Employment of semi-rigid *N*-donor ligands towards the synthesis of functional coordination polymers with low dimensionality

Appendix

Edouardos Loukopoulos

Submitted for degree of Doctor of Philosophy
University of Sussex
August 2018

TABLE OF CONTENTS

Chapter 1

. 1.1 Crystal Structures of Ligands……. 1

1.2 Characterization spectra (^{1}H NMR, ^{13}C NMR, HRMS, FT-IR) of ligands…… 3

Chapter 2

2.1 π-π interactions……... 17

2.2 Magnetic Measurements……. 21

2.3 Characterization data of **1** – **10**…… 22

Chapter 3

3.1 Synthesis of starting azines……. 33

3.2 Characterization data of **11** – **13**……. 33

3.3 Catalytic Experiments……. 41

3.4 ^{1}H and ^{13}C NMR data of selected isolated pyrazoles ……. 46

3.5 ^{1}H, ^{13}C NMR and HRMS spectra of the 1,4-dihydropyridine products……. 47

3.6 ^{1}H, ^{13}C NMR and HRMS spectra of selected isolated pyrazoles……... 64

Chapter 4

4.1 Characterization data of **14** – **21**……. 69

4.2 ^{1}H, ^{13}C NMR and HRMS spectra of propargylamine products…….. 78

Chapter 5

5.1 Characterization data of **22** – **26**……. 105

5.2 ^{1}H, ^{13}C NMR and HRMS spectra of triazole products……. 116

Chapter 6

6.1 Weak interactions……... 136

6.2 Additional Figures of Crystal Structures……. 139

6.3 Characterization data of **27** – **35**……. 140

6.4 ^{1}H, ^{13}C NMR and HRMS spectra of ketone products……. 158

Chapter 1

1.1. Crystal Structures of ligands

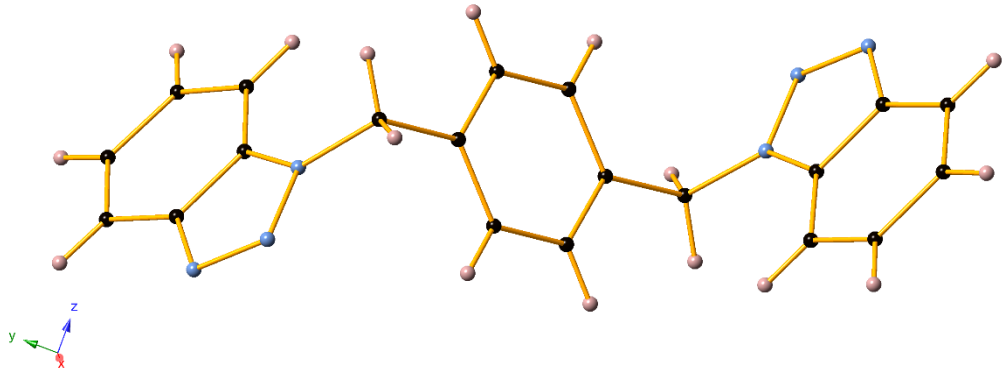

Figure S1.1. The structure of **L**[1]. Colour code C (black), H (light pink), N (light blue).

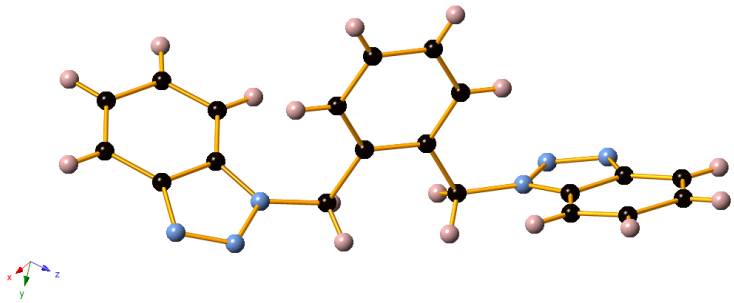

Figure S1.2. The structure of **L**[3]. Colour code C (black), H (light pink), N (light blue).

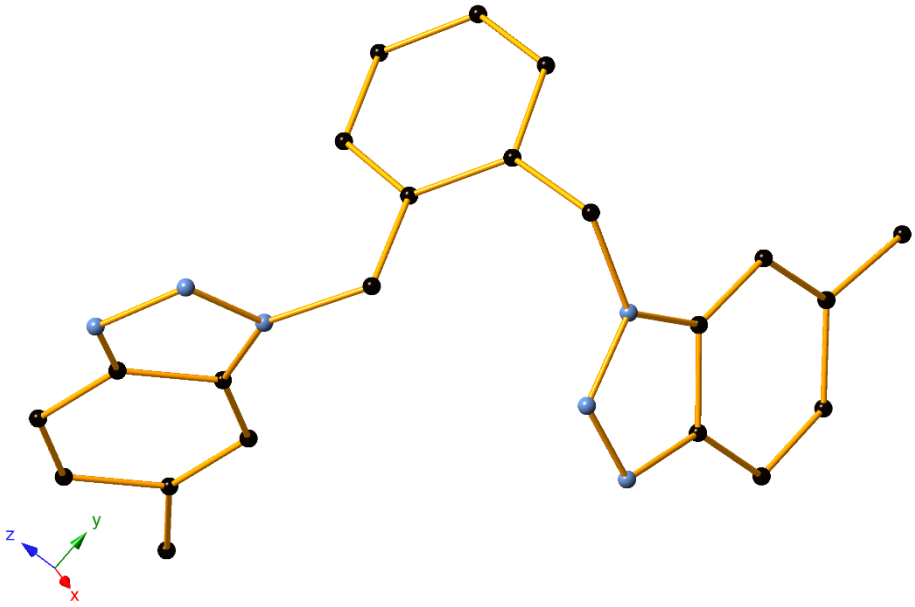

Figure S1.3. The structure of **L**[4]. H atoms have been omitted to enhance clarity. Colour code C (black), N (light blue).

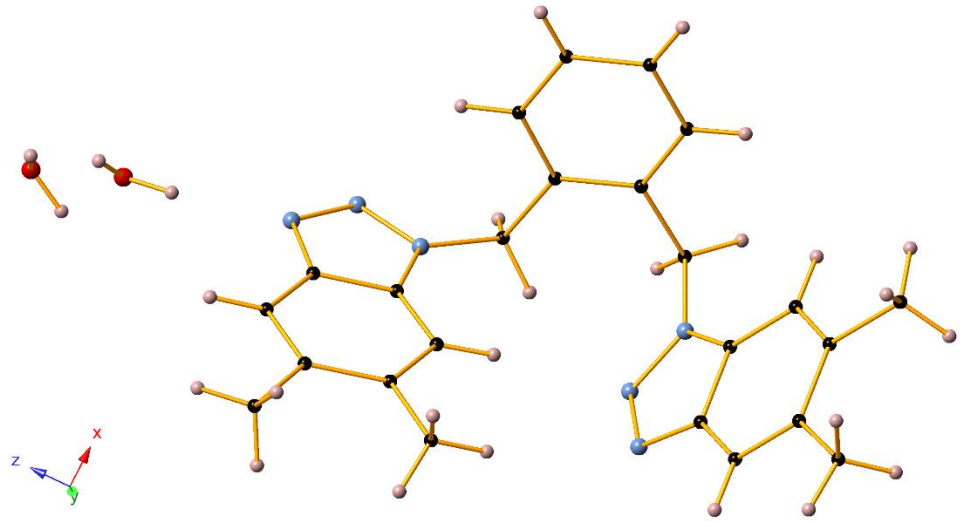

Figure S1.4. The structure of $\mathbf{L^5}\cdot 2H_2O$. Colour code C (black), H (light pink), N (light blue), O (red).

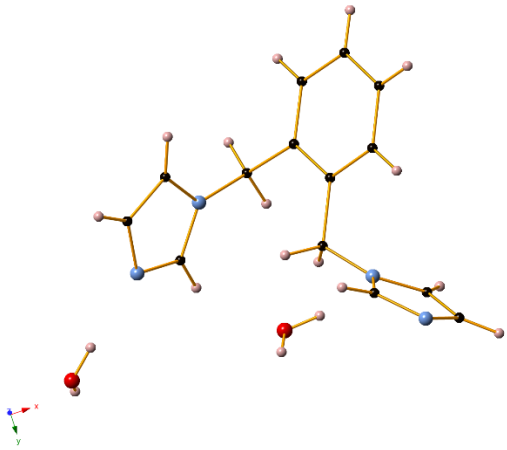

Figure S1.5. The structure of $\mathbf{L^7}\cdot 2H_2O$. Colour code C (black), H (light pink), N (light blue), O (red).

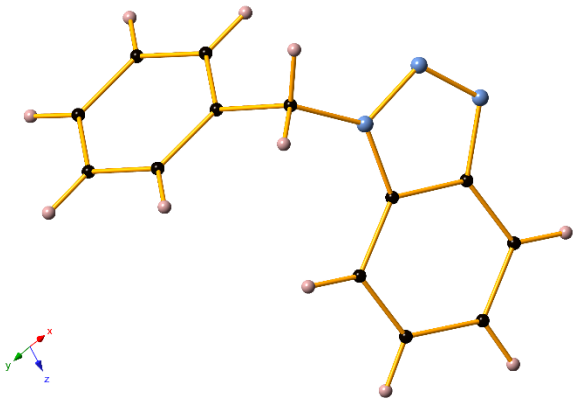

Figure S1.6. The structure of $\mathbf{L^8}$. Colour code C (black), H (light pink), N (light blue).

1.2. Characterization spectra (^{1}H NMR, ^{13}C NMR, HRMS, FT-IR) of ligands

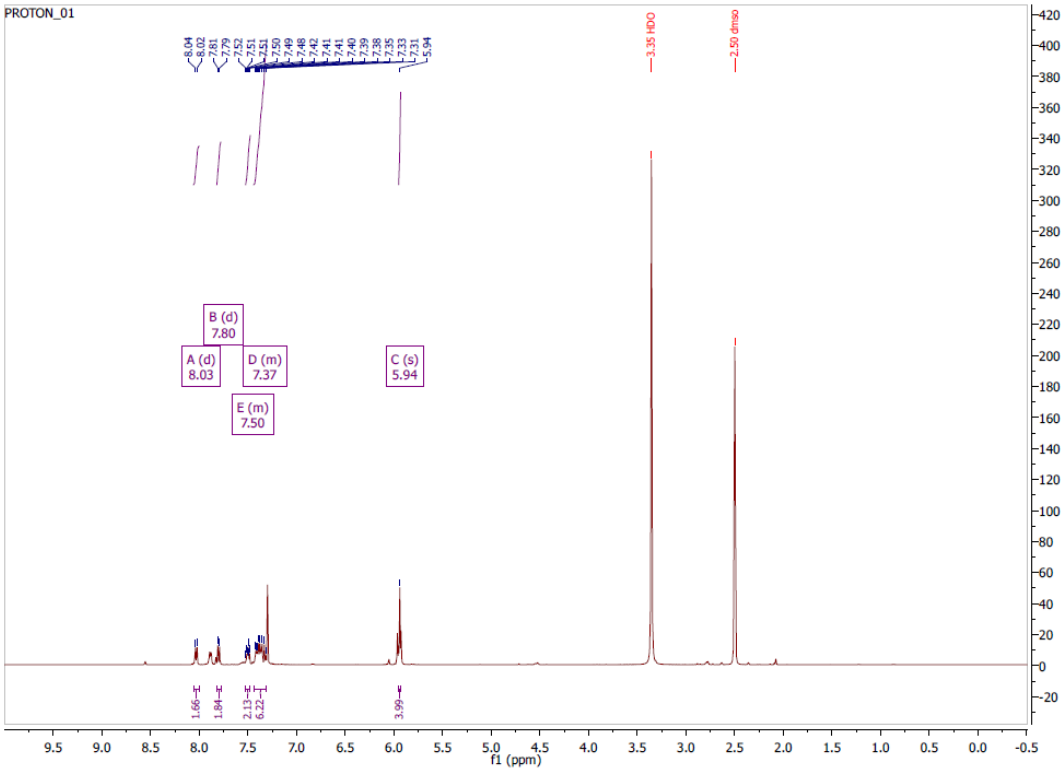

Figure S1.7. ^{1}H NMR spectrum of **L^{1}**.

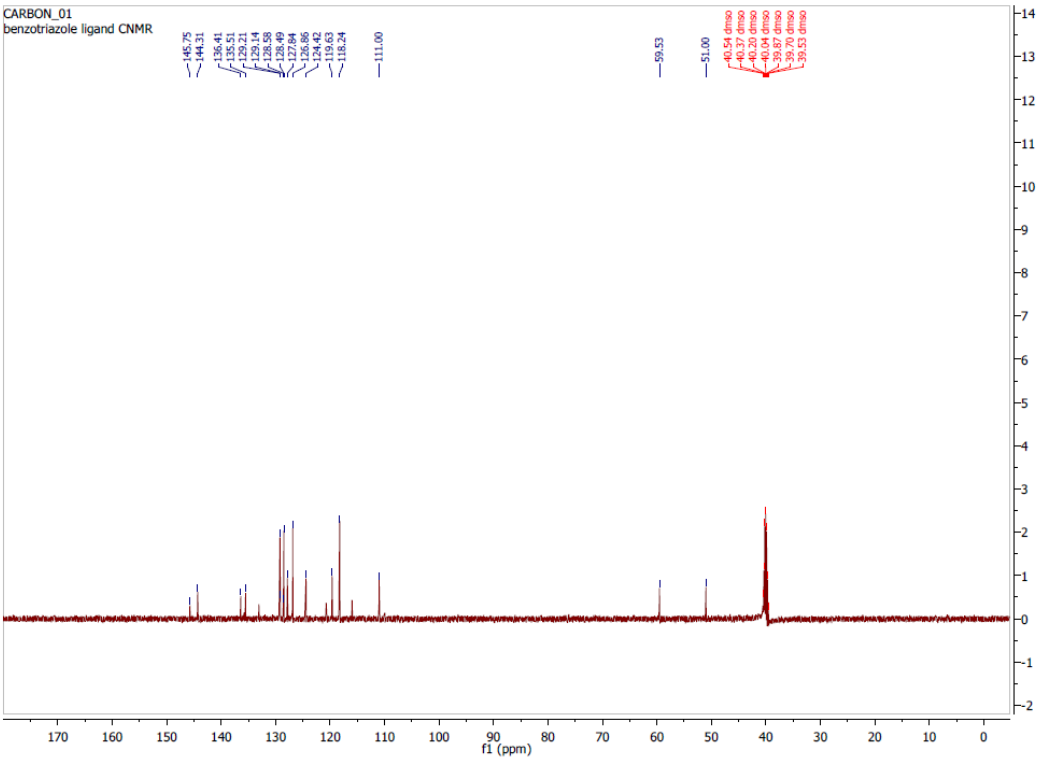

Figure S1.8. ^{13}C NMR spectrum of **L^{1}**.

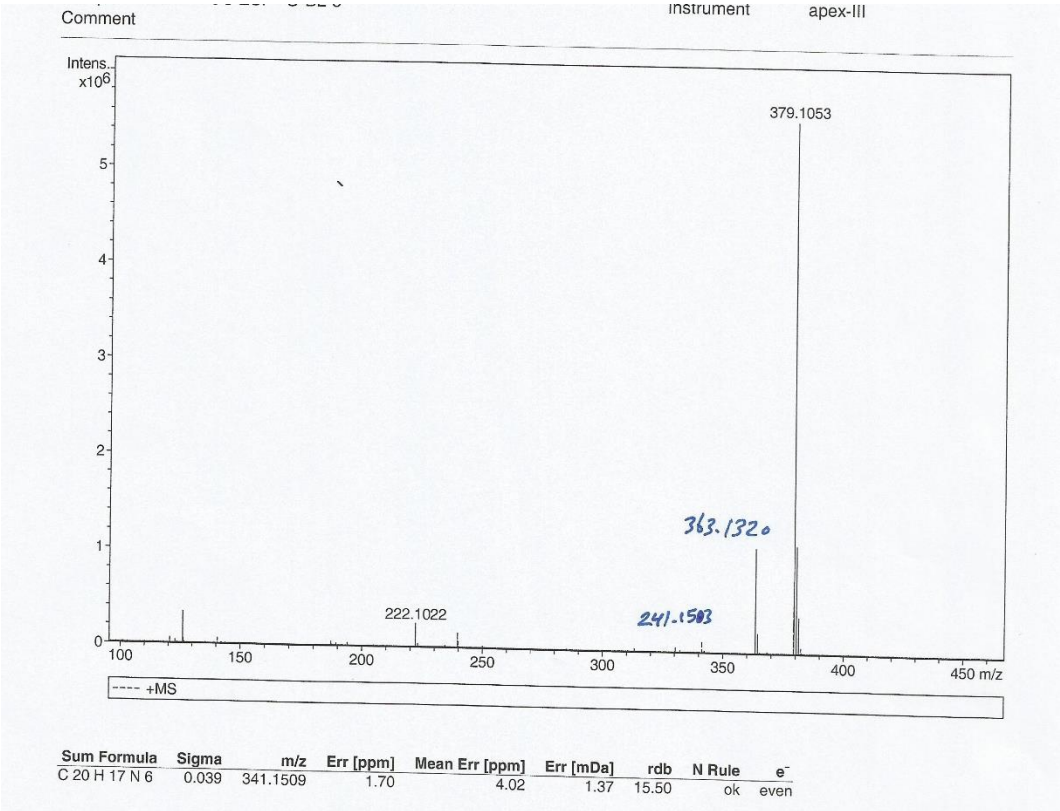

Figure S1.9. HRMS spectrum of **L**[1].

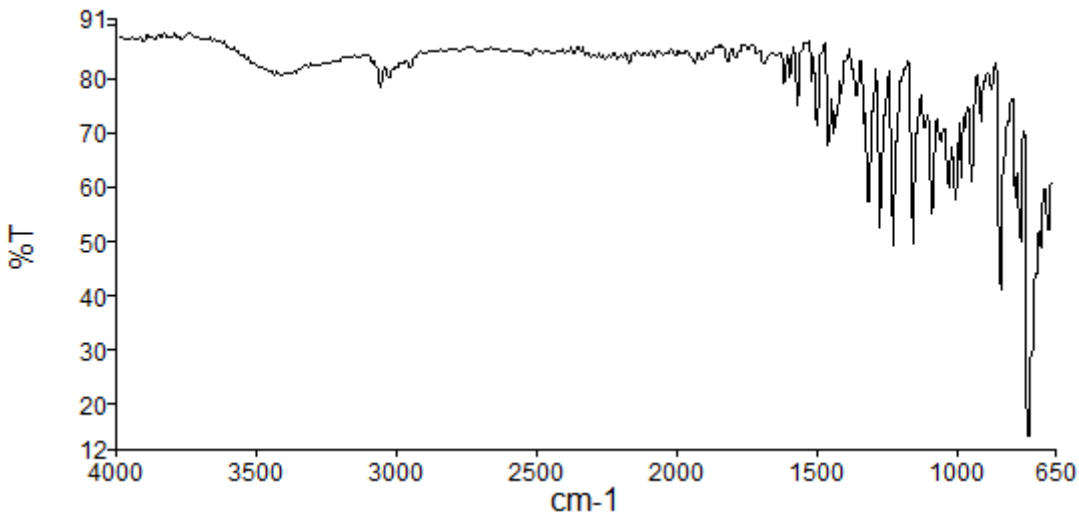

Figure S1.10. IR spectrum of **L**[1].

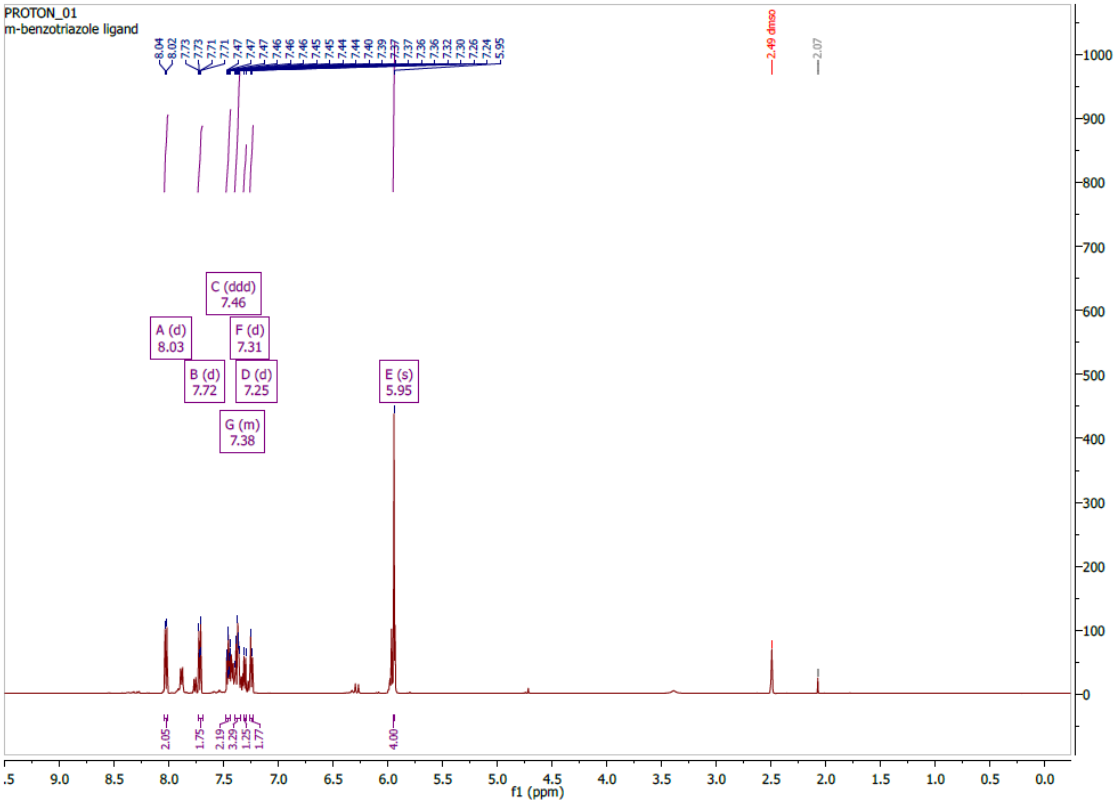

Figure S1.11. ^{1}H NMR spectrum of **L²**.

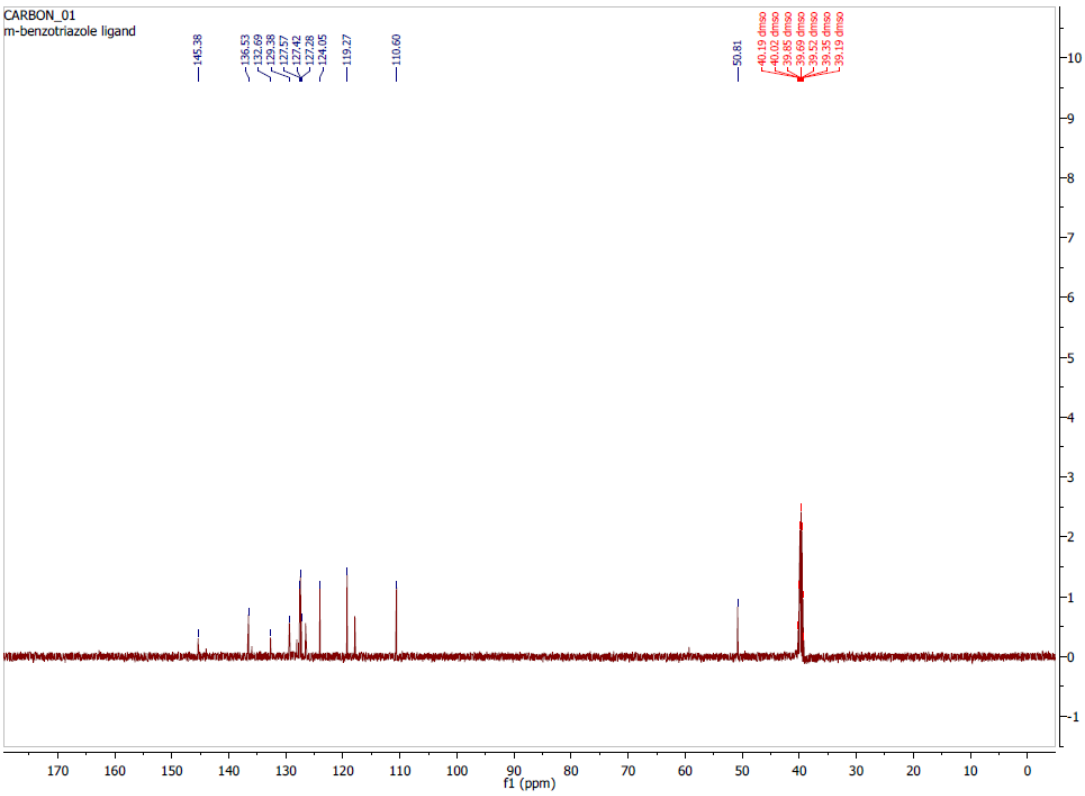

Figure S1.12. ^{13}C NMR spectrum of **L²**.

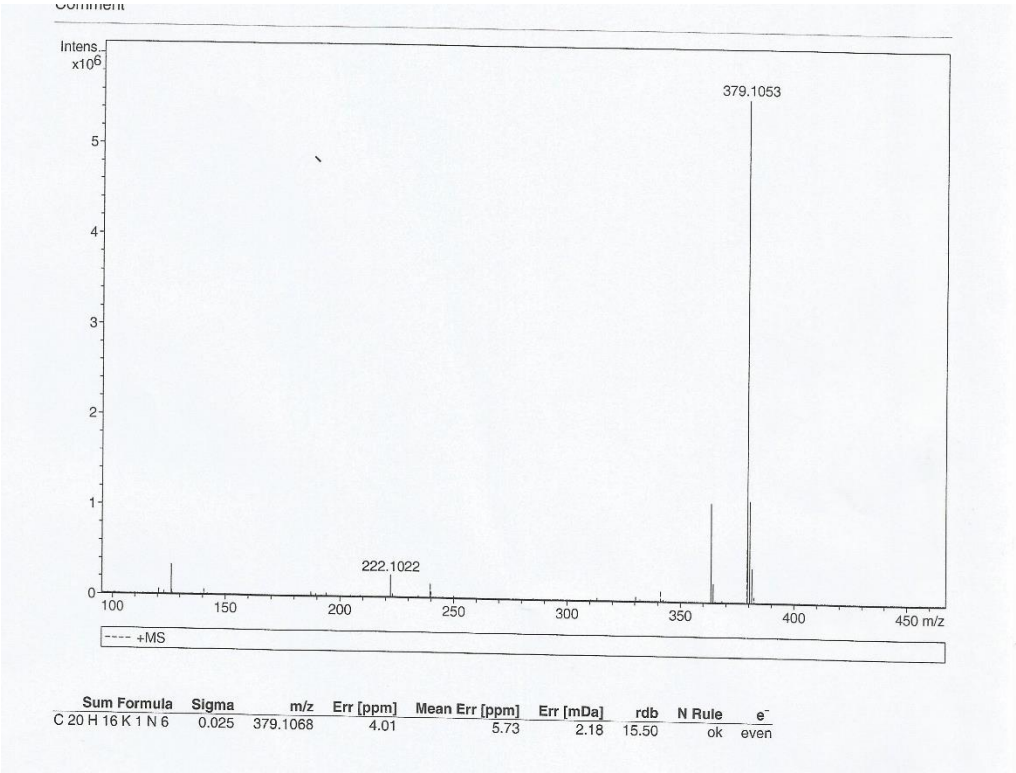

Figure S1.13. HRMS spectrum of **L²**.

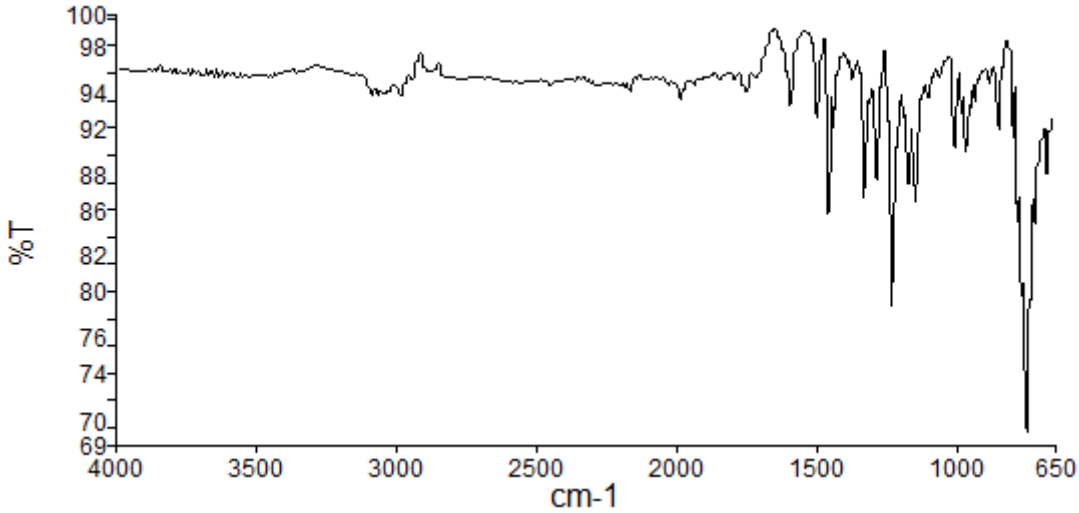

Figure S1.14. IR spectrum of **L²**.

Figure S1.15. ^{1}H NMR spectrum of **L^{3}**.

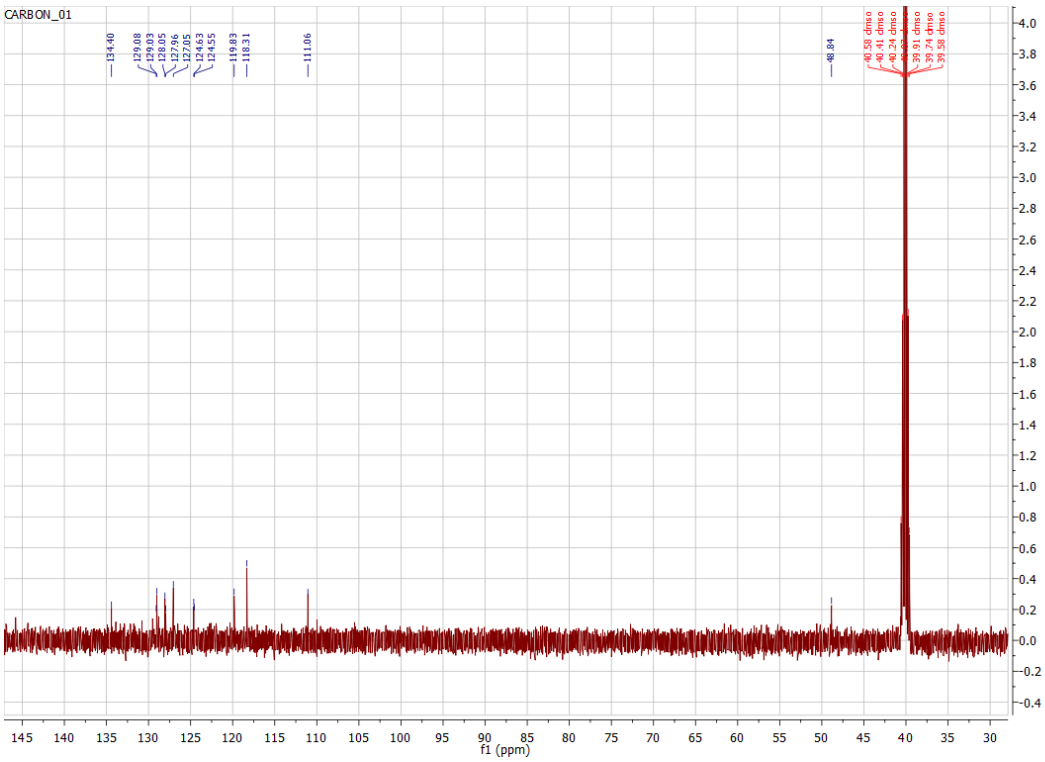

Figure S1.16. ^{13}C NMR spectrum of **L^{3}**.

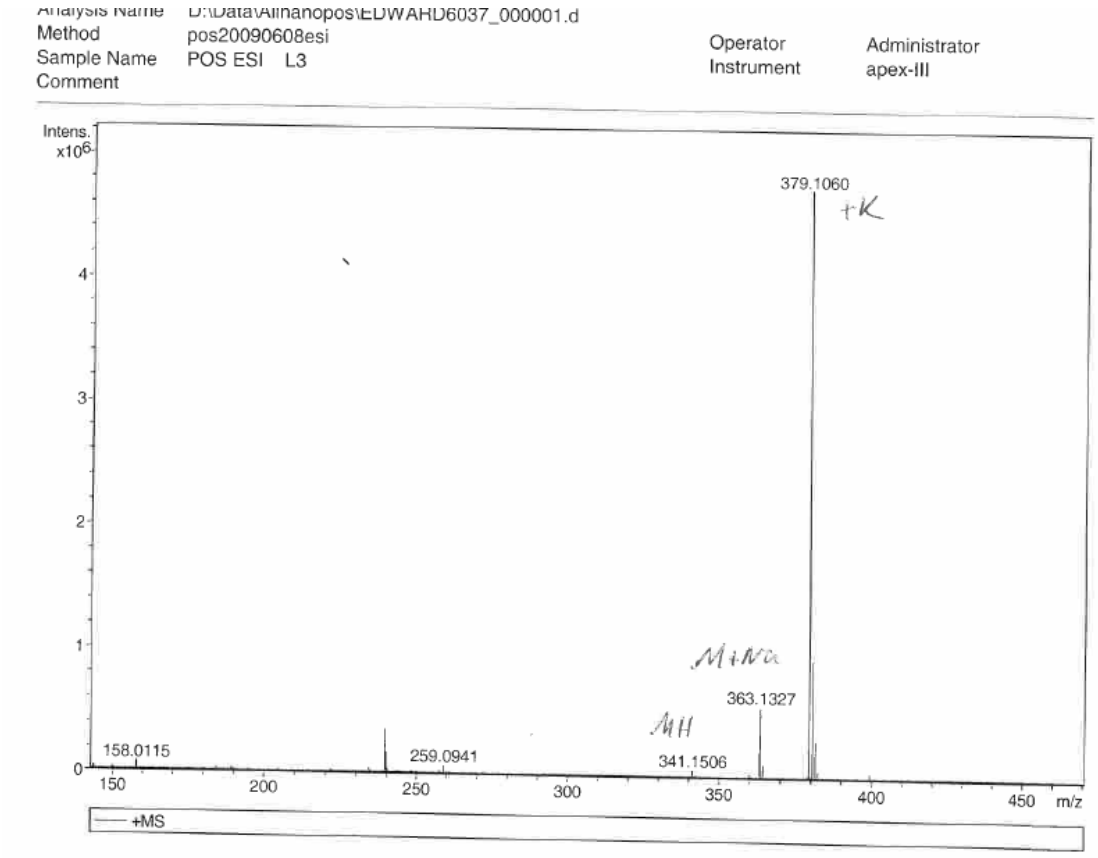

Figure S1.17. HRMS spectrum of **L³**.

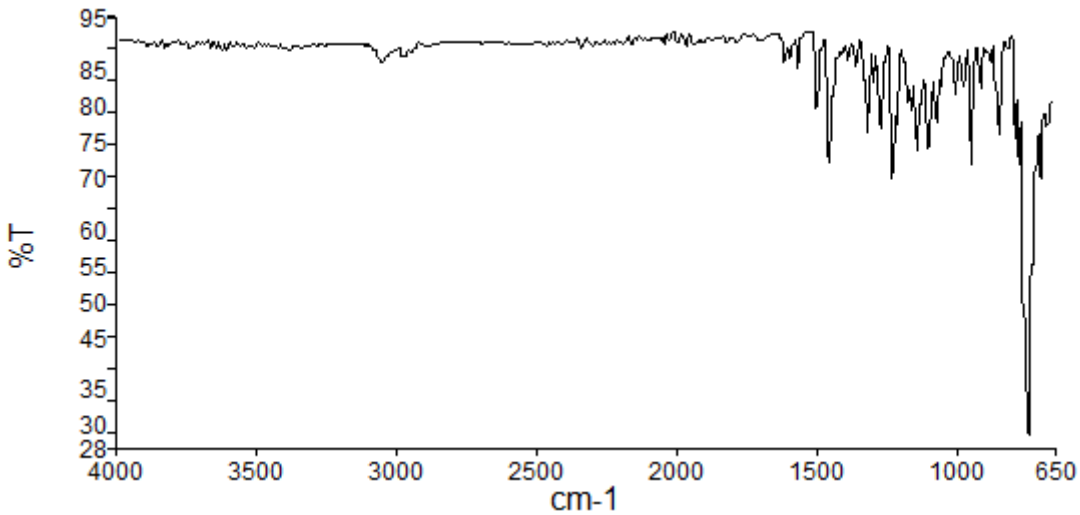

Figure S1.18. IR spectrum of **L³**.

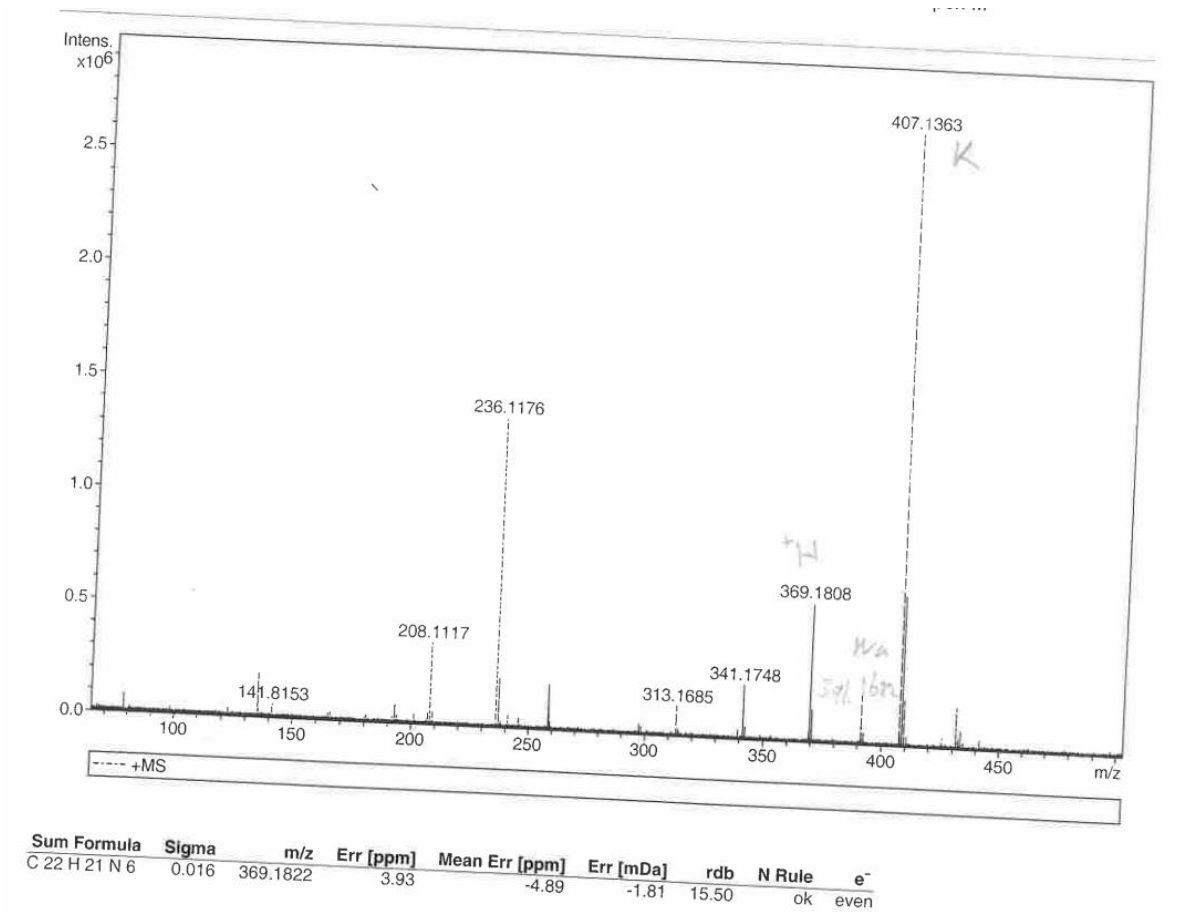

Figure S1.19. HRMS spectrum of **L**^{4}.

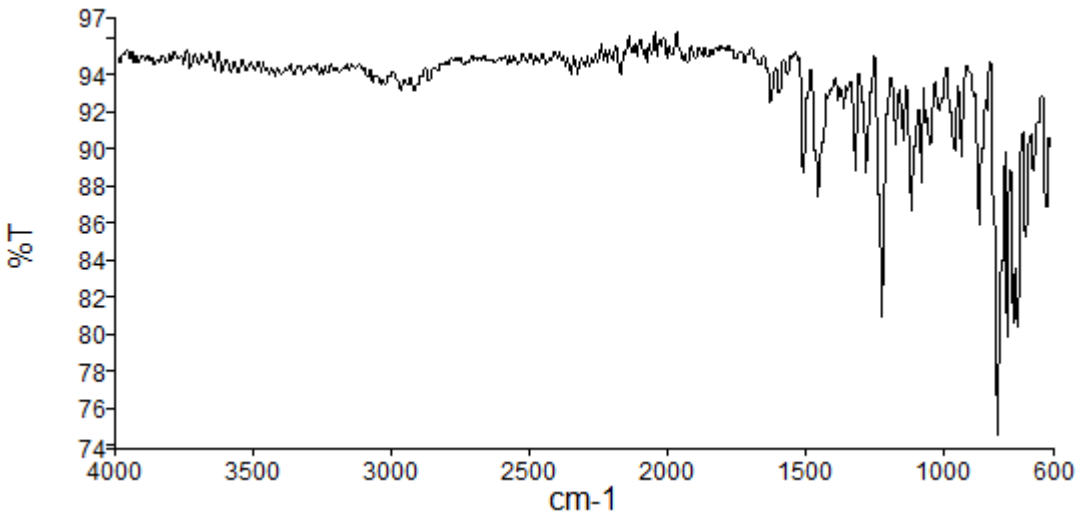

Figure S1.20. IR spectrum of **L**^{4}.

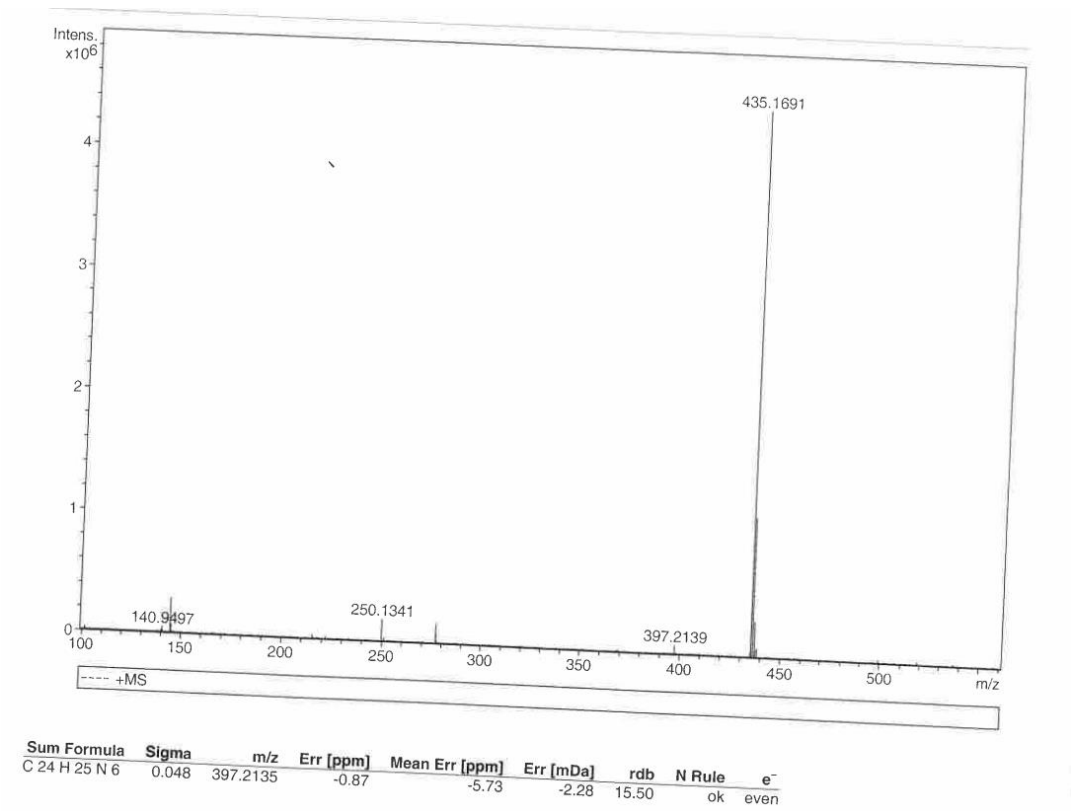

Figure S1.21. HRMS spectrum of **L**^{5}.

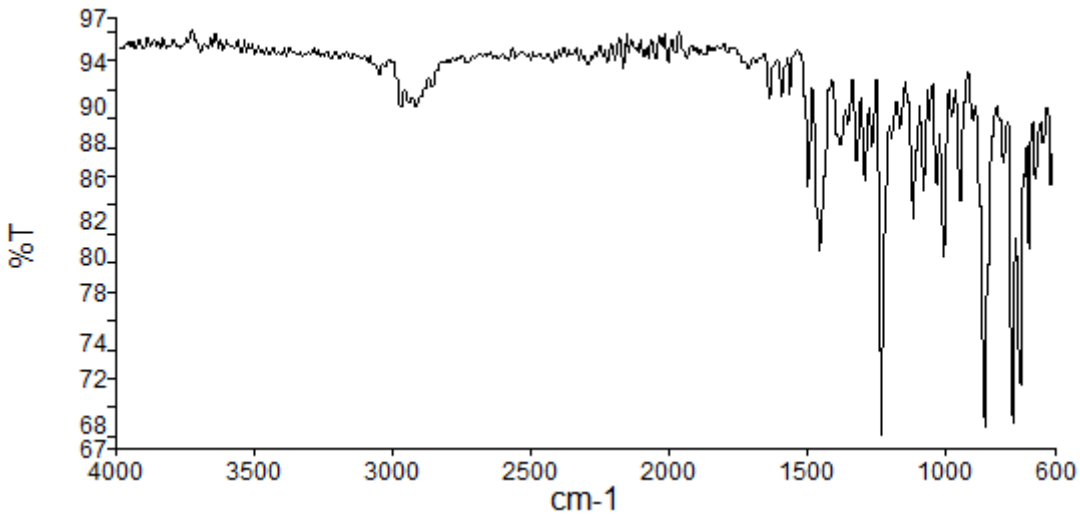

Figure S1.22. IR spectrum of **L**^{5}.

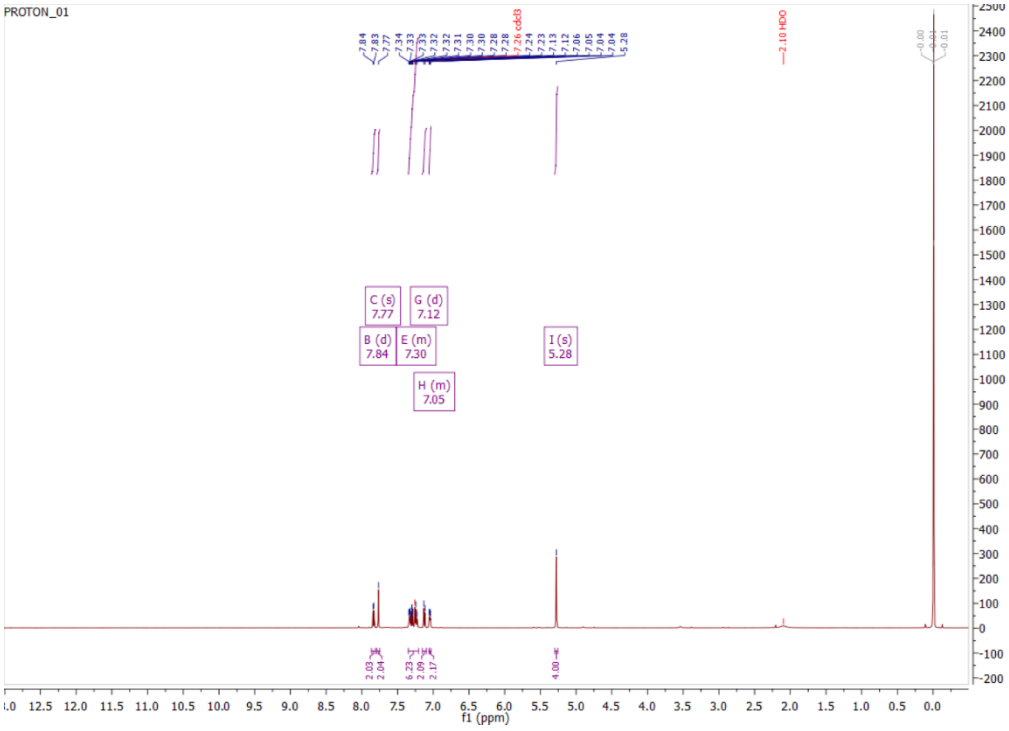

Figure S1.23. ^{1}H NMR spectrum of **L^{6}**.

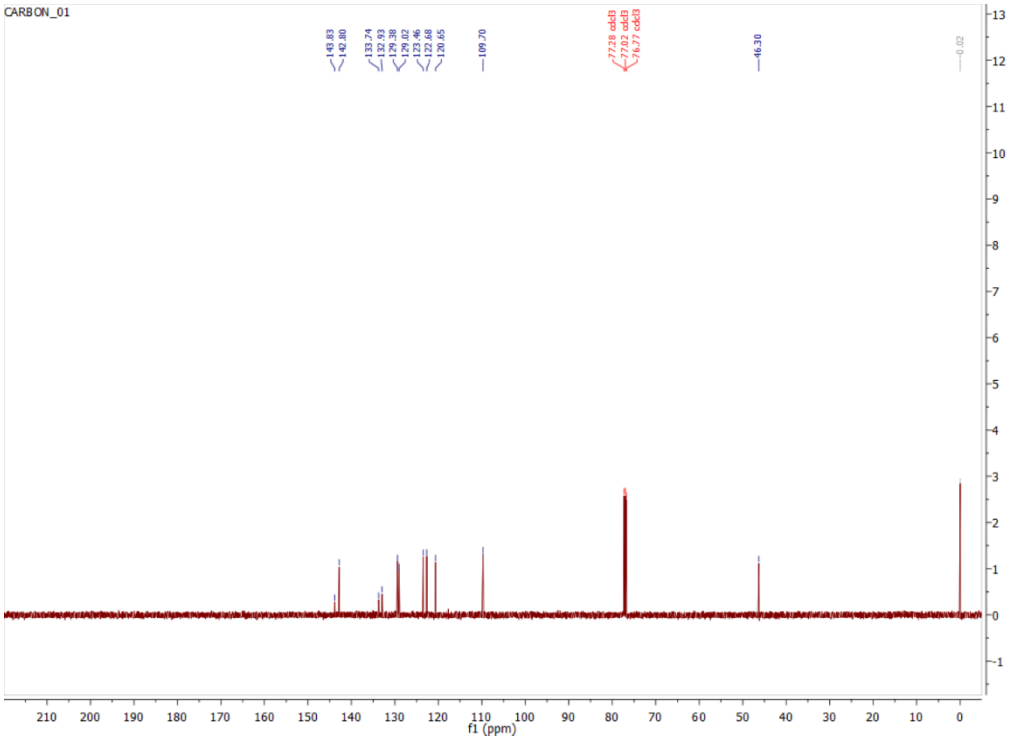

Figure S1.24. ^{13}C NMR spectrum of **L^{6}**.

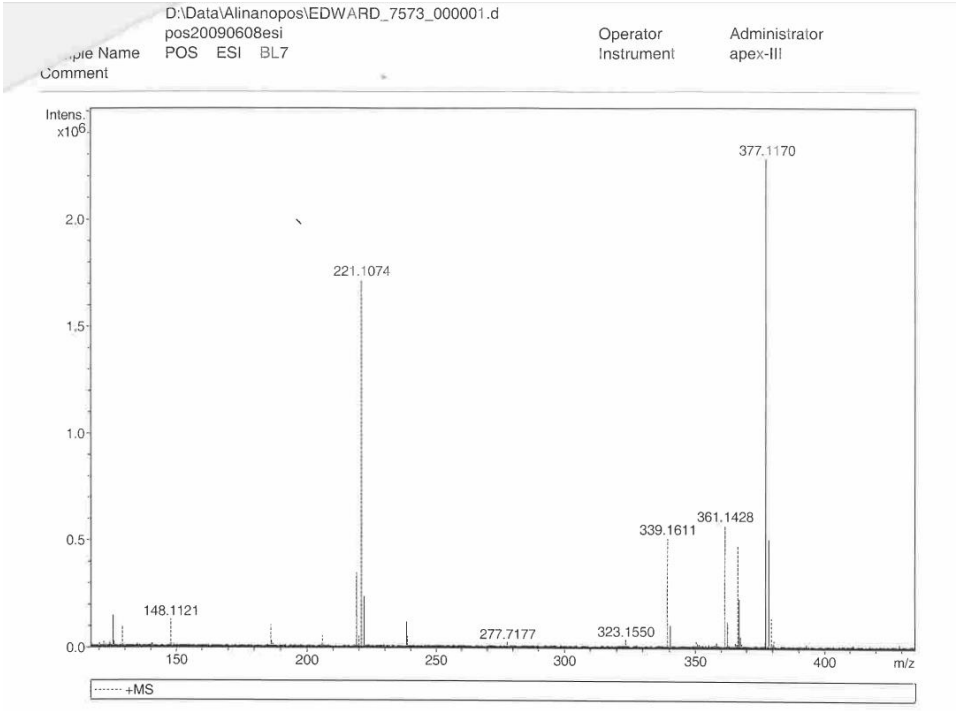

Sum Formula	Sigma	m/z	Err [ppm]	Mean Err [ppm]	Err [mDa]	rdb	N Rule	e⁻
C 22 H 19 N 4	0.027	339.1604	-2.04	4.54	1.54	15.50	ok	even

Figure S1.25. HRMS spectrum of **L**^{6}.

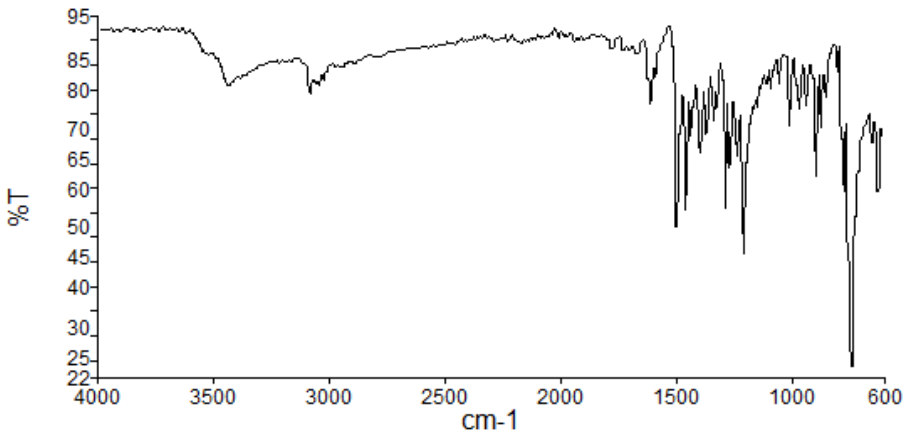

Figure S1.26. IR spectrum of **L**^{6}.

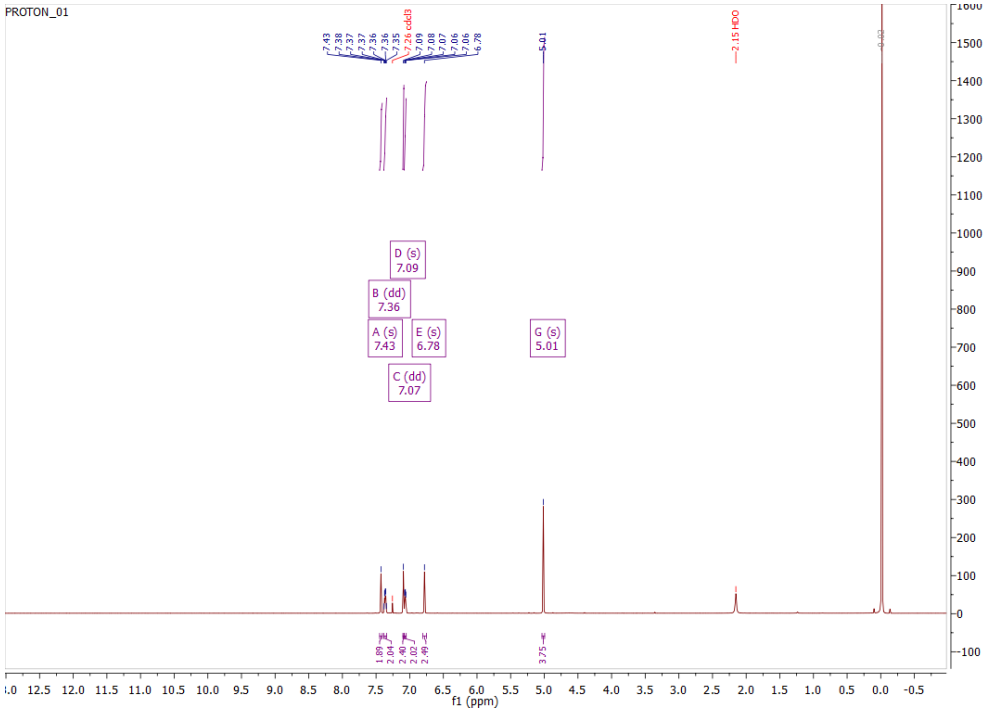

Figure S1.27. ^{1}H NMR spectrum of **L**^{7}.

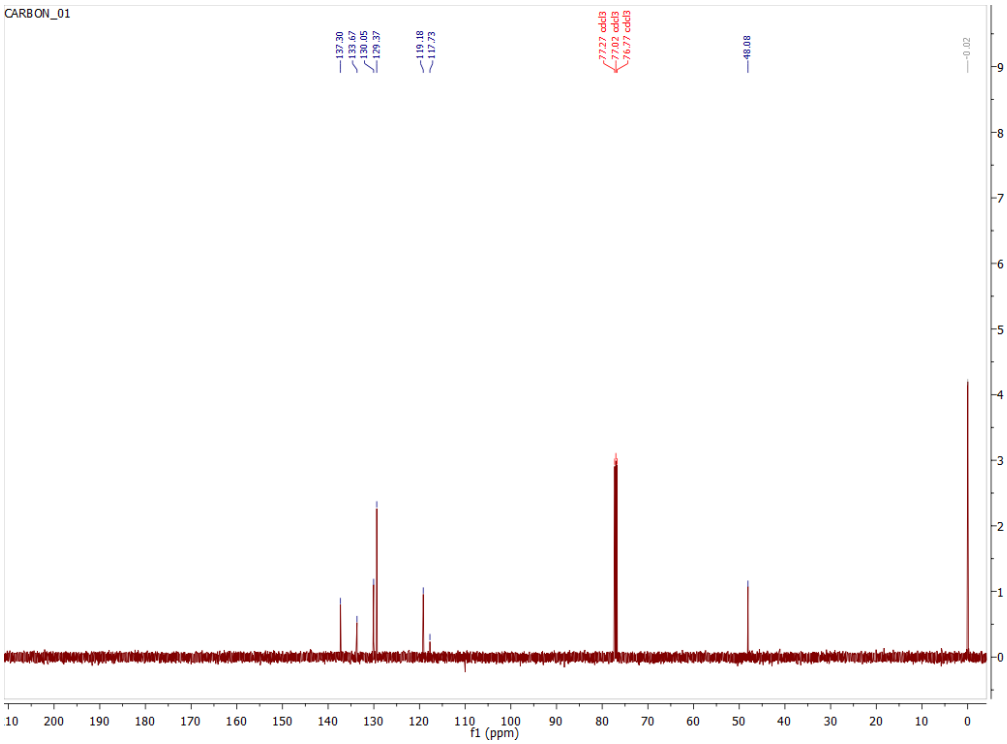

Figure S1.28. ^{13}C NMR spectrum of **L**^{7}.

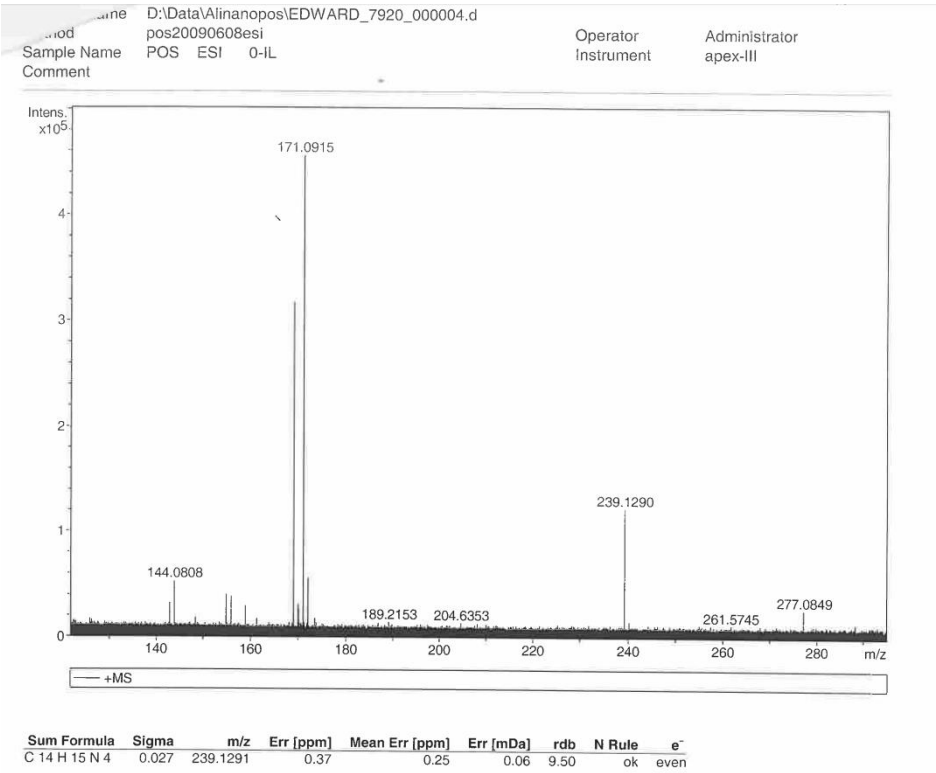

Figure S1.29. HRMS spectrum of **L**^{7}.

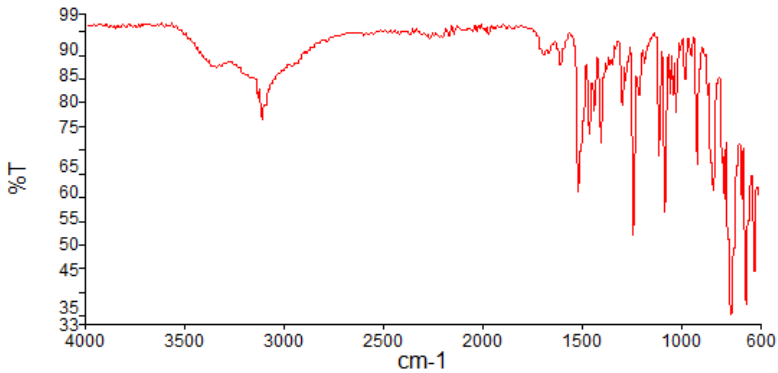

Figure S1.30. IR spectrum of **L**^{7}.

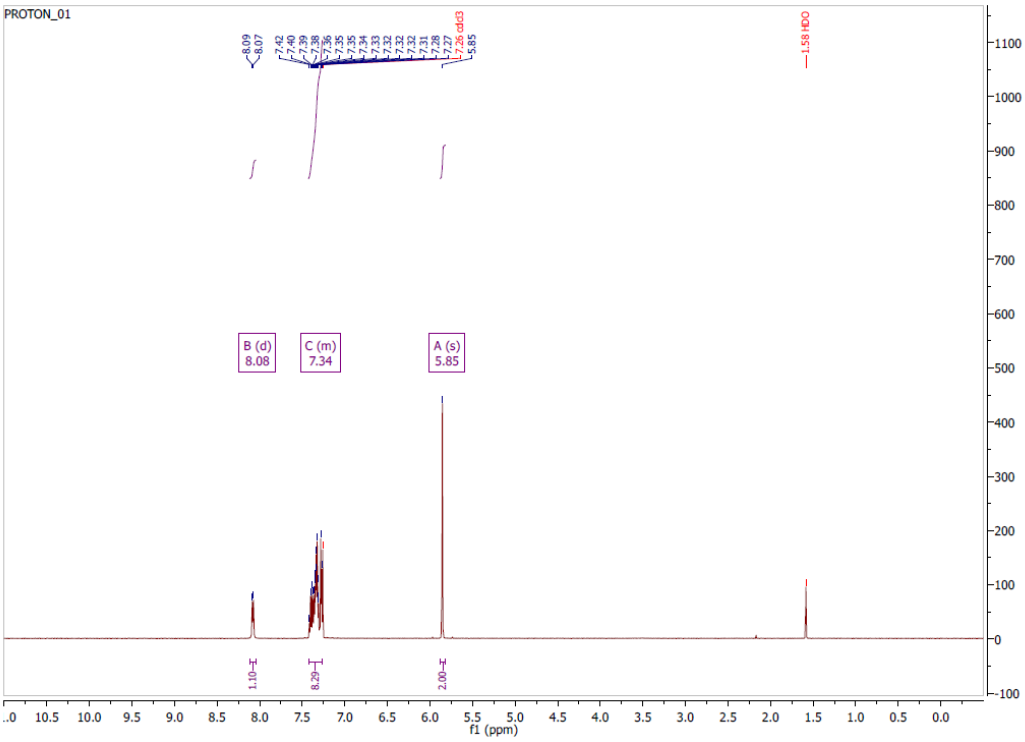

Figure S1.31. ^{1}H NMR spectrum of **L^{8}**.

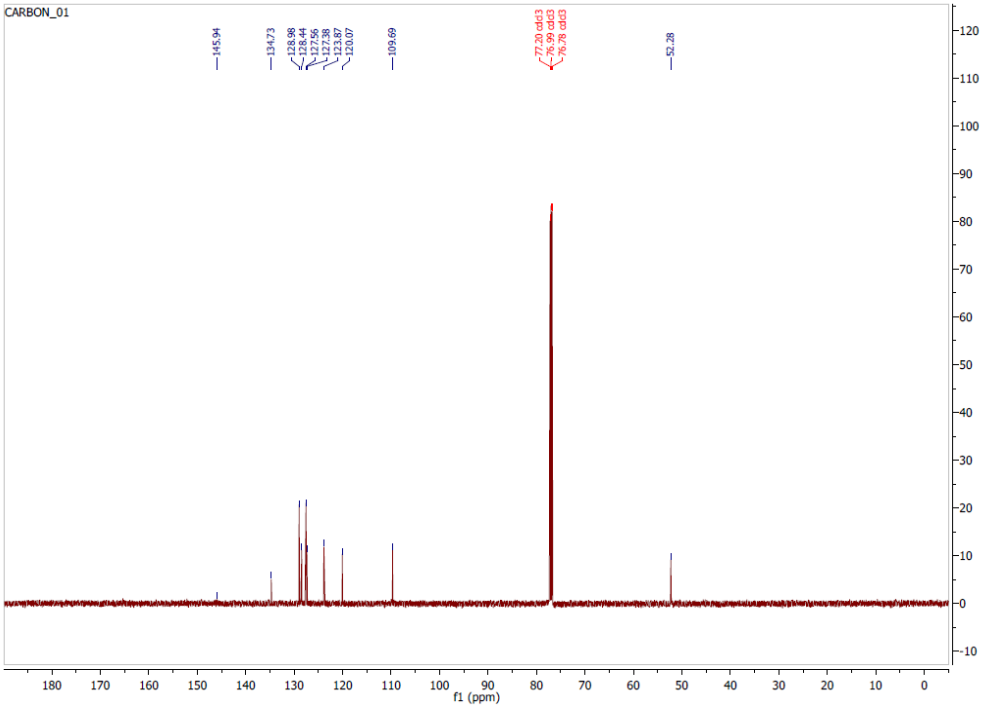

Figure S1.32. ^{13}C NMR spectrum of **L^{8}**.

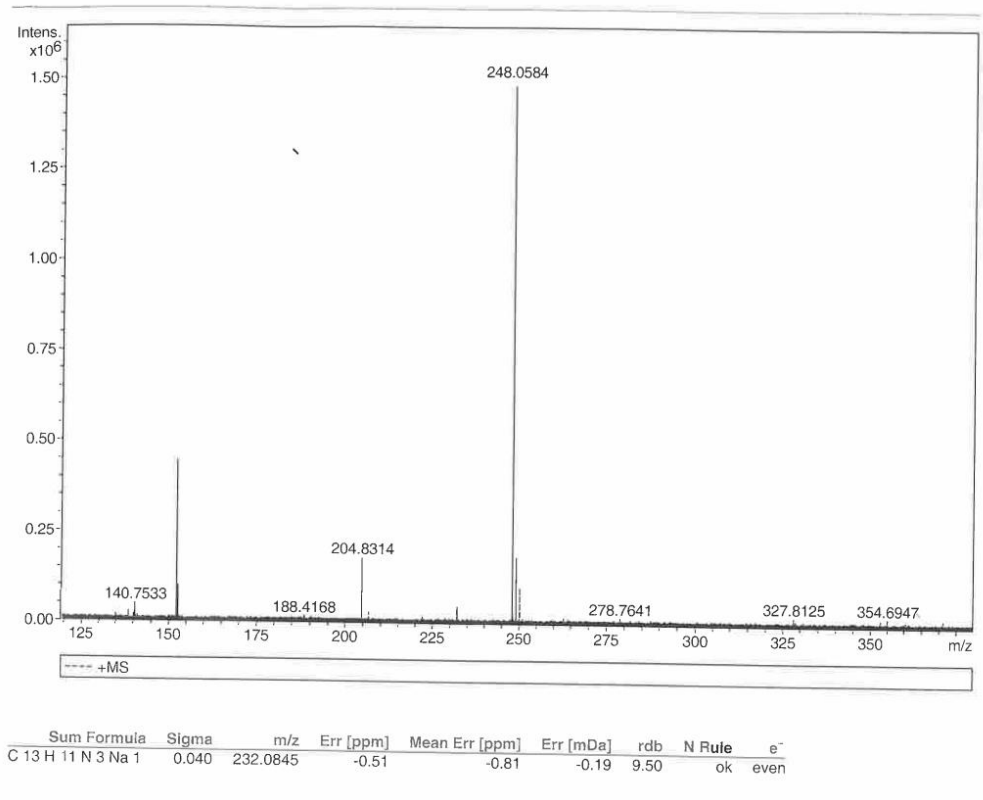

Figure S1.33. HRMS spectrum of **L**[8].

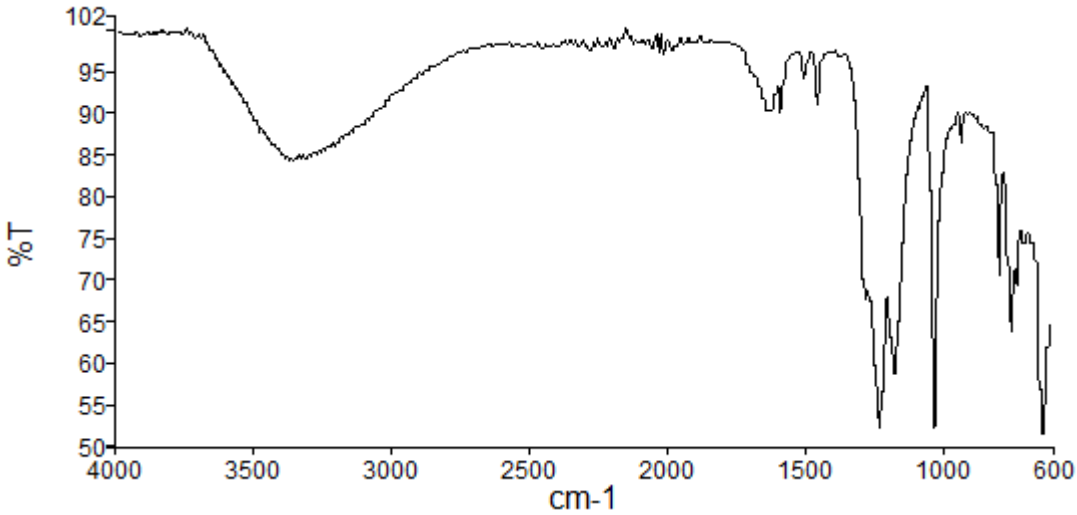

Figure S1.34. IR spectrum of **L**[8].

Chapter 2

2.1. π-π interactions

Table S2.1. π–π stacking distances (Å) and angles (º) in compound **1**.

Rings	Distance between ring centroids (Å)	Perpendicular distance between ring planes (Å)	Centroid offset (Å)	Dihedral angle between ring mean-planes (˚)
A-A^{i}	3.708(3)	3.433(2)	1.400(2)	0.0
A-B^{i}	3.596(3)	3.436(2)	1.400(2)	0.8(3)
C-C^{ii}	3.755(3)	3.472(2)	1.430(2)	0.0

Rings: A: C15-C16-N4-N5-N6. B: C15-C16-C17-C18-C19-C20. C: C2-C3-C4-C5-C6-C7.

Symmetry codes: ^{i}: 2-x, -y, 1-z. ^{ii}: 1-x, 1-y, 2-z.

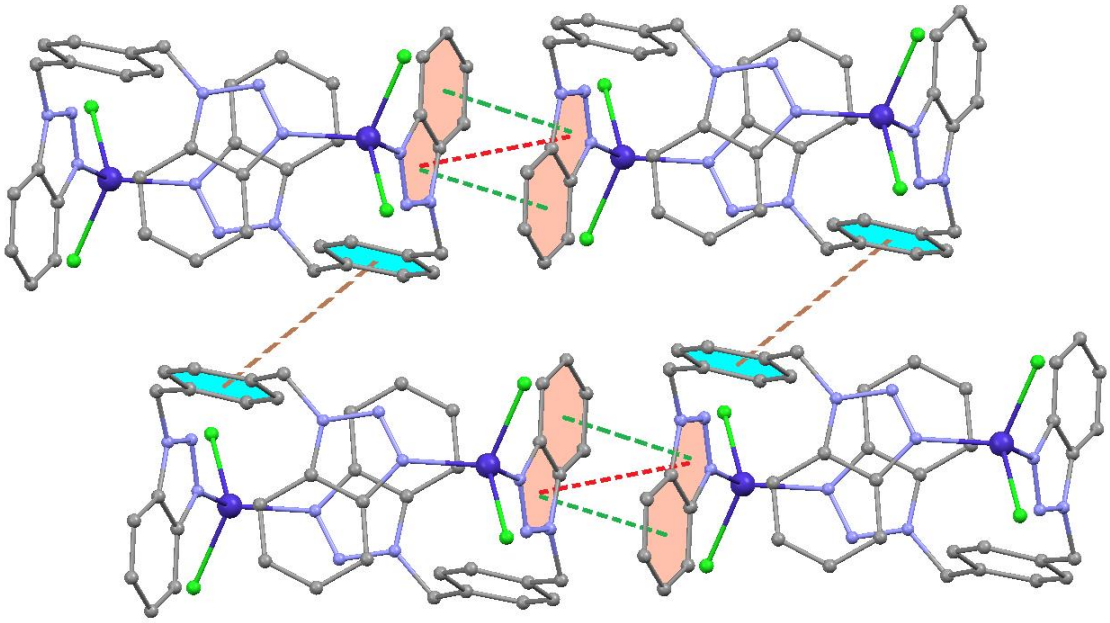

Figure S2.1. Part of the supramolecular architecture of compound **1**, stabilised by intermolecular π···π interactions (brown, green and red dashed lines), as described in Table S3. Solvent molecules and hydrogen atoms have been omitted. Colour code Co (blue), Cl (green), C (grey), N (light blue).

Table S2.2. π–π stacking distances (Å) and angles (º) in compound **3**.

Rings	Distance between ring centroids (Å)	Perpendicular distance between ring planes (Å)	Centroid offset (Å)	Dihedral angle between ring mean-planes (˚)
A-A^{i}	3.6485(13)	3.3288(9)	1.413(8)	0.00 (13)
A-B^{i}	3.4601(13)	3.3291 (9)	0.938(8)	0.08(12)

Rings: A: C1-C6-N1-N2-N3. B: C1-C2-C3-C4-C5-C6. Symmetry codes: ^{i}: 2-x, 1-y, 1-z.

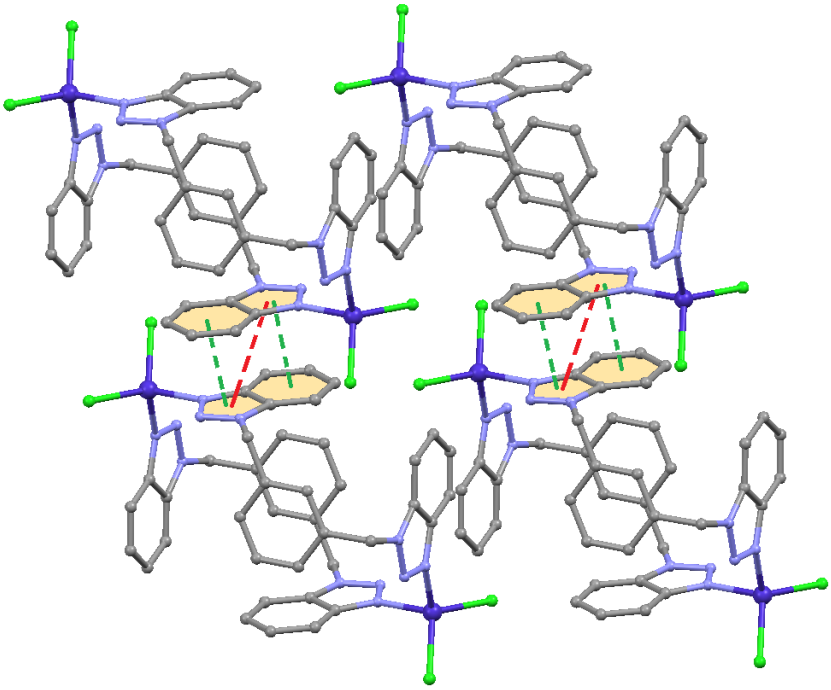

Figure S2.2. Part of the supramolecular architecture of compound **3**, stabilised by intermolecular π···π interactions (green and red dashed lines), as described in Table S4. Solvent molecules and hydrogen atoms have been omitted. Colour code Co (blue), Cl (green), C (grey), N (light blue).

Table S2.3. π–π stacking distances (Å) and angles (º) in compound **4**.

Rings	Distance between ring centroids (Å)	Perpendicular distance between ring planes (Å)	Centroid offset (Å)	Dihedral angle between ring mean-planes (˚)
A-A^{i}	3.641(3)	3.2927(17)	1.554(2)	0.0(2)
A-B^{i}	3.801(3)	3.3155(17)	1.902(2)	0.8(2)

Rings: A: C1-C2-C3-C4-C5-C6. B: C1-C6-N1-N2-N3. Symmetry codes: ^{i}: -x, 1-y, -z.

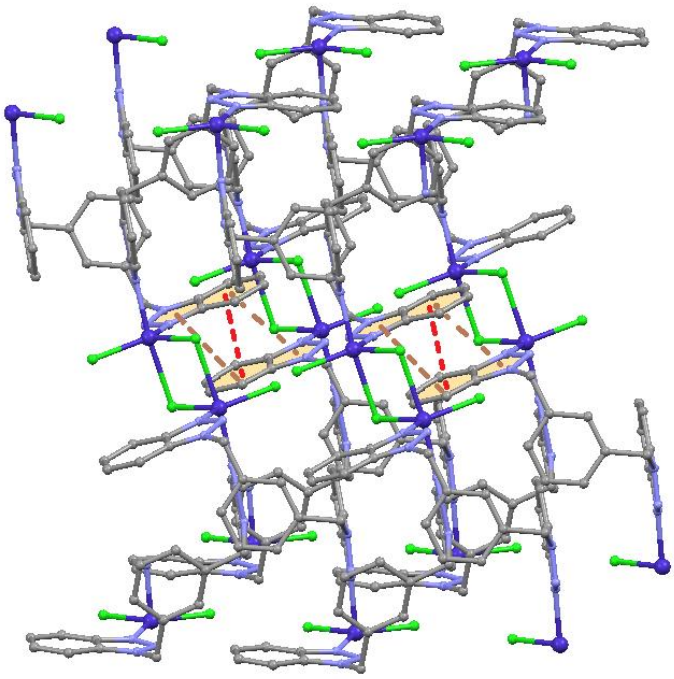

Figure S2.3. Part of the supramolecular architecture of compound **4**, in which the intermolecular π···π interactions (described in Table S5, noted with brown and red dashed lines), further stabilise the 2D framework. Hydrogen atoms have been omitted. Colour code Co (blue), Cl (green), C (grey), N (light blue).

Table S2.4. π–π stacking distances (Å) and angles (º) in compound **8**.

Rings	Distance between ring centroids (Å)	Perpendicular distance between ring planes (Å)	Centroid offset (Å)	Dihedral angle between ring mean-planes (˚)
A-B^{i}	3.782(3)	3.3773(17)	1.661(3)	0.9(2)
C-C^{ii}	3.688(3)	3.2972(18)	1.651(3)	0.0(2)

Rings: A: C1-C6-N1-N2-N3. B: C1-C2-C3-C4-C5-C6. C: C15-C16-C17-C18-C19-C20.

Symmetry codes: ^{i}: -x, 1-y, 1-z. ^{ii}: 1-x, -y, 2-z.

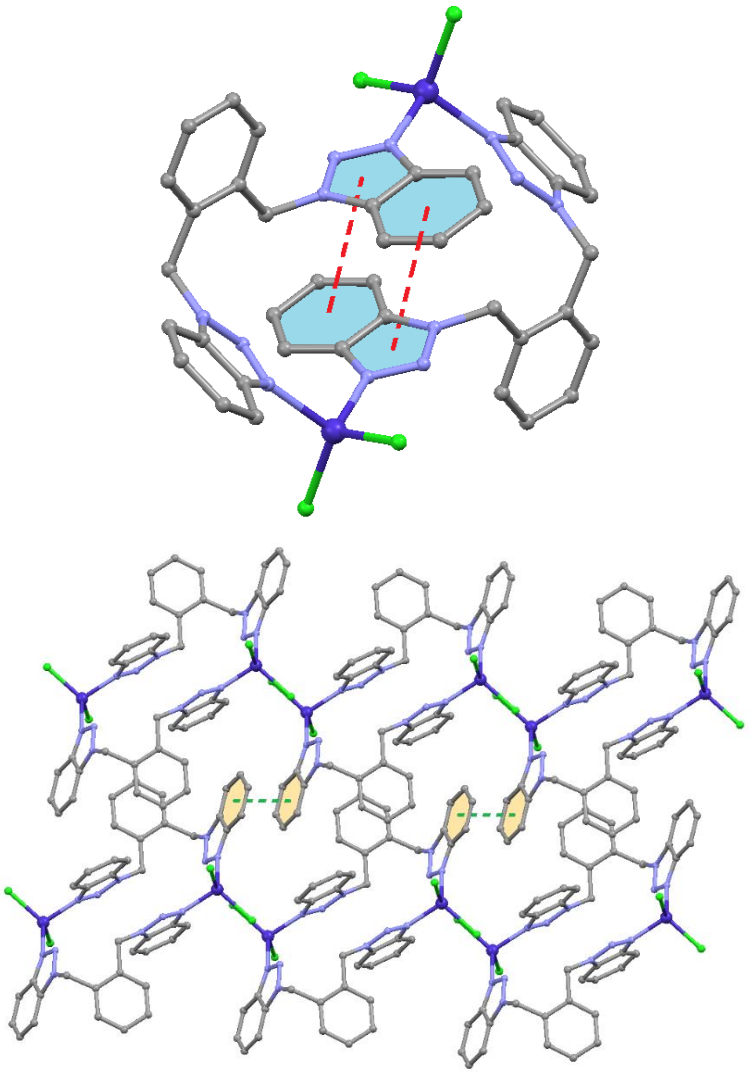

Figure S2.4. (upper) The intramolecular π···π interactions observed in compound **8**, noted with red dashed lines. (lower) Part of the supramolecular architecture of the compound **8**, stabilised by the intermolecular π···π interactions (noted with green dashed lines). Hydrogen atoms have been omitted. Colour code Co (blue), Cl (green), C (grey), N (light blue).

2.2. Magnetic Measurements

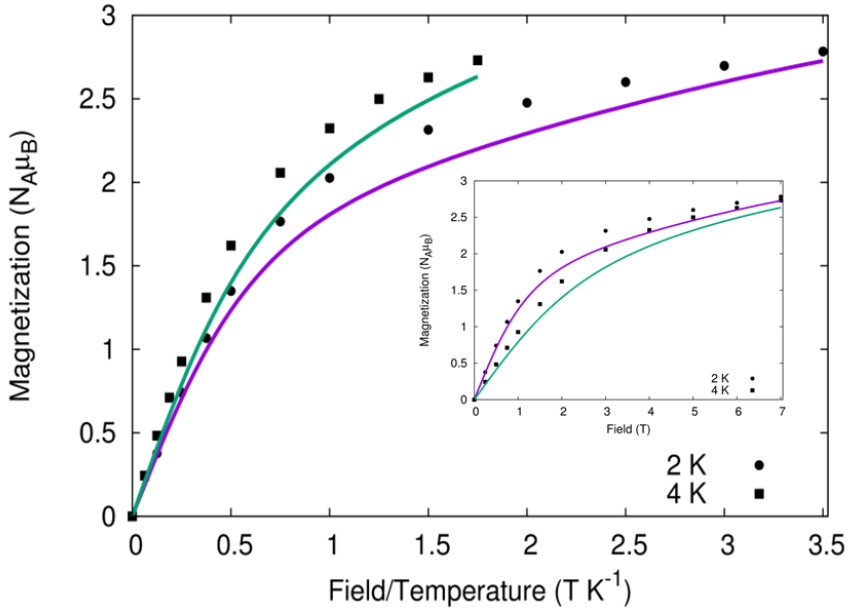

Figure S2.5. Experimental (black circles and squares) and fitted (purple and green lines, parameters in text) reduced magnetization for **7** at 2 and 4 K. (inset) Experimental (black circles and squares) and fitted (purple and green lines, parameters in text) magnetization for **7** at 2 and 4 K.

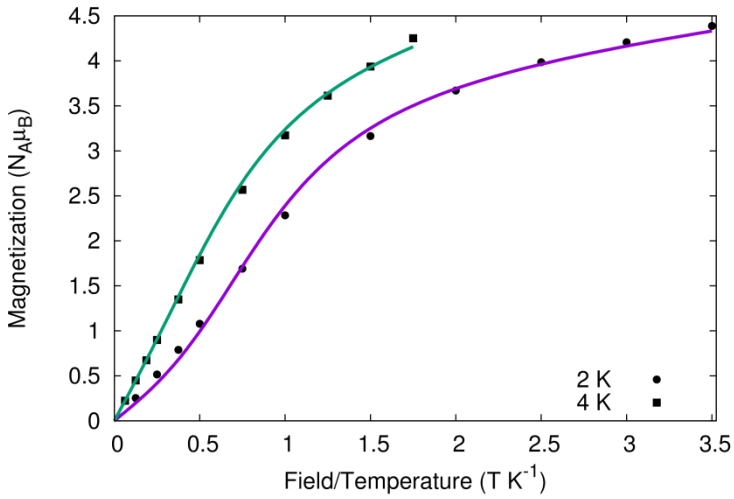

Figure S2.6. Experimental (black circles and squares) and fitted (purple and green lines) reduced magnetization for **9** at 2 and 4 K.

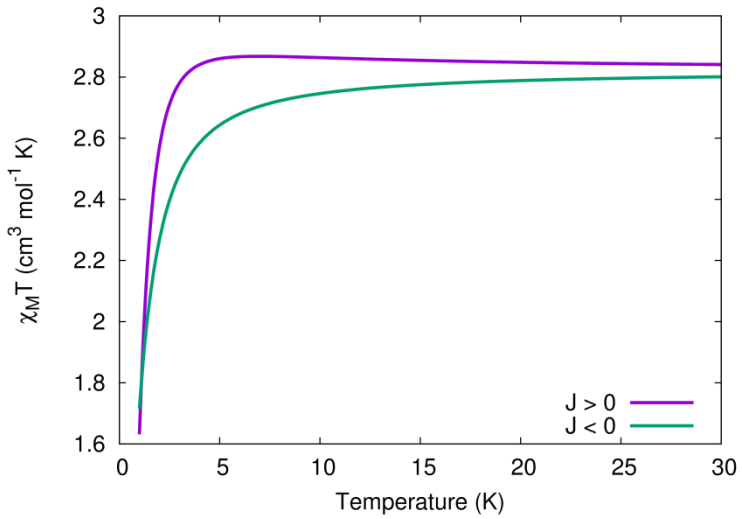

Figure S2.7. Simulated $\chi_M T$ in an 0.5 T field for $J > 0$ and $J < 0$ using the $S = 1/2$ model used to simulate the EPR spectra of compound **4**.

2.3. Characterization data of 1 – 10

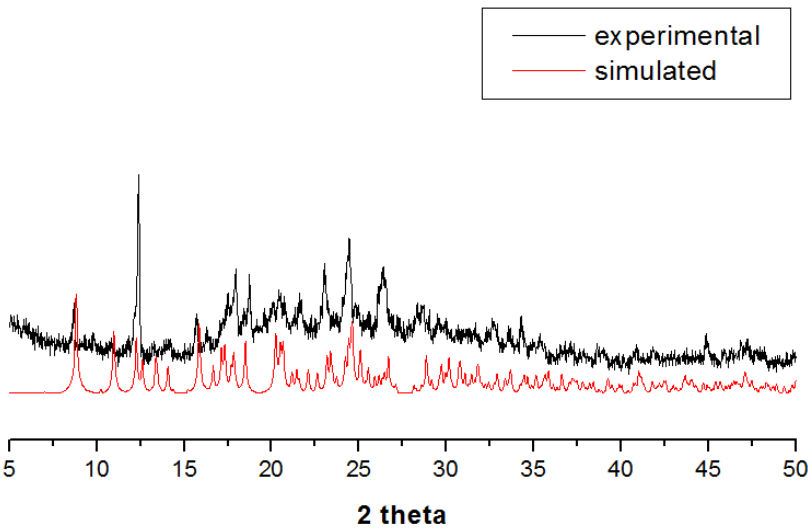

Figure S2.8. The powder XRD pattern of compound **7** (experimental and simulated from the crystal structure).

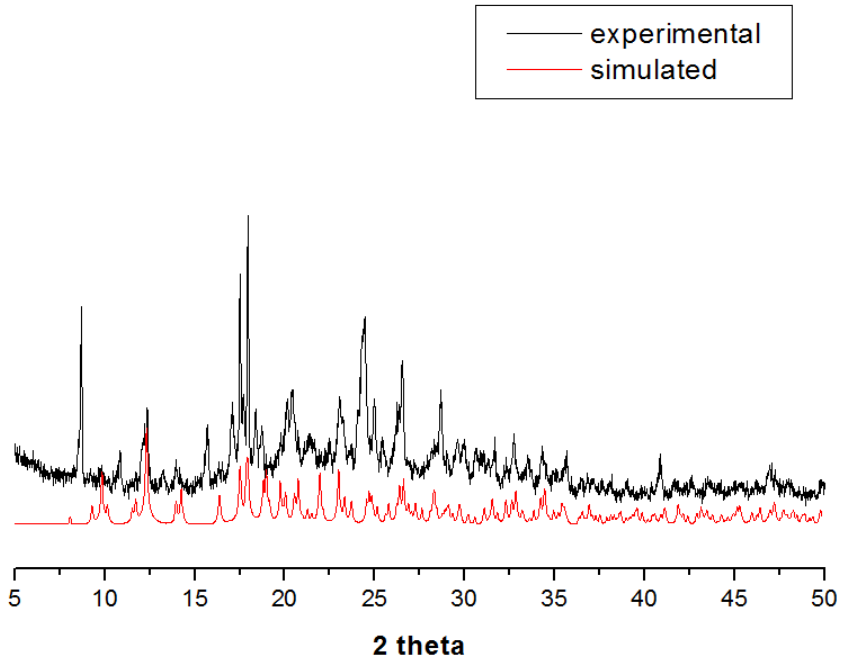

Figure S2.9. The powder XRD pattern of compound **8** (experimental and simulated from the crystal structure).

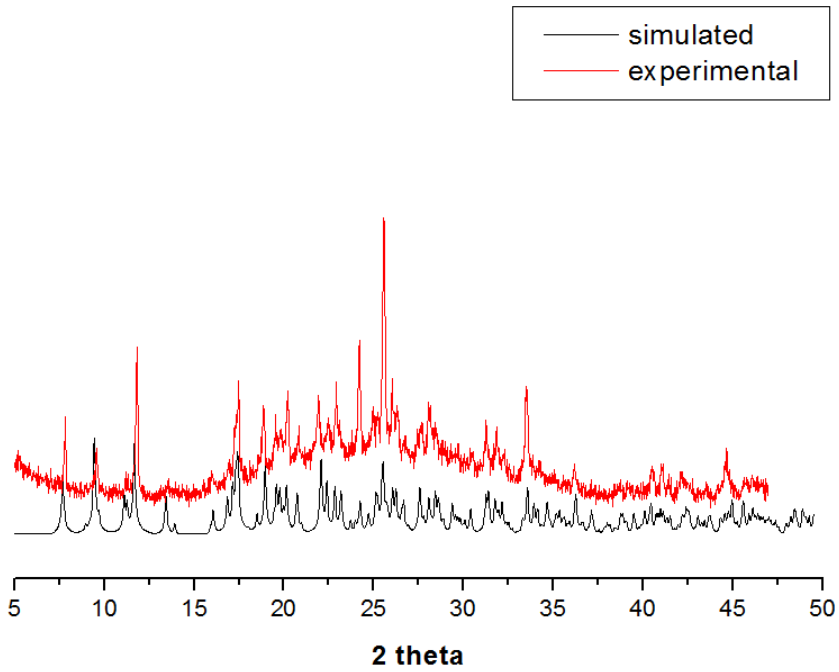

Figure S2.10. The powder XRD pattern of compound **9** (experimental and simulated from the crystal structure).

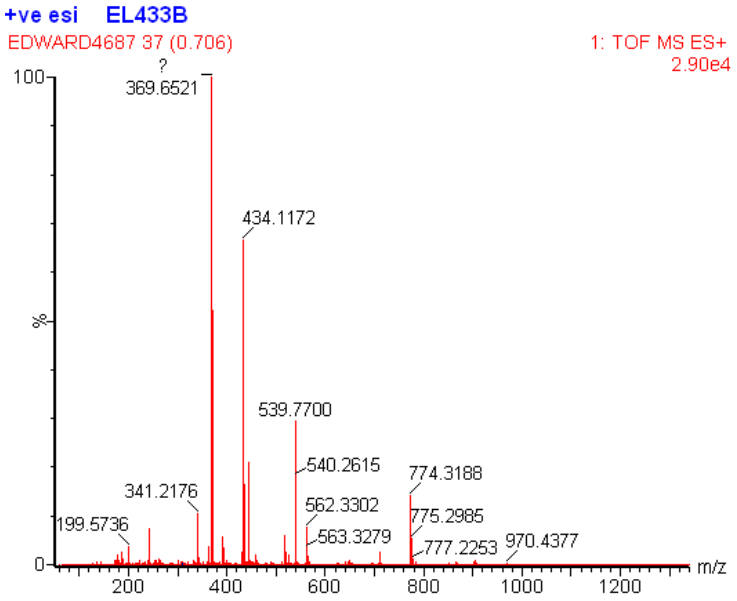

Figure S2.11. ESI-MS graph for compound **3** in methanol. Main fragments: 341.21 m/z [(**L²**) + H]$^{1+}$, 369.65 m/z [Co(**L²**)$_2$ – H]$^{2+}$, 434.12 m/z [Co(**L²**)Cl – H]$^{1+}$, 539.77 m/z [Co(**L²**)$_3$ – H]$^{2+}$, 562.33 m/z [Co$_2$(**L²**)Cl$_3$ – H]$^{2+}$, 774.32 m/z [Co(**L²**)$_2$Cl – H]$^{1+}$.

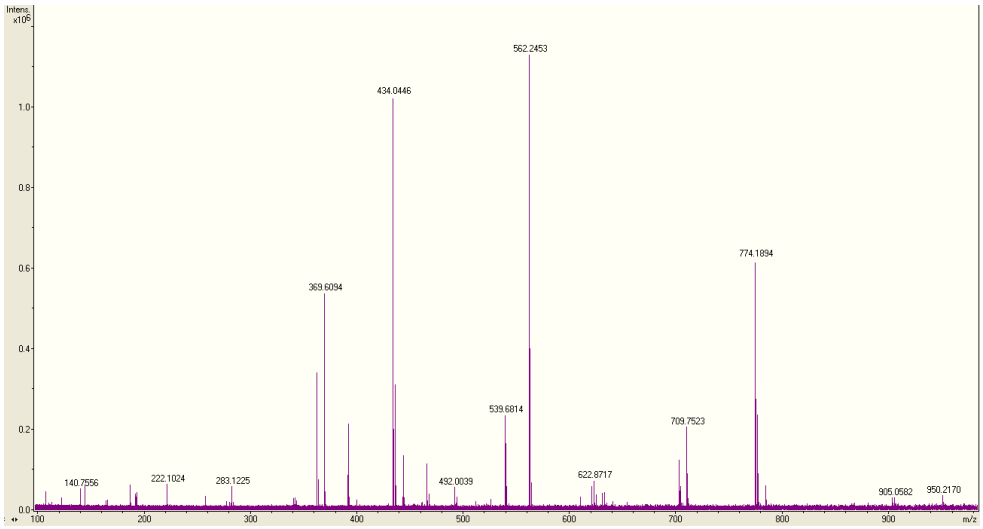

Figure S2.12. ESI-MS graph for compound **4** in methanol. Main fragments: 369.61 m/z [Co(**L²**)$_2$ – H]$^{2+}$, 387.10 m/z [Co(**L²**)$_2$Cl – H]$^{2+}$, 434.04 m/z [Co(**L²**)Cl – H]$^{1+}$, 492.00 m/z [Co$_2$(**L²**)Cl – H]$^{1+}$, 539.69 m/z [Co(**L²**)$_3$ – H]$^{2+}$, 562.24 m/z [Co$_2$(**L²**)Cl$_3$ – H]$^{2+}$, 709.75 m/z [Co(**L²**)$_4$ – H]$^{2+}$, 774.19 m/z [Co(**L²**)$_2$Cl – H]$^{1+}$.

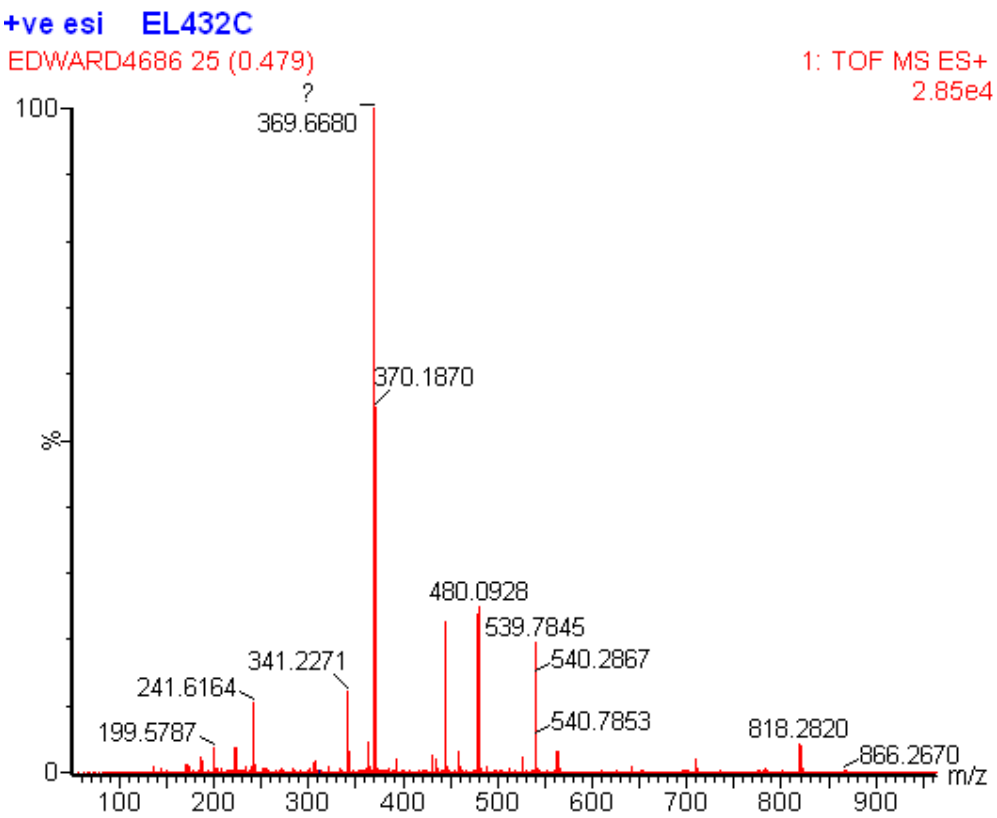

Figure S2.13. ESI-MS graph for compound **5** in methanol. Main fragments: 369.67 m/z $[Co(\mathbf{L^2})_2 - H]^{2+}$, 480.09 m/z $[Co(\mathbf{L^2})Br - H]^{1+}$, 539.78 m/z $[Co(\mathbf{L^2})_3 - H]^{2+}$, 709.75 m/z $[Co(\mathbf{L^2})_4 - H]^{2+}$, 818.28 m/z $[Co(\mathbf{L^2})_2Br - H]^{1+}$.

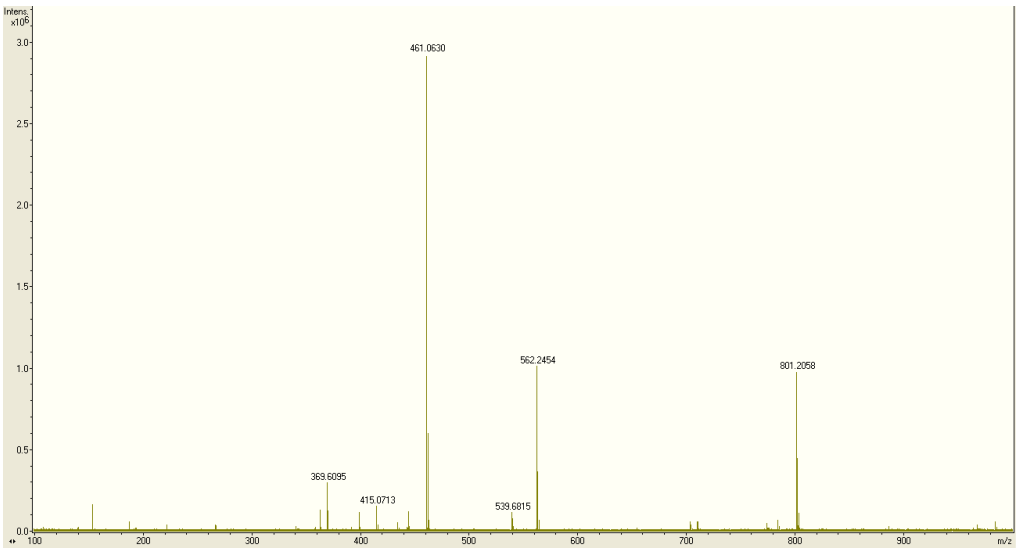

Figure S2.14. ESI-MS graph for compound **6** in methanol. Main fragments: 369.61 m/z $[Co(\mathbf{L^2})_2 - H]^{2+}$, 461.06 m/z $[Co(\mathbf{L^2})(NO_3) - H]^{1+}$, 539.69 m/z $[Co(\mathbf{L^2})_3 - H]^{2+}$, 568.25 m/z $[Co(\mathbf{L^2})_3(NO_3)_2 - H]^{2+}$, 709.75 m/z $[Co(\mathbf{L^2})_4 - H]^{2+}$, 801.21 m/z $[Co(\mathbf{L^2})_2(NO_3) - H]^{1+}$.

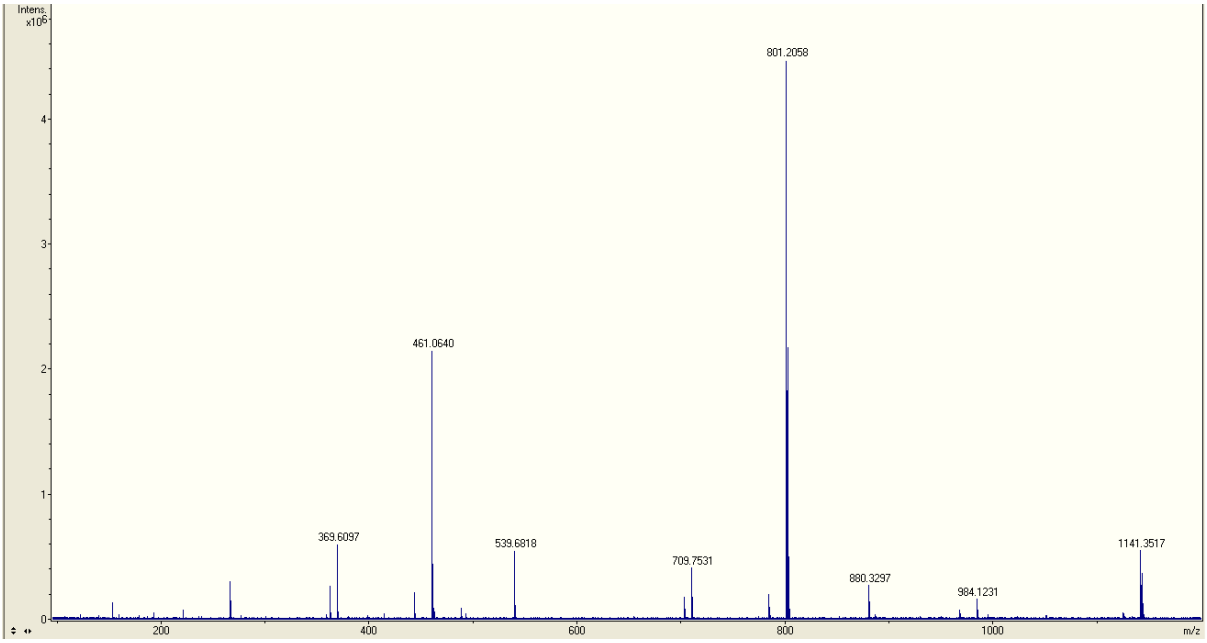

Figure S2.15. ESI-MS graph for compound **10** in methanol. Main fragments: 369.61 m/z $[Co(\mathbf{L^3})_2 - H]^{2+}$, 461.06 m/z $[Co(\mathbf{L^3})(NO_3) - H]^{1+}$, 539.18 m/z $[Co(\mathbf{L^3})_3 - H]^{2+}$, 709.75 m/z $[Co(\mathbf{L^3})_4 - H]^{2+}$, 801.20 m/z $[Co(\mathbf{L^3})_2(NO_3) - H]^{1+}$, 880.33 m/z $[Co(\mathbf{L^3})_5 - H]^{2+}$, 1141.35 m/z $[Co(\mathbf{L^3})_2(NO_3) - H]^{1+}$.

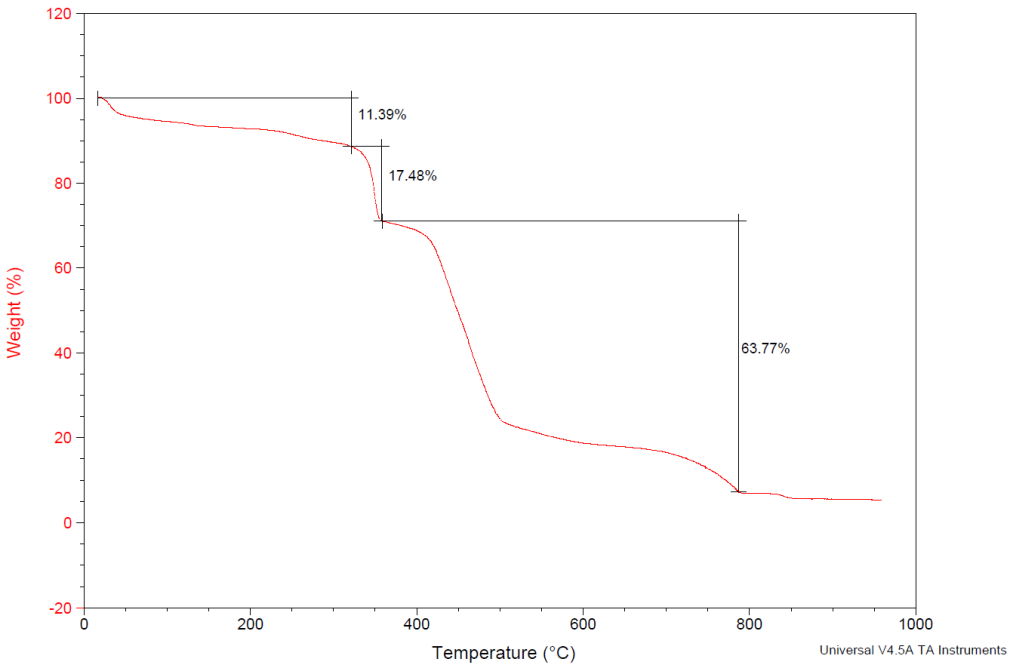

Figure S2.16. TGA graph for compound **1**. 1st mass loss: 9.02% calc. for two MeCN solvents. 2nd mass loss: 13.87% for four Cl atoms. 3rd mass loss: 63.45% calc. for framework decomposition.

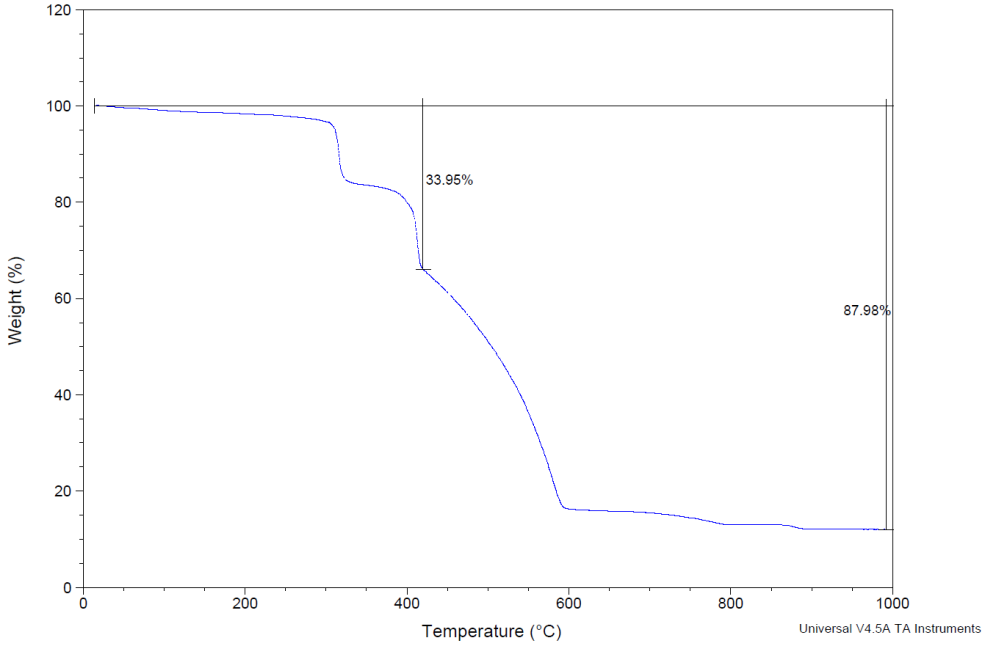

Figure S2.17. TGA graph for compound **5**. 1st mass loss: 33.47% calc. for two MeCN solvents and four Br atoms. 2nd mass loss: 54.03% obs., 54.04% calc. for framework decomposition.

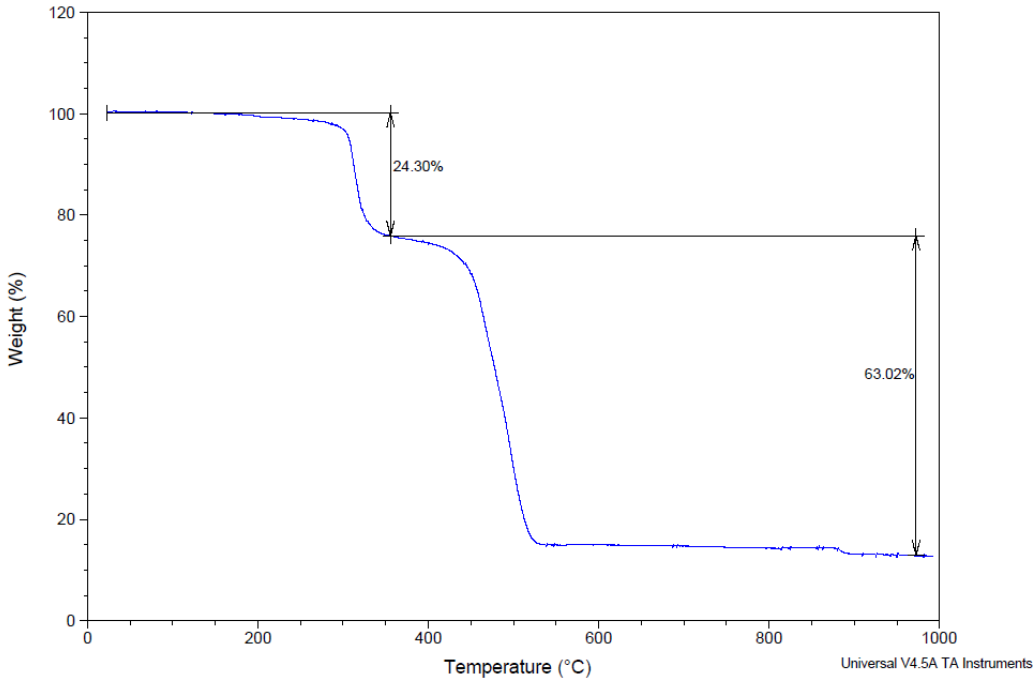

Figure S2.18. TGA graph for compound **7**. 1st mass loss: 22.09% calc. for one MeCN solvent and two Cl atoms. 2nd mass loss: 63.25% calc. for framework decomposition.

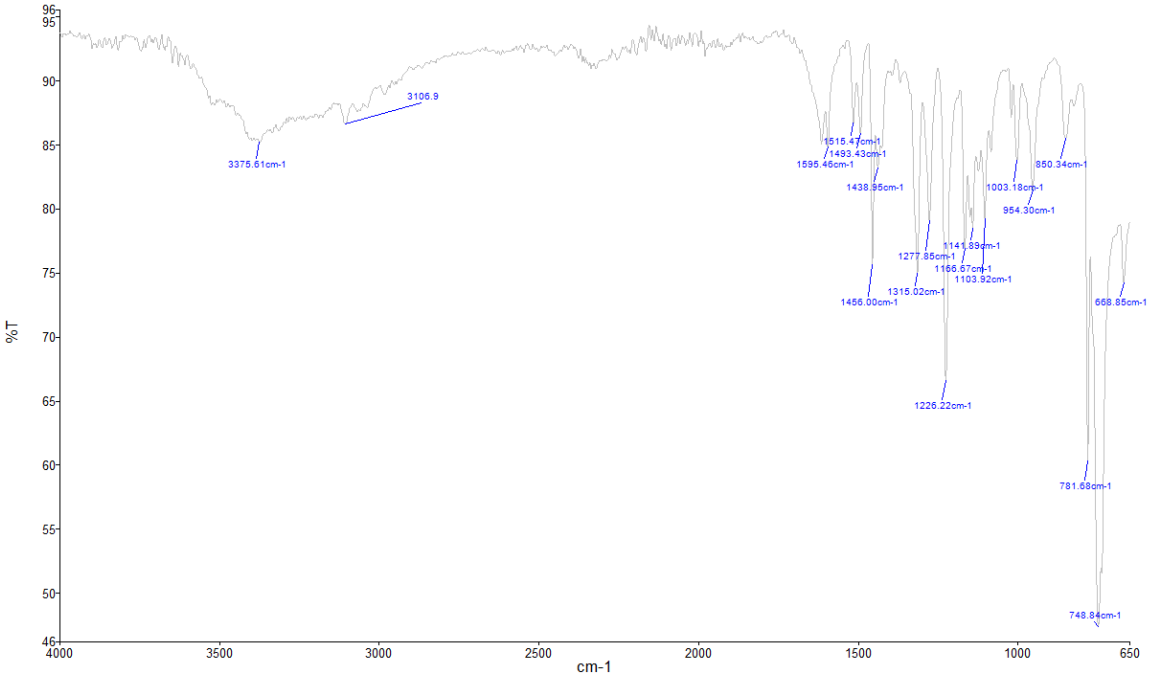

Figure S2.19. FT-IR of compound **1**.

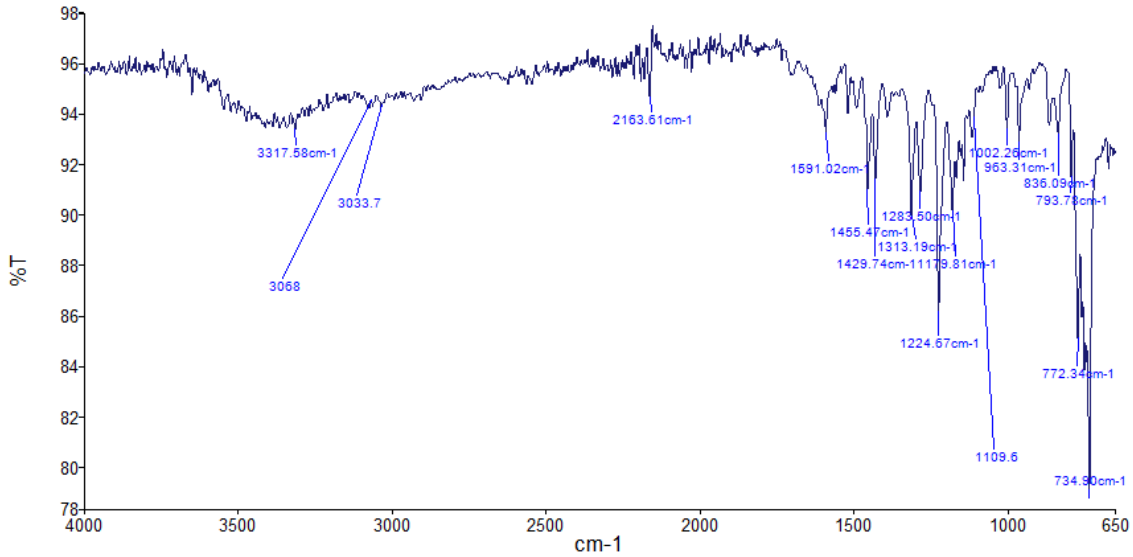

Figure S2.20. FT-IR of compound **2**.

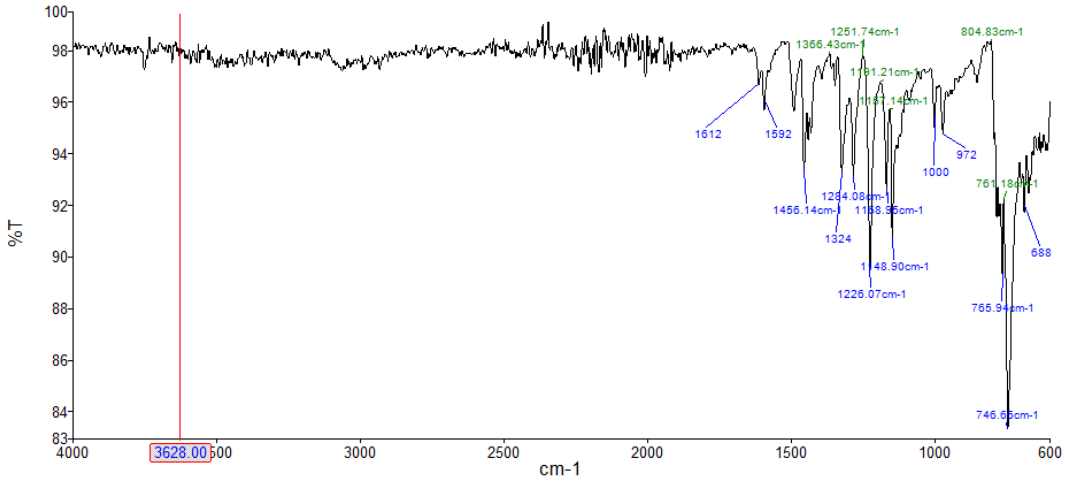

Figure S2.21. FT-IR of compound **3**.

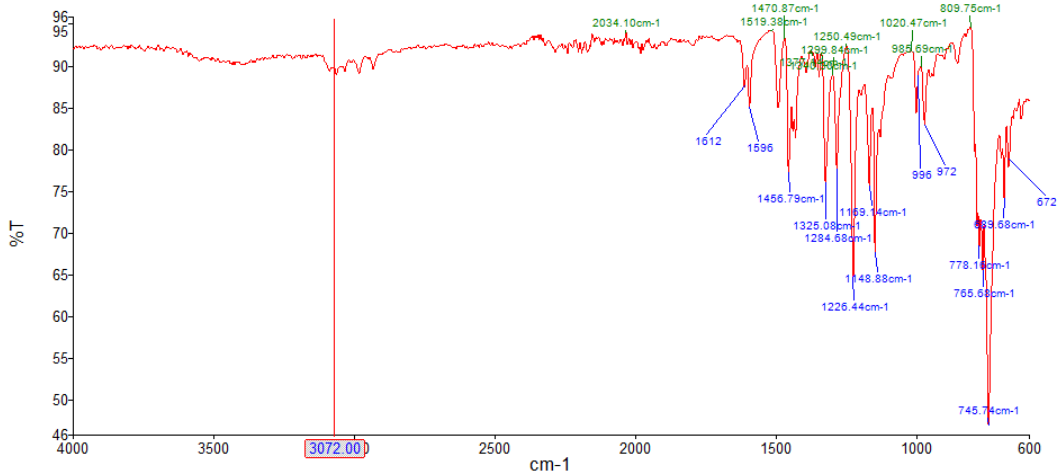

Figure S2.22. FT-IR of compound **4**.

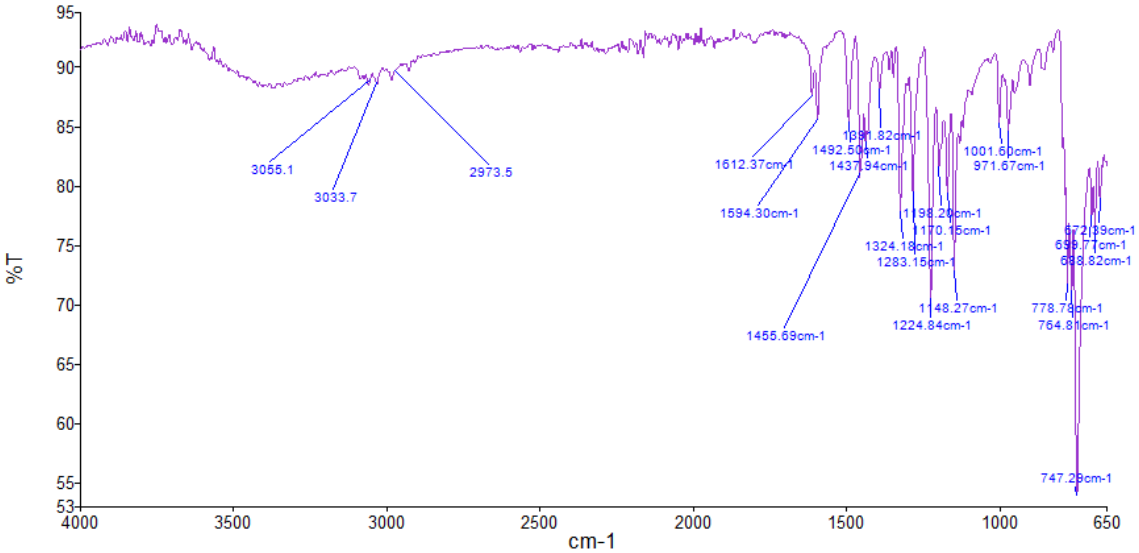

Figure S2.23. FT-IR of compound **5**.

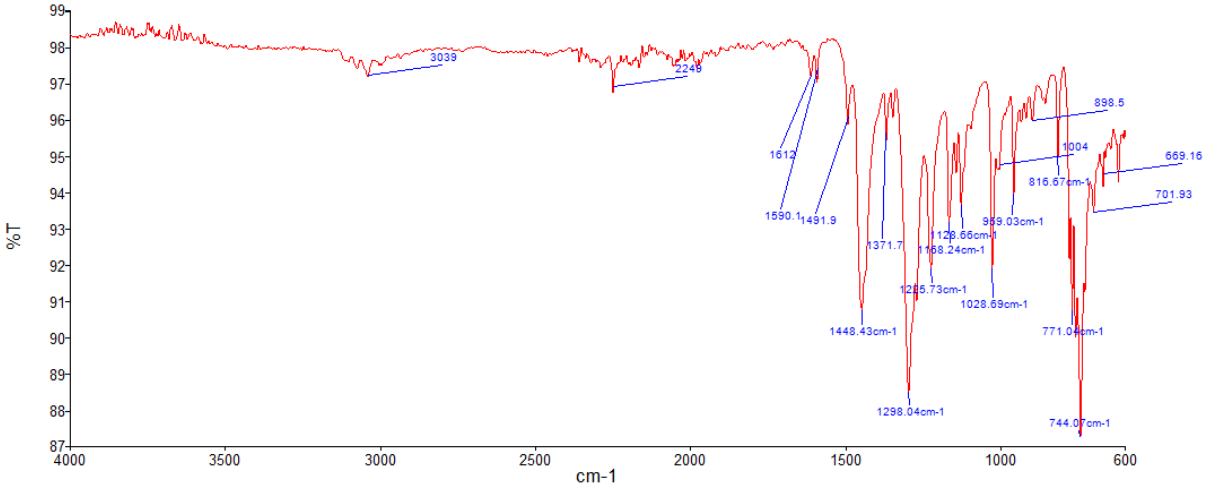

Figure S2.24. FT-IR of compound **6**.

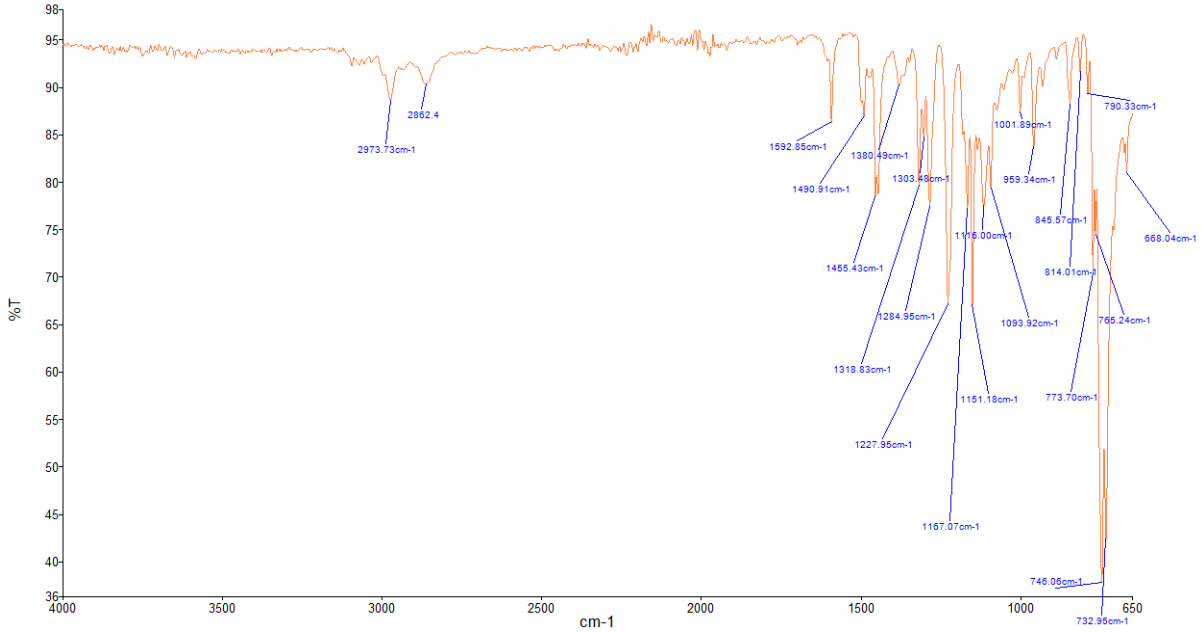

Figure S2.25. FT-IR of compound **7**.

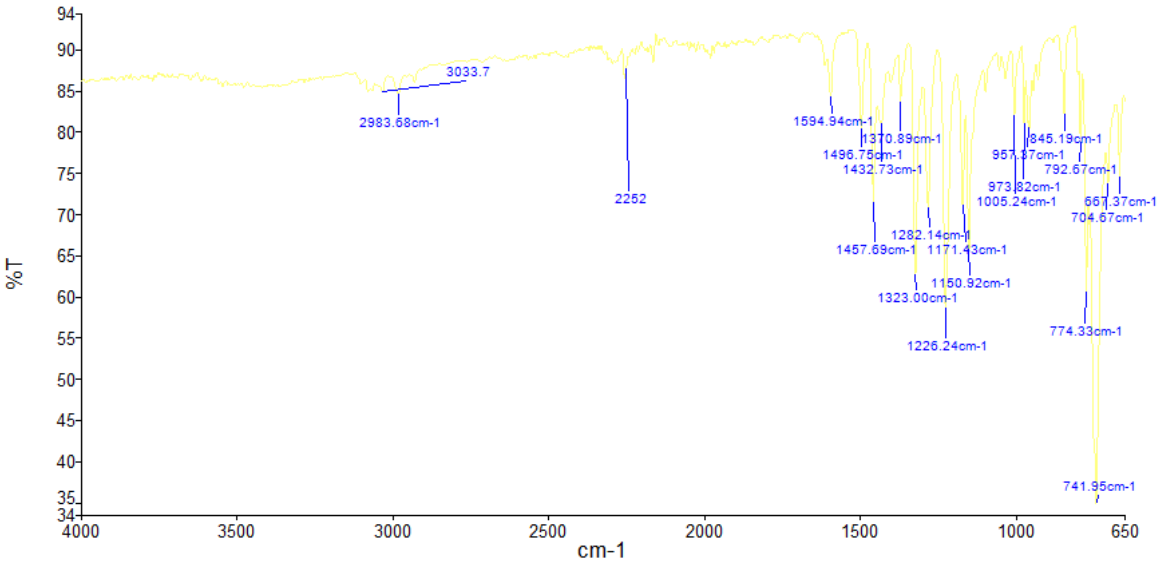

Figure S2.26. FT-IR of compound **8**.

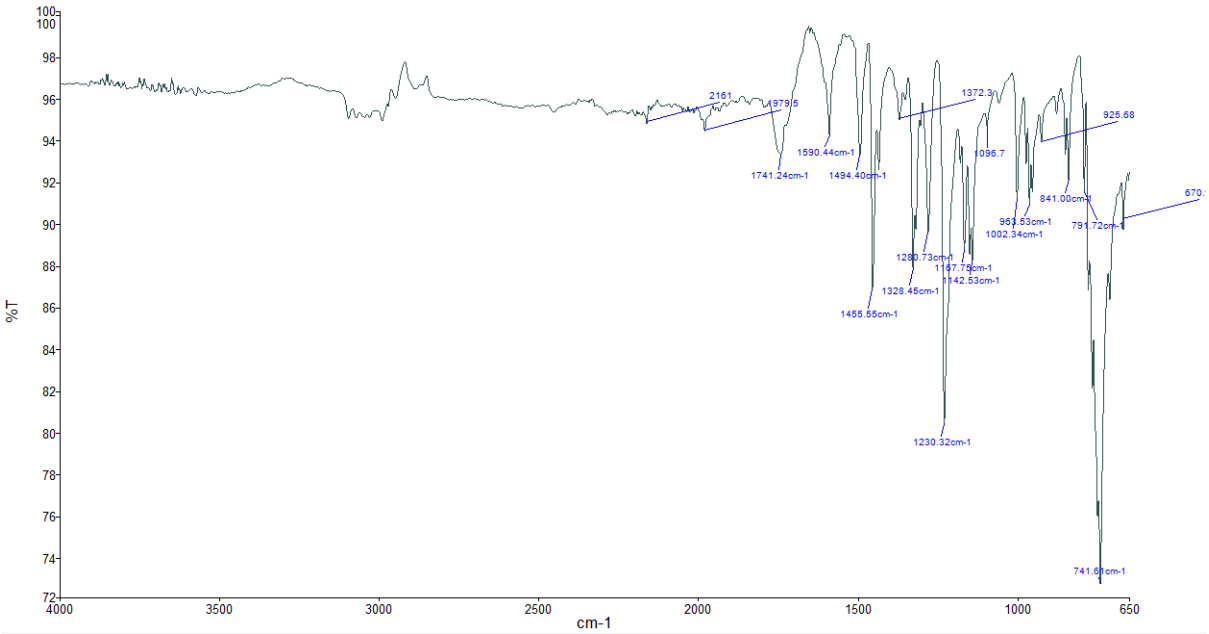

Figure S2.27. FT-IR of compound **9**.

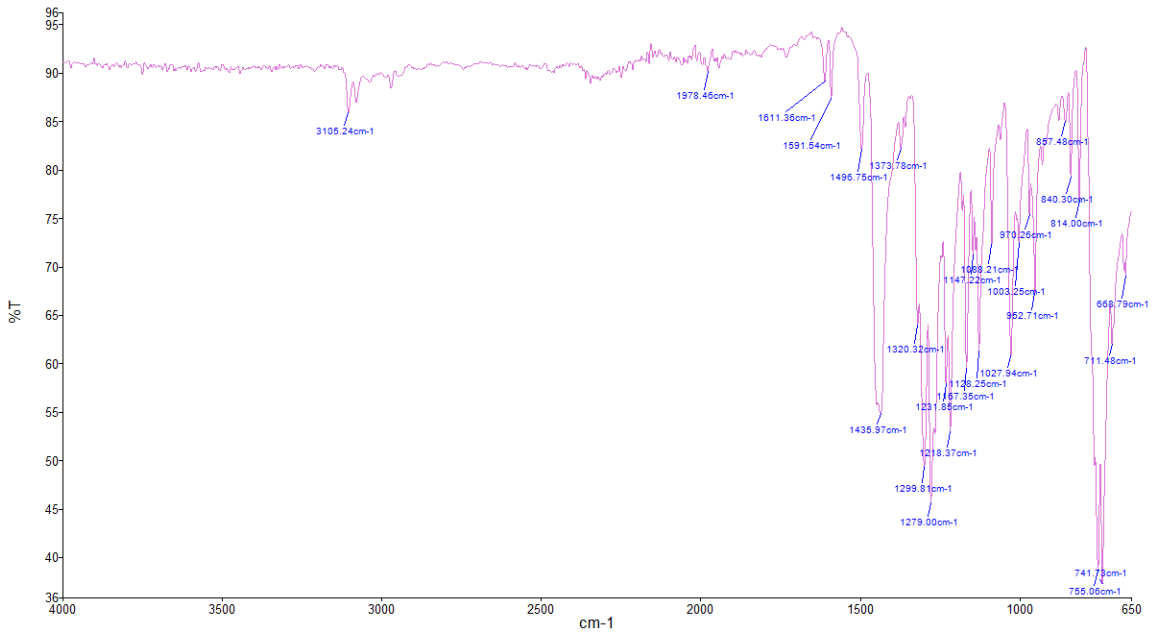

Figure S2.28. FT-IR of compound **10**.

Chapter 3

3.1. Synthesis of starting azines

Synthesis of azines. Into a sealed tube containing the aldehyde (0.5 mmol) and methanol (10 mL), 0.3 mmol of $NH_2NH_2 \cdot H_2O$ were added. The reaction was stirred at room temperature for selected time. The reaction was monitored by thin layer chromatography (TLC), and after completion the slurry was filtered and the yellow solid product washed with the aid of ether or ethyl acetate (~5 mL). In most cases the corresponding azine was formed in clean and high yields.

3.2. Characterization data of 11-13

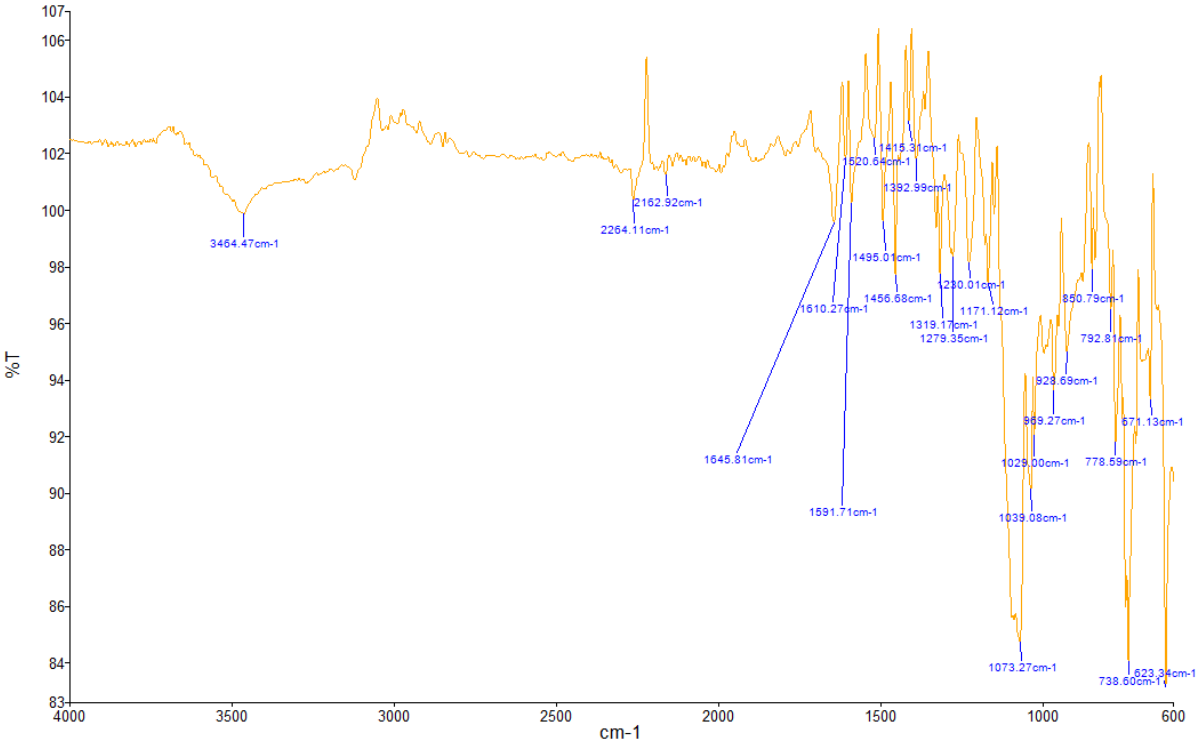

Figure S3.1. FT-IR of compound **11**.

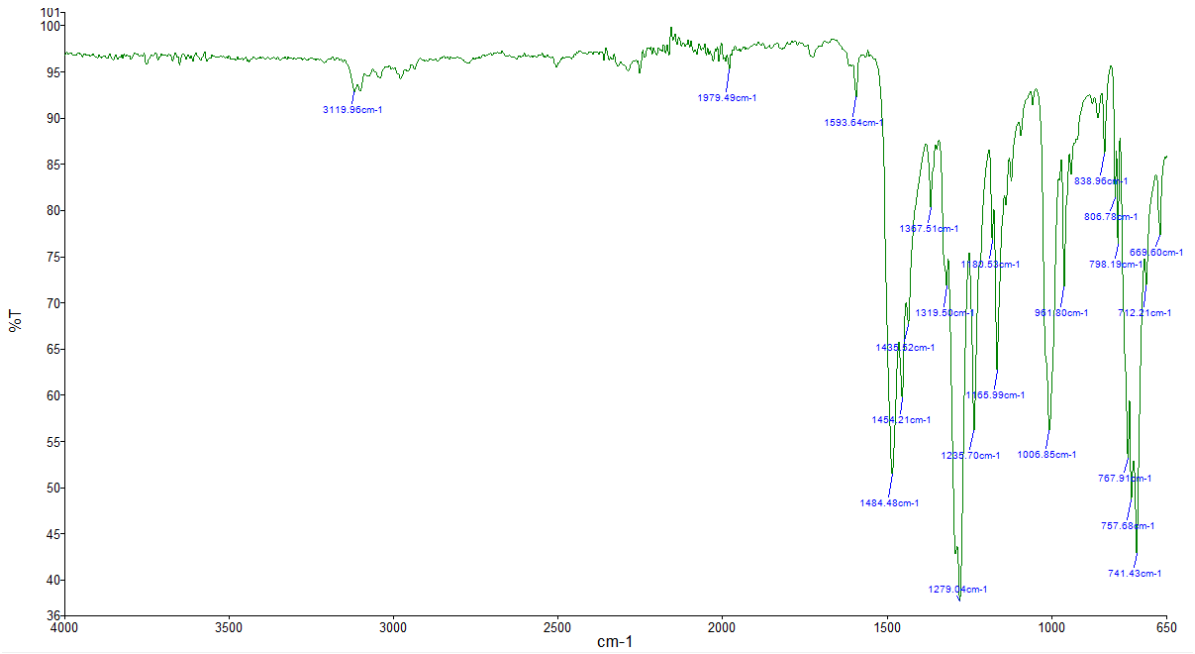

Figure S3.2. FT-IR of compound **12**.

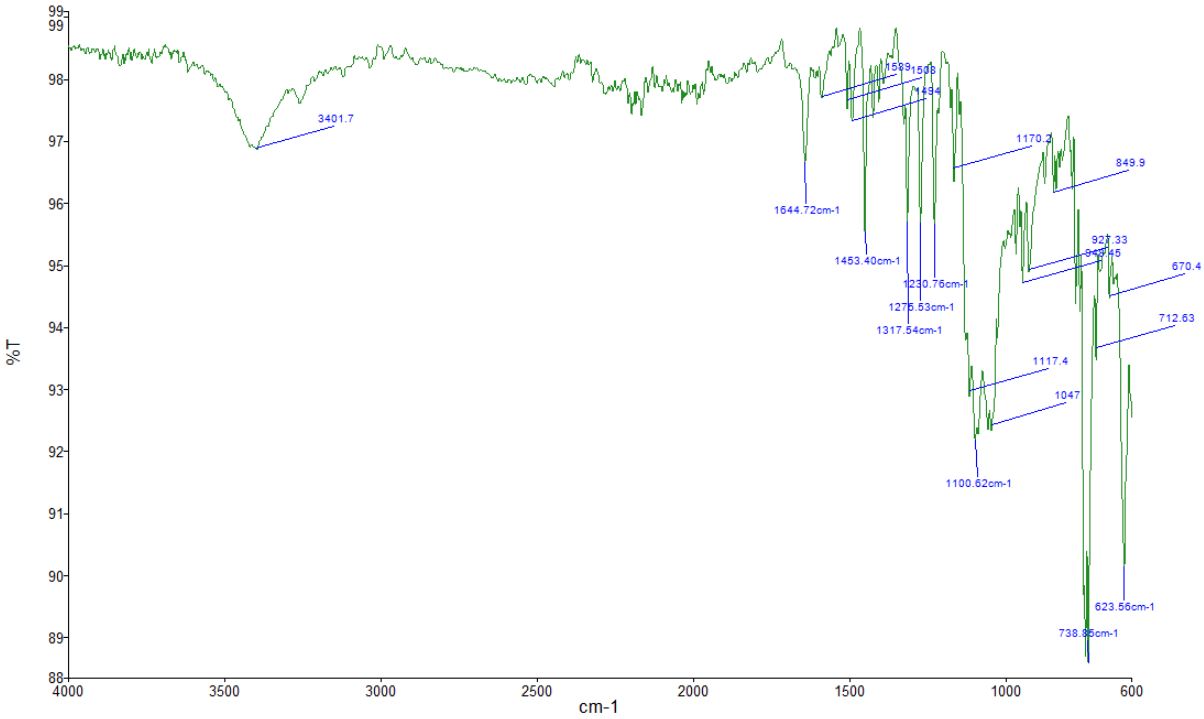

Figure S3.3. FT-IR of compound **13**.

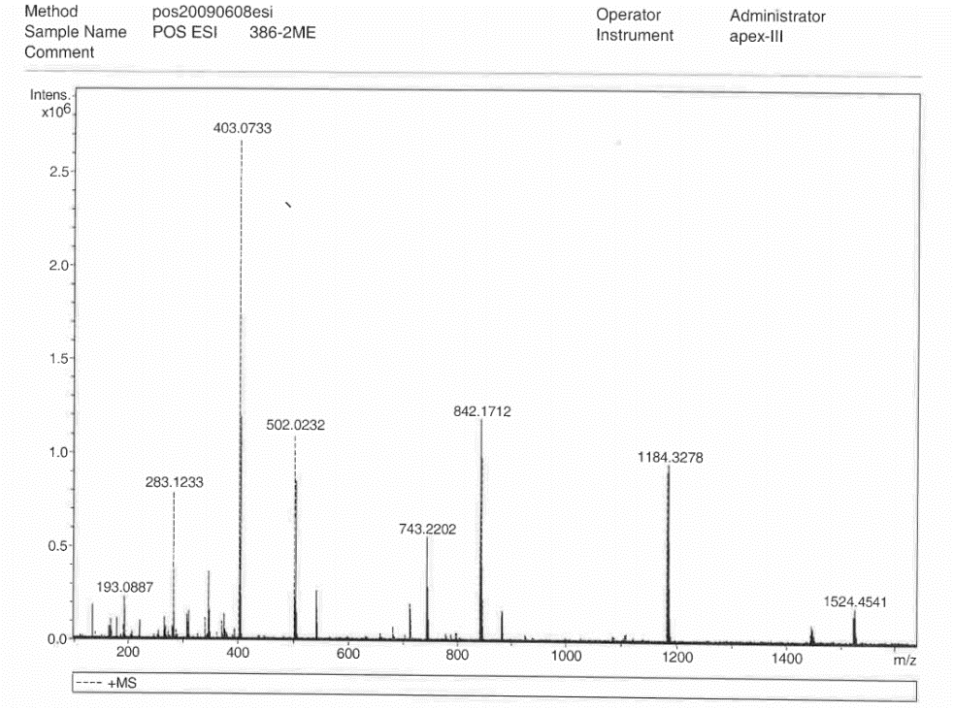

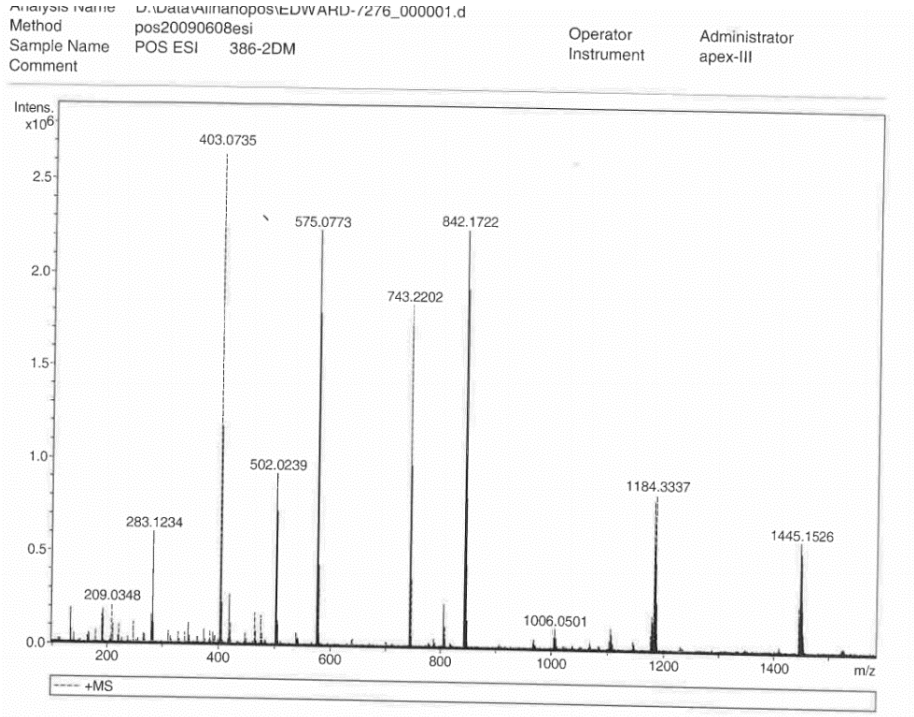

Figure S3.4. ESI-MS data for compound **11** in methanol (upper) and dimethylformamide (lower). Main fragments: 403.07 m/z $[Cu(\mathbf{L^3})]^{1+}$, 502.02 m/z $[Cu(\mathbf{L^3})(ClO_4)]^{1+}$, 743.22 m/z $[Cu(\mathbf{L^3})_2]^{1+}$, 842.16 m/z $[Cu(\mathbf{L^3})_2(ClO_4)]^{1+}$, 1184.31 m/z $[Cu(\mathbf{L^3})_3(ClO_4) + H]^{1+}$. ESI –MS in DMF solution shows identical peaks as above and an additional peak at 575.07 m/z $[Cu(\mathbf{L^3})(DMF)(ClO_4)]^{1+}$.

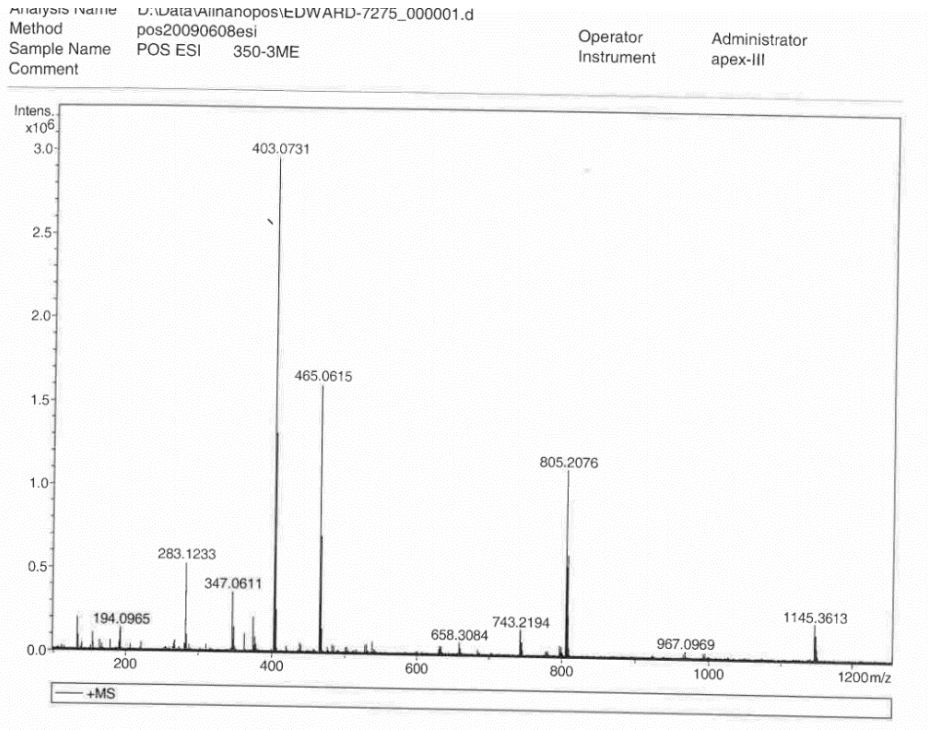

Figure S3.5. ESI-MS data for compound **12** in methanol. Main fragments: 403.07 m/z $[Cu(\mathbf{L^3})]^{1+}$, 465.06 m/z $[Cu(\mathbf{L^3})(NO_3)]^{1+}$, 743.22 m/z $[Cu(\mathbf{L^3})_2]^{1+}$, 805.20 m/z $[Cu_2(\mathbf{L^3})_2 - H]^{1+}$, 1145.36 m/z $[Cu(\mathbf{L^3})_3(NO_3) + H]^{1+}$

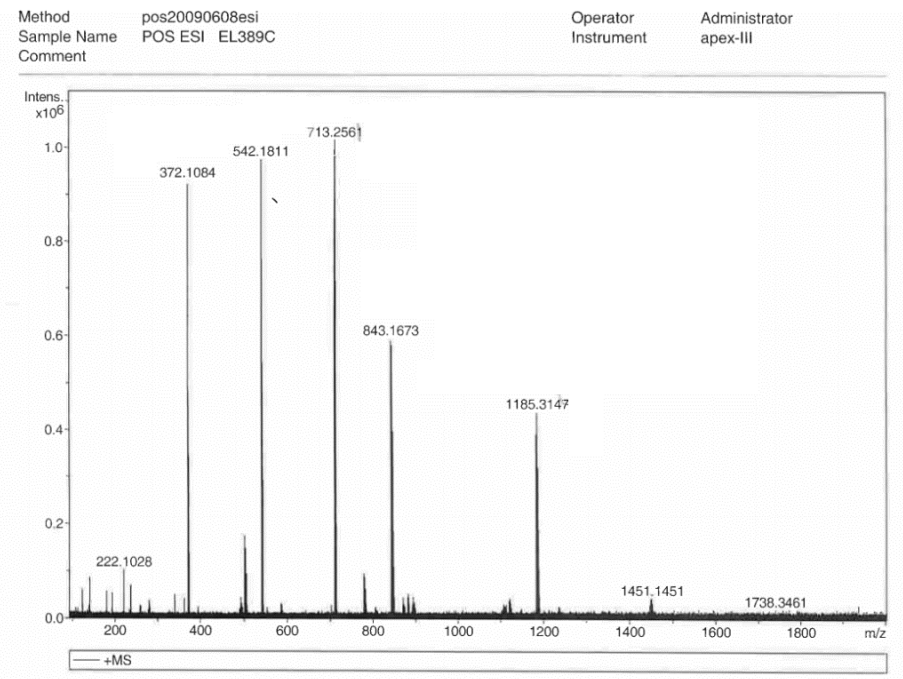

Figure S3.6. ESI-MS data for compound **13** in methanol. Main fragments: 372.10 m/z $[(\mathbf{L^3}) + MeOH]^{1+}$, 542.18 m/z $[Zn(\mathbf{L^3})_3]^{2+}$, 713.25 m/z $[(\mathbf{L^3})_2 + MeOH]^{1+}$, 843.16 m/z $[Zn(\mathbf{L^3})_2(ClO_4)]^{1+}$, 1185.31 m/z $[Zn(\mathbf{L^3})_3(ClO_4) + H]^{1+}$

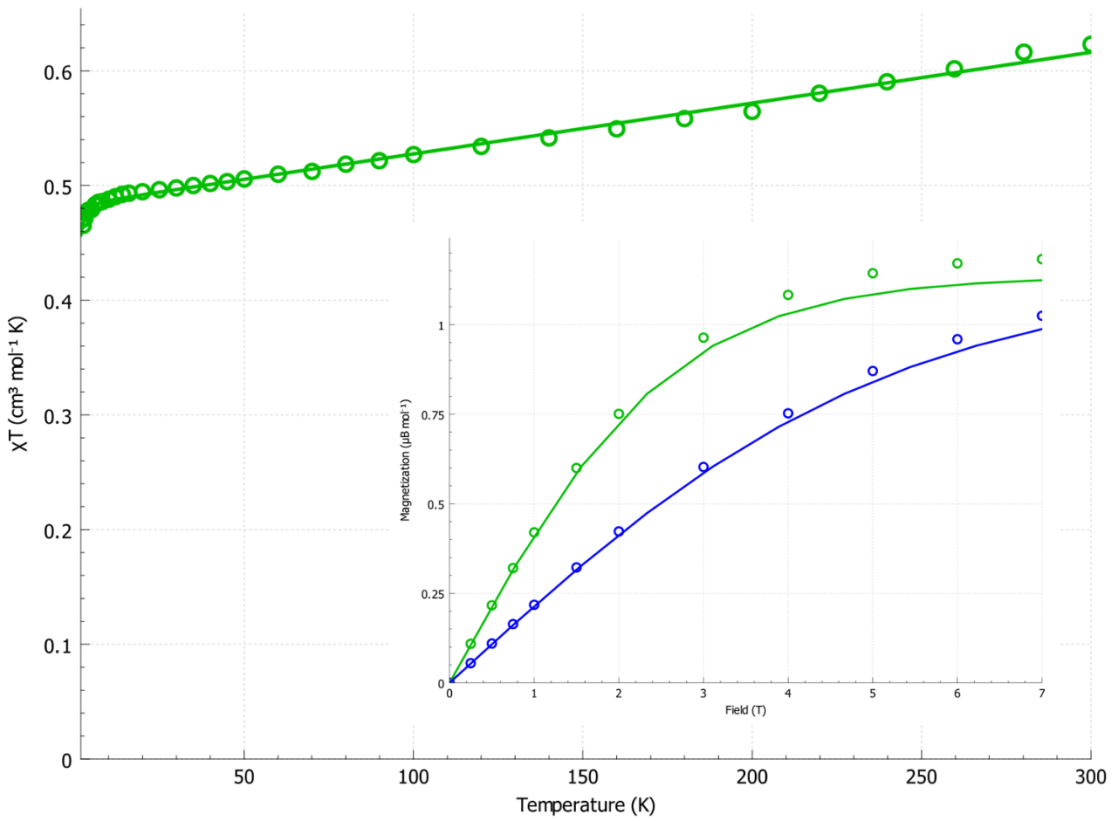

Figure S3.7. Product of χT *vs.* T for compound **11** under an applied susceptibility field of 1 T. (Inset) magnetization plots in the range 0-7 T for T = 2K (green) and 4K (blue). Solid lines show the best obtained fits.

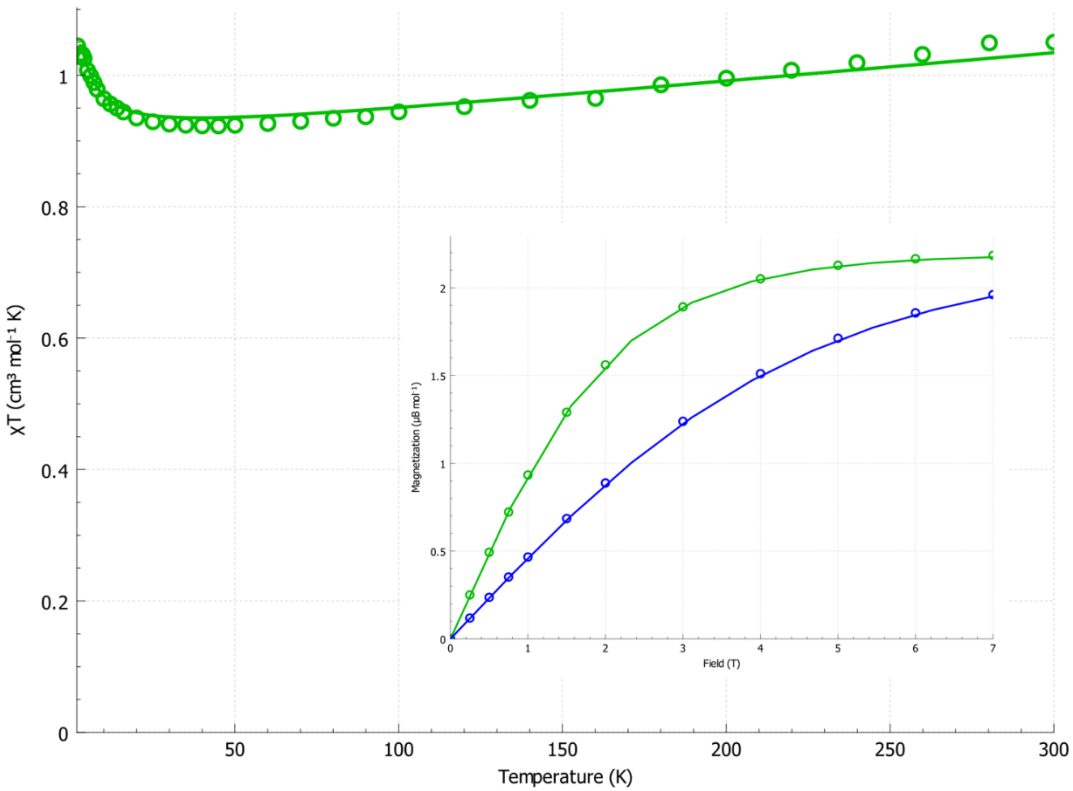

Figure S3.8. Product of χT *vs.* T for compound **12** under an applied susceptibility field of 1 T. (Inset) magnetization plots in the range 0-7 T for T = 2K (green) and 4K (blue). Solid lines show the best obtained fits.

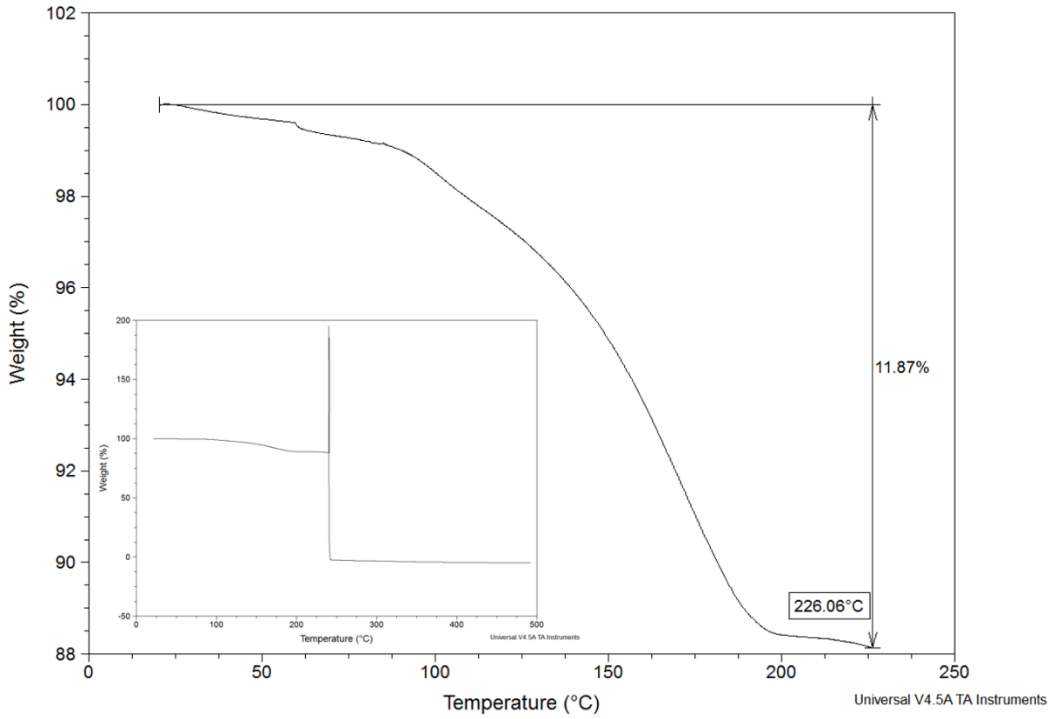

Figure S3.9. TGA graph for compound **11** up to 230 °C. (inset) The same graph up to 500 °C.

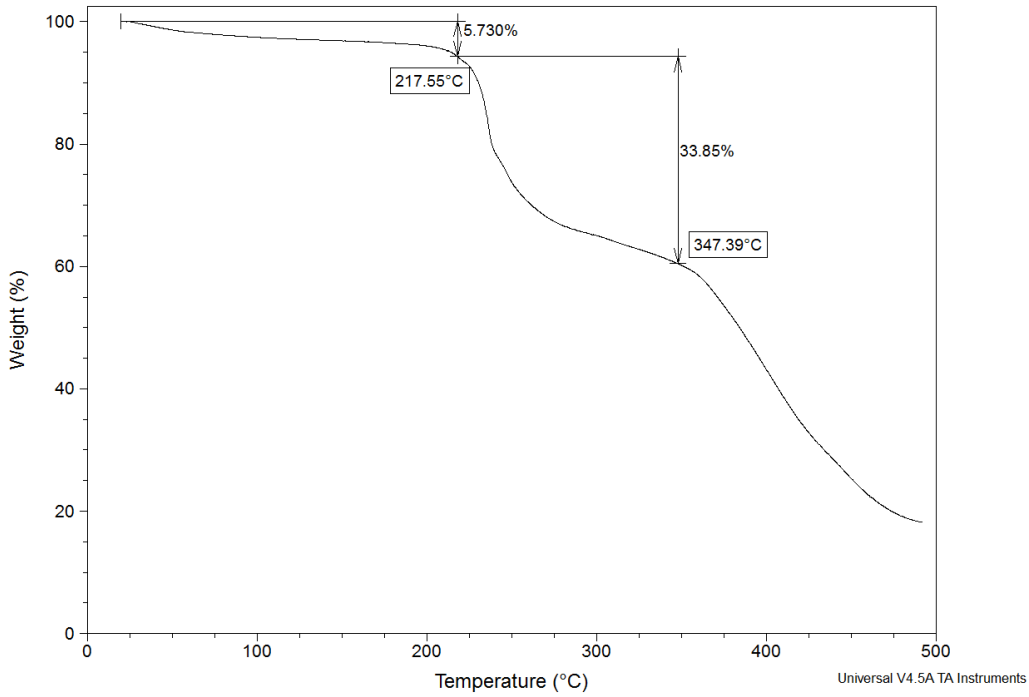

Figure S3.10. TGA graph for compound **12**.

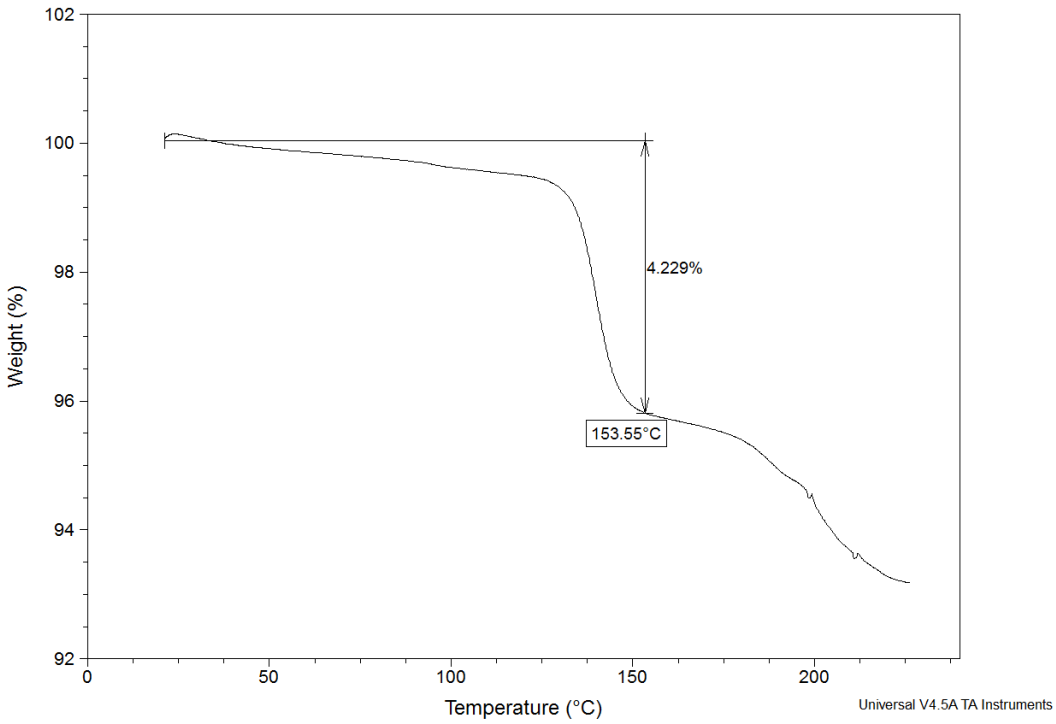

Figure S3.11. TGA graph for compound **13**.

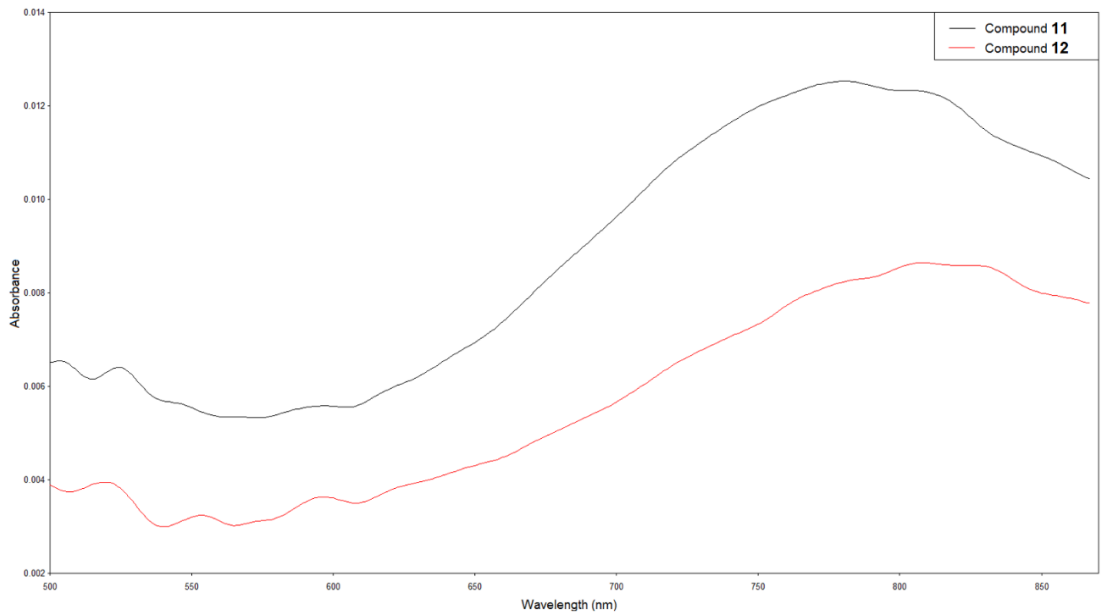

Figure S3.12. UV-Vis spectra for compounds **11** and **12** in methanol, in the region of 500-870 nm.

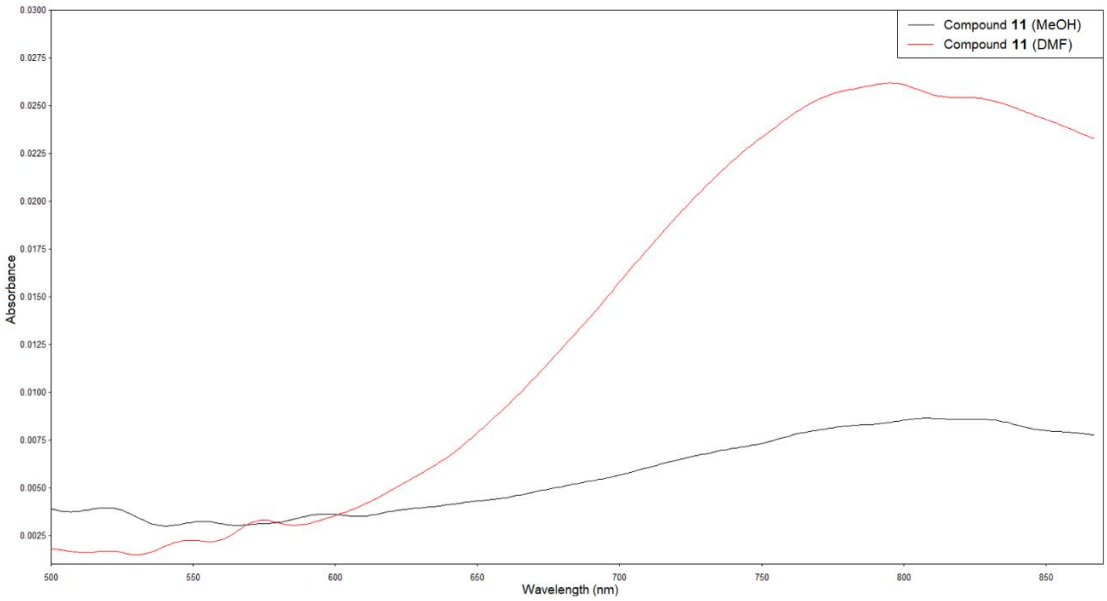

Figure S3.13. UV-Vis spectra of compound **11** in methanol and dimethylformamide, in the region of 500-870 nm.

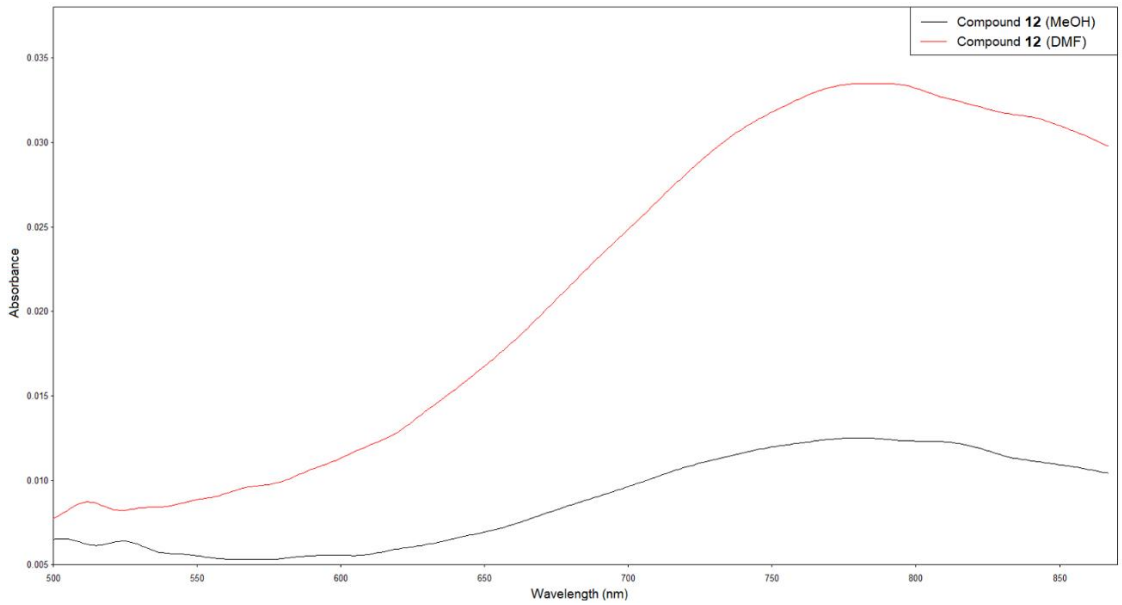

Figure S3.14. UV-Vis spectra of compound **12** in methanol and dimethylformamide, in the region of 500-870 nm.

3.3. Catalytic experiments

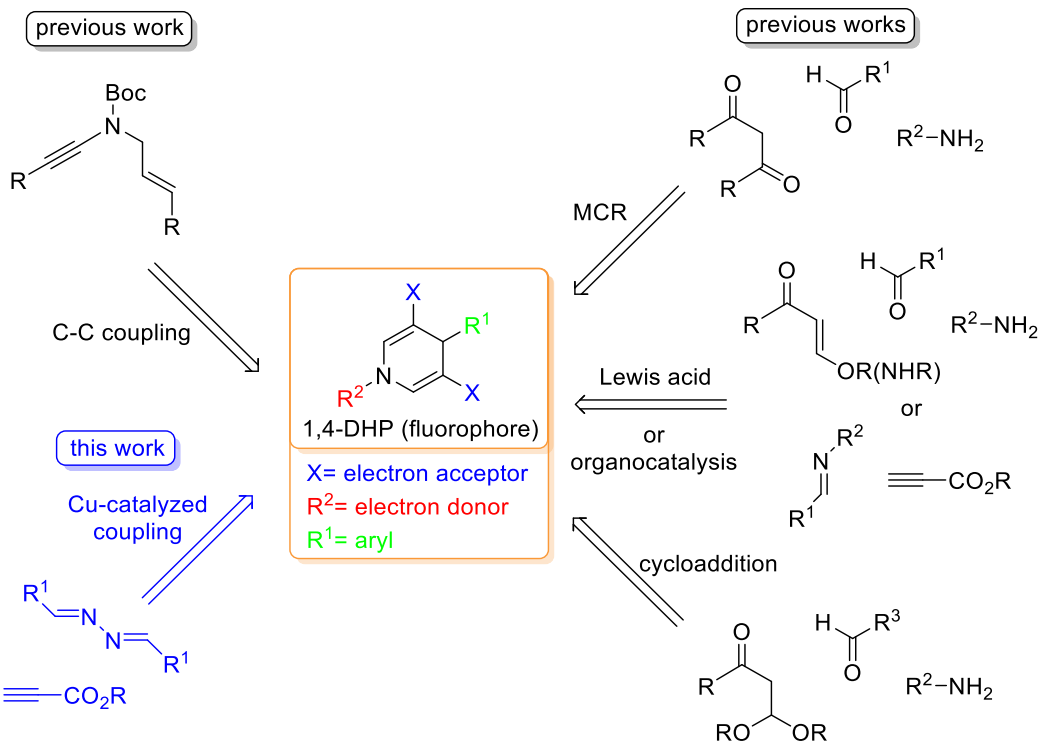

Scheme S3.1. Design and retrosynthetic scheme for substituted 1,4-DHP synthesis.

Table S3.1. Relative yields for the catalytic 1,4-DHP products (**C3D**) and non-catalytic pyrazoles products (**C3P**).

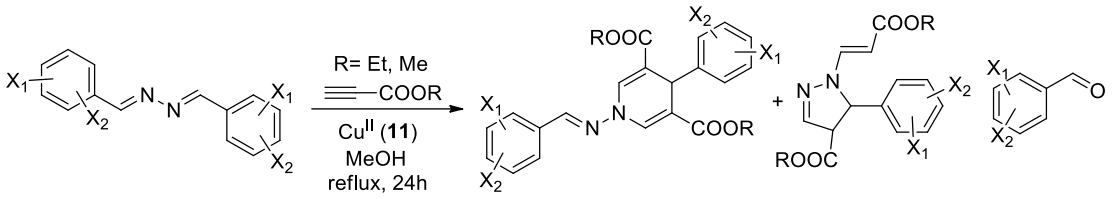

A/A	Aromatic ring (X_1, X_2)	R	C3D	C3P	C3A	C3Z
1	4-Me	Et	65	13	22	-
2	4-MeO	Et	59	12	29	-
3	2-MeO	Et	44	21	35	-
4	3,4-diMeO	Et	68	5	27	-
5	2,4-diMe	Et	51	19	30	-
6	3-Cl	Et	53[a]	-	47	-
7	H	Et	25	<10	30	35
8	4-NO_2	Et	-	-	30	70
9	4-CF_3	Et	<10	-	33	57
10	2-OH, 3-OMe	Et	-	-	-	>99
11	4-Me	Me	58	16	26	-
12	4-MeO	Me	60	10	30	-
13	4-MeO	Me	47	17	36	-
14	3,4-diMeO	Me	64	8	28	-
15	4-Cl	Me	55[a]	-	45	-
16	naphthyl	Et	<5%	71	-	24
17	furyl	Et	<10	24	14	47
18	thiophenyl	Et	67	-	9	24

a: 3 days

Table S3.2. Alkynes evaluation in the catalytic procedure using azine **C3Z1** and **11** as the catalyst under the conditions noted in Table 3.2.

Entry	dipolophile	Result
1	≡—COOEt	**C3D1**
2	EtOOC—≡—COOEt	NR
3	≡—Ph	NR

4	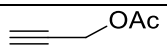	NR
5	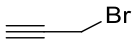	NR
6	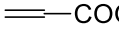	NR
7	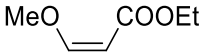	NR

NR = No reaction

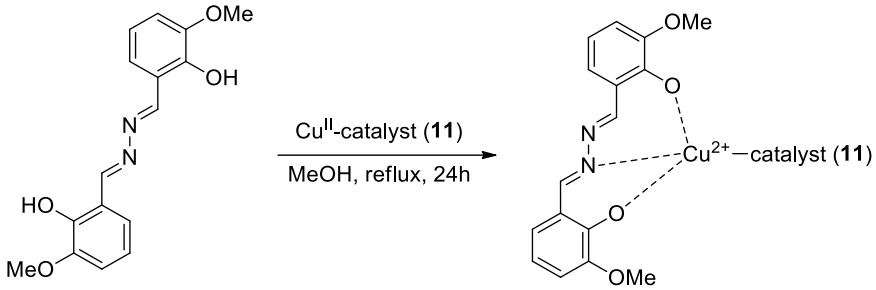

Figure S3.15. Proposed coordinated complex between azine **C3Z10** and the Cu^{II}-catalyst **11** under catalytic conditions. The colour of the solution changed during the reaction process from yellow to red-purple, probably due to the binding of azine to Cu^{II}.

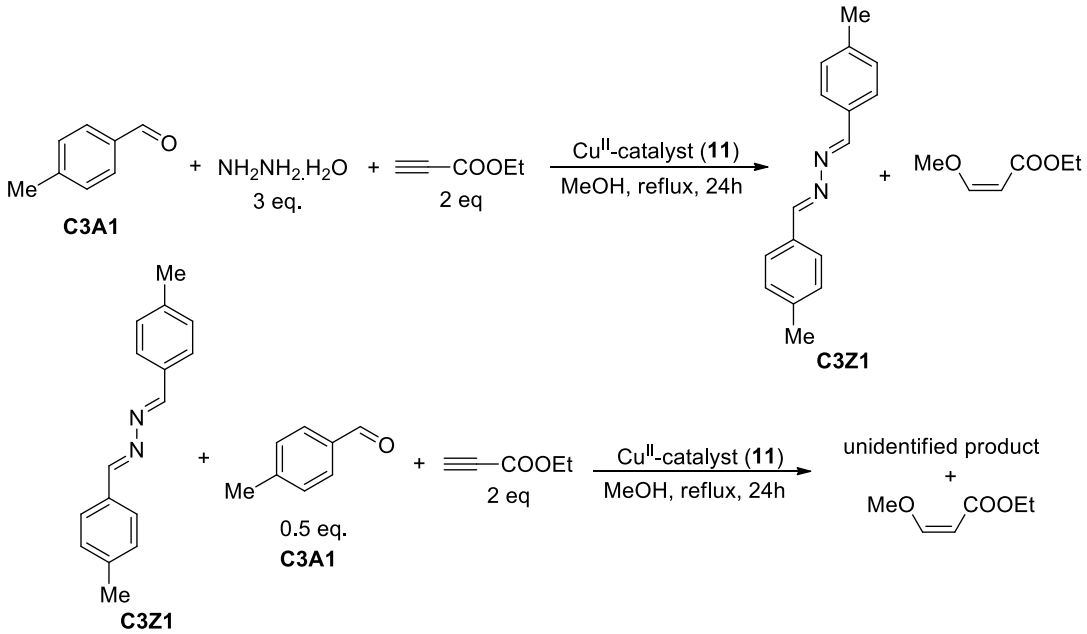

Figure S3.16. MCR type procedure evaluation for the synthesis of 1,4-DHP derivatives under the proposed catalytic conditions.

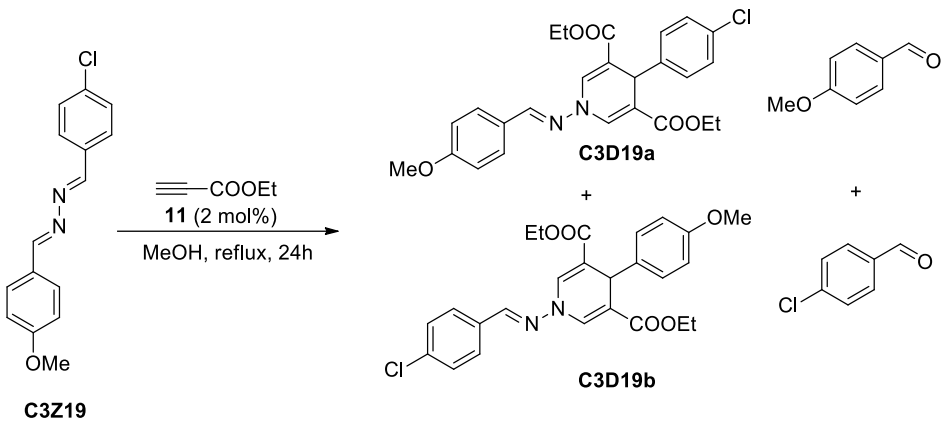

Figure S3.17. Catalytic transformation of hetero-azine **C3Z19** to the corresponding 1,4-DHP derivatives **C3D19a** and **C3D19b** using **11** as catalyst in MeOH.

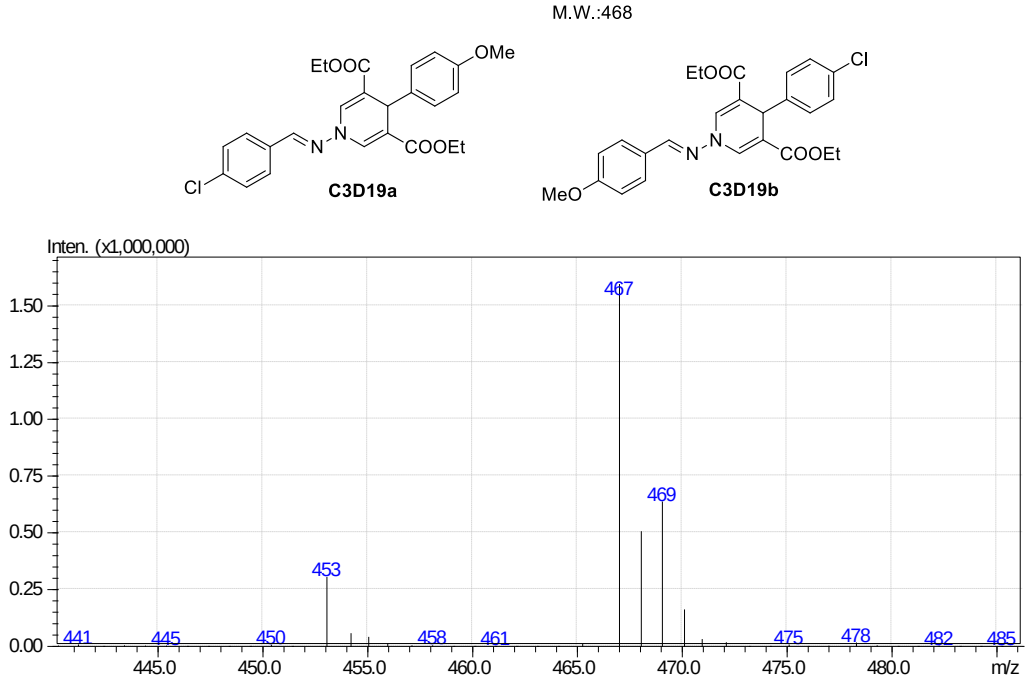

Figure S3.18. MS chromatographic spectrum for the mixture of the two isomers **C3D19a** and **C3D19b**.

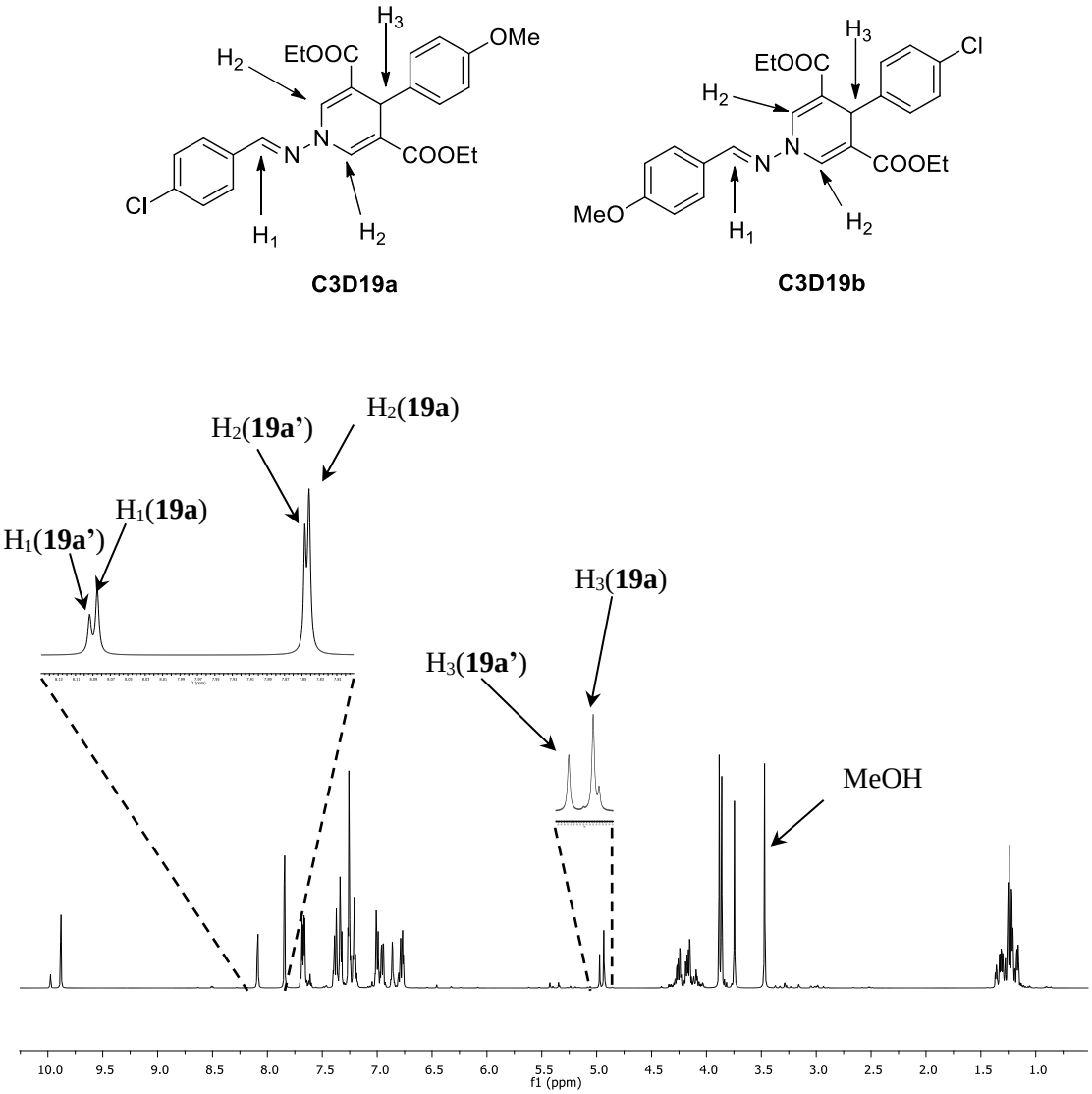

Figure S3.19. ^{1}H NMR spectrum of the crude mixture after catalytic formation of **C3D19a** and **C3D19b**.

3.4. ^{1}H and ^{13}C NMR data of selected isolated pyrazoles

(*E*)-Ethyl 1-(3-ethoxy-3-oxoprop-1-en-1-yl)-5-(p-tolyl)-4,5-dihydro-1H-pyrazole-4-Carboxylate (C3P1)

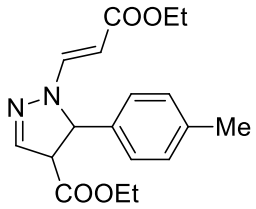

^{1}H NMR (500 MHz, $CDCl_3$): 7.95 (d, *J* = 13.7 Hz, 1H), 7.17 (d, *J* = 8.1 Hz, 2H), 7.10 (d, *J* = 8.1 Hz, 2H), 6.85 (d, *J* = 1.9 Hz, 1H), 5.25 (d, *J* = 7.3 Hz, 1H), 4.68 (d, *J* = 13.7 Hz, 1H), 4.29 (q, *J* = 7.1 Hz, 2H), 4.16-4.02 (m, 2H), 3.90 (dd, *J* = 7.3, 1.9 Hz, 1H), 2.34 (s, 3H), 1.31 (t, *J* = 7.2 Hz, 3H), 1.21 (t, *J* = 7.1 Hz, 3H). ^{13}C-NMR (125 MHz, $CDCl_3$): 168.4, 167.7, 144.3, 139.0, 138.4, 135.6, 130.1, 125.8, 90.7, 63.6, 63.3, 62.4, 59.5, 21.2, 14.5, 14.2. HRMS calcd.: 330.1509 m/z, HRMS found: 329.1496 [M-H^{+}].

(*E*)-Ethyl 1-(3-ethoxy-3-oxoprop-1-en-1-yl)-5-(4-methoxyphenyl)-4,5-dihydro-1H-pyrazole-4-carboxylate (C3P2)

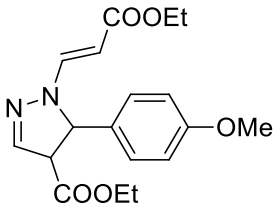

^{1}H NMR (500 MHz, $CDCl_3$): 7.95 (d, *J* = 13.6 Hz, 1H), 7.14 (d, *J* = 8.6 Hz, 2H), 6.91-6.85 (m, 3H), 5.24 (d, *J* = 7.4 Hz, 1H), 4.66 (d, *J* = 13.6 Hz, 1H), 4.25 (q, *J* = 7.2 Hz, 2H), 4.19-4.02 (m, 2H), 3.91 (dd, *J* = 7.4, 1.7 Hz, 1H), 3.80 (s, 3H), 1.31 (t, *J* = 7.2 Hz, 3H), 1.21 (t, *J* = 7.2 Hz, 3H). ^{13}C-NMR (125 MHz, $CDCl_3$): 168.4, 167.7, 159.7, 144.2, 139.0, 130.6, 127.2, 114.8, 90.7, 63.4, 63.3, 62.4, 59.5, 55.4, 14.5, 14.2. HRMS calcd.: 346.1529 m/z, HRMS found: 345.1445 [M-H^{+}].

(*E*)-Ethyl 1-(3-ethoxy-3-oxoprop-1-en-1-yl)-5-(2-methoxyphenyl)-4,5-dihydro-1H-pyrazole-4-carboxylate (C3P3)

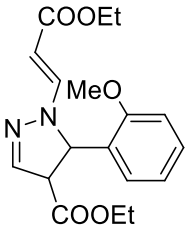

^{1}H NMR (500 MHz, $CDCl_3$): 7.98 (d, *J* = 13.1 Hz, 1H), 7.31-7.26 (m, 1H), 7.06 (d, *J* = 7.4 Hz, 1H), 6.95-6.88 (m, 2H), 6.81 (d, *J* = 1.7 Hz, 1H), 5.55 (d, *J* = 6.2 Hz, 1H), 4.66 (d, *J* = 13.1 Hz, 1H), 4.25 (q, *J* = 7.1 Hz, 2H), 4.15-4.03 (m, 2H), 3.87 (dd, *J* = 6.2, 1.7 Hz, 1H), 3.82 (s, 3H), 1.31 (t, *J* = 7.1 Hz, 3H), 1.22 (t, *J* = 7.1 Hz, 3H). ^{13}C NMR (125 MHz, $CDCl_3$): 168.5, 167.9, 156.5, 144.3, 139.7, 129.7, 127.2, 125.6, 121.0, 111.1, 90.0, 62.1, 61.8, 60.1, 59.4, 55.5, 14.5, 14.2. HRMS calcd.: 346.1528 m/z, HRMS found: 347.1601 [M+H^{+}].

3.5. ^{1}H, ^{13}C NMR and HRMS spectra of the 1,4-dihydropyridine products

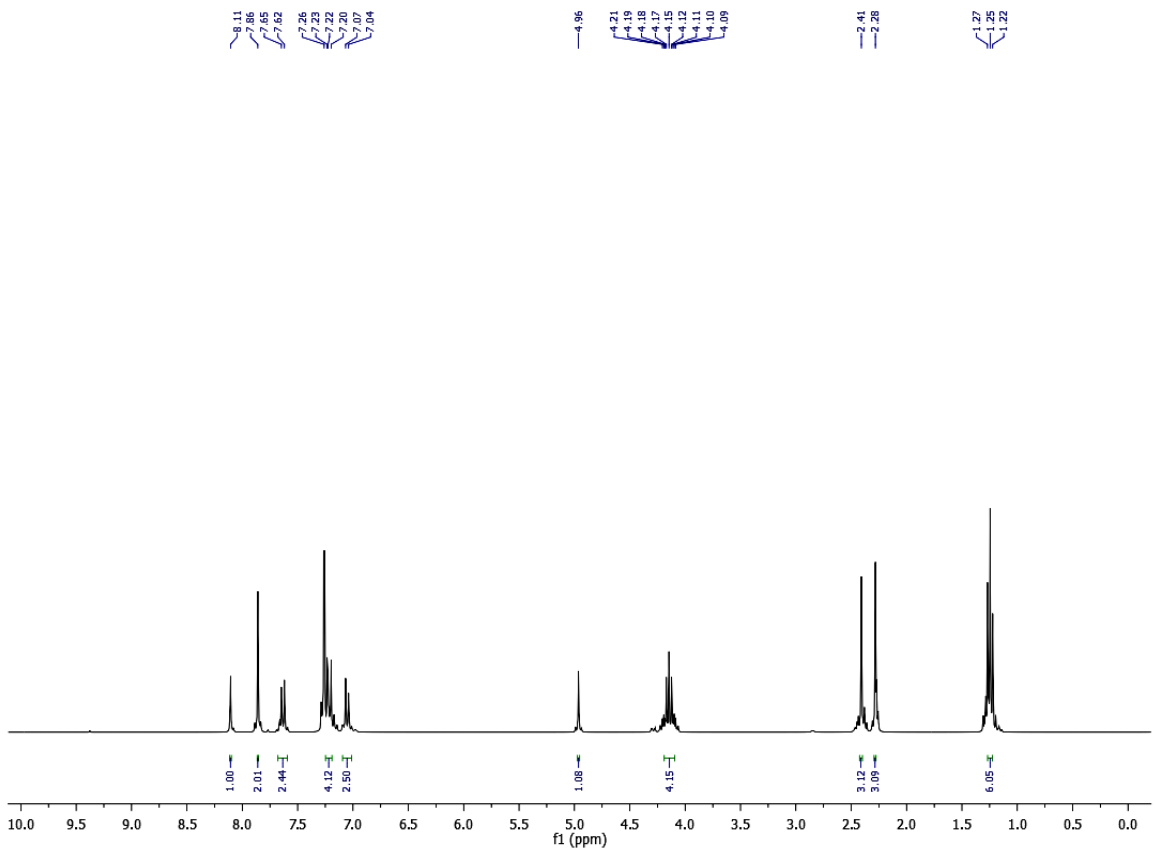

Figure S3.20. ^{1}H NMR spectrum of dihydropyridine **C3D1**.

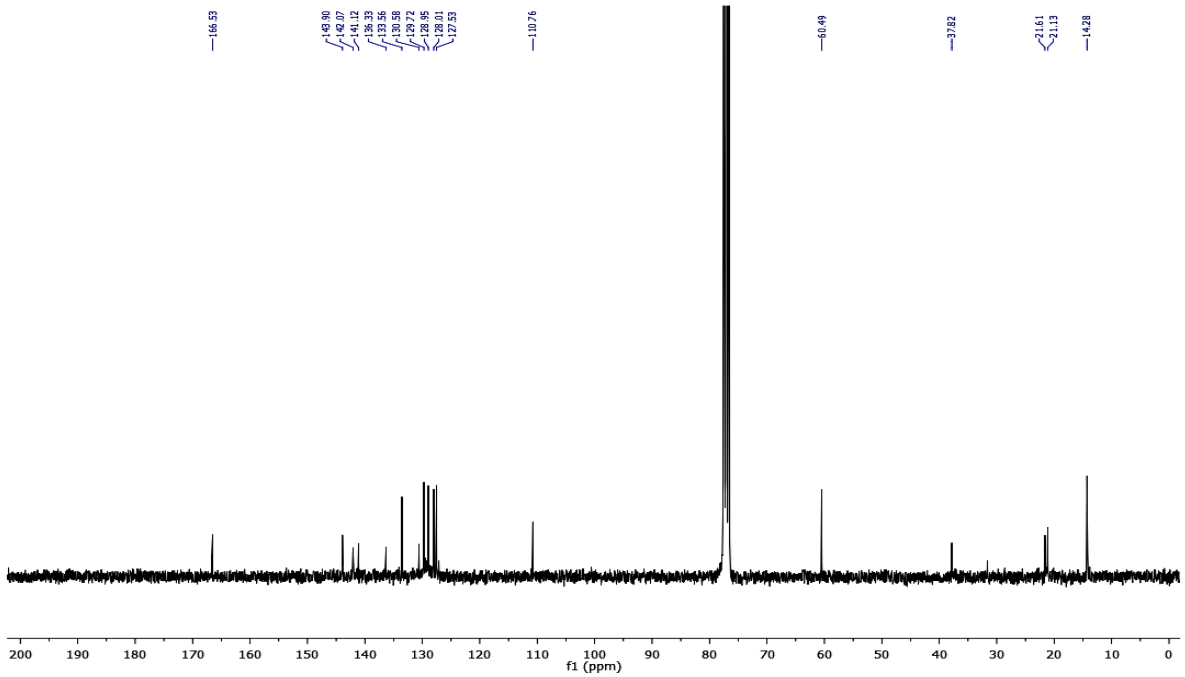

Figure S3.21. ^{13}C NMR spectrum of dihydropyridine **C3D1**.

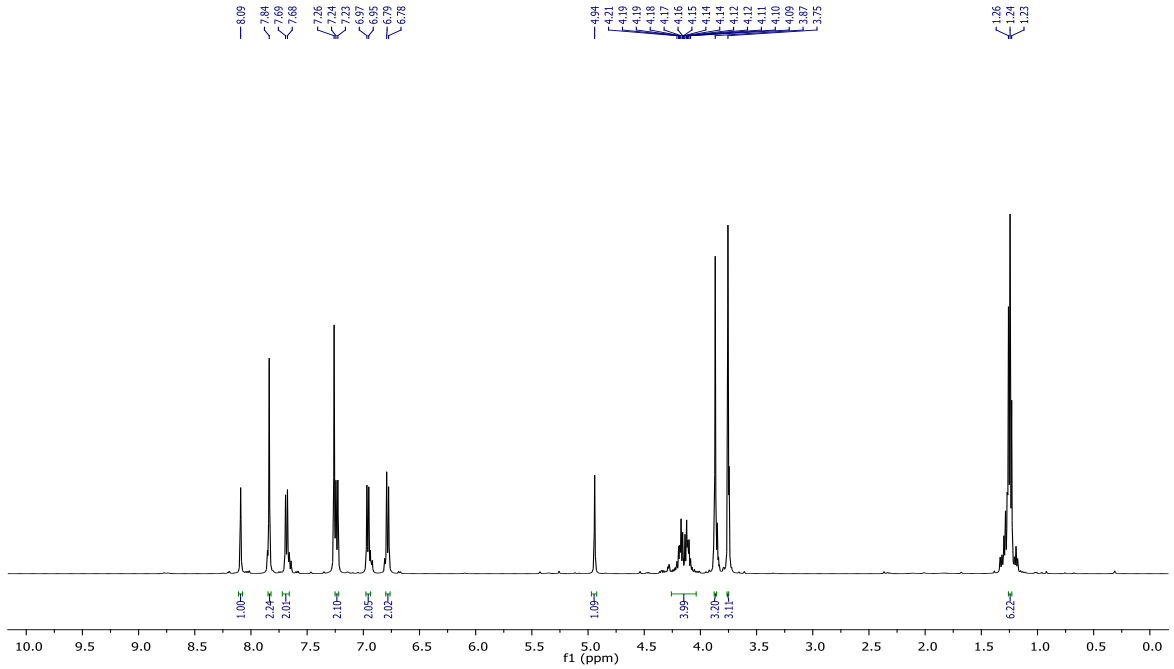

Figure S3.22. ^{1}H NMR spectrum of dihydropyridine **C3D2**.

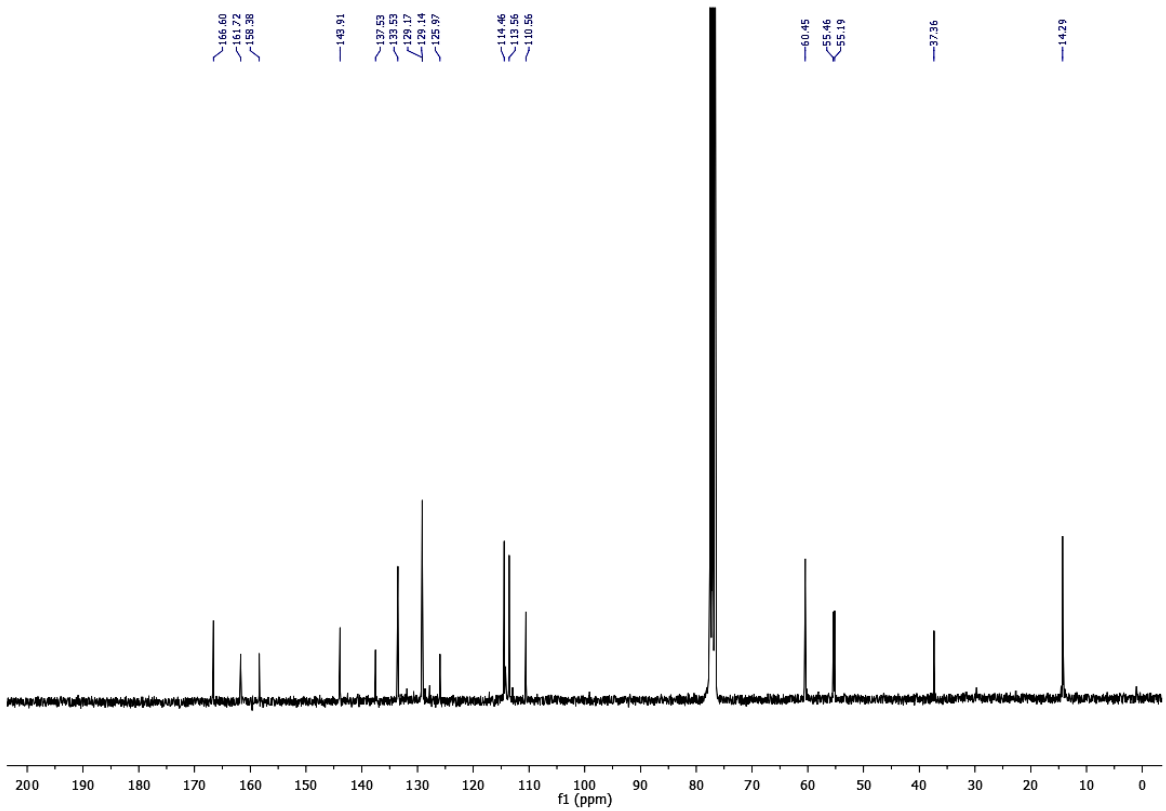

Figure S3.23. ^{13}C NMR spectrum of dihydropyridine **C3D2**.

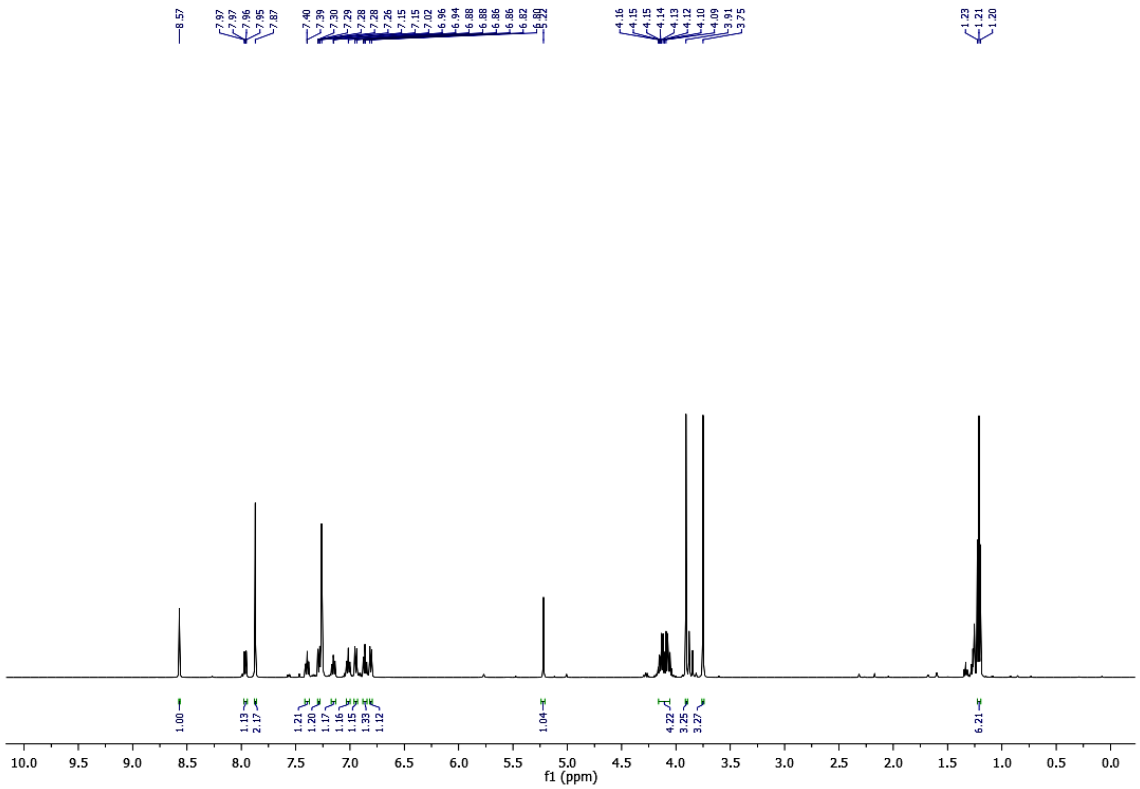

Figure S3.24. ^{1}H NMR spectrum of dihydropyridine **C3D3**.

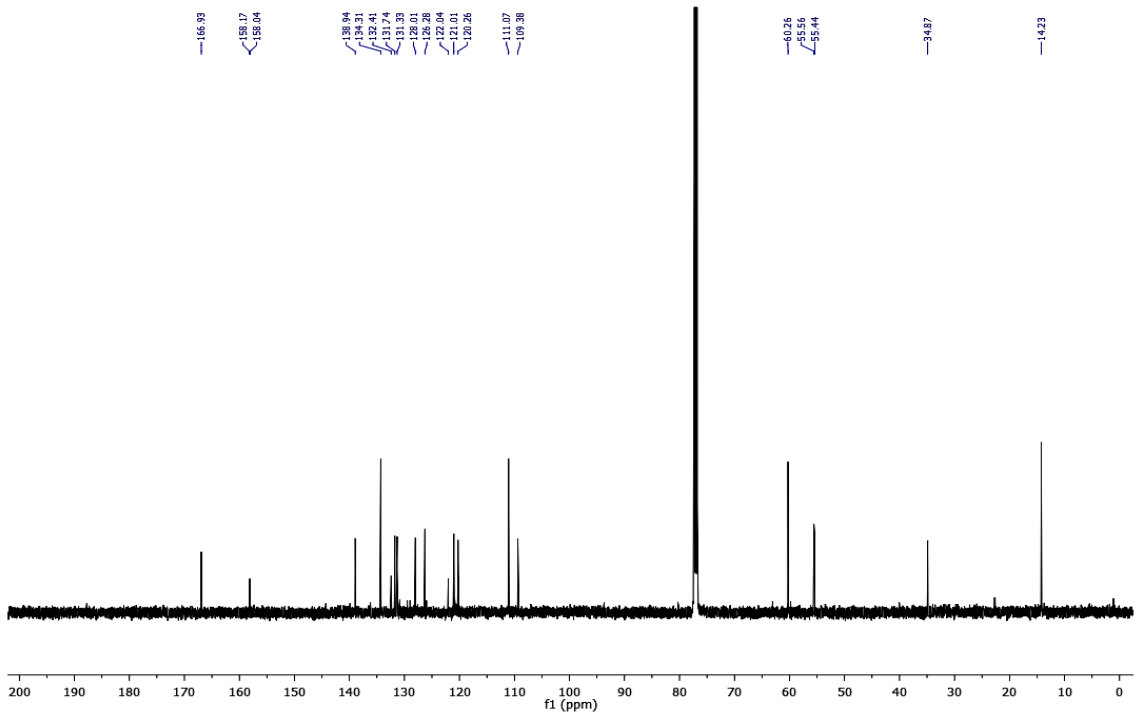

Figure S3.25. ^{13}C NMR spectrum of dihydropyridine **C3D3**.

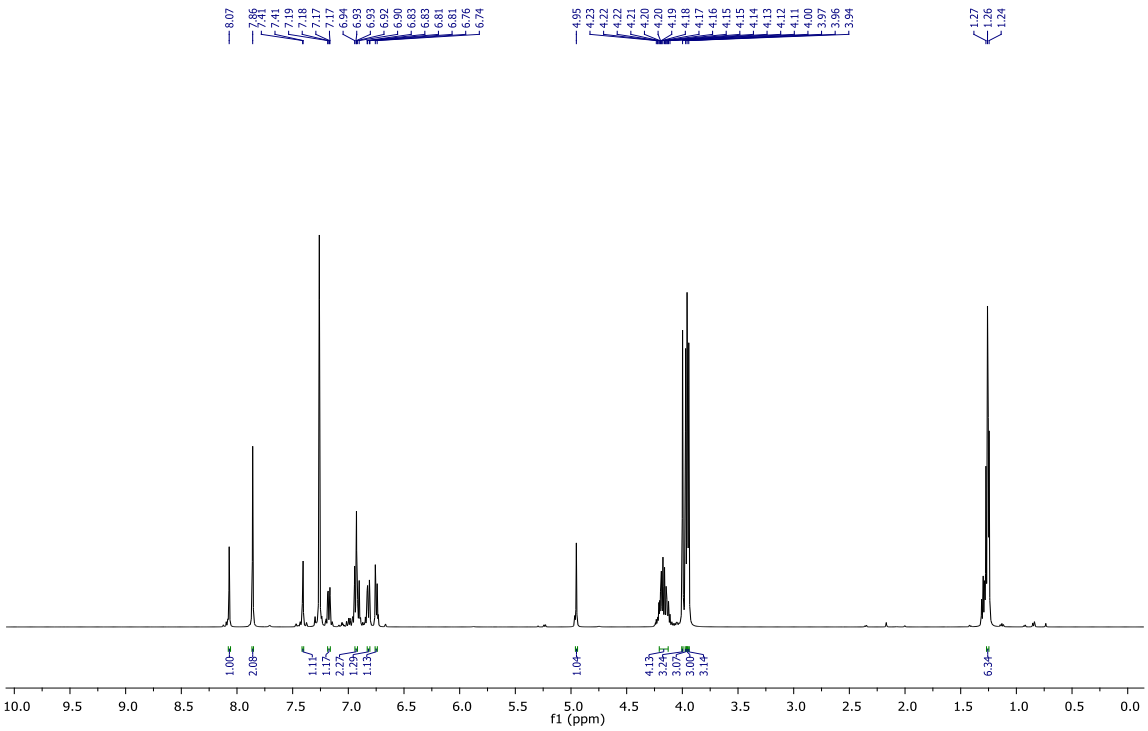

Figure S3.26. ^{1}H NMR spectrum of dihydropyridine **C3D4**.

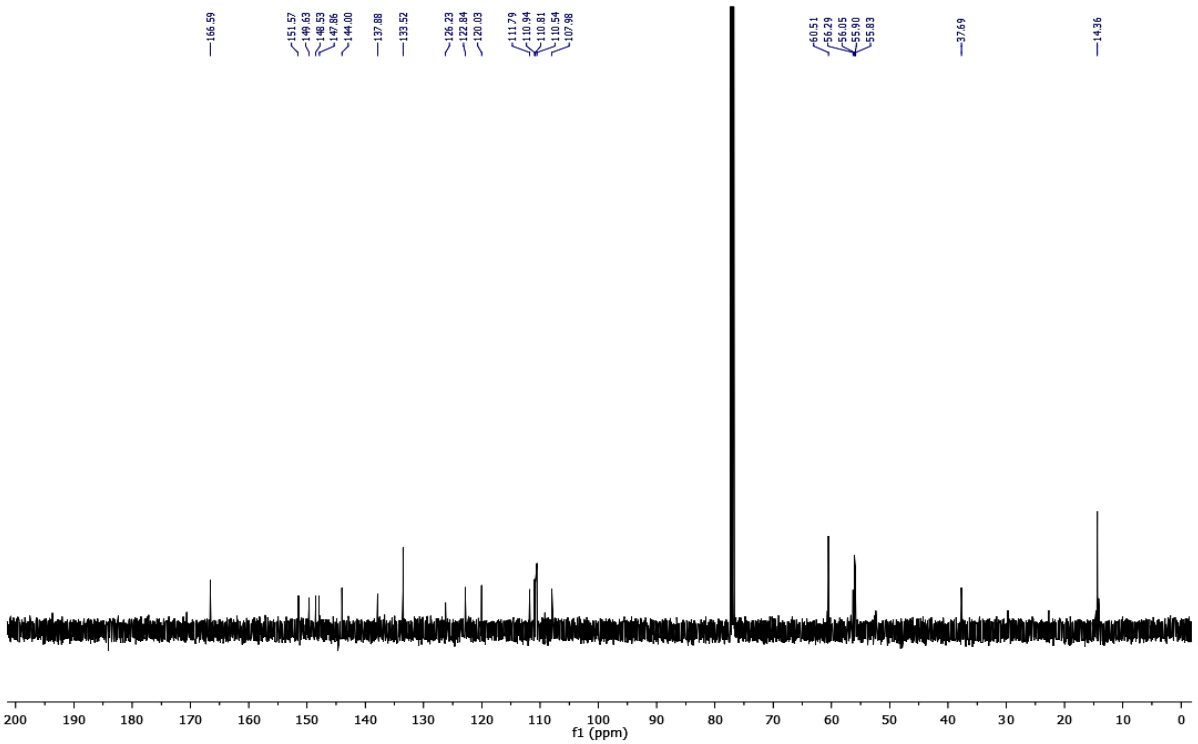

Figure S3.27. ^{13}C NMR spectrum of dihydropyridine **C3D4**.

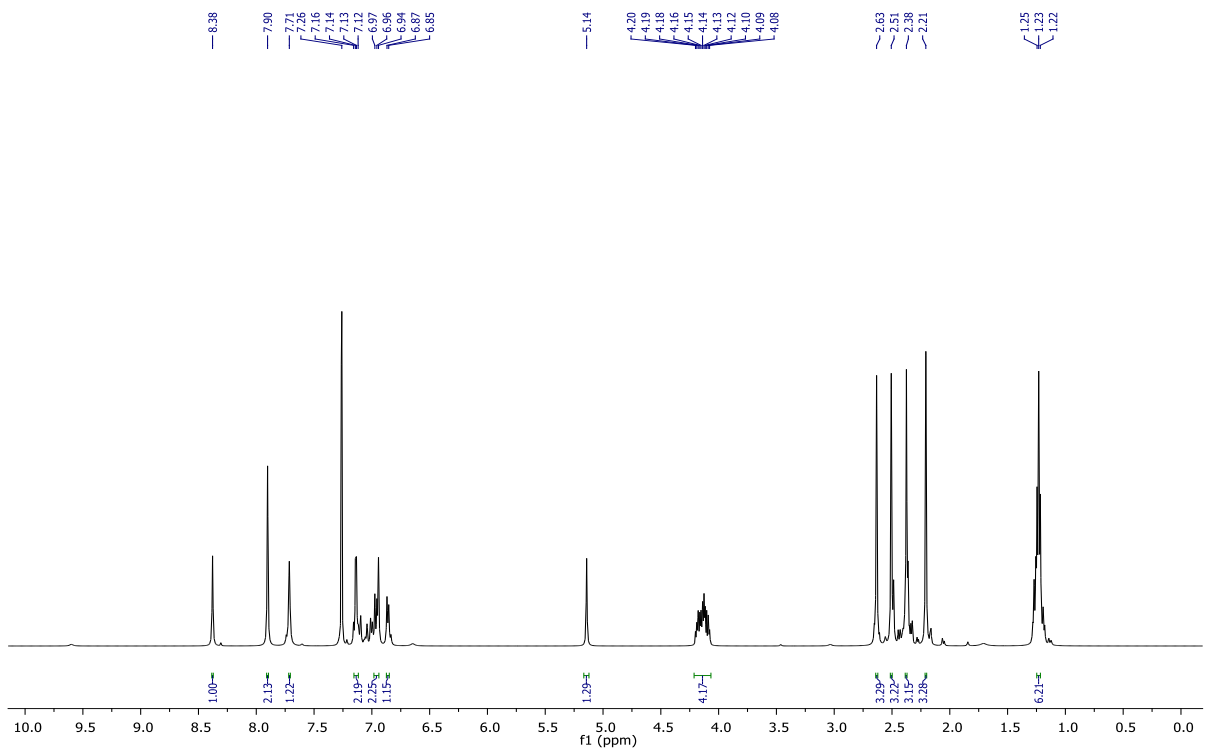

Figure S3.28. ^{1}H NMR spectrum of dihydropyridine **C3D5**.

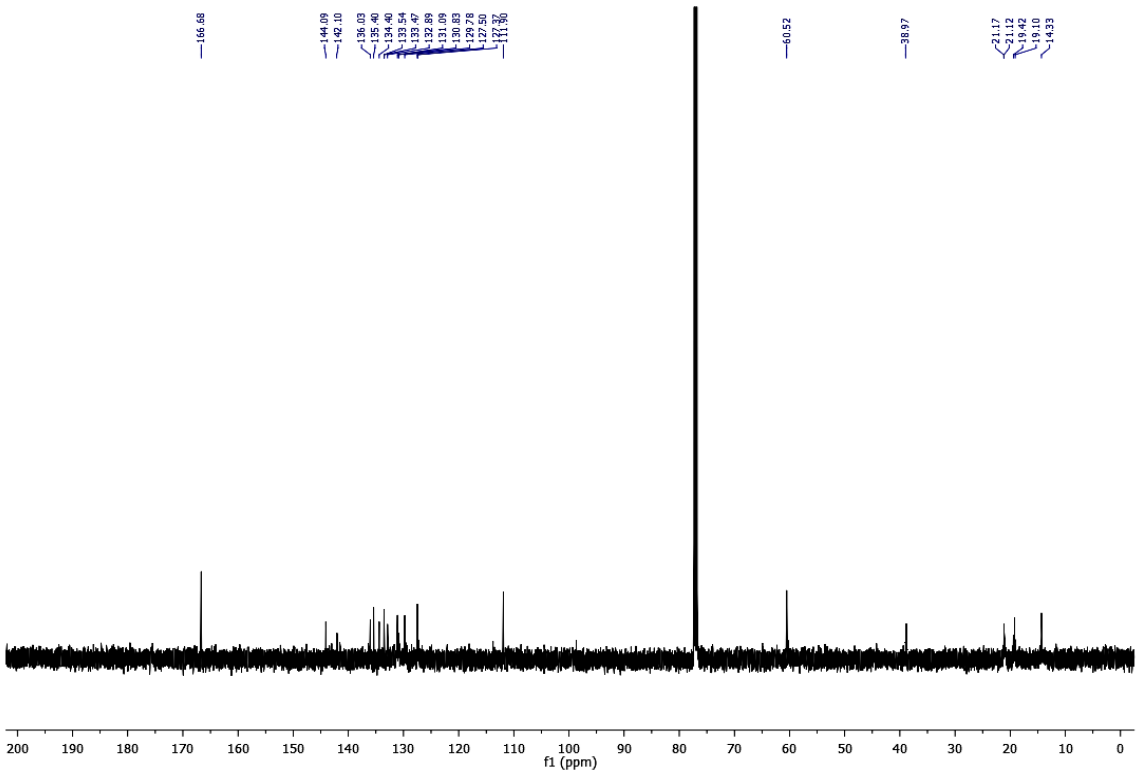

Figure S3.29. ^{13}C NMR spectrum of dihydropyridine **C3D5**.

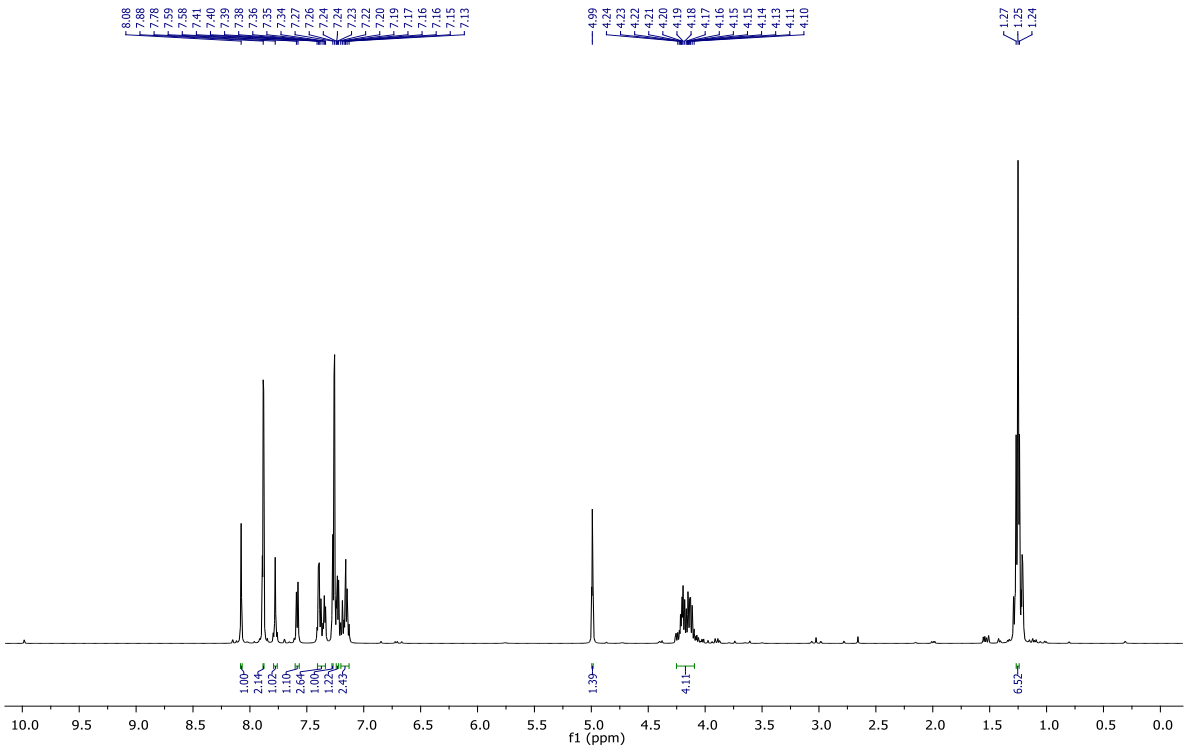

Figure S3.30. ^{1}H NMR spectrum of dihydropyridine **C3D6**.

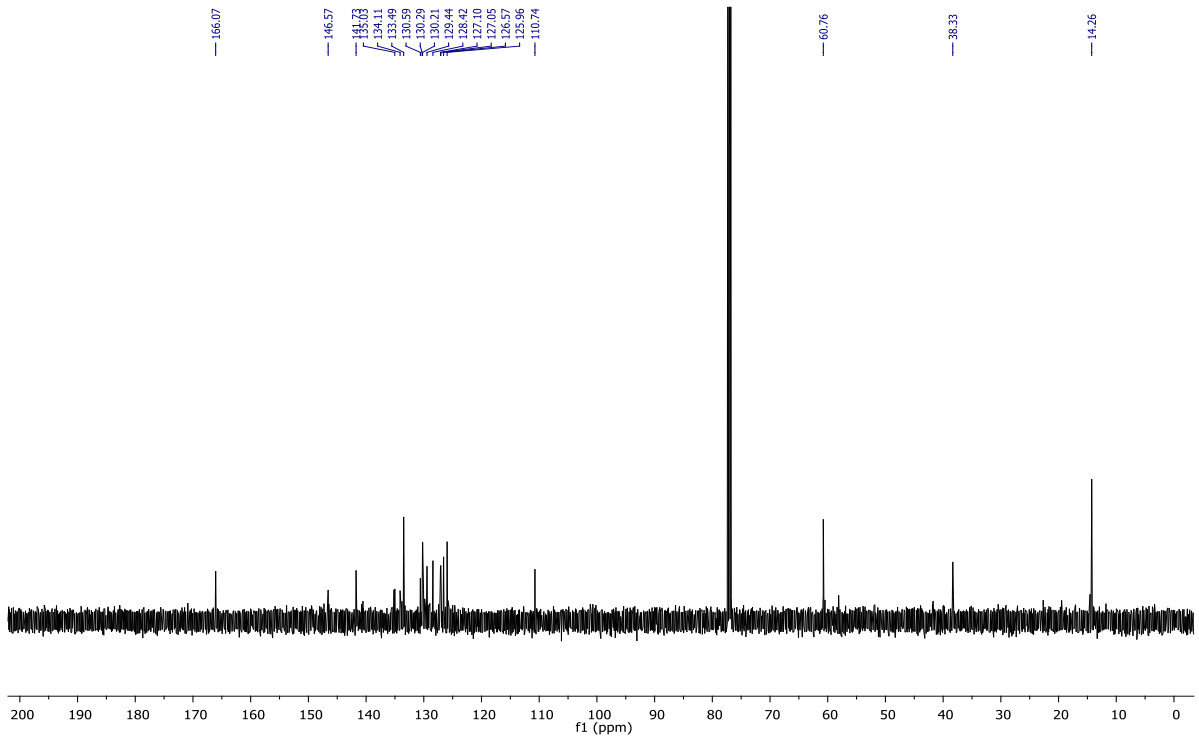

Figure S3.31. ^{13}C NMR spectrum of dihydropyridine **C3D6**.

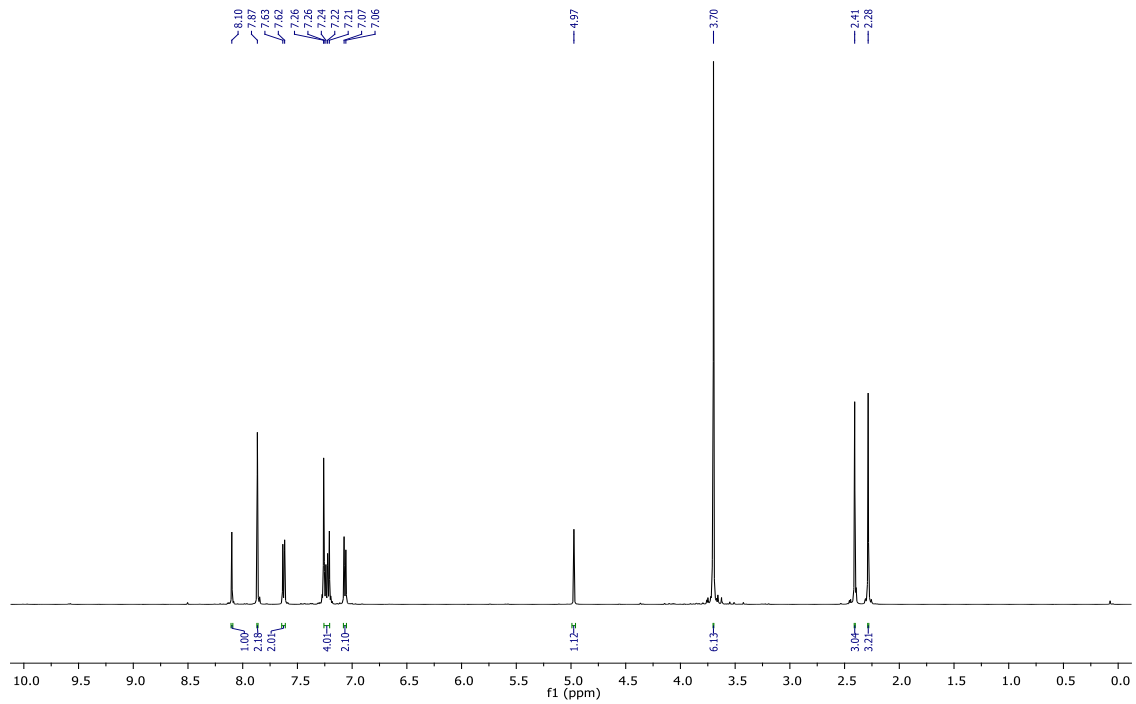

Figure S3.32. ^{1}H NMR spectrum of dihydropyridine **C3D11**.

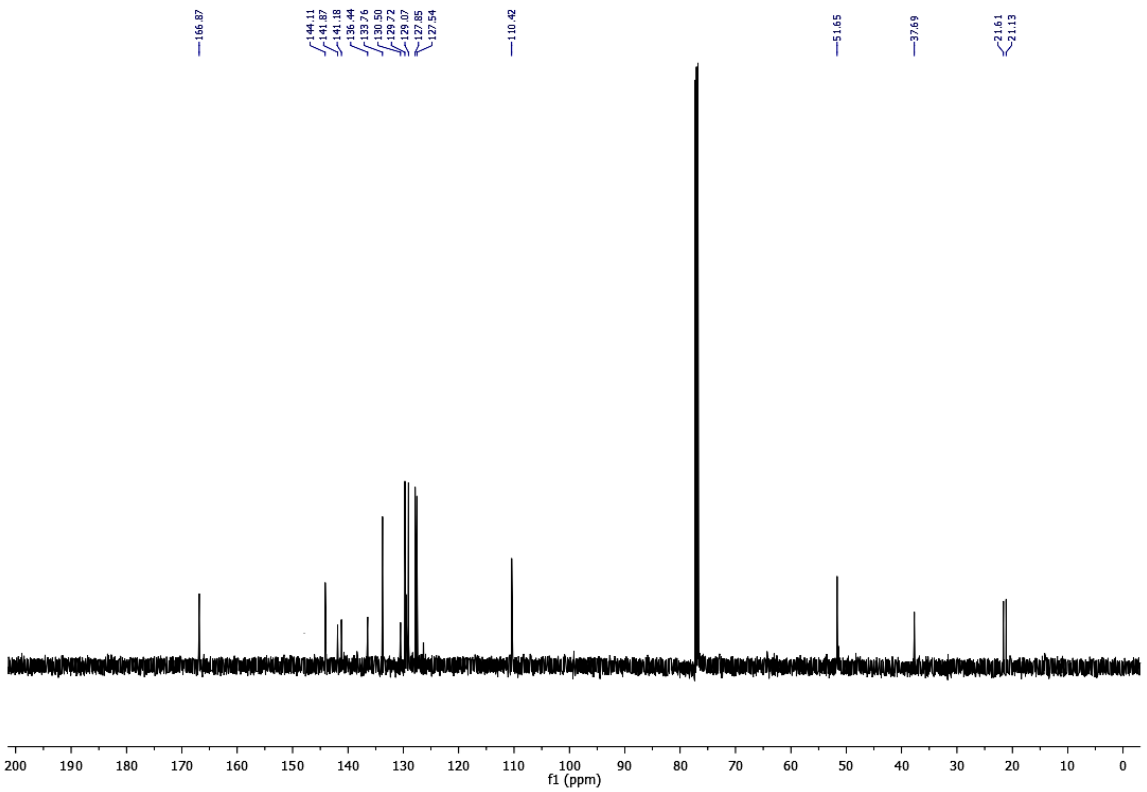

Figure S3.33. ^{13}C NMR spectrum of dihydropyridine **C3D11**.

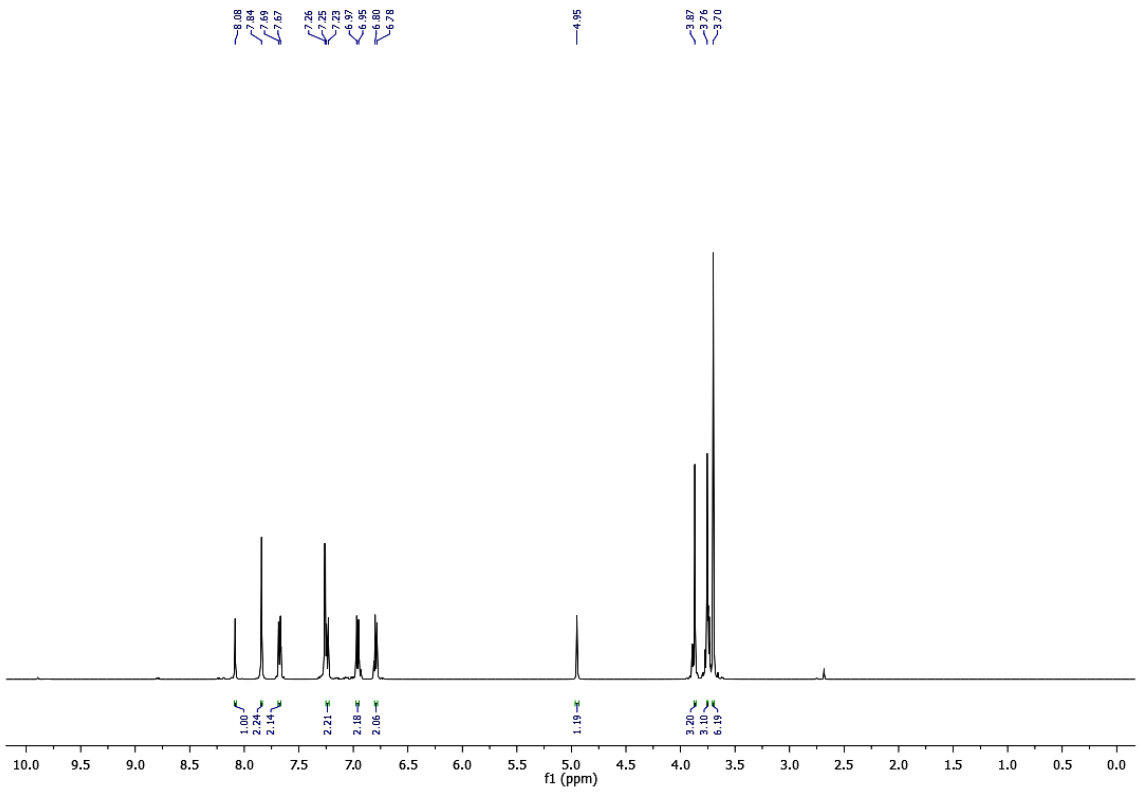

Figure S3.34. ^{1}H NMR spectrum of dihydropyridine **C3D12**.

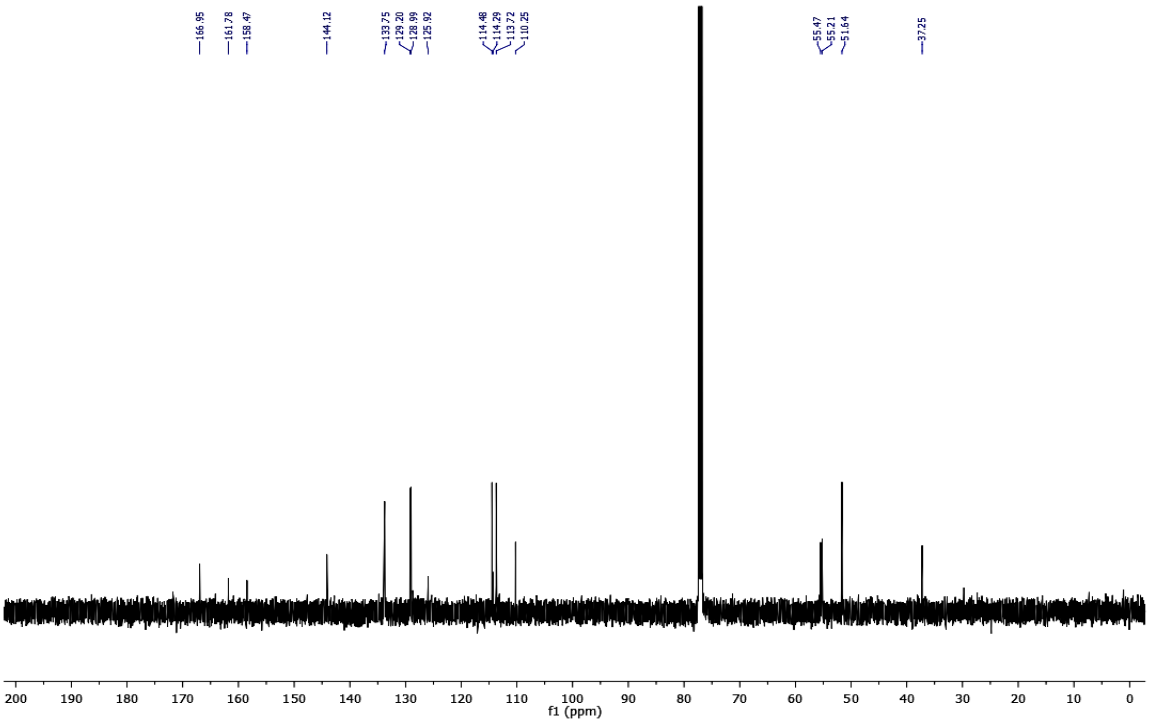

Figure S3.35. ^{13}C NMR spectrum of dihydropyridine **C3D12**.

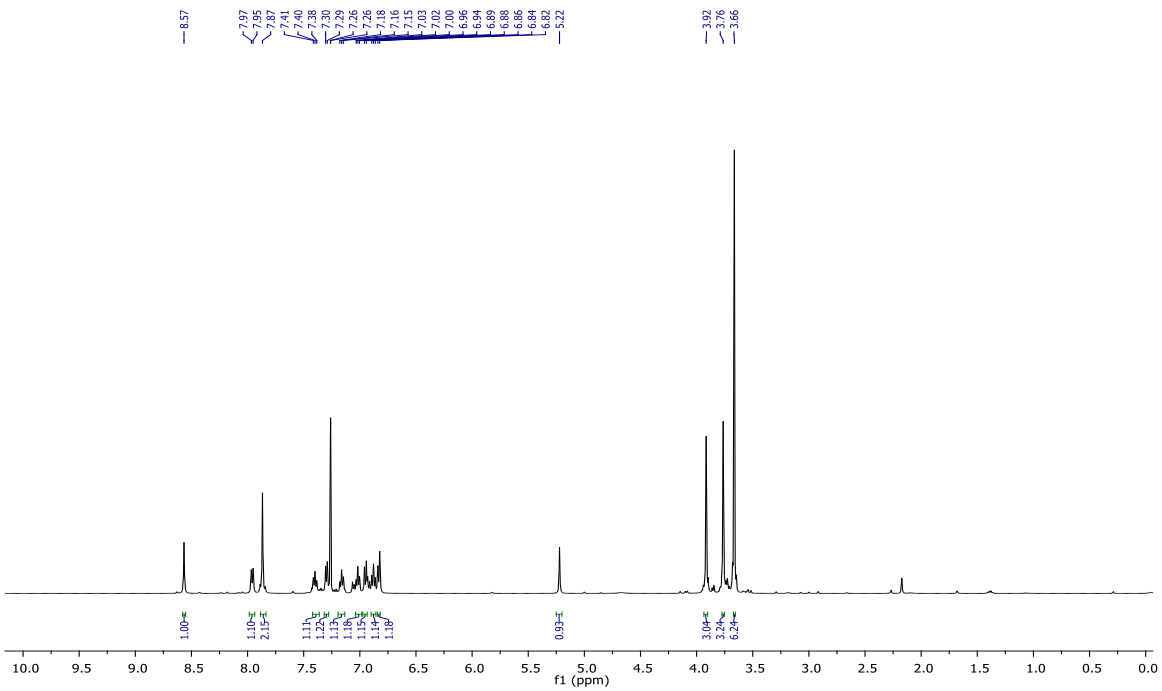

Figure S3.36. ^{1}H NMR spectrum of dihydropyridine **C3D13**.

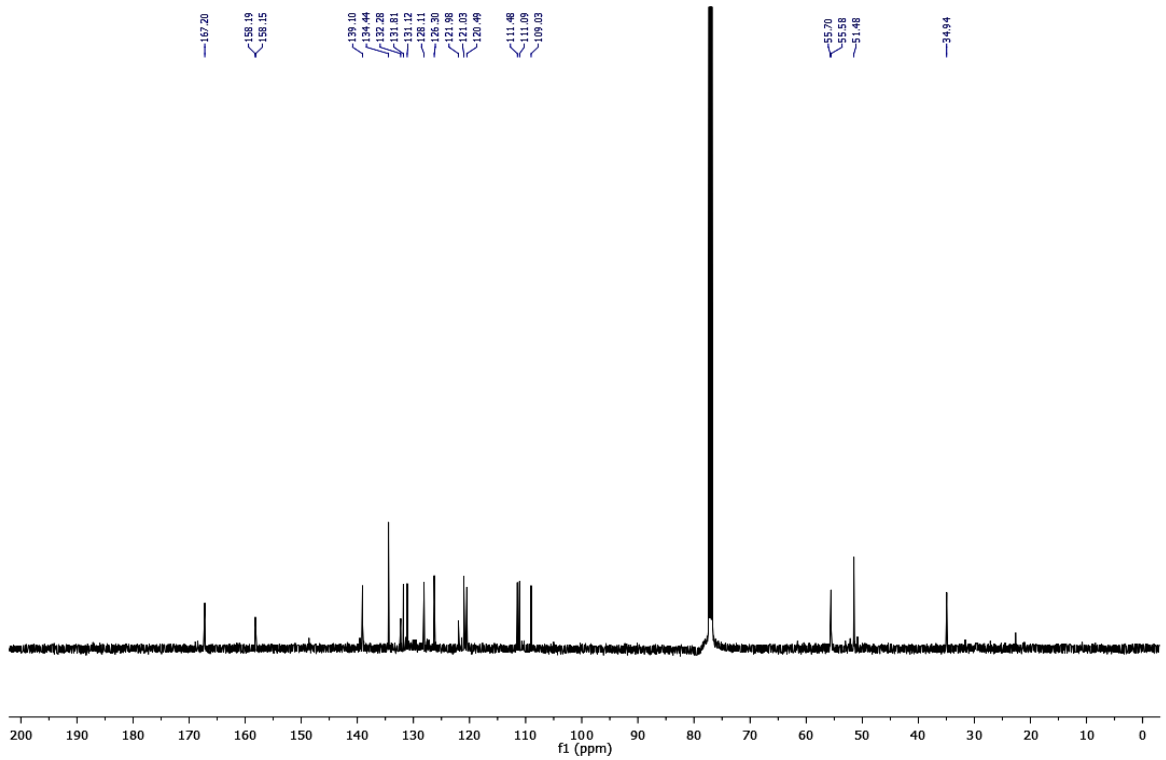

Figure S3.37. ^{13}C NMR spectrum of dihydropyridine **C3D13**.

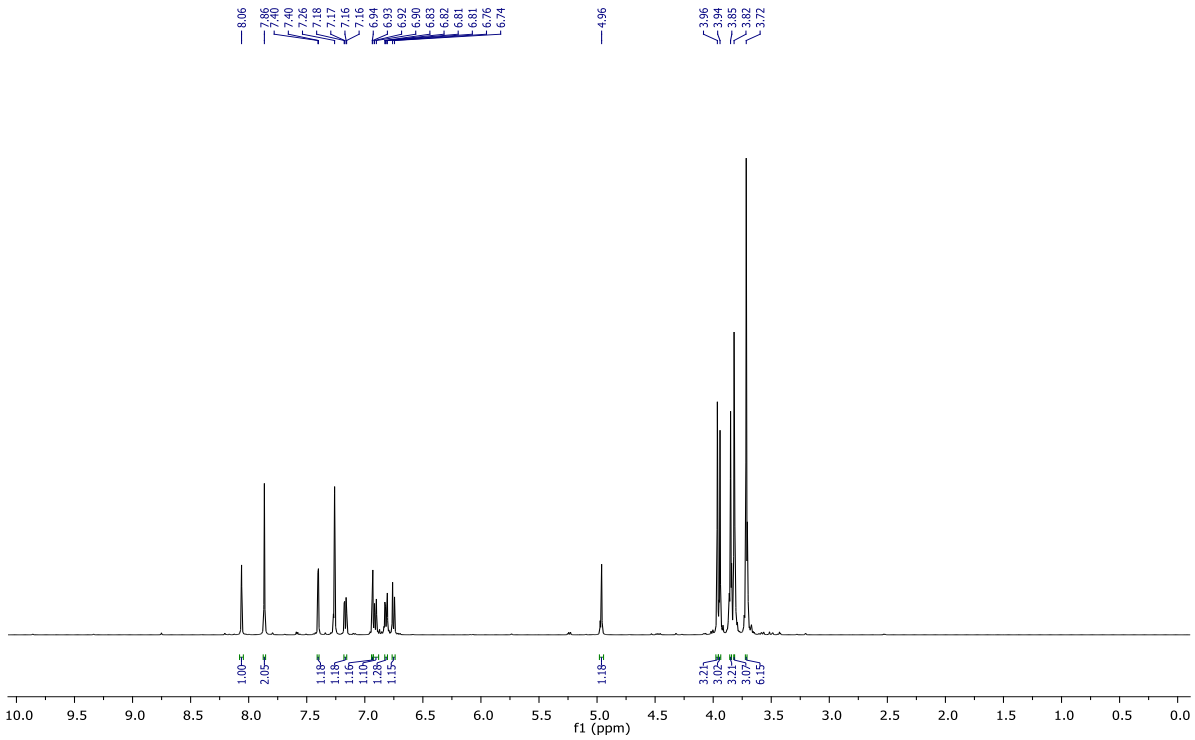

Figure S3.38. ^{1}H NMR spectrum of dihydropyridine **C3D14**.

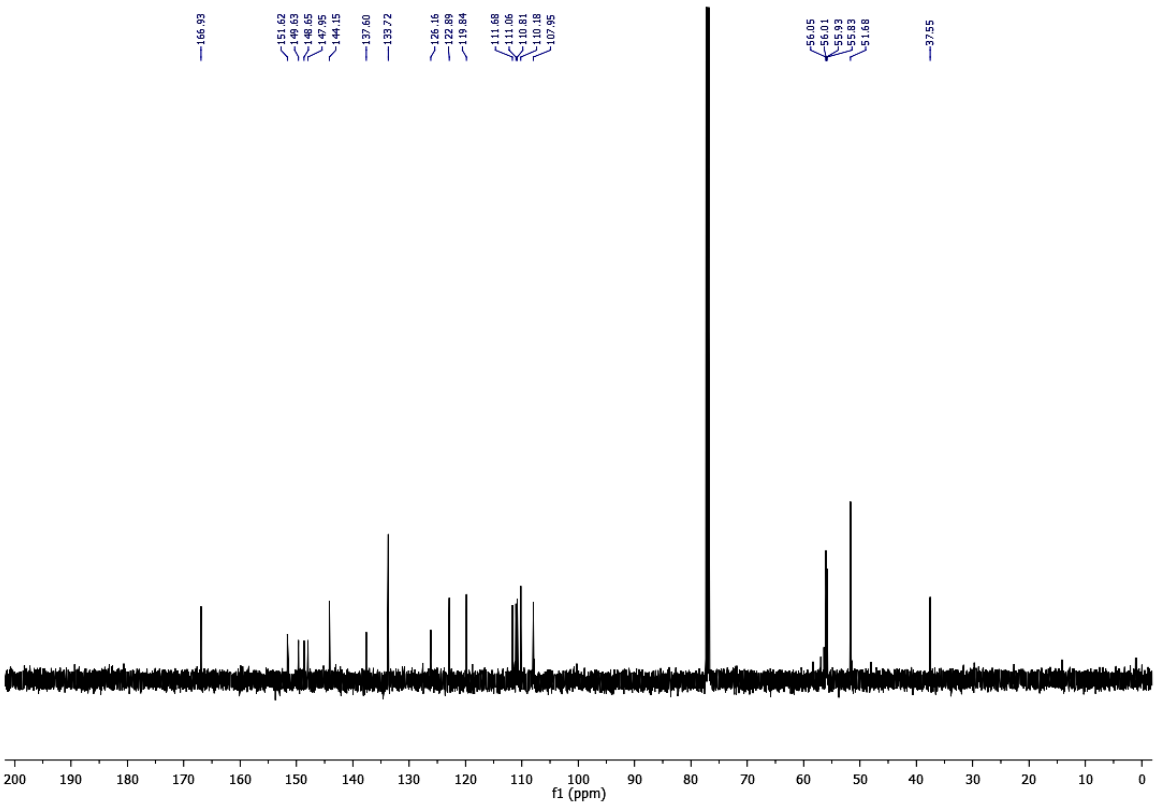

Figure S3.39. ^{13}C NMR spectrum of dihydropyridine **C3D14**.

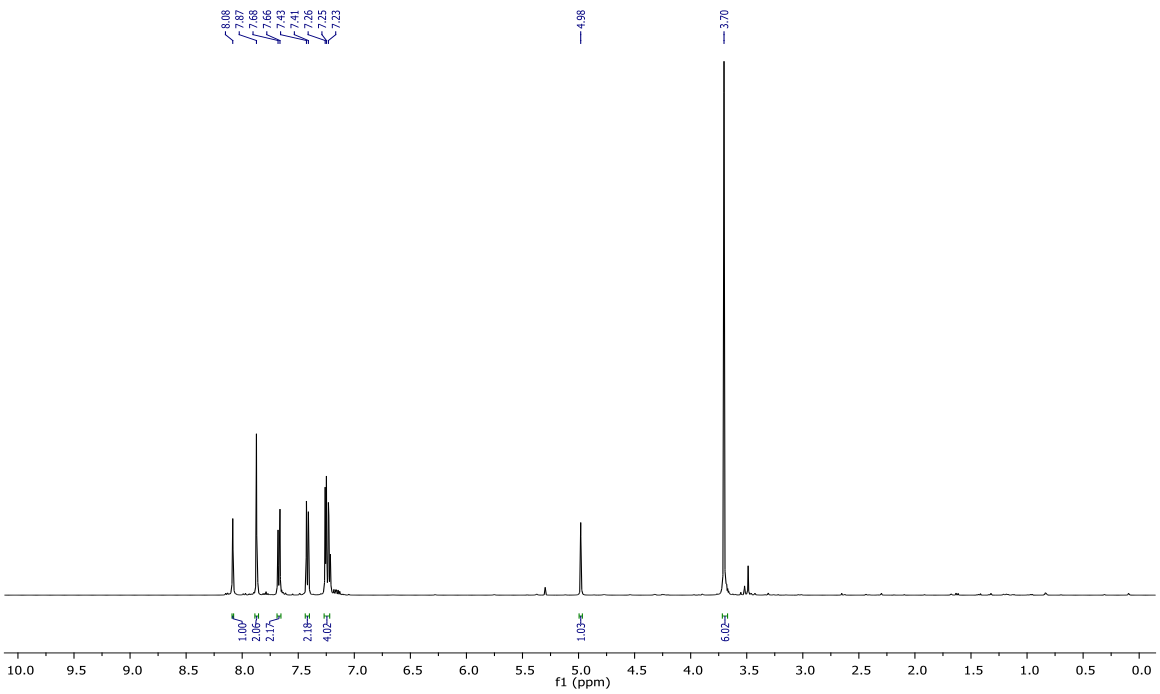

Figure S3.40. ^{1}H NMR spectrum of dihydropyridine **C3D15**.

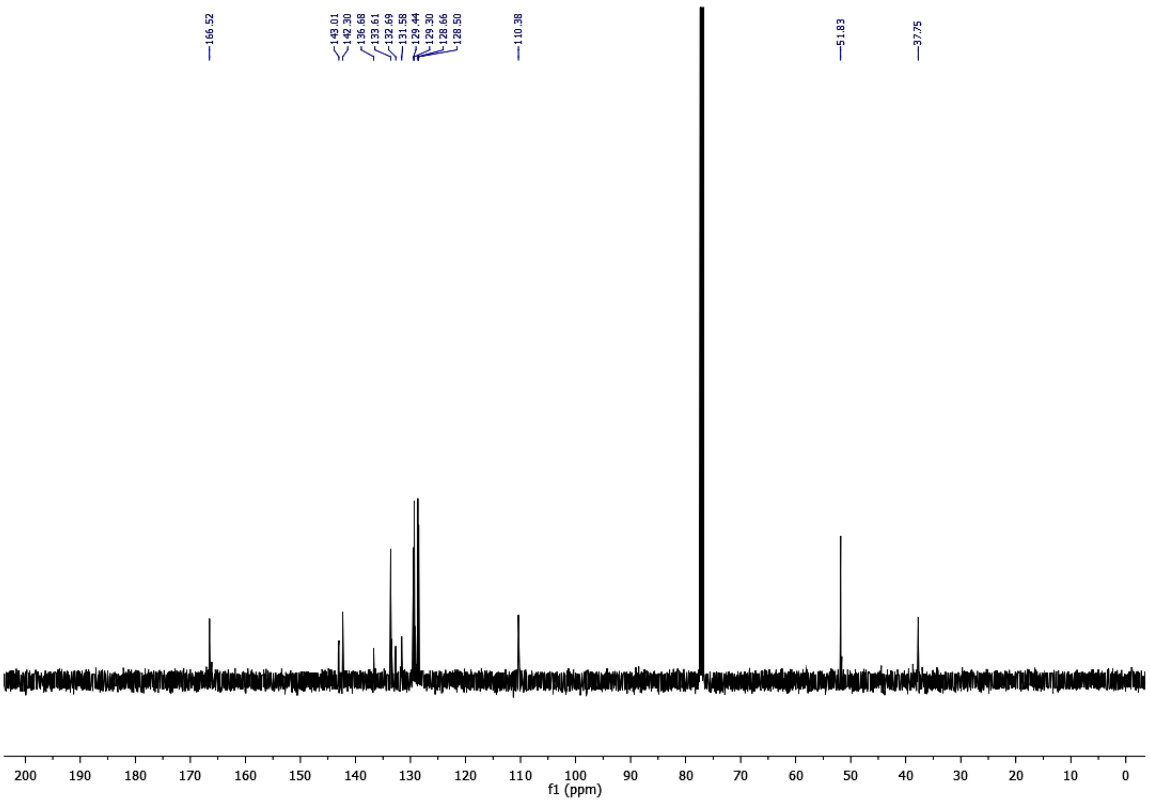

Figure S3.41. ^{13}C NMR spectrum of dihydropyridine **C3D15**.

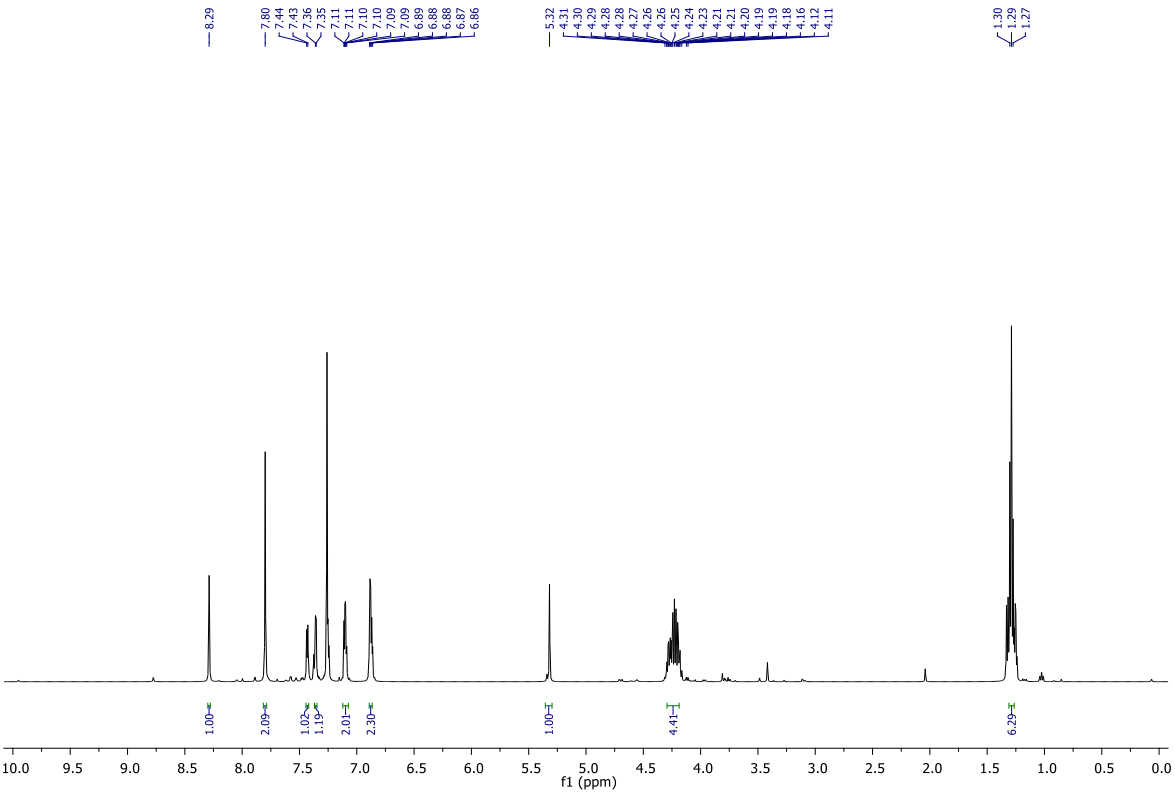

Figure S3.42. ^{1}H NMR spectrum of dihydropyridine **C3D16**.

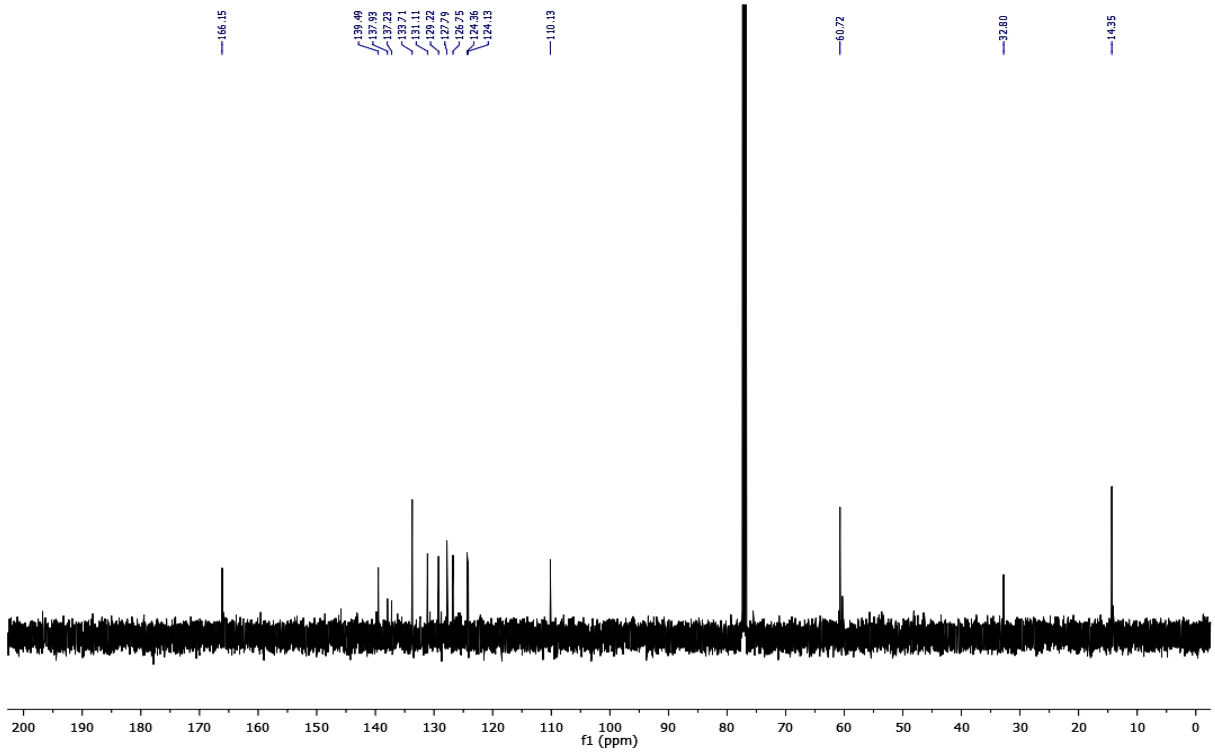

Figure S3.43. ^{13}C NMR spectrum of dihydropyridine **C3D16**.

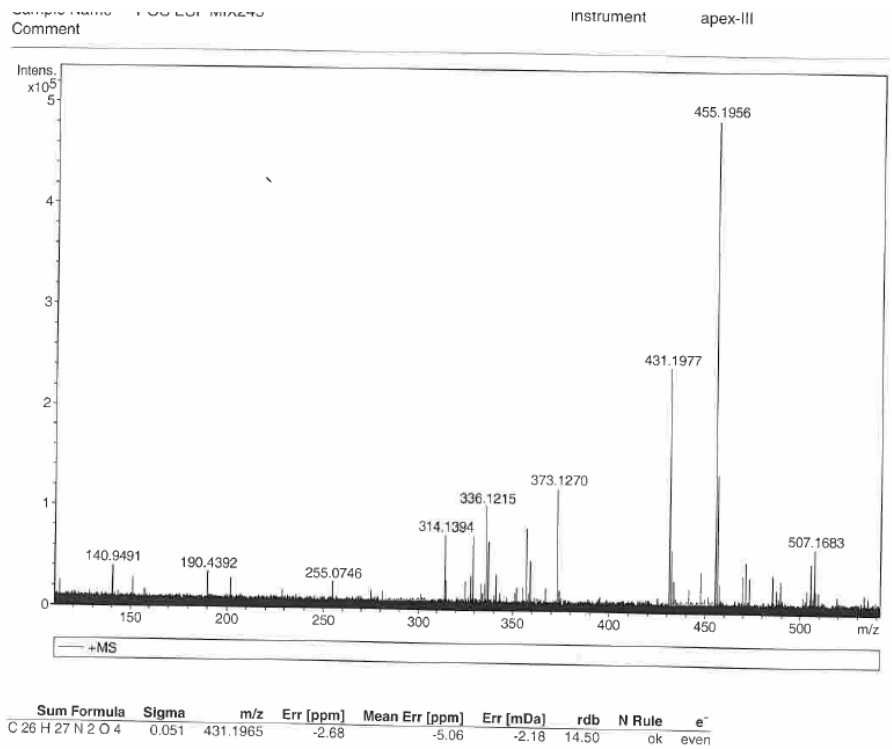

Figure S3.44. HRMS spectrum of dihydropyridine **C3D1**.

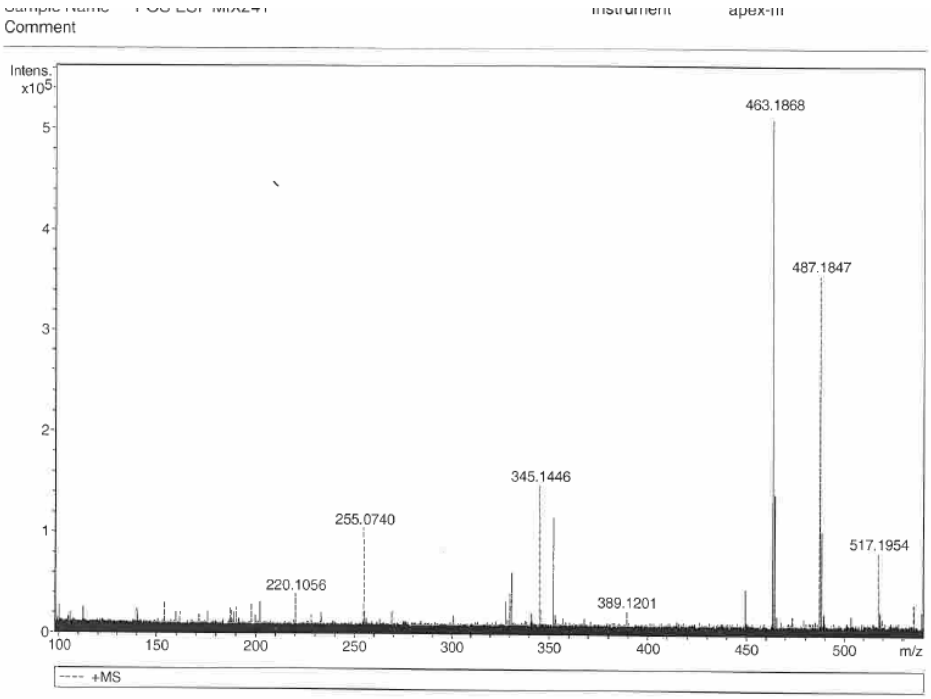

Sum Formula	Sigma	m/z	Err [ppm]	Mean Err [ppm]	Err [mDa]	rdb	N Rule	e⁻
C 26 H 27 N 2 O 6	0.026	463.1864	-0.96	-3.67	-1.70	14,50	ok	even

Figure S3.45. HRMS spectrum of dihydropyridine **C3D2**.

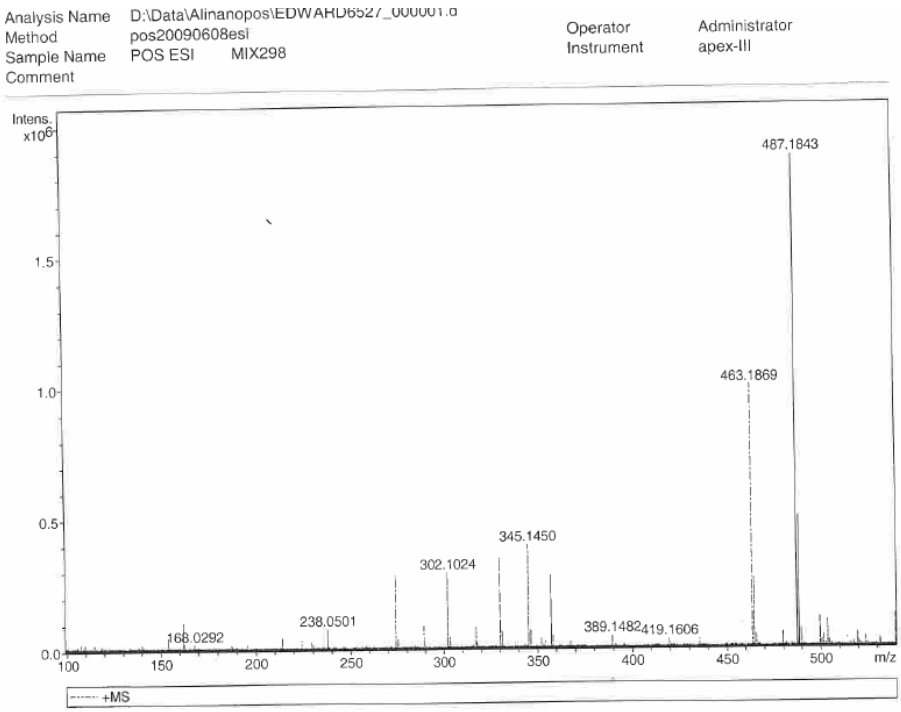

Sum Formula	Sigma	m/z	Err [ppm]	Mean Err [ppm]	Err [mDa]	rdb	N Rule	e⁻
C 26 H 27 N 2 O 6	0.032	463.1864	-1.15	-4.46	-2.07	14.50	ok	even

Figure S3.46. HRMS spectrum of dihydropyridine **C3D3**.

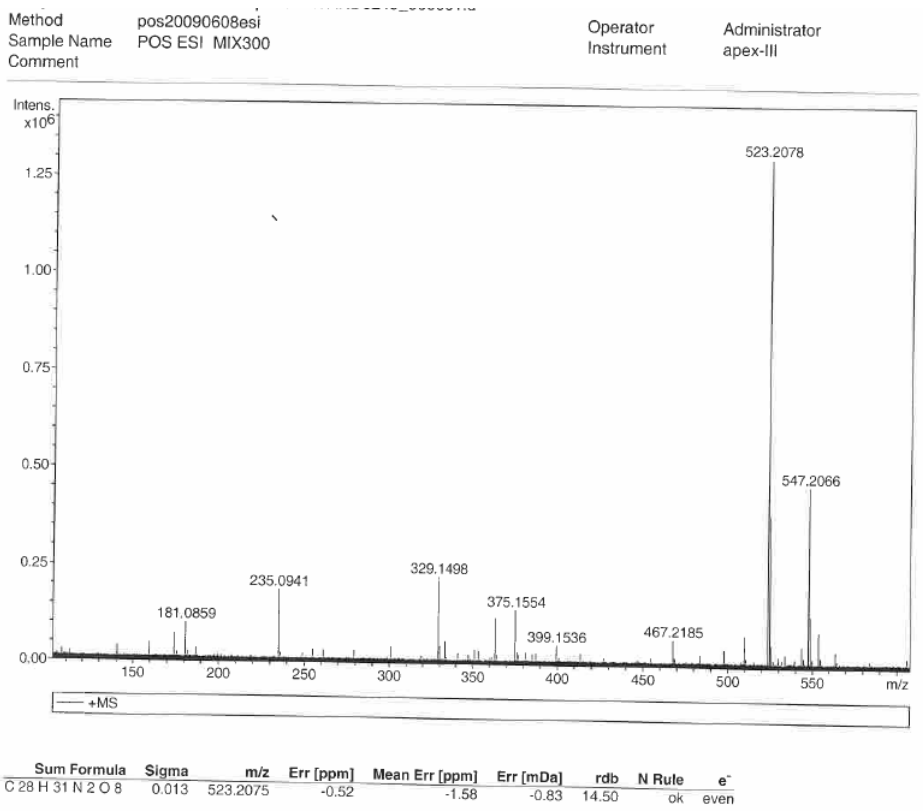

Figure S3.47. HRMS spectrum of dihydropyridine **C3D4**.

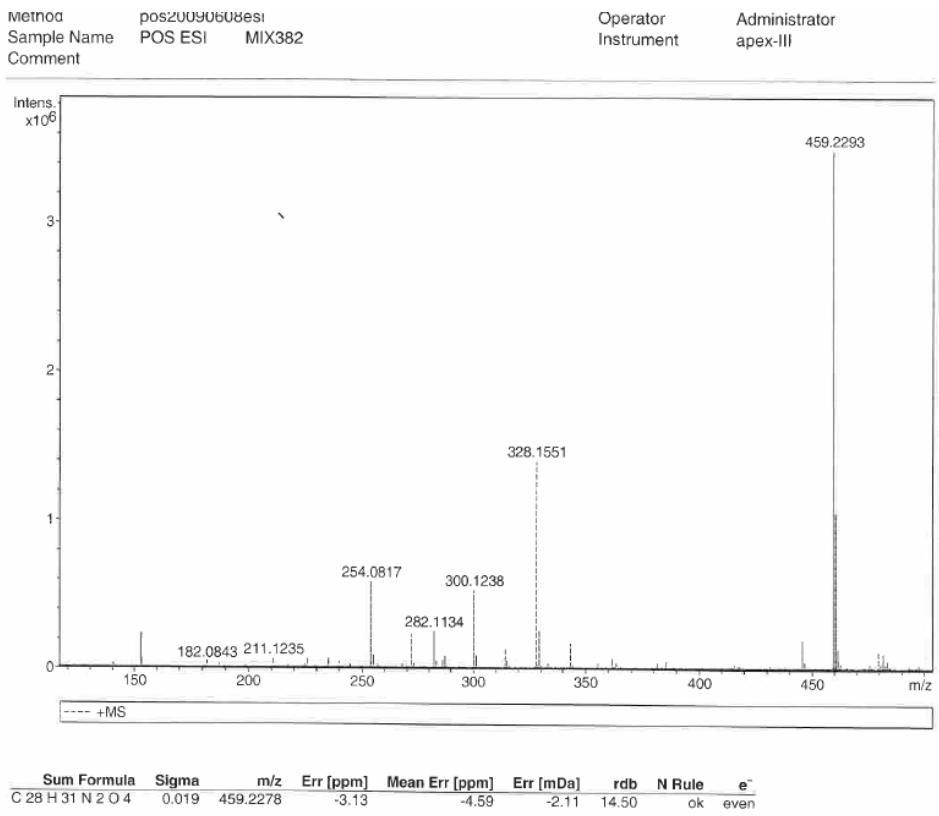

Figure S3.48. HRMS spectrum of dihydropyridine **C3D5**.

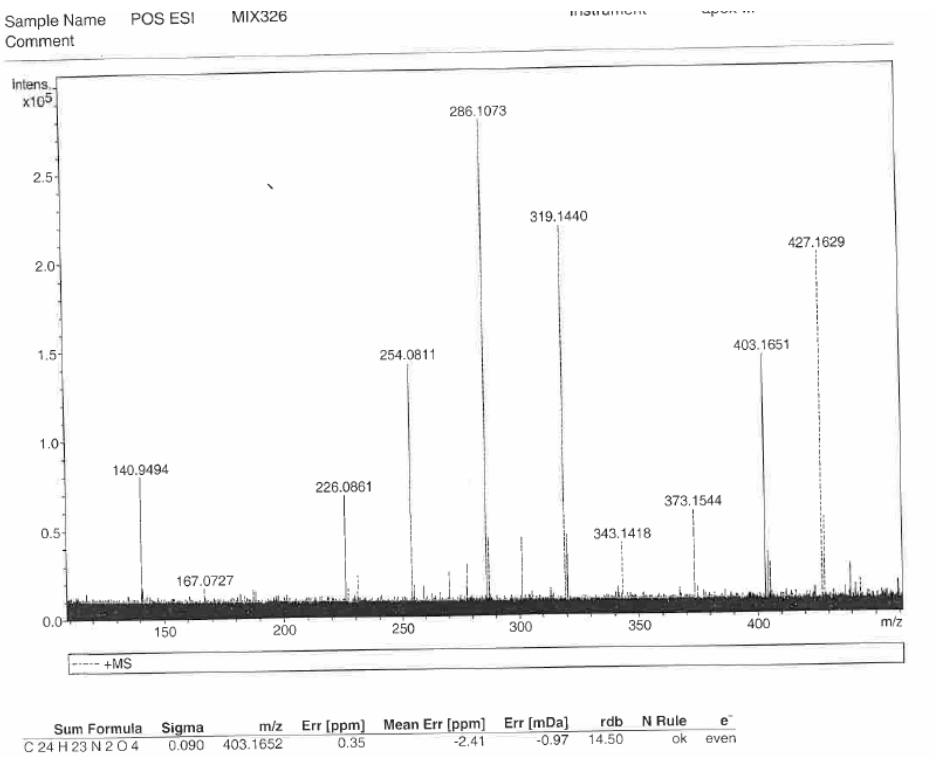

Figure S3.49. HRMS spectrum of dihydropyridine **C3D11**.

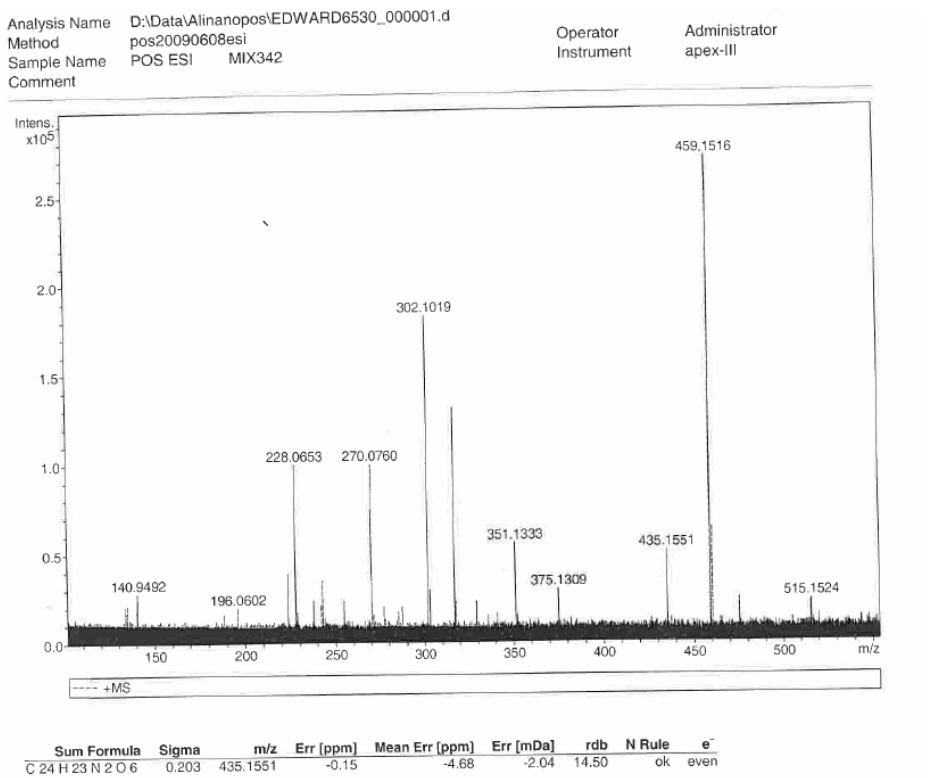

Figure S3.50. HRMS spectrum of dihydropyridine **C3D12**.

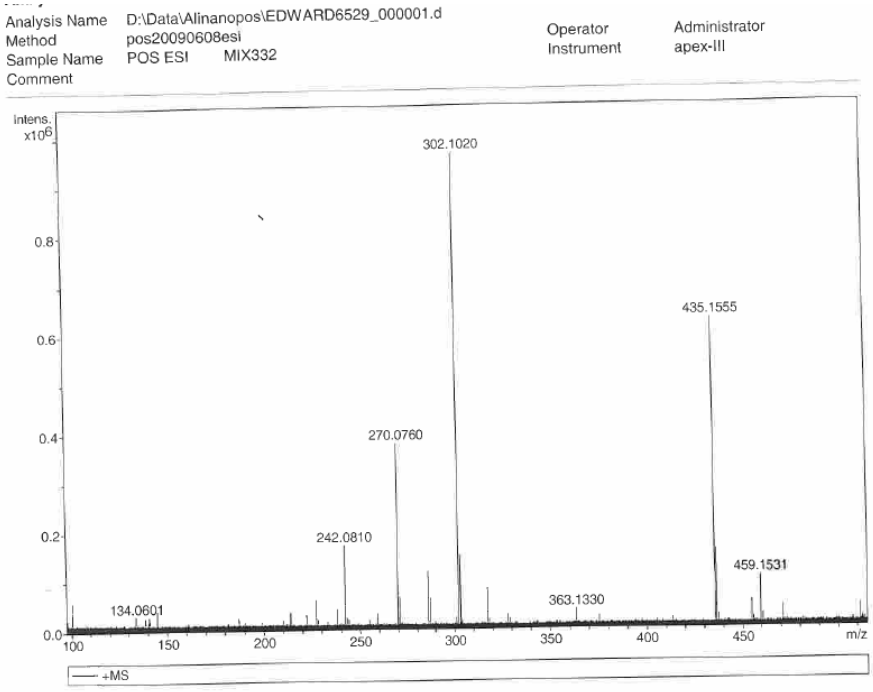

Sum Formula	Sigma	m/z	Err [ppm]	Mean Err [ppm]	Err [mDa]	rdb	N Rule	e⁻
C 24 H 23 N 2 O 6	0.014	435.1551	-1.05	-1.50	-0.65	14.50	ok	even

Figure S3.51. HRMS spectrum of dihydropyridine **C3D13**.

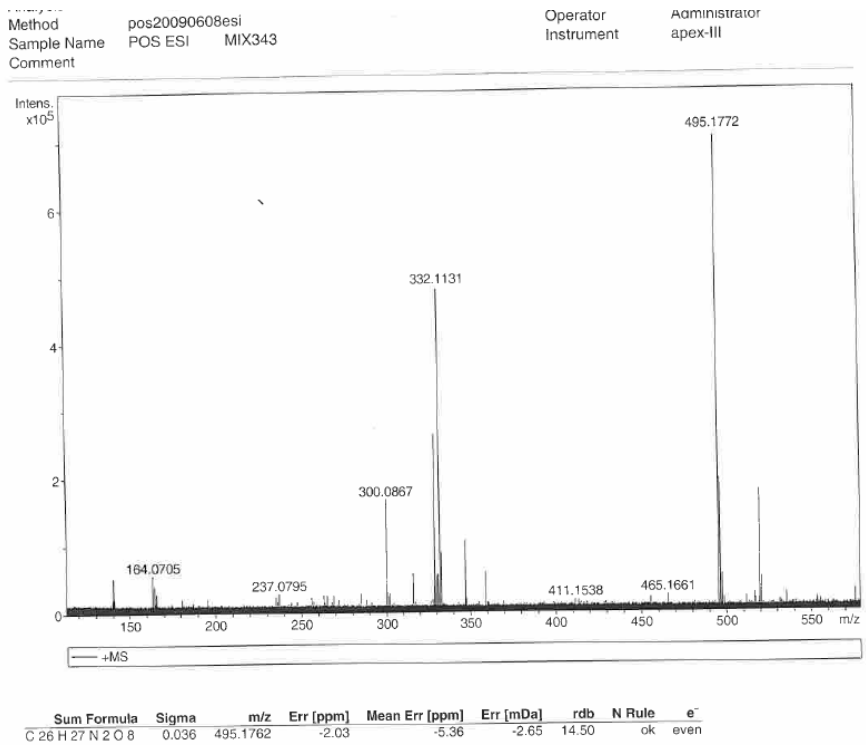

Sum Formula	Sigma	m/z	Err [ppm]	Mean Err [ppm]	Err [mDa]	rdb	N Rule	e⁻
C 26 H 27 N 2 O 8	0.036	495.1762	-2.03	-5.36	-2.65	14.50	ok	even

Figure S3.52. HRMS spectrum of dihydropyridine **C3D14**.

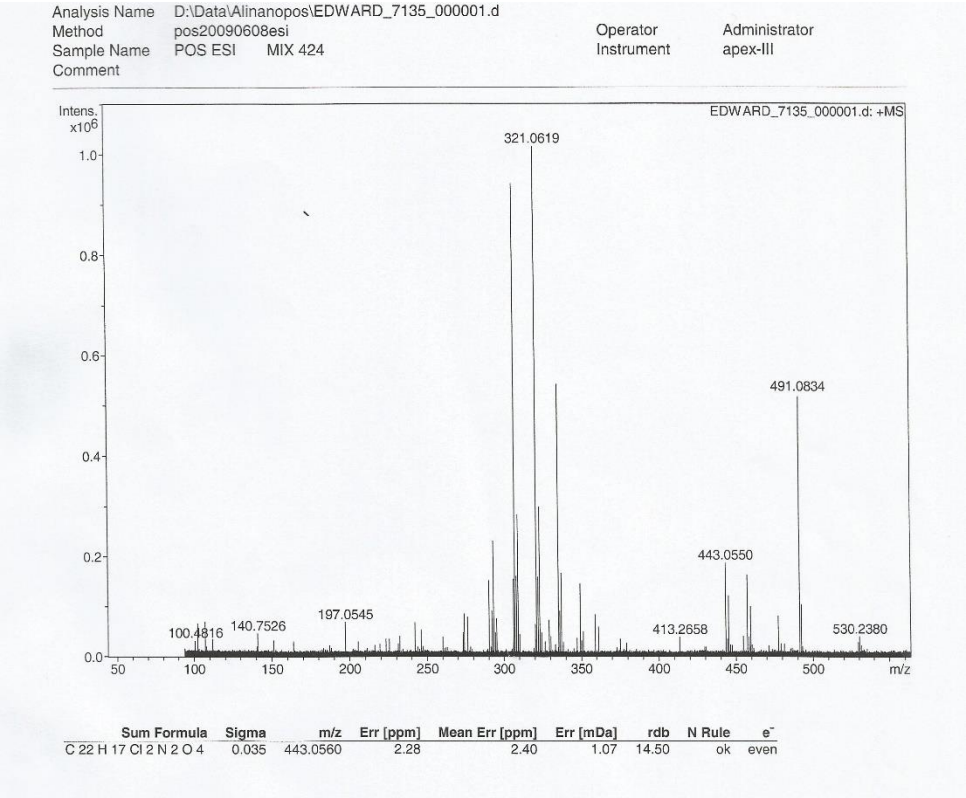

Figure S3.53. HRMS spectrum of dihydropyridine **C3D15**.

3.6. ^{1}H, ^{13}C NMR and HRMS spectra of selected isolated pyrazoles

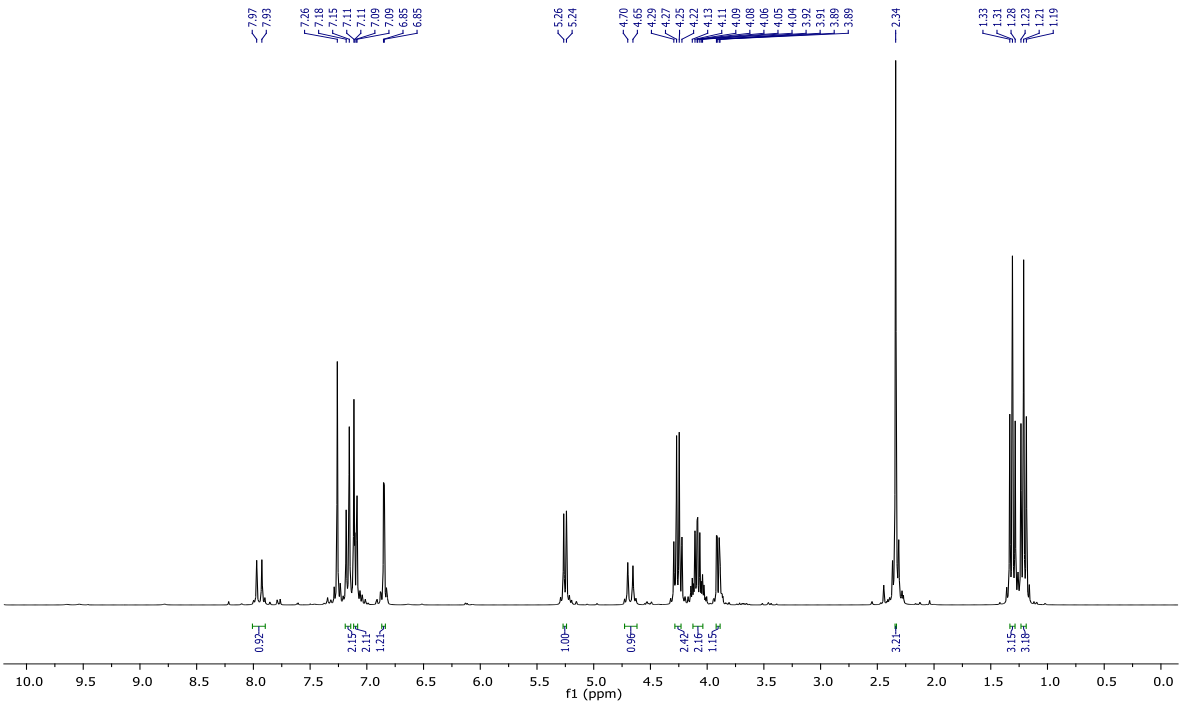

Figure S3.54. ^{1}H NMR spectrum of pyrazole **C3P1**.

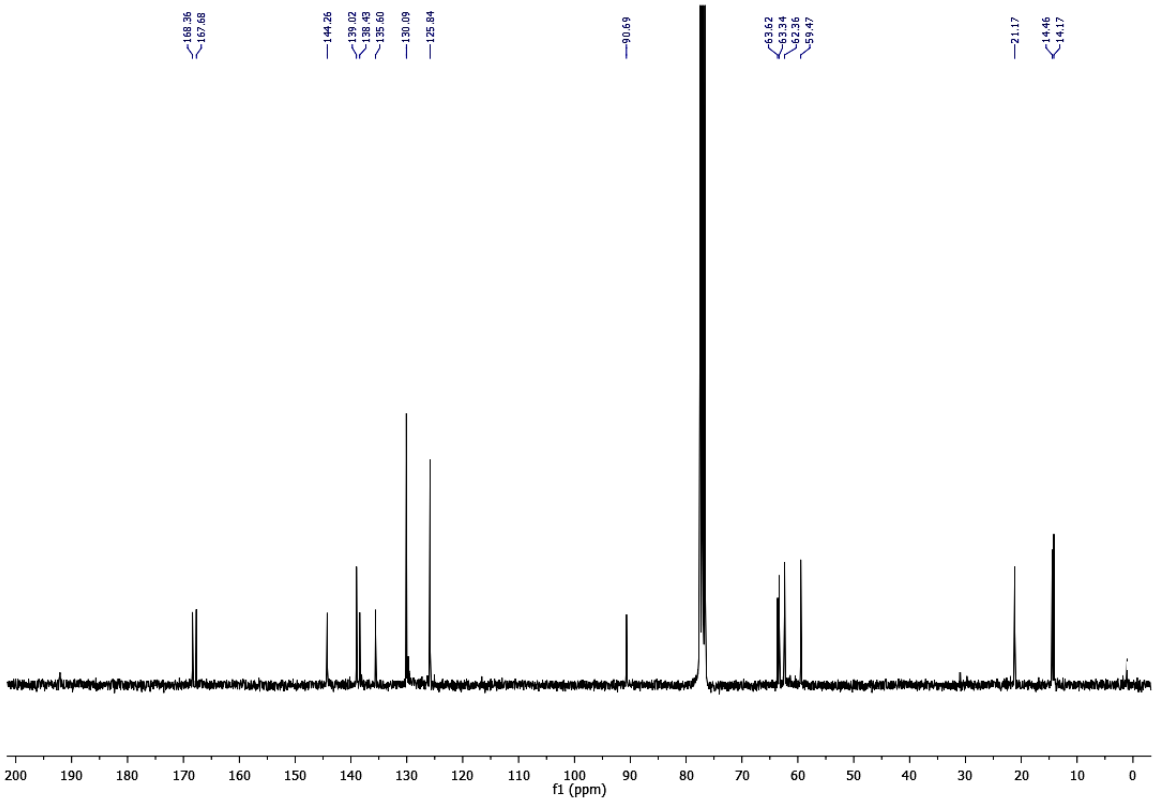

Figure S3.55. ^{13}C NMR spectrum of pyrazole **C3P1**.

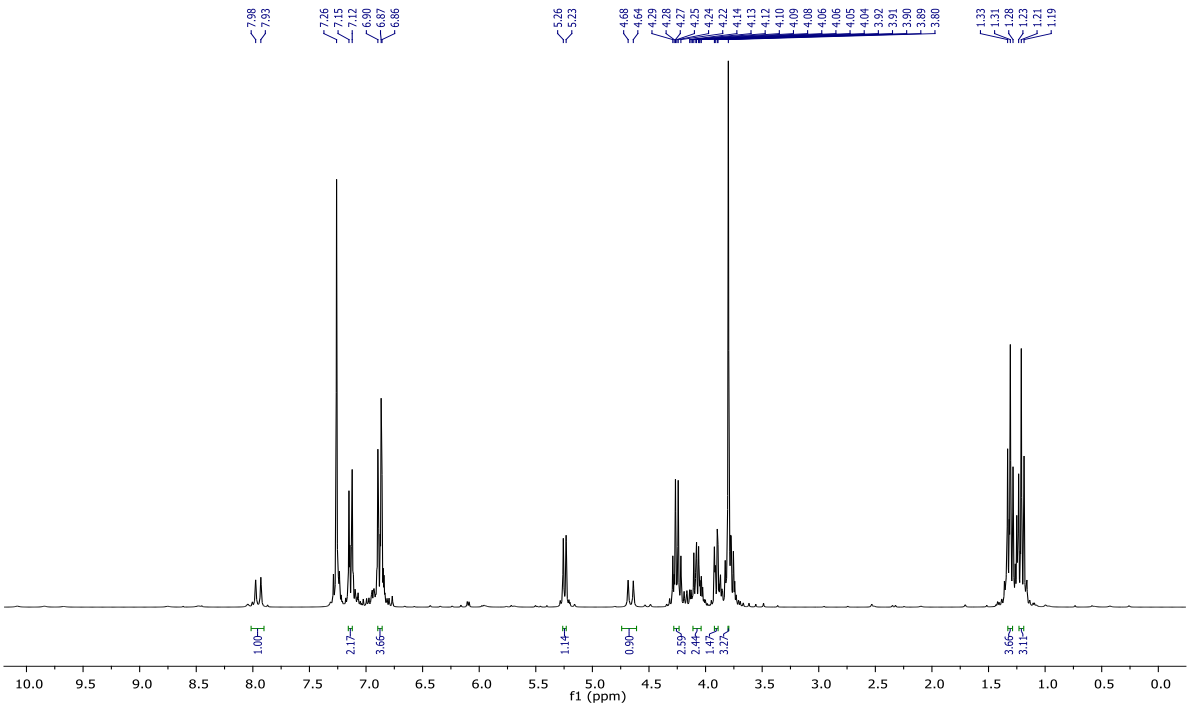

Figure S3.56. ^{1}H NMR spectrum of pyrazole **C3P2**.

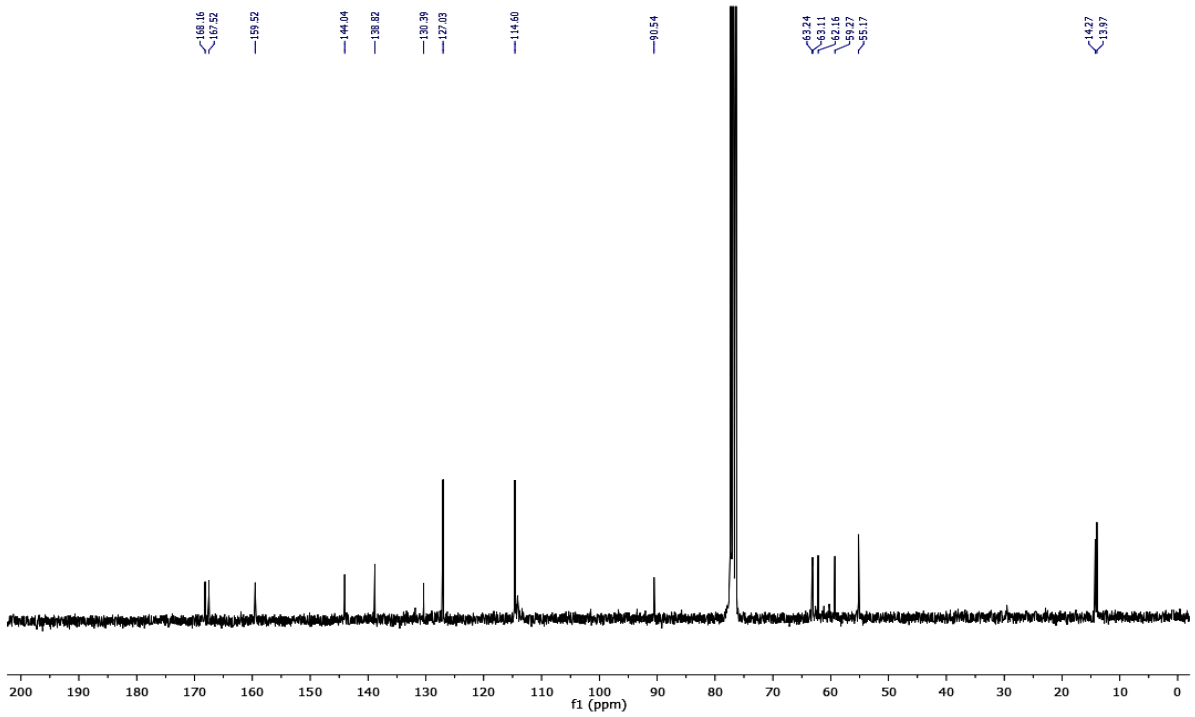

Figure S3.57. ^{13}C NMR spectrum of pyrazole **C3P2**.

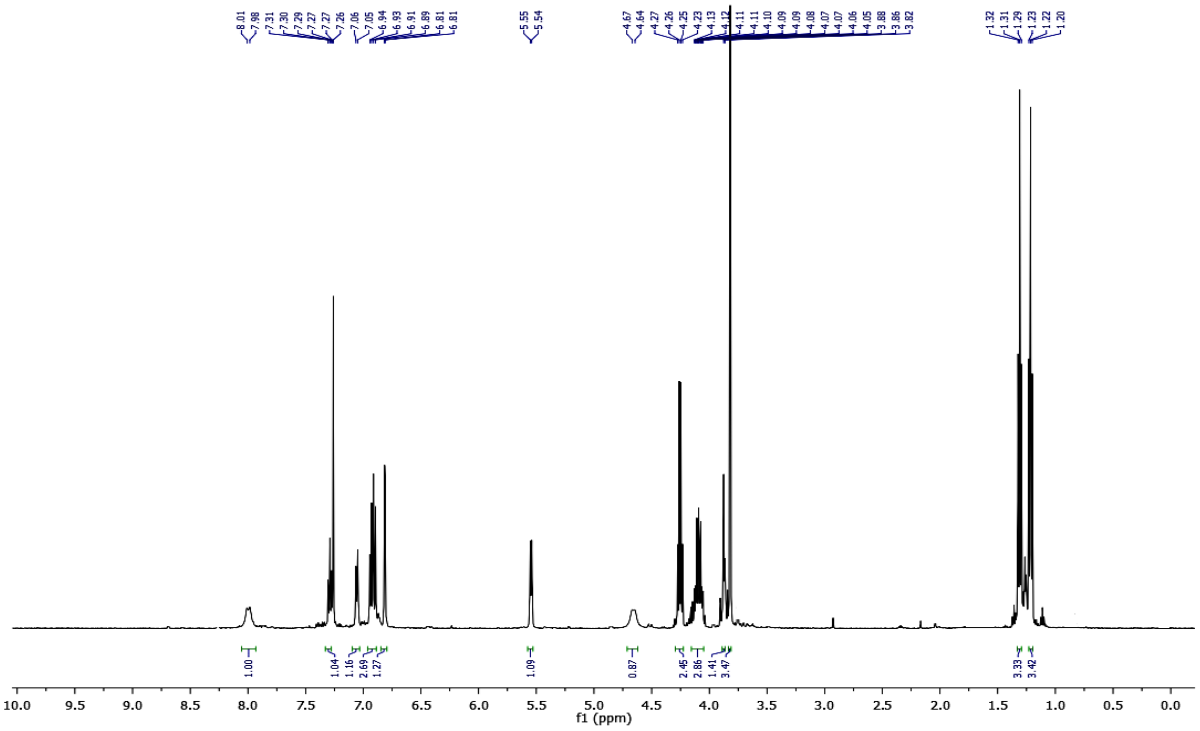

Figure S3.58. ^{1}H NMR spectrum of pyrazole **C3P3**.

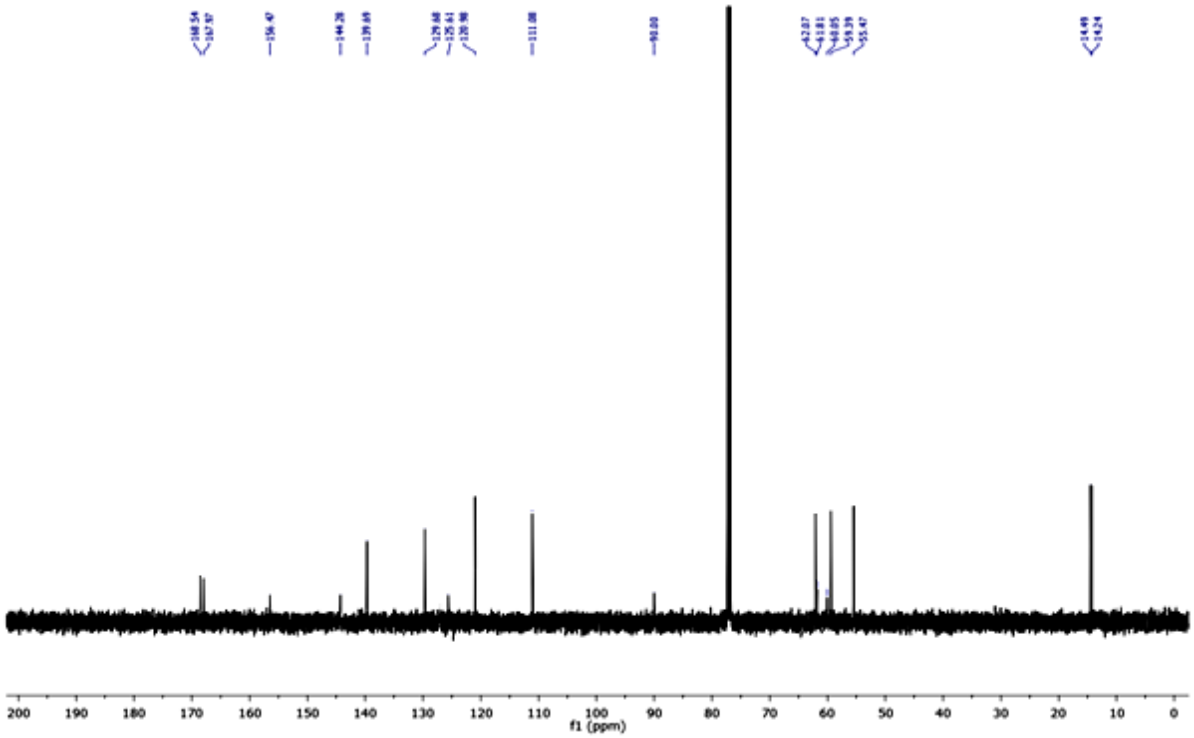

Figure S3.59. ^{13}C NMR spectrum of pyrazole **C3P3**.

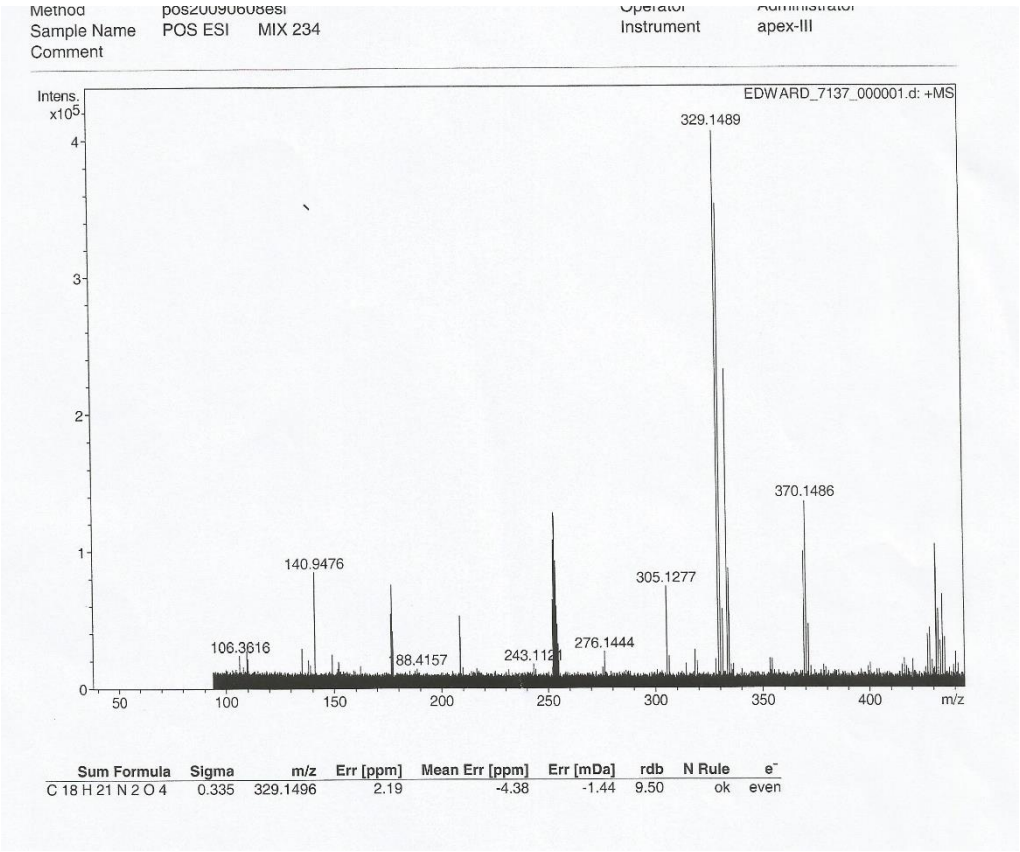

Figure S3.60. HRMS spectrum of pyrazole **C3P1**.

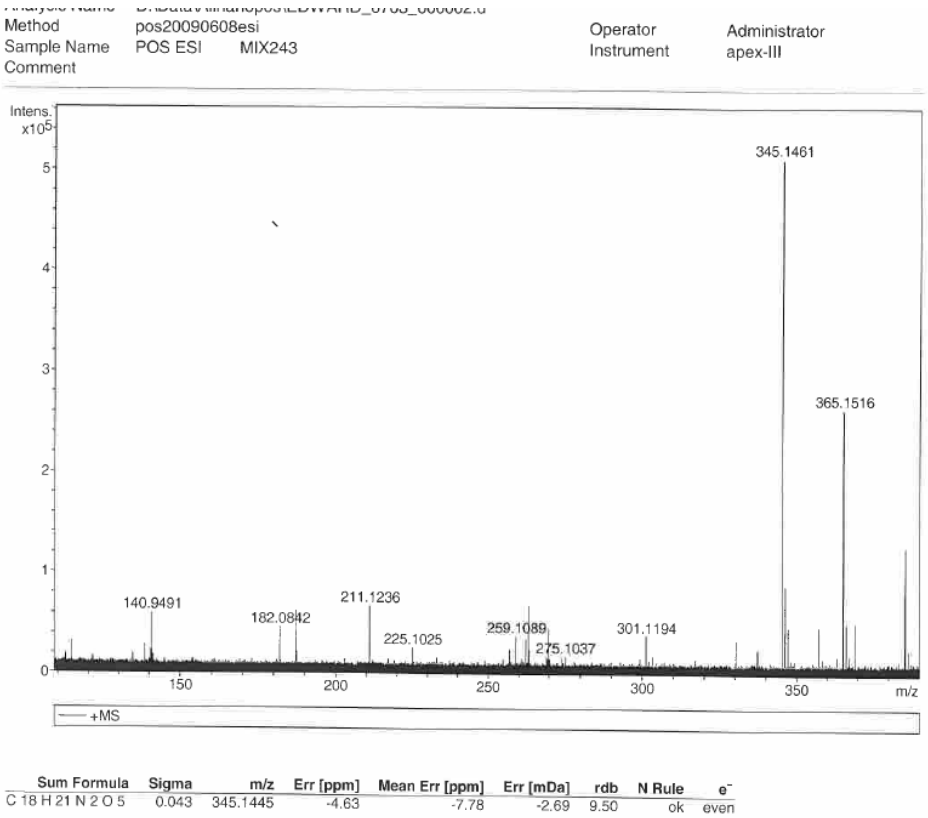

Figure S3.61. HRMS spectrum of pyrazole **C3P2**.

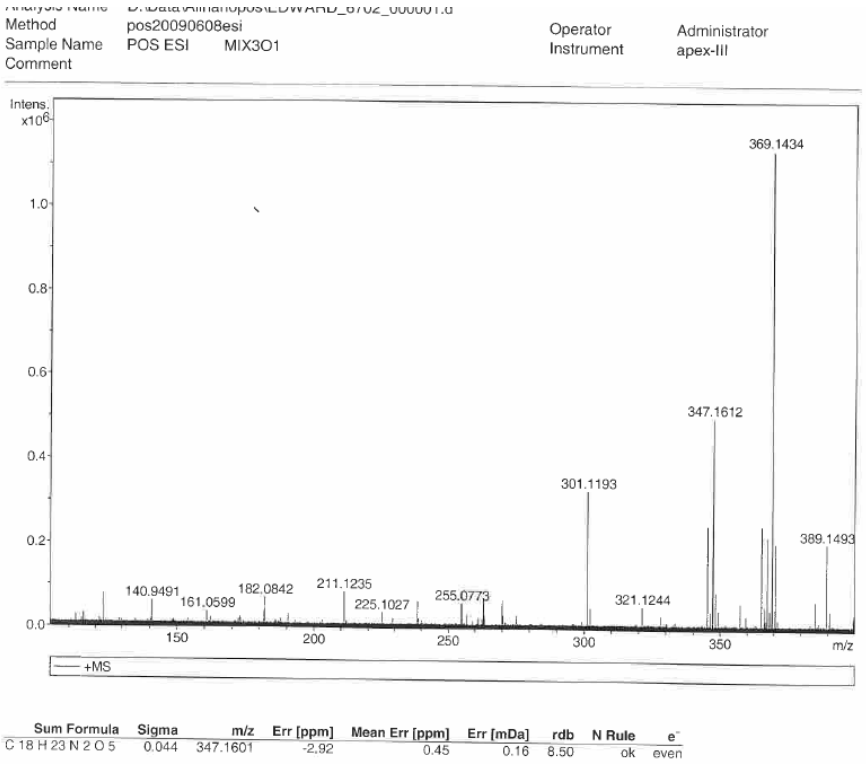

Figure S3.62. HRMS spectrum of pyrazole **C3P3**.

Chapter 4

4.1. Characterization data of 14 – 21

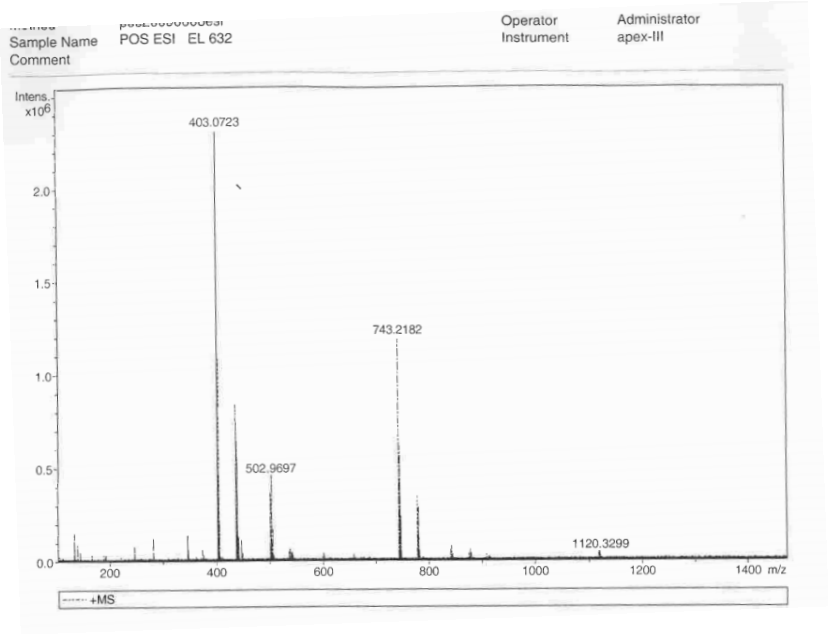

Figure S4.1. ESI-MS data for compound **14** in methanol. Main fragments: 403.07 m/z $[Cu(\mathbf{L^3})]^{1+}$, 438.04 m/z $[Cu(\mathbf{L^3})(Cl)]^{1+}$, 502.96 m/z $[Cu_2(\mathbf{L^3})(Cl)]^{1+}$, 535.95 m/z $[Cu_2(\mathbf{L^3})(Cl)_2]^{1+}$, 743.22 m/z $[Cu(\mathbf{L^3})_2]^{1+}$, 778.18 m/z $[Cu_2(\mathbf{L^3})_2(Cl)]^{1+}$, 1120.33 m/z $[Cu(\mathbf{L^3})_3(Cl) + H]^{1+}$

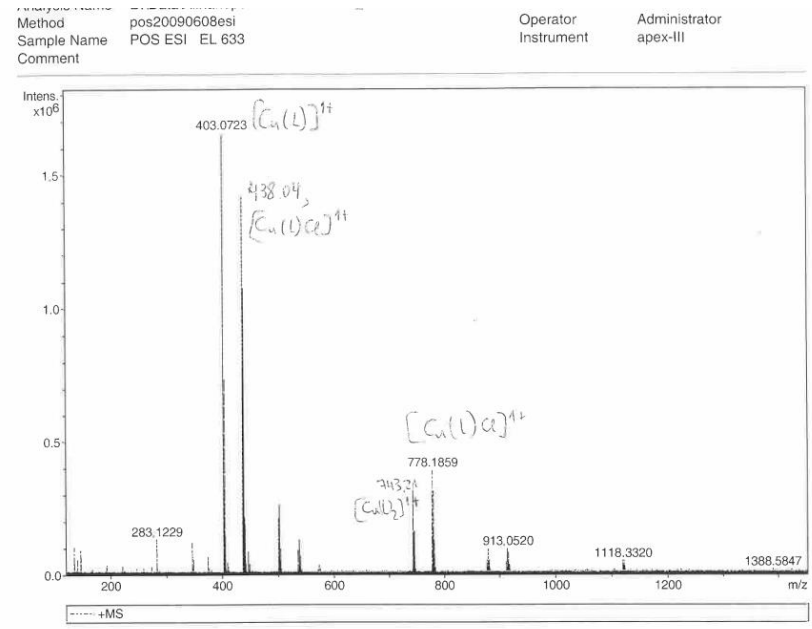

Figure S4.2. ESI-MS data for compound **15** in methanol. Main fragments: Main fragments: 403.07 m/z $[Cu(\mathbf{L^3})]^{1+}$, 438.04 m/z $[Cu(\mathbf{L^3})(Cl)]^{1+}$, 502.96 m/z $[Cu_2(\mathbf{L^3})(Cl)]^{1+}$, 535.95 m/z

$[Cu_2(\mathbf{L^3})(Cl)_2]^{1+}$, 743.22 m/z $[Cu(\mathbf{L^3})_2]^{1+}$, 778.18 m/z $[Cu_2(\mathbf{L^3})_2(Cl)]^{1+}$, 913.05 m/z $[Cu_2(\mathbf{L^3})_2(Cl)_3]^{+1}$, 1118.33 m/z $[Cu(\mathbf{L^3})_3(Cl) + H]^{1+}$

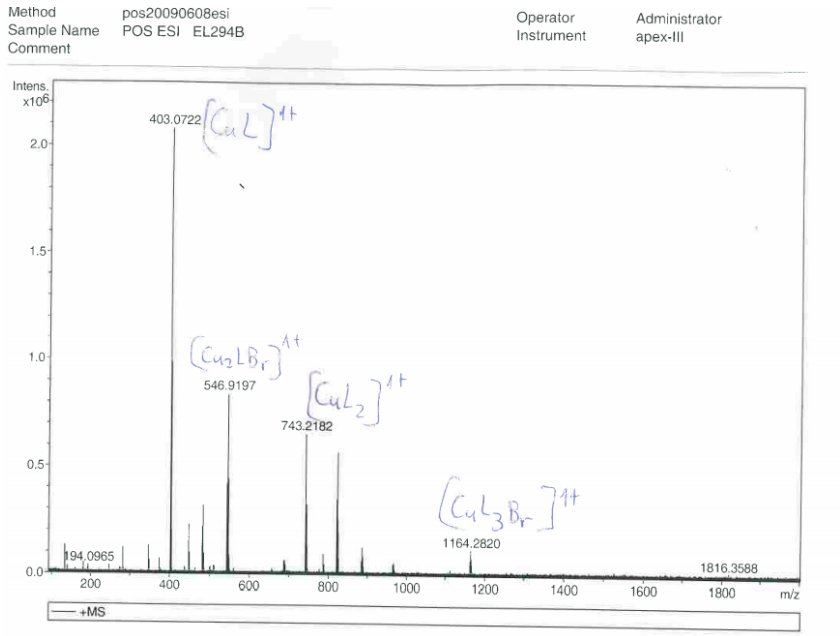

Figure S4.3. ESI-MS data for compound **16** in methanol. Main fragments: 403.07 m/z $[Cu(\mathbf{L^3})]^{1+}$, 443.55 m/z $[Cu_2(\mathbf{L^3})_2(Br)]^{2+}$, 484.00 m/z $[Cu(\mathbf{L^3})(Br)]^{1+}$, 546.91 m/z $[Cu_2(\mathbf{L^3})(Br)]^{1+}$, 743.21 m/z $[Cu(\mathbf{L^3})_2]^{1+}$, 824.13 m/z $[Cu(\mathbf{L^3})_2(Br)]^{1+}$, 887.08 m/z $[Cu_2(\mathbf{L^3})_2(Br)]^{1+}$, 967.98 m/z $[Cu_2(\mathbf{L^3})_2(Br)_2]^{1+}$, 1164.28 m/z $[Cu(\mathbf{L^3})_3(Br)]^{1+}$

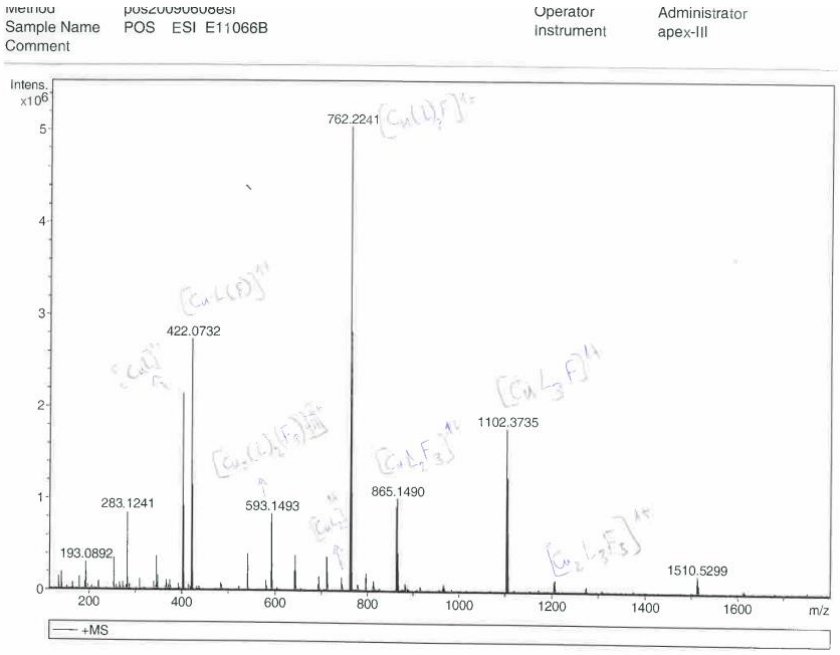

Figure S4.4. ESI-MS data for compound **17** in methanol. Main fragments: 403.07 m/z $[Cu(\mathbf{L^3})]^{1+}$, 422.07 m/z $[Cu(\mathbf{L^3})(F)]^{1+}$, 491.07 m/z $[Cu(\mathbf{L^3})(BF_4)]^{1+}$ (low intensity), 553.04 m/z

$[Cu_2(\mathbf{L^3})(BF_4)]^{1+}$, 593.14 m/z $[Cu_2(\mathbf{L^3})_2(F)_3]^{2+}$, 640.05 m/z $[Cu_2(\mathbf{L^3})(BF_4)_2]^{1+}$, 743.22 m/z $[Cu(\mathbf{L^3})_2]^{1+}$, 762.22 m/z $[Cu(\mathbf{L^3})_2(F)]^{1+}$, 1102.37 m/z $[Cu(\mathbf{L^3})_3(F)]^{1+}$, 1171.39 m/z $[Cu(\mathbf{L^3})_3(BF_4)]^{1+}$ (low intensity), 1203.31 m/z $[Cu_2(\mathbf{L^3})_2(F)_3]^{1+}$

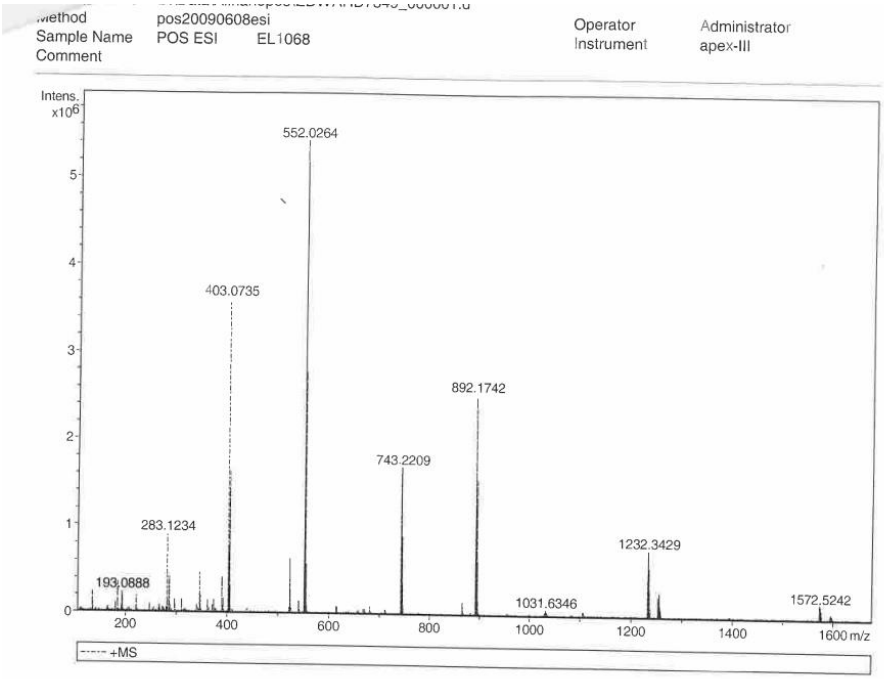

Figure S4.5. ESI-MS data for compound **18** in methanol. Main fragments: 403.07 m/z $[Cu(\mathbf{L^3})]^{+1}$, 552.02 m/z $[Cu(\mathbf{L^3})(CF_3SO_3)]^{+1}$, 614.95 m/z $[Cu_2(\mathbf{L^3})(CF_3SO_3)]^{+1}$, 743.22 m/z $[Cu(\mathbf{L^3})_2]^{1+}$, 892.18 m/z $[Cu(\mathbf{L^3})_2(CF_3SO_3)]^{+1}$, 1106.10 m/z $[Cu_2(\mathbf{L^3})_2(CF_3SO_3)2]^{+1}$, 1232.34 m/z $[Cu(\mathbf{L^3})_3(CF_3SO_3)]^{+1}$, 1255.03 m/z $[Cu_2(\mathbf{L^3})_2(CF_3SO_3)_3]^{+1}$, 1572.52 m/z $[Cu(\mathbf{L^3})_4(CF_3SO_3)]^{+1}$

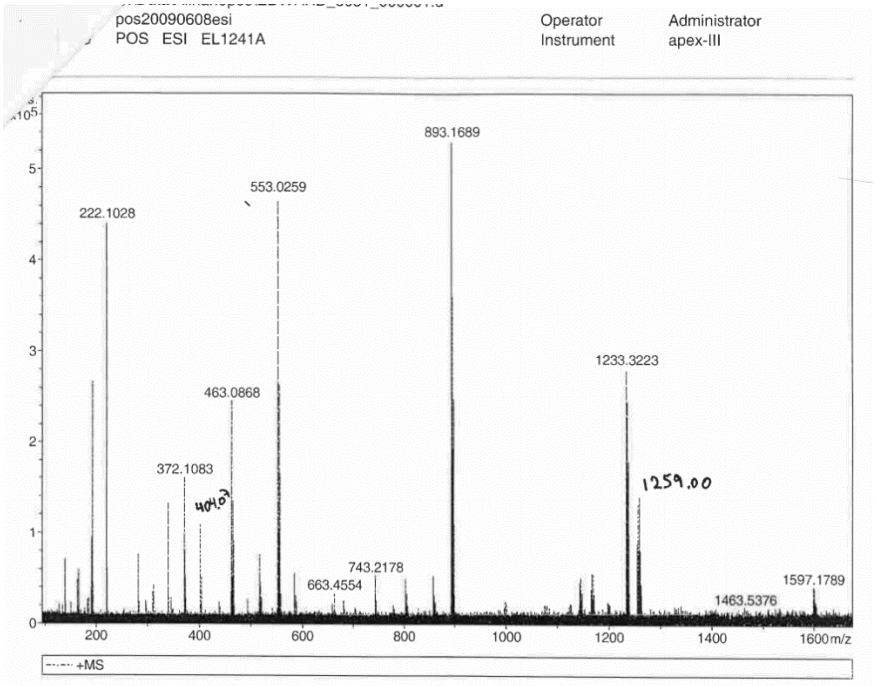

Figure S4.6. ESI-MS data for compound **19** in methanol. Main fragments: 372.10 m/z [$\mathbf{L^3}$ + MeOH]$^{1+}$, 404.07 m/z [Zn($\mathbf{L^3}$)]$^{+1}$, 468.08 m/z [Zn_2($\mathbf{L^3}$)]$^{+1}$, 553.02 m/z [Zn($\mathbf{L^3}$)(CF_3SO_3)]$^{+1}$, 743.22 m/z [Zn($\mathbf{L^3}$)$_2$]$^{1+}$, 893.17 m/z [Zn($\mathbf{L^3}$)$_2$(CF_3SO_3)]$^{+1}$, 1233.32 m/z [Zn($\mathbf{L^3}$)$_3$(CF_3SO_3)]$^{+1}$, 1259.00 m/z [Zn_2($\mathbf{L^3}$)$_2$(CF_3SO_3)$_3$]$^{+1}$, 1597.18 m/z [Zn_2($\mathbf{L^3}$)$_3$(CF_3SO_3)$_3$]$^{+1}$

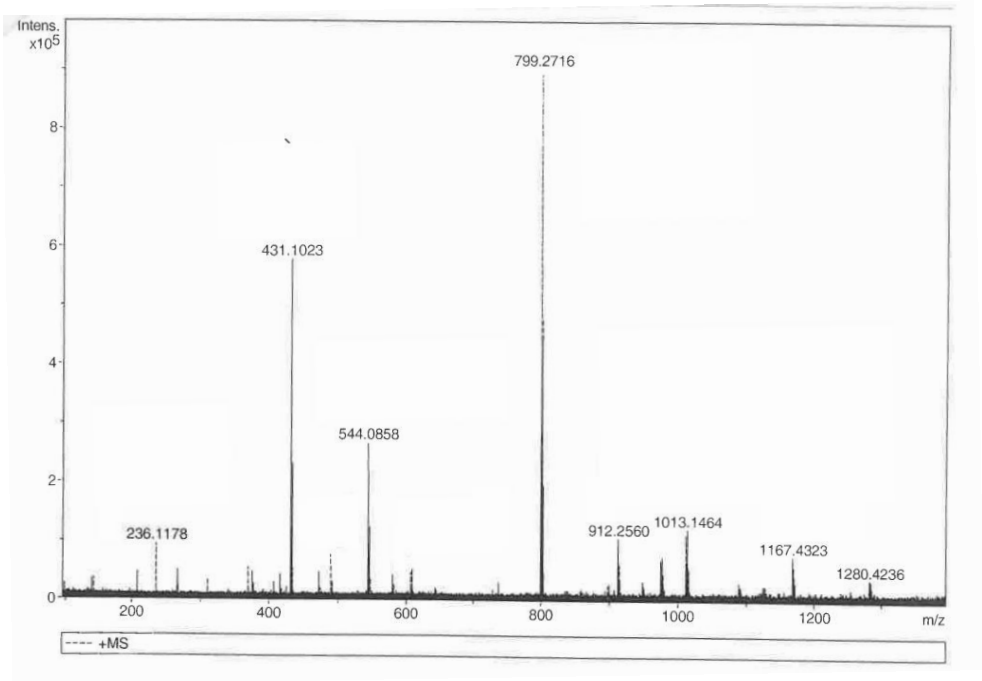

Figure S4.7. ESI-MS data for compound **20** in methanol. Main fragments: 431.10 m/z [Cu($\mathbf{L^4}$)]$^{+1}$, 494.09 m/z [Cu_2($\mathbf{L^4}$)]$^{1+}$, 544.08 m/z [Cu_2($\mathbf{L^4}$)(MeOH)(H_2O)]$^{1+}$, 580.06 m/z

$[Cu(\mathbf{L^4})(CF_3SO_3)]^{+1}$, 799.27 m/z $[Cu(\mathbf{L^4})_2]^{1+}$, 912.25 m/z $[Cu_2(\mathbf{L^4})_2(MeOH)(H_2O)]^{1+}$, 948.22 m/z $[Cu(\mathbf{L^4})_2(CF_3SO_3)]^{+1}$, 977.18 m/z $[Cu_3(\mathbf{L^4})_2(MeOH)(H_2O)]^{1+}$, 1013.14 m/z $[Cu_2(\mathbf{L^4})_2(CF_3SO_3)]^{+1}$, 1167.43 m/z $[Cu(\mathbf{L^4})_3]^{+1}$, 1280.42 m/z $[Cu_2(\mathbf{L^4})_3(MeOH)(H_2O)]^{1+}$

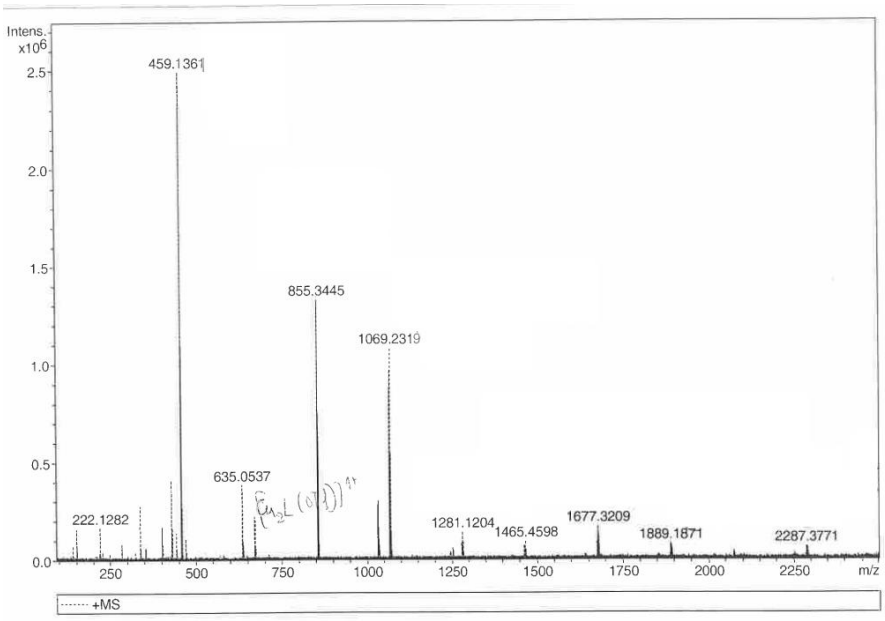

Figure S4.8. ESI-MS data for compound **21** in methanol. Main fragments: 459.19 m/z $[Cu(\mathbf{L^5})]^{+1}$, 635.05 m/z $[Cu(\mathbf{L^5})_2(CF_3SO_3)_3]^{+2}$, 671.03 m/z $[Cu_2(\mathbf{L^5})(CF_3SO_3)]^{+1}$, 855.34 m/z $[Cu(\mathbf{L^5})_2]^{1+}$, 1069.23 m/z $[Cu_2(\mathbf{L^5})_2(CF_3SO_3)]^{+1}$, 1281.12 m/z $[Cu_3(\mathbf{L^5})_2(CF_3SO_3)_2]^{+1}$, 1465.46 m/z $[Cu_2(\mathbf{L^5})_2(CF_3SO_3)]^{+1}$, 1677.32 m/z $[Cu_3(\mathbf{L^5})_3(CF_3SO_3)_2]^{+1}$, 1889.18 m/z $[Cu_4(\mathbf{L^5})_3(CF_3SO_3)_3]^{+1}$, 2287.37 m/z $[Cu_4(\mathbf{L^5})_4(CF_3SO_3)_3]^{+1}$

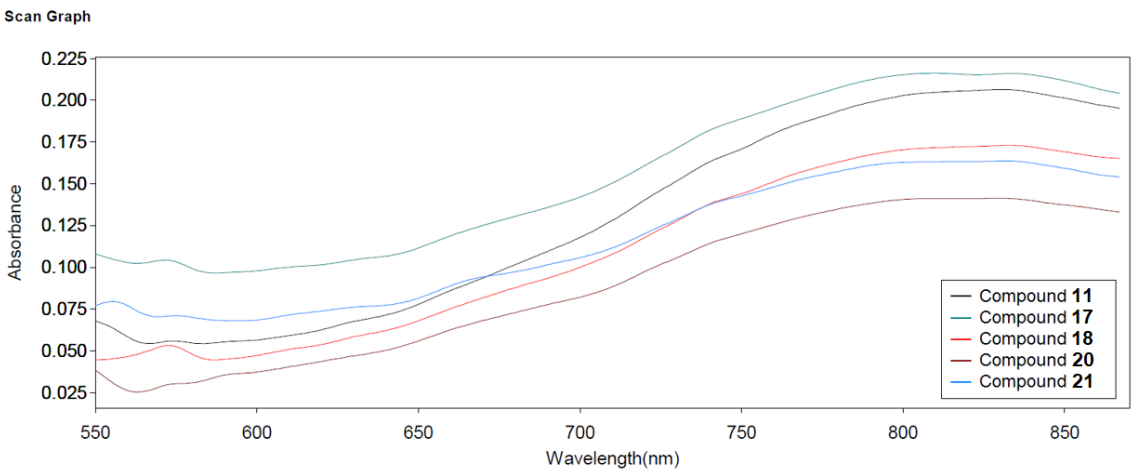

Figure S4.9. Overlay of the UV-Vis spectra for compounds **11**, **17**, **18**, **20**, **21** in methanol, in the region of 550-870 nm.

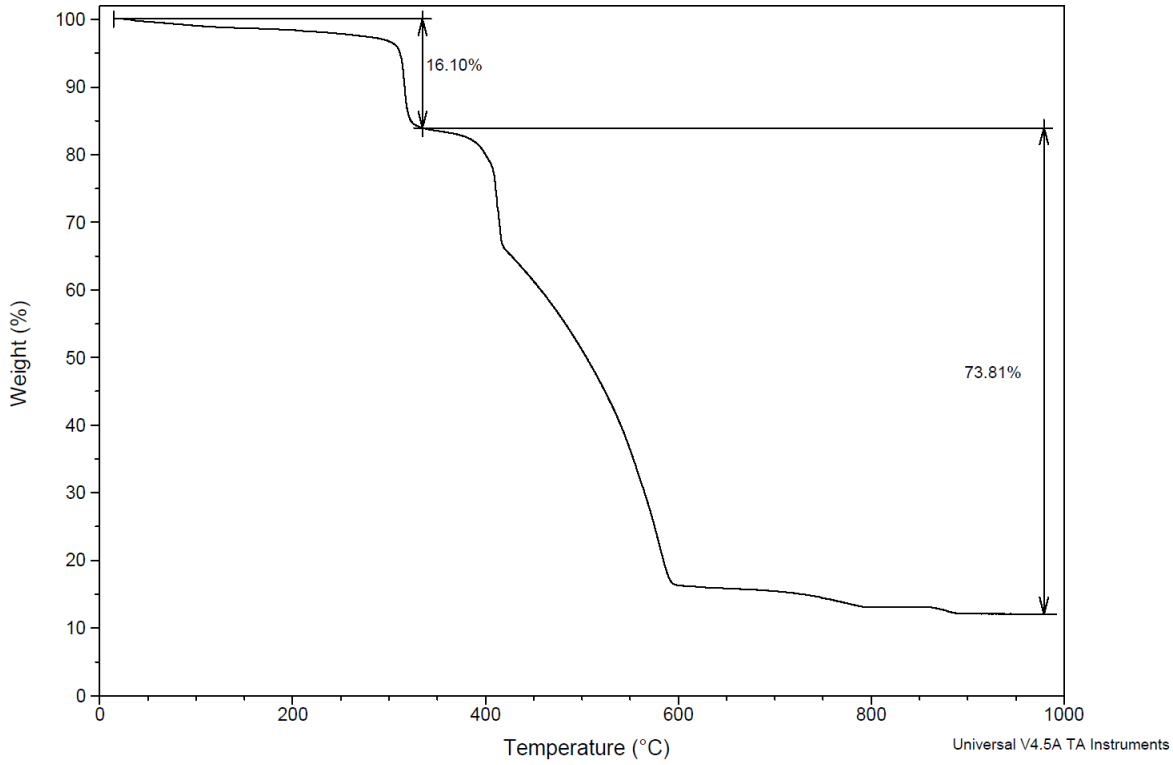

Figure S4.10. TGA graph for compound **14**.

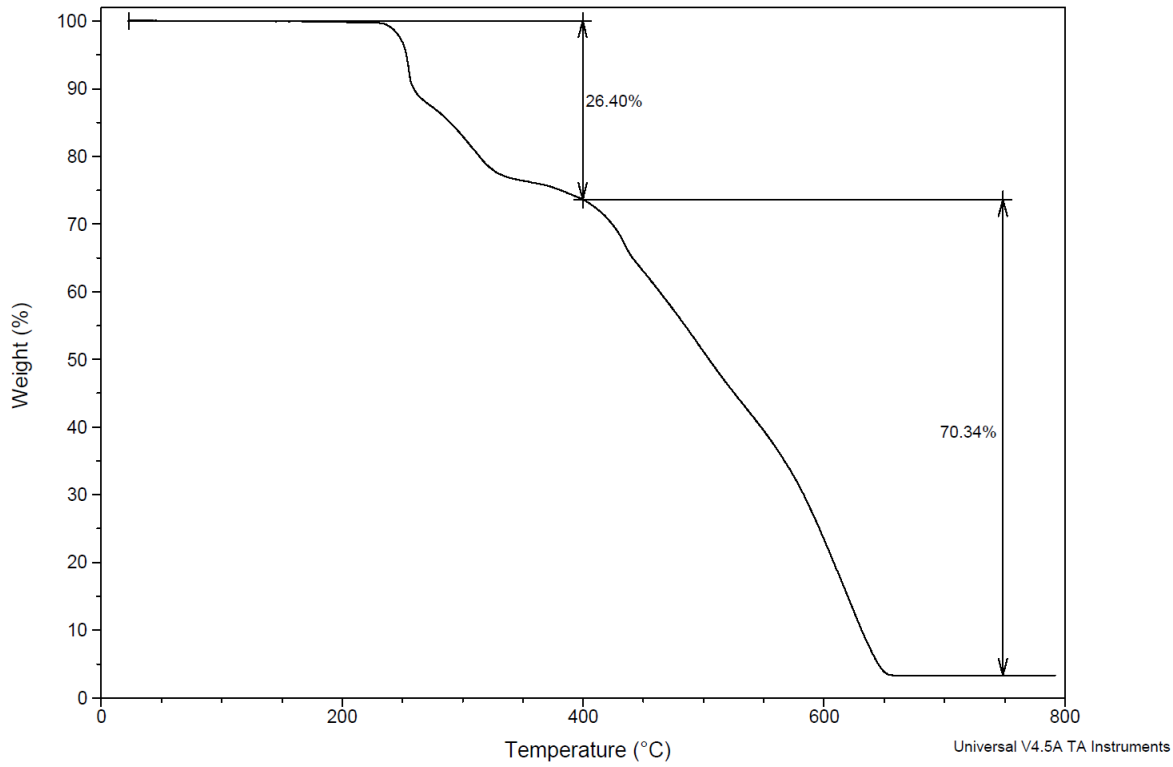

Figure S4.11. TGA graph for compound **15**.

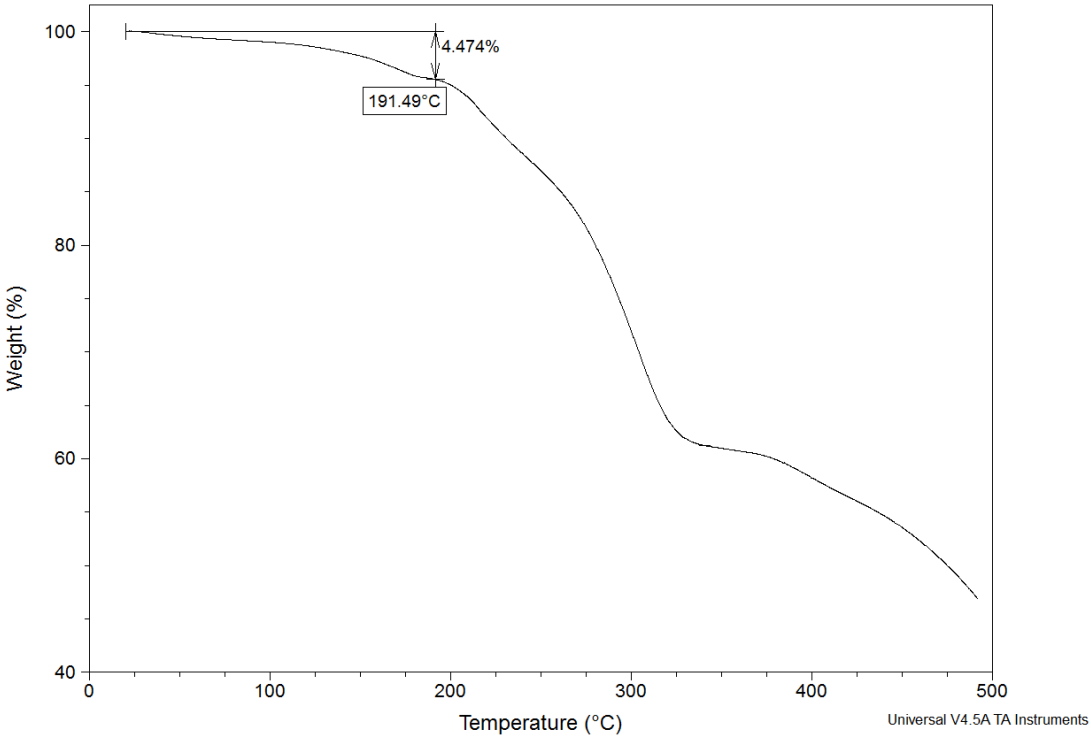

Figure S4.12. TGA graph for compound **16**.

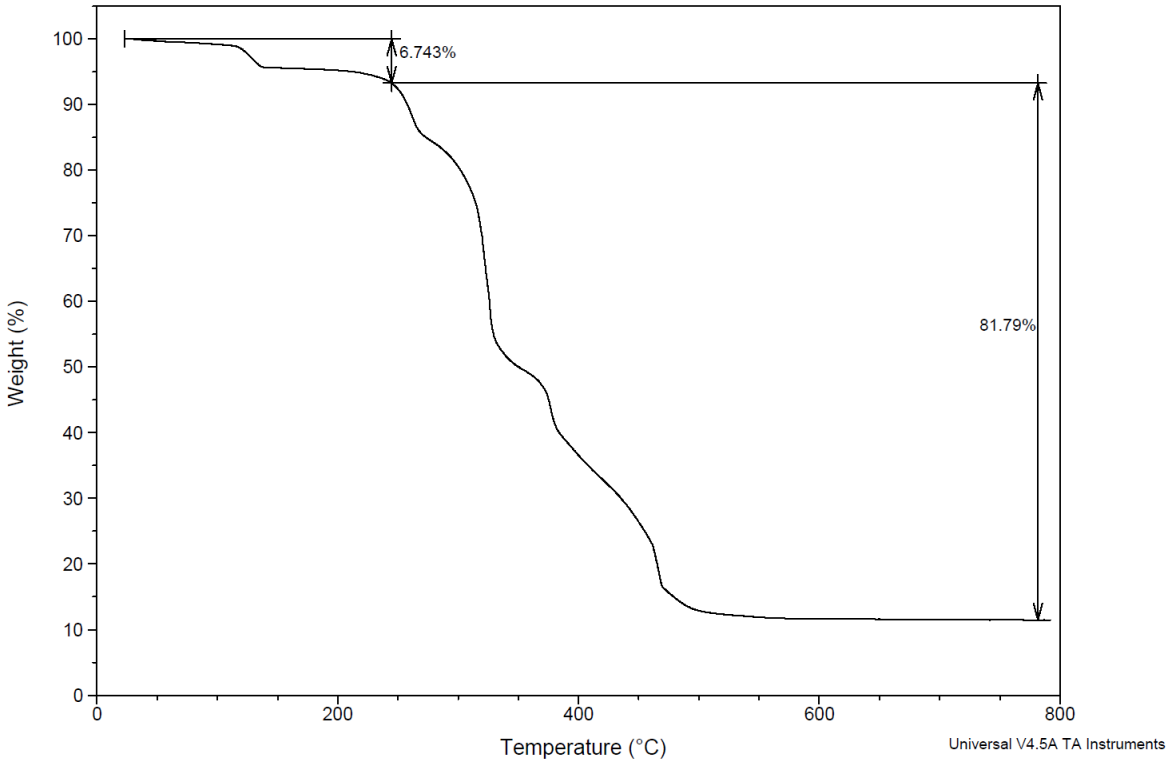

Figure S4.13. TGA graph for compound **17**.

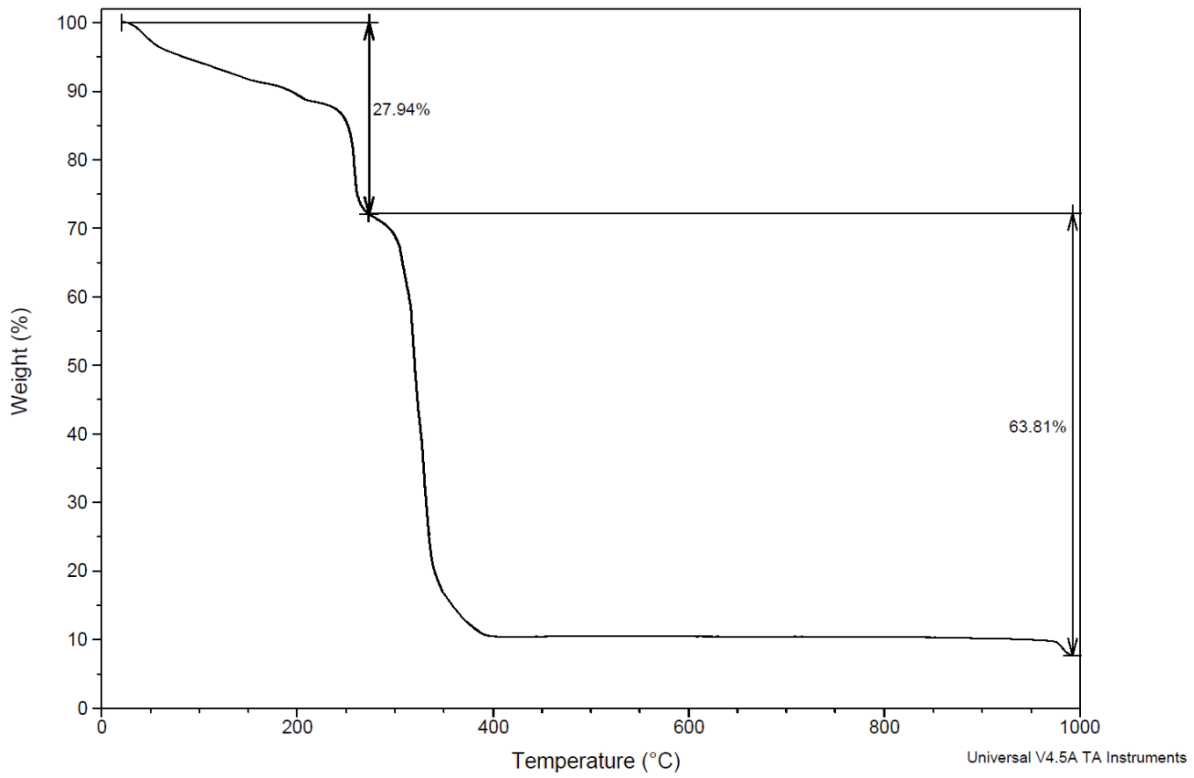

Figure S4.14. TGA graph for compound **18**.

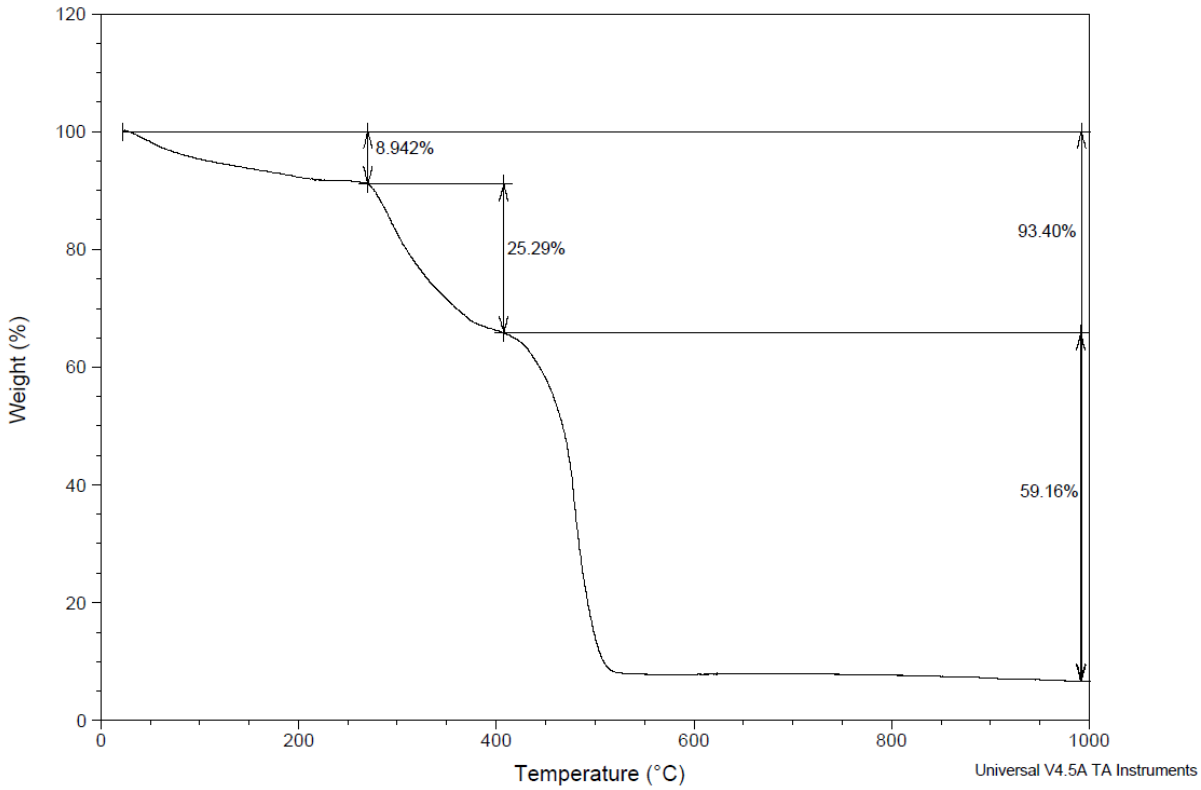

Figure S4.15. TGA graph for compound **19**.

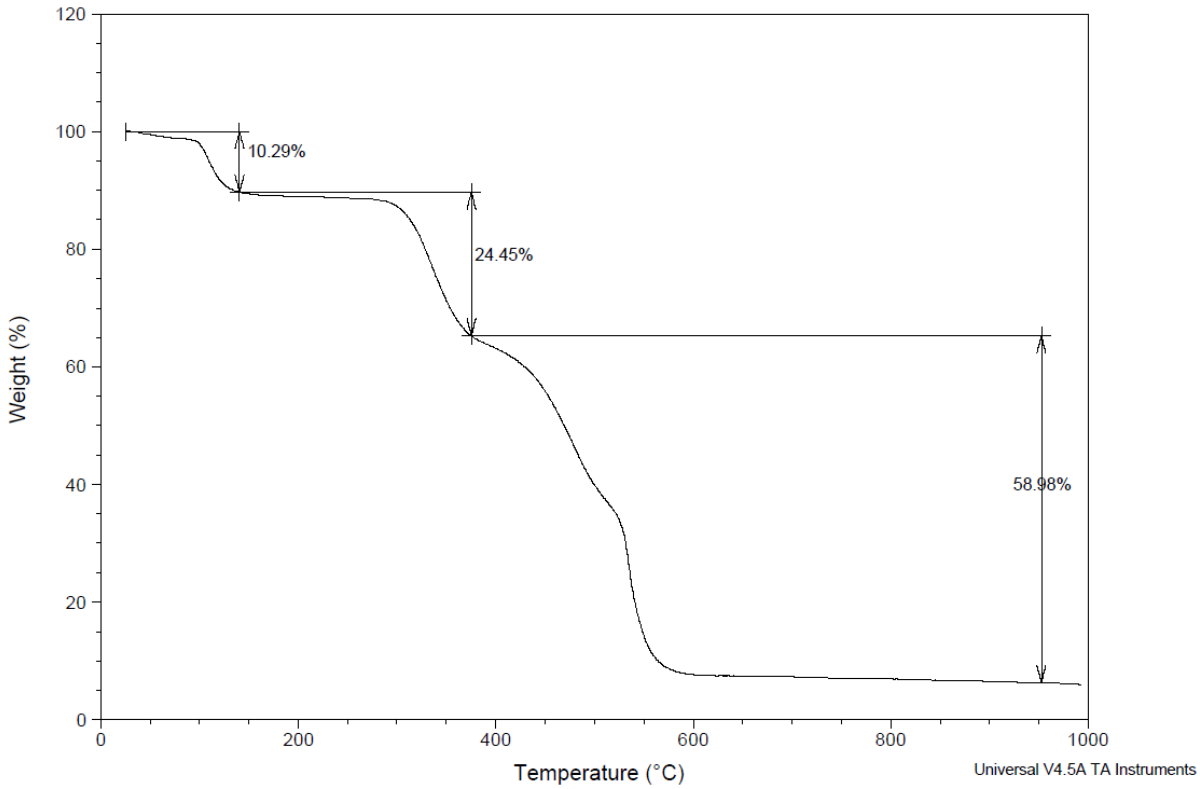

Figure S4.16. TGA graph for compound **20**.

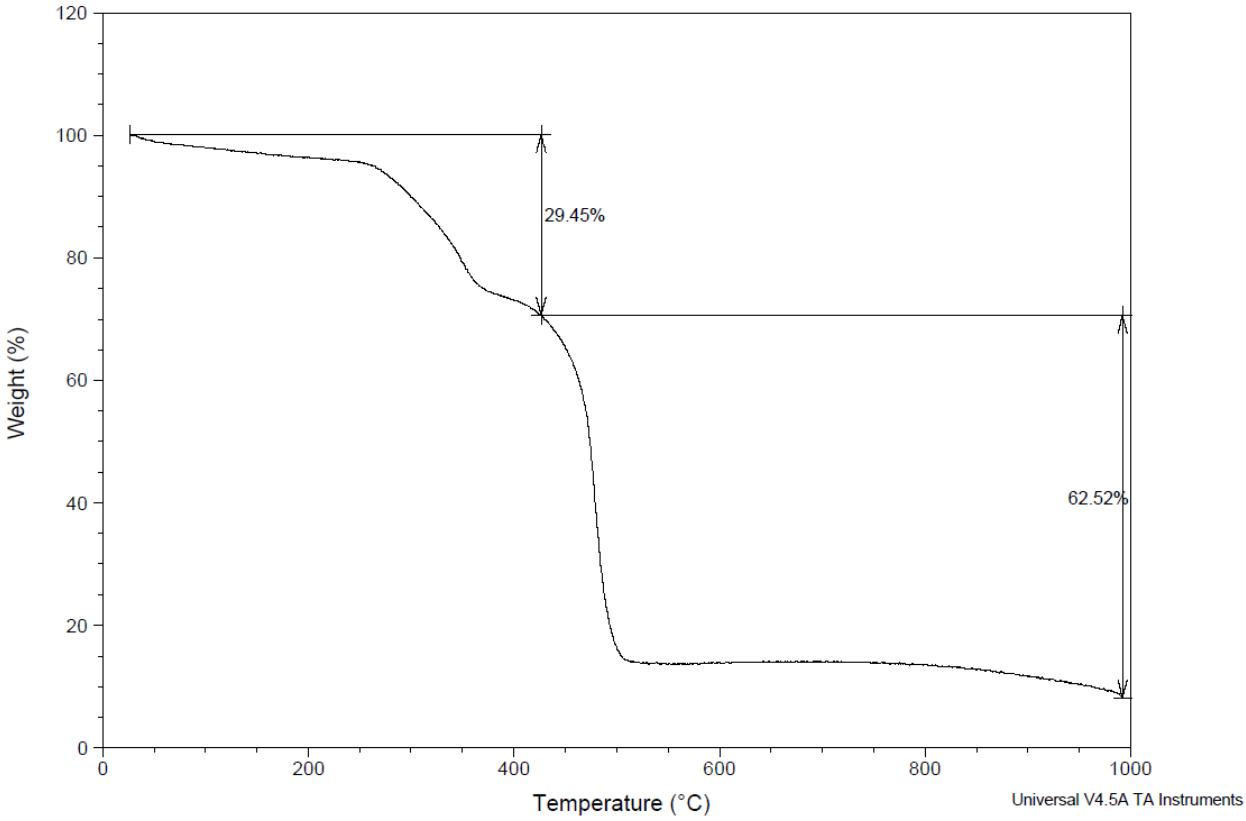

Figure S4.17. TGA graph for compound **21**.

4.2. ^{1}H, ^{13}C NMR and HRMS spectra of propargylamines

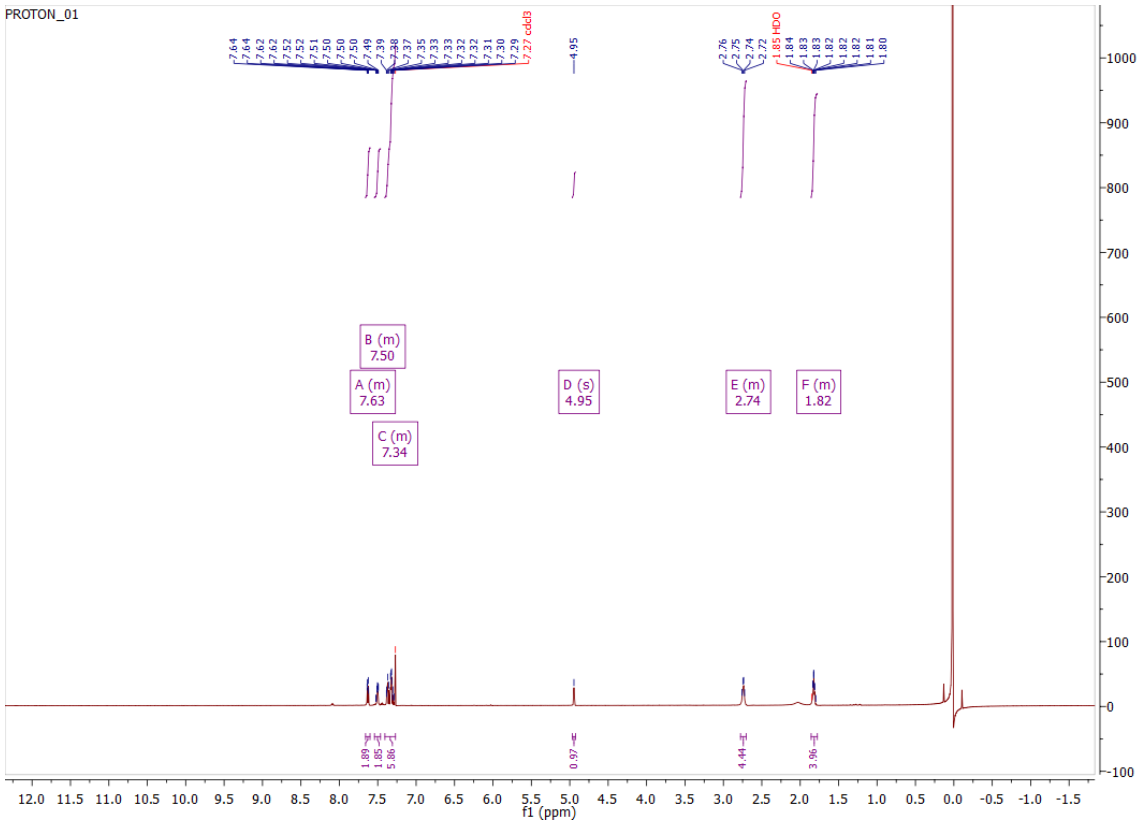

Figure S4.18. ^{1}H NMR spectrum of propargylamine **C4P1**.

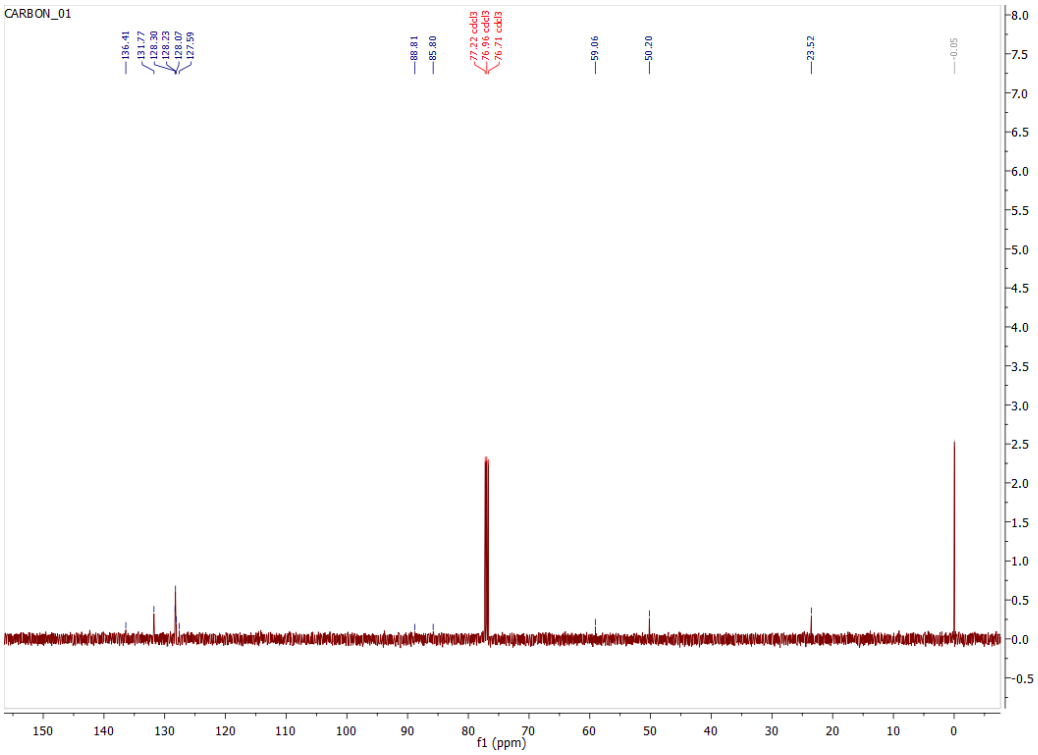

Figure S4.19. ^{13}C NMR spectrum of propargylamine **C4P1**.

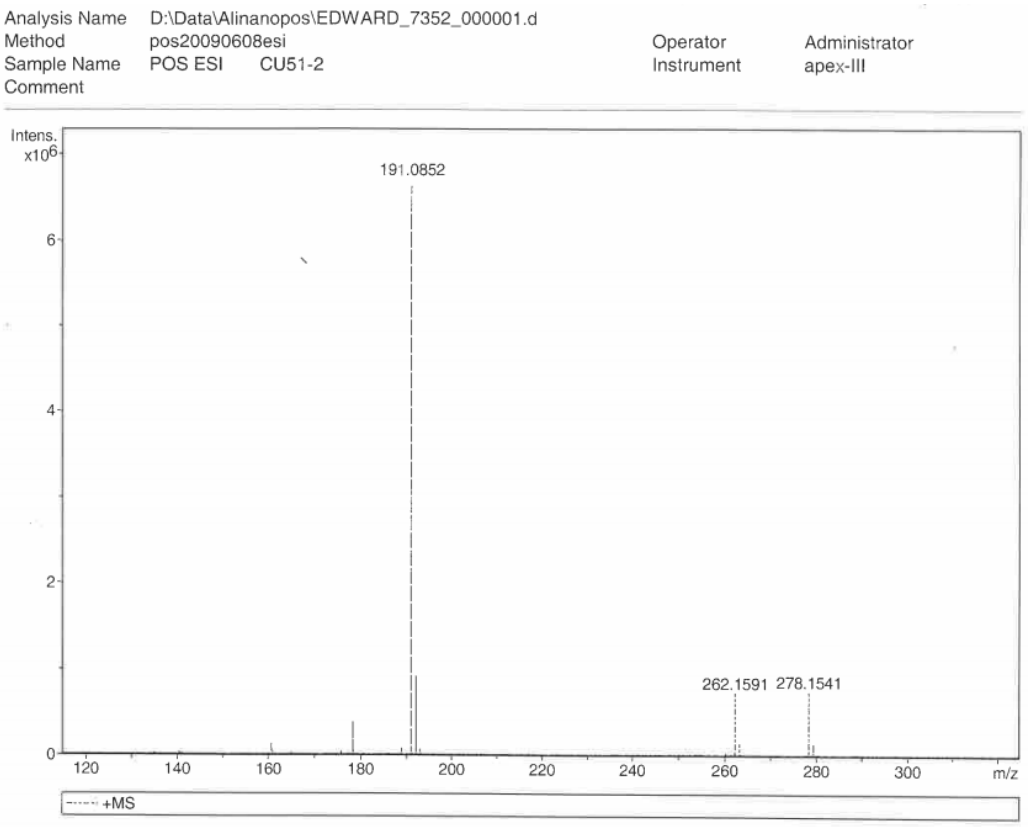

Sum Formula	Sigma	m/z	Err [ppm]	Mean Err [ppm]	Err [mDa]	rdb	N Rule	e⁻
C 19 H 20 N 1	0.017	262.1590	-0.32	-1.00	-0.26	10.50	ok	even

Figure S4.20. HRMS spectrum of propargylamine **C4P1**.

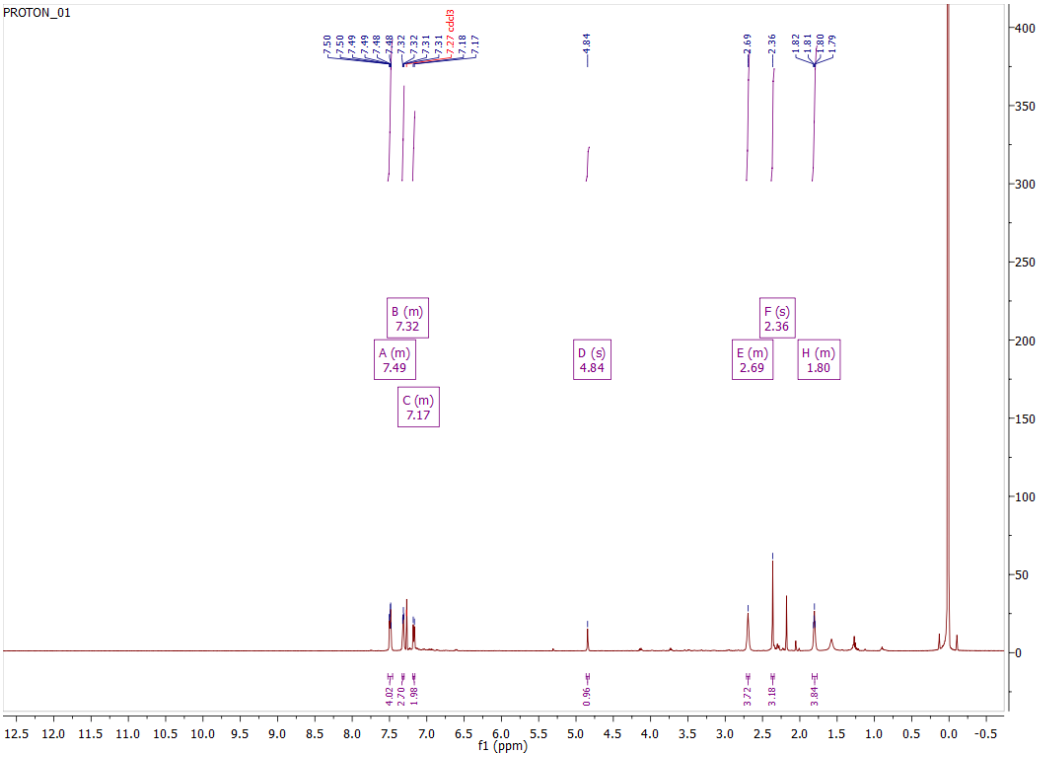

Figure S4.21. ^{1}H NMR spectrum of propargylamine **C4P2**.

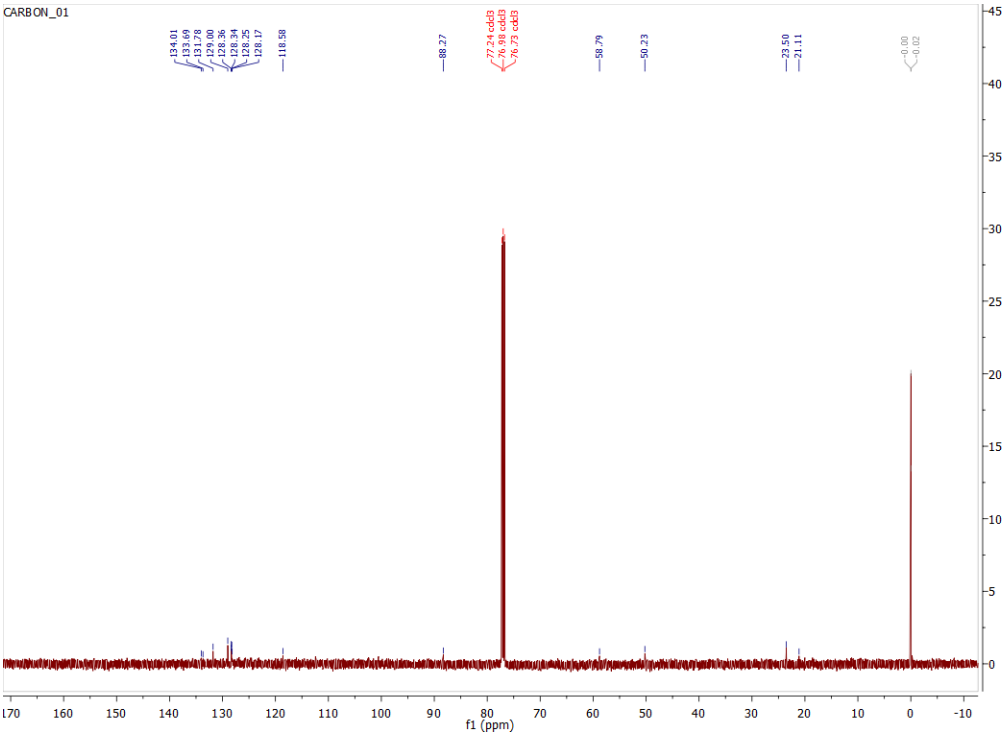

Figure S4.22. ^{13}C NMR spectrum of propargylamine **C4P2**.

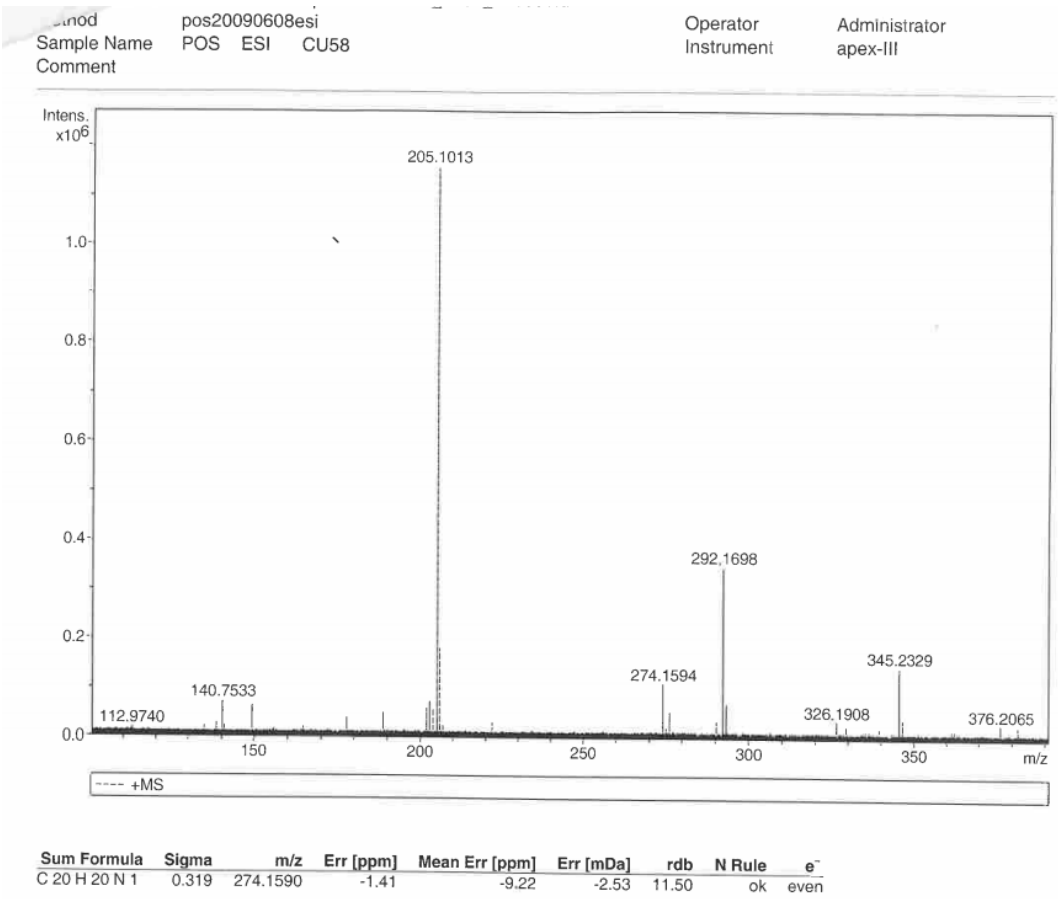

Figure S4.23. HRMS spectrum of propargylamine **C4P2**.

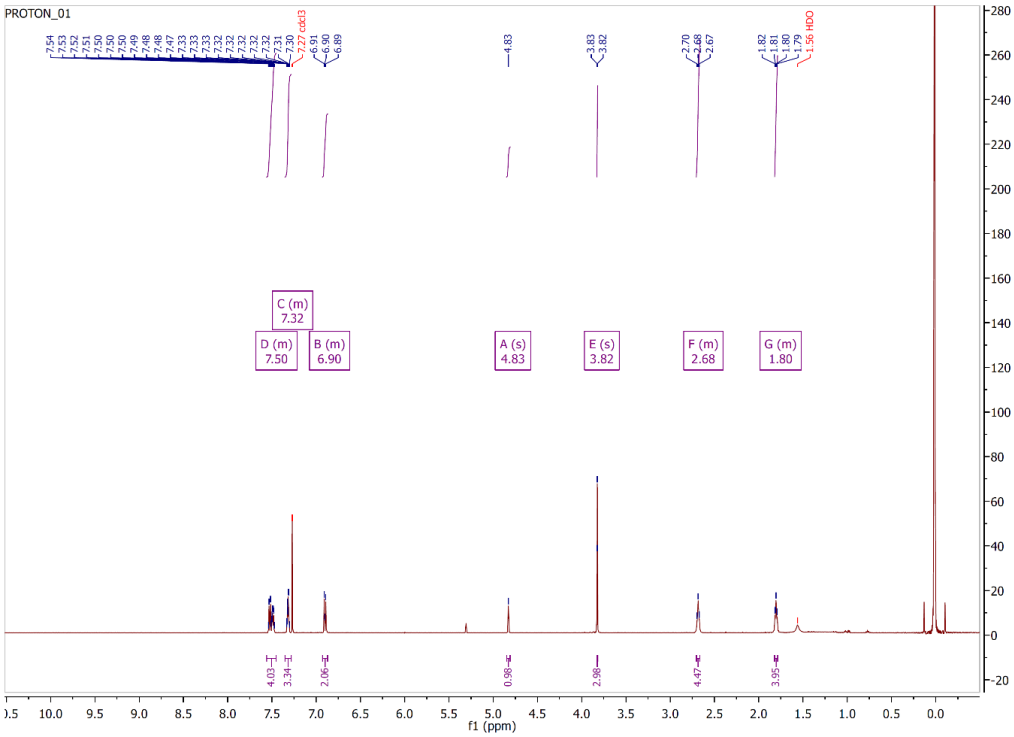

Figure S4.24. ^{1}H NMR spectrum of propargylamine **C4P3**.

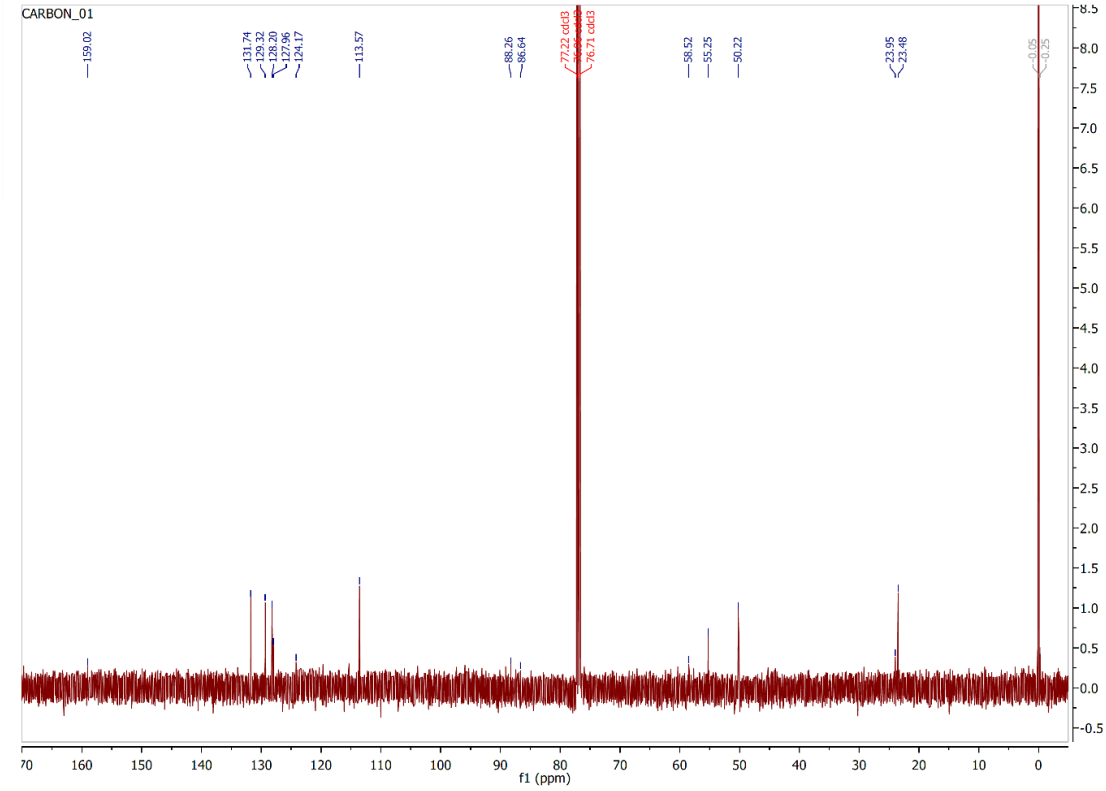

Figure S4.25. ^{13}C NMR spectrum of propargylamine **C4P3**.

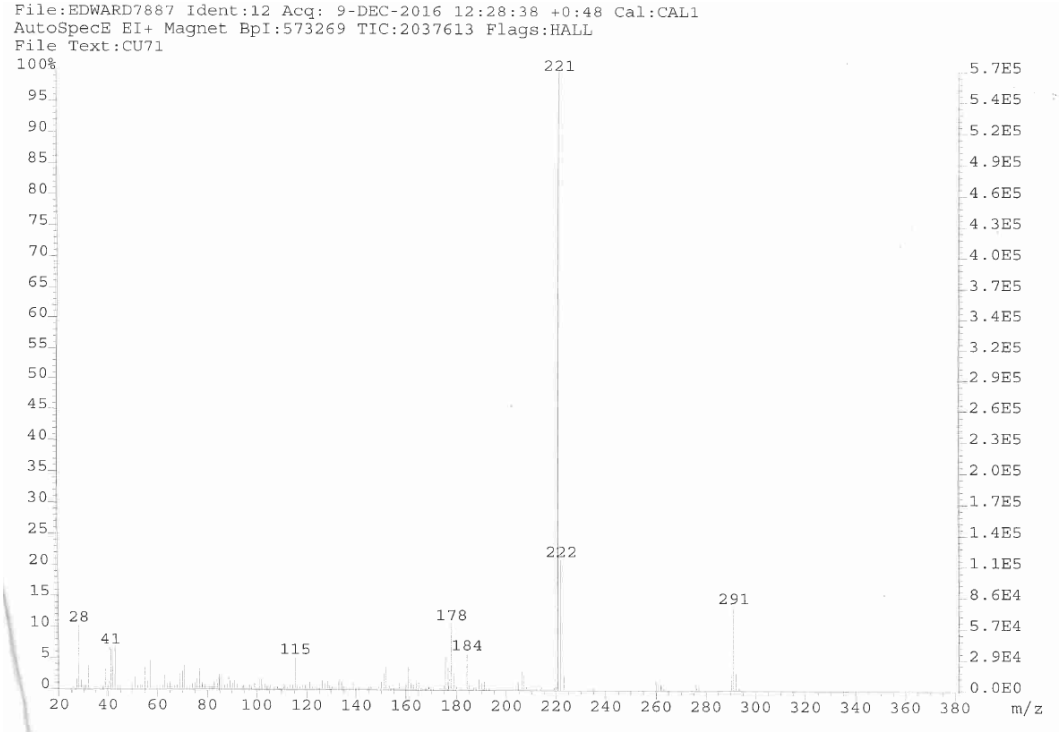

Figure S4.26. EI spectrum of propargylamine **C4P3**.

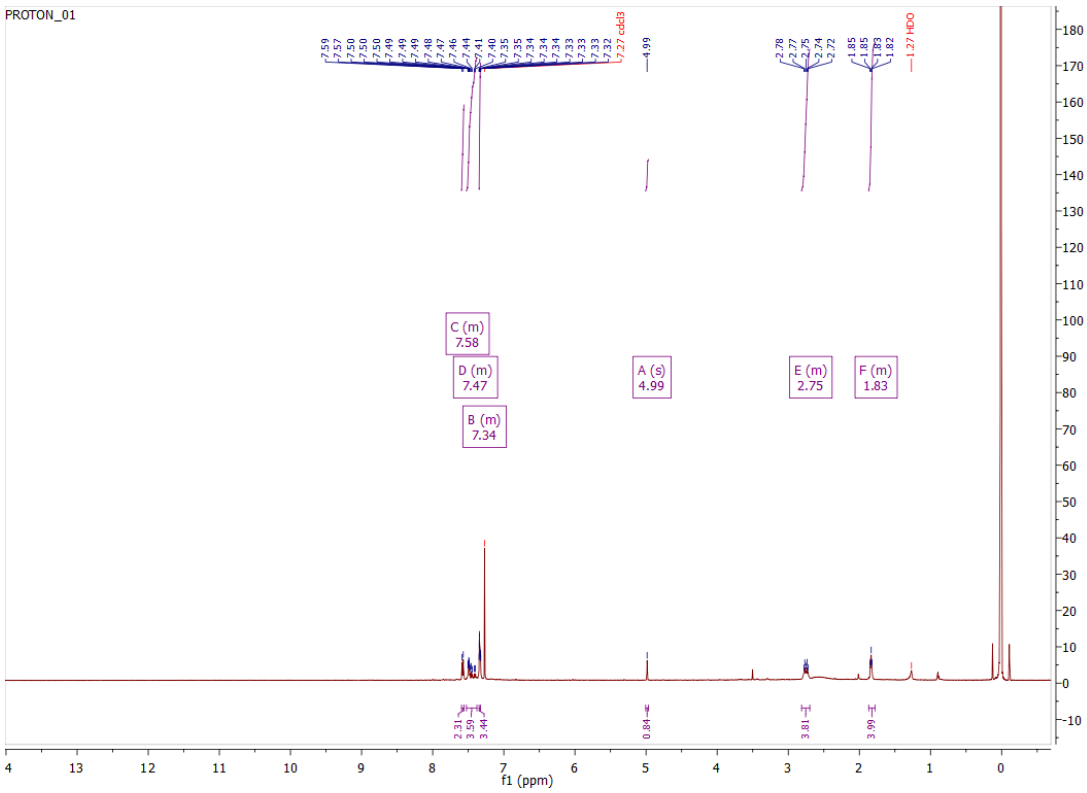

Figure S4.27. ^{1}H NMR spectrum of propargylamine **C4P4**.

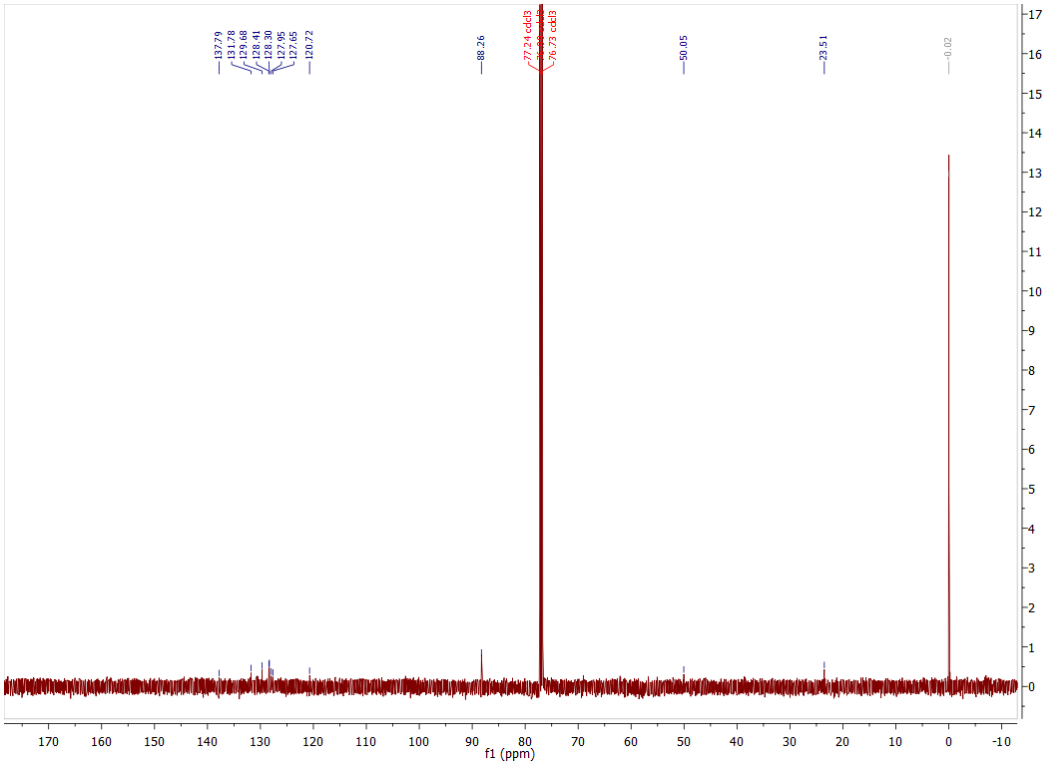

Figure S4.28. ^{13}C NMR spectrum of propargylamine **C4P4**.

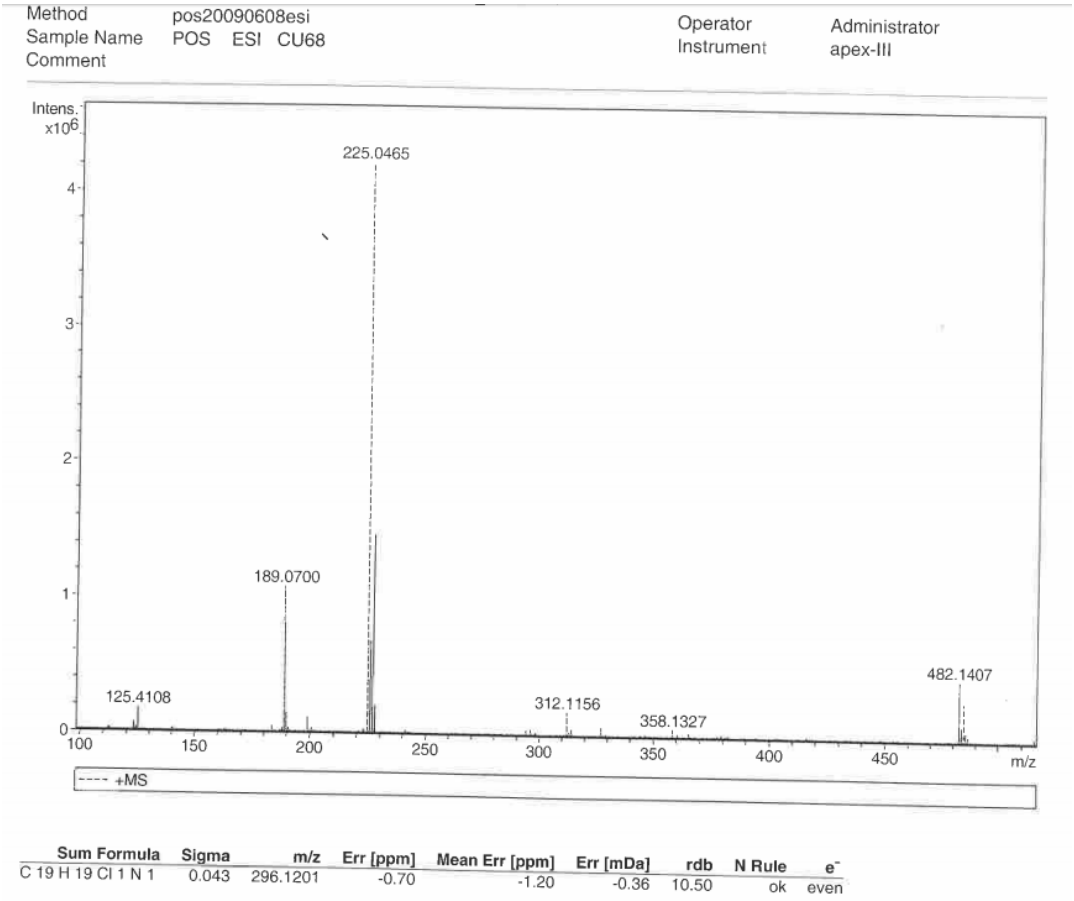

Figure S4.29. HRMS spectrum of propargylamine **C4P4**.

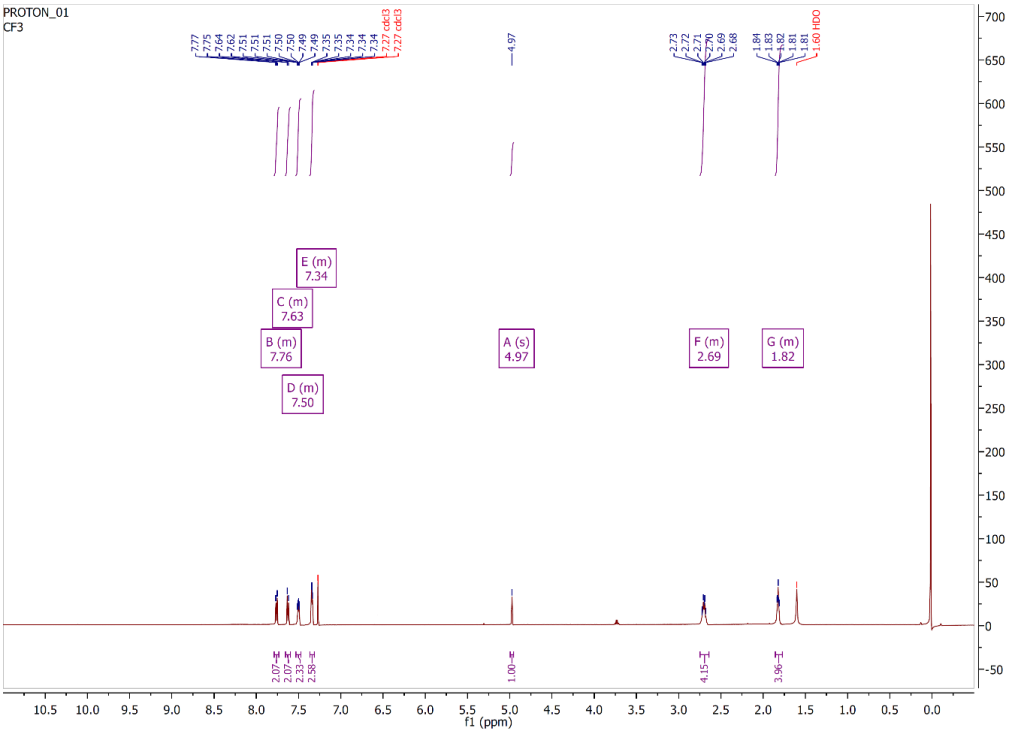

Figure S4.30. ^{1}H NMR spectrum of propargylamine **C4P5**.

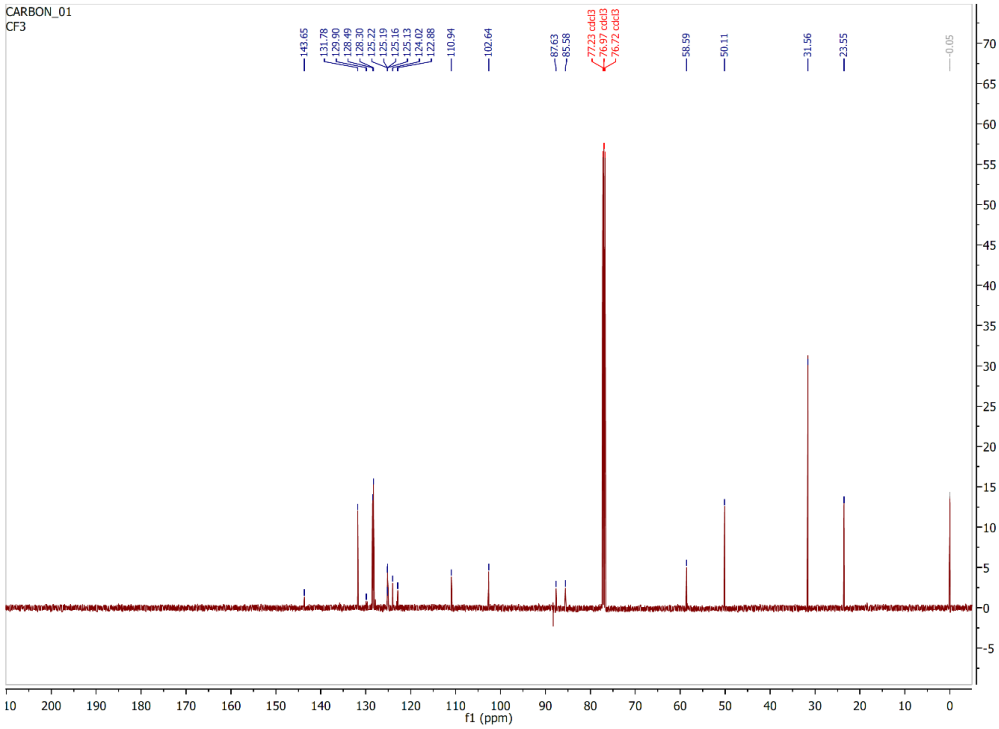

Figure S4.31. ^{13}C NMR spectrum of propargylamine **C4P5**.

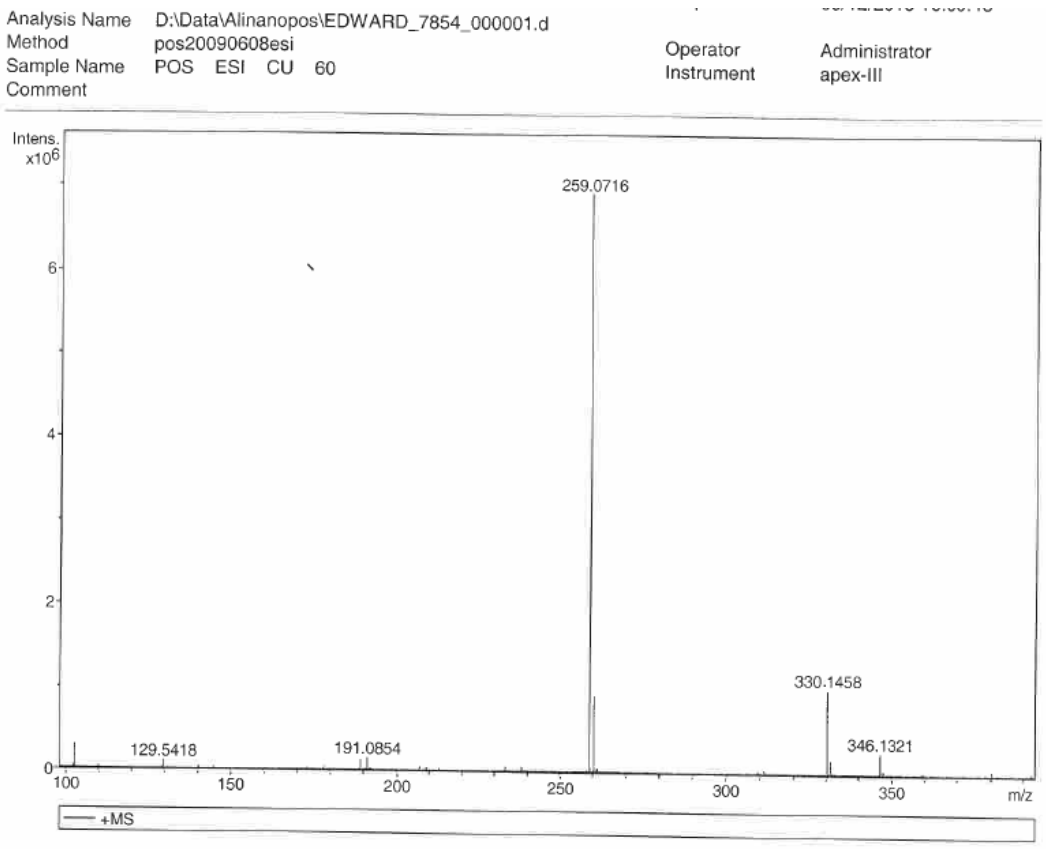

Sum Formula	Sigma	m/z	Err [ppm]	Mean Err [ppm]	Err [mDa]	rdb	N Rule	e⁻
C 20 H 19 F 3 N 1	0.009	330.1464	1.82	10.00	3.30	10.50	ok	even

Figure S4.32. HRMS spectrum of propargylamine **C4P5**.

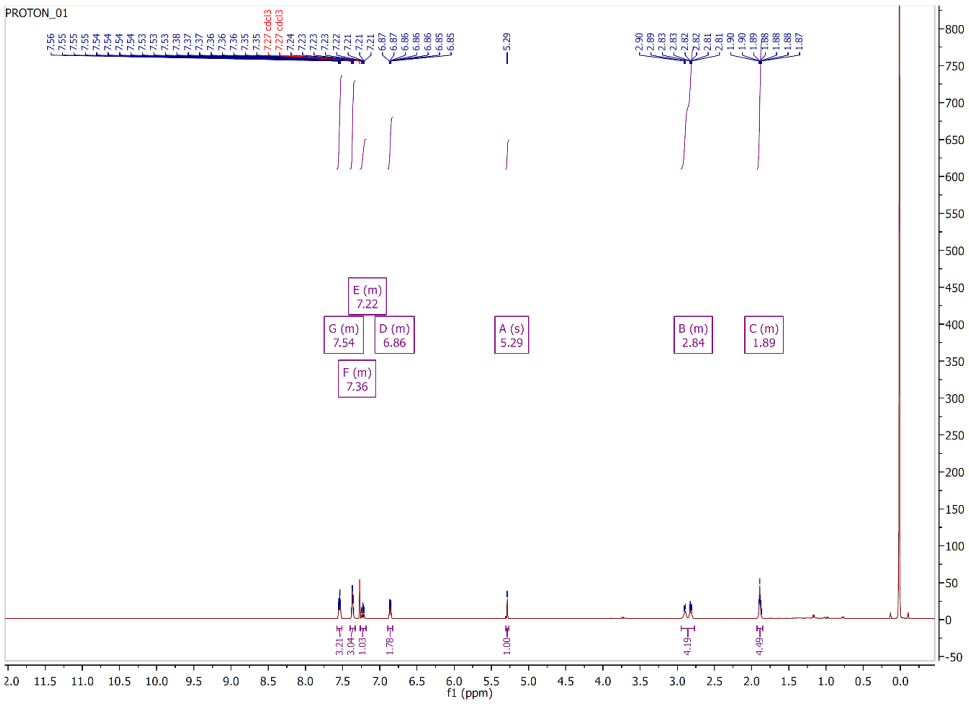

Figure S4.33. ^{1}H NMR spectrum of propargylamine **C4P6**.

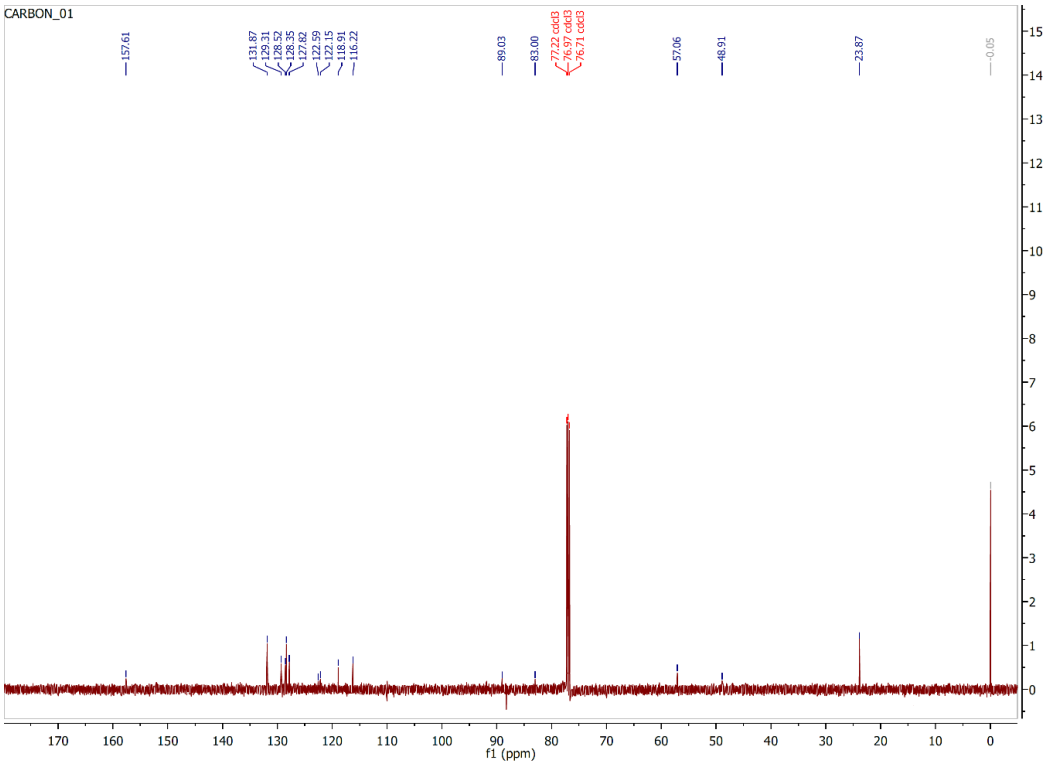

Figure S4.34. ^{13}C NMR spectrum of propargylamine **C4P6**.

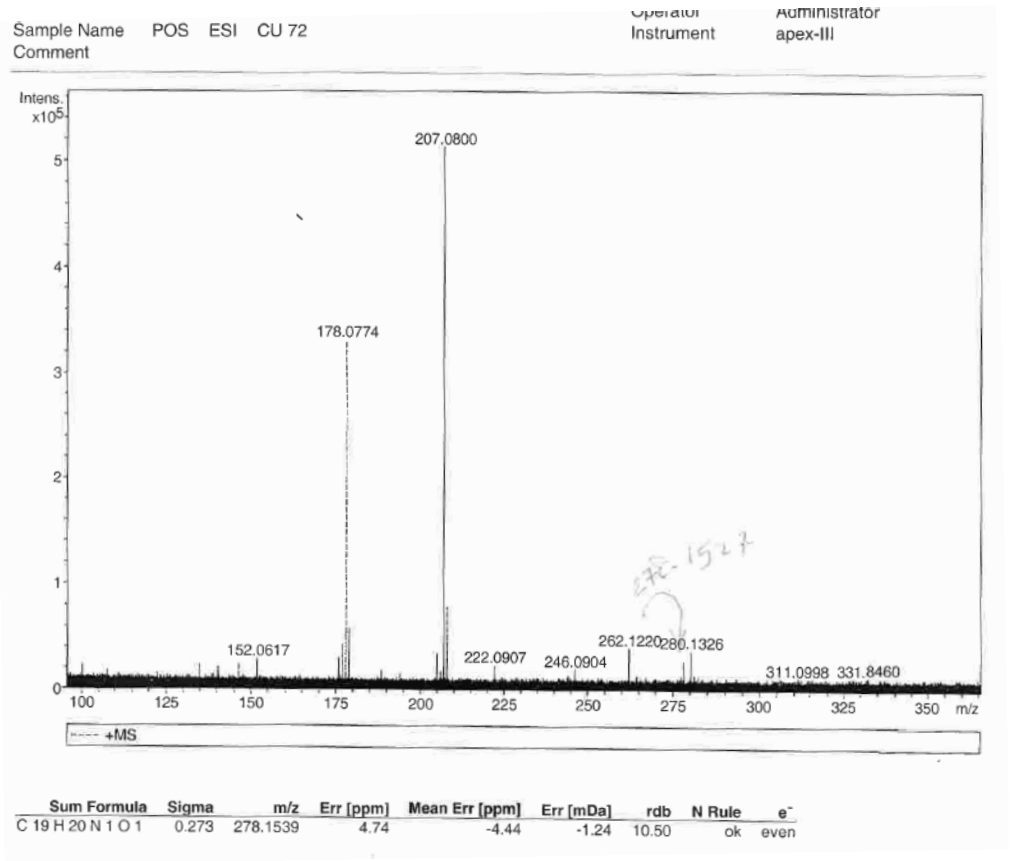

Figure S4.35. HRMS spectrum of propargylamine **C4P6**.

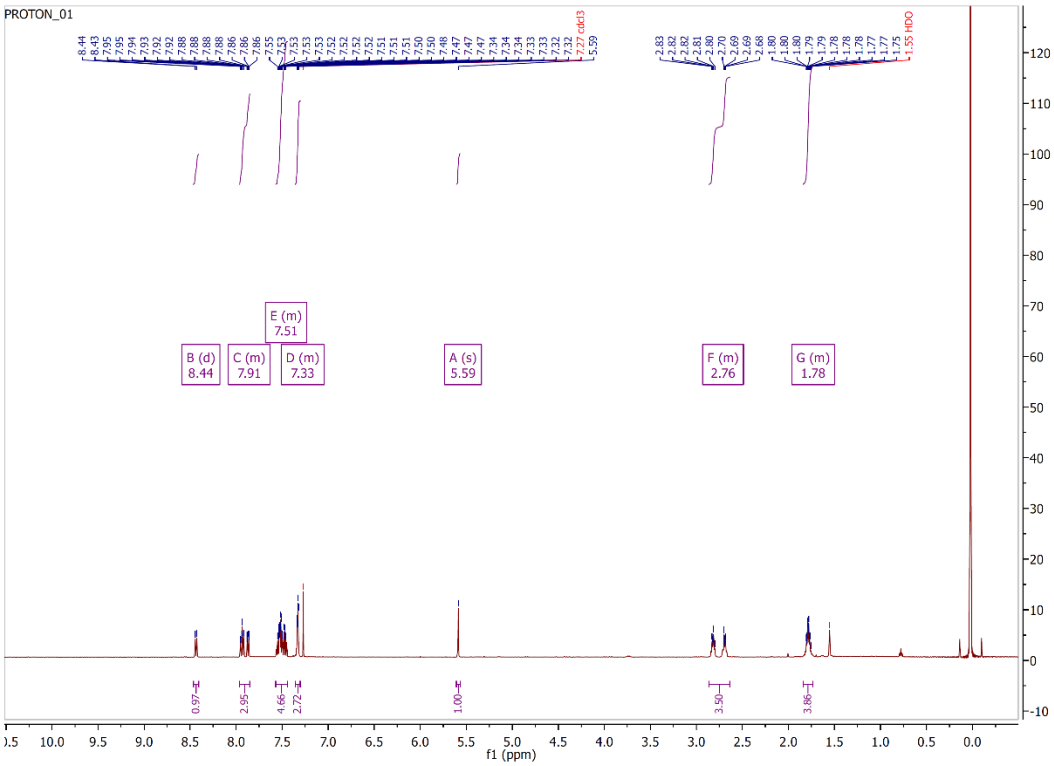

Figure S4.36. ^{1}H NMR spectrum of propargylamine **C4P7**.

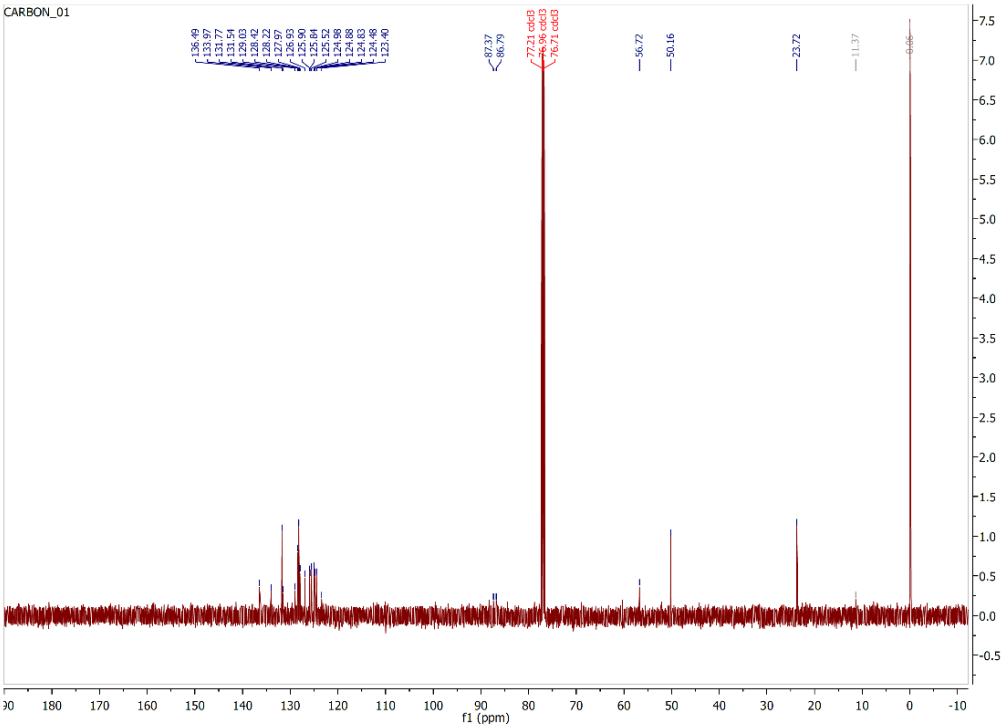

Figure S4.37. ^{13}C NMR spectrum of propargylamine **C4P7.**

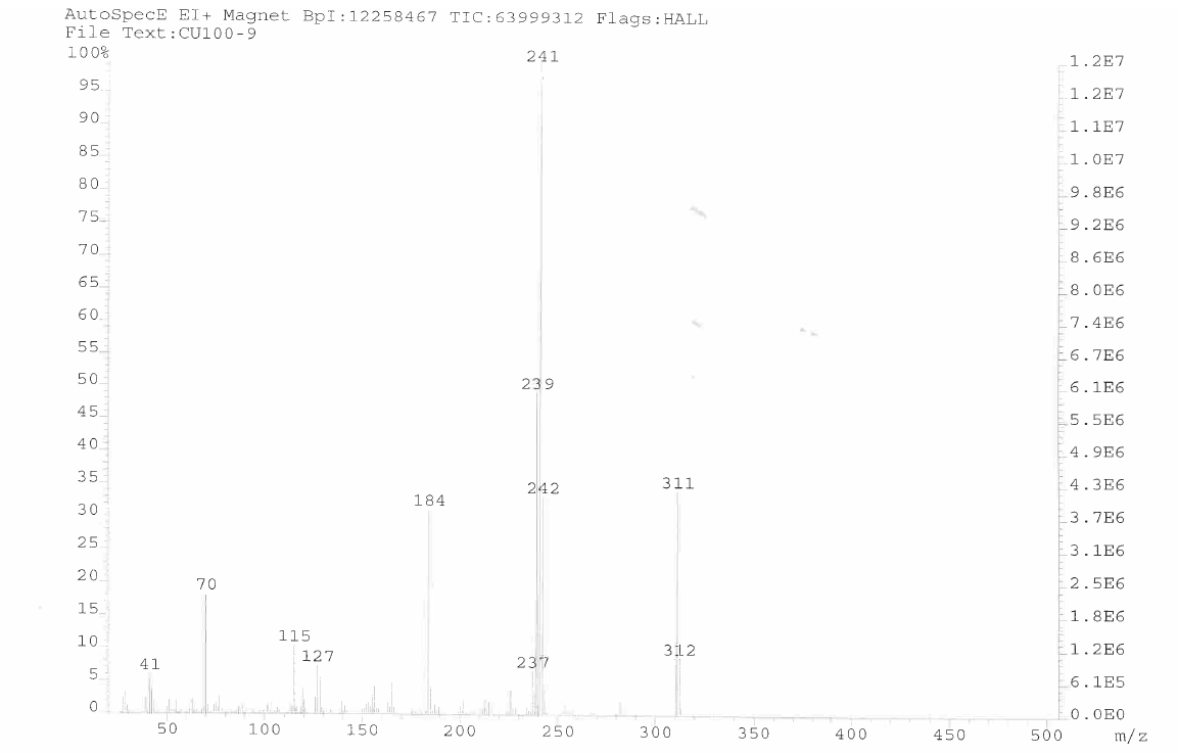

Figure S4.38. EI spectrum of propargylamine **C4P7**.

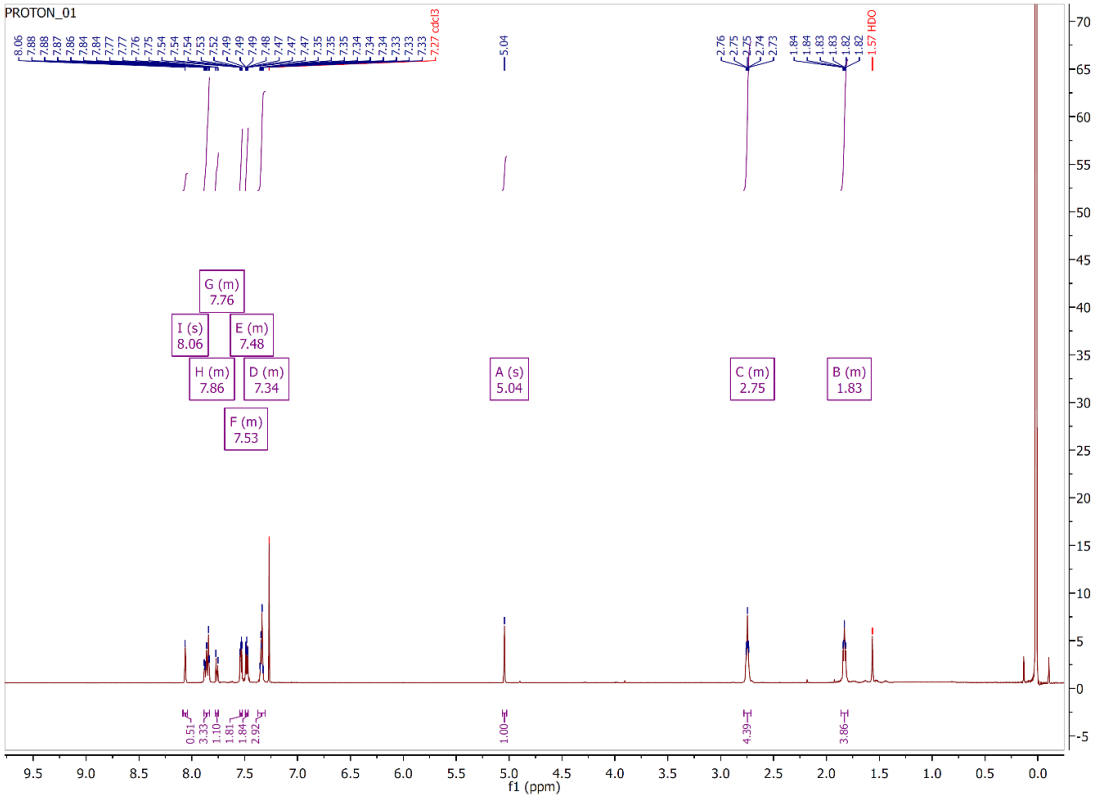

Figure S4.39. ^{1}H NMR spectrum of propargylamine **C4P8**.

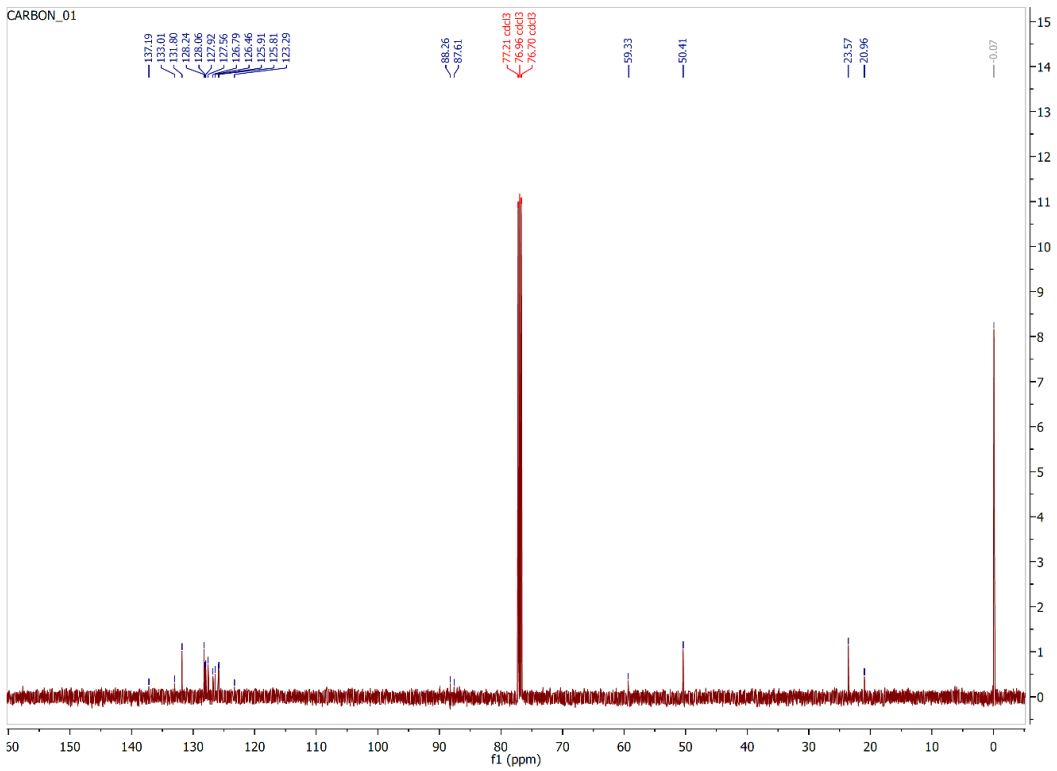

Figure S4.40. ^{13}C NMR spectrum of propargylamine **C4P8**.

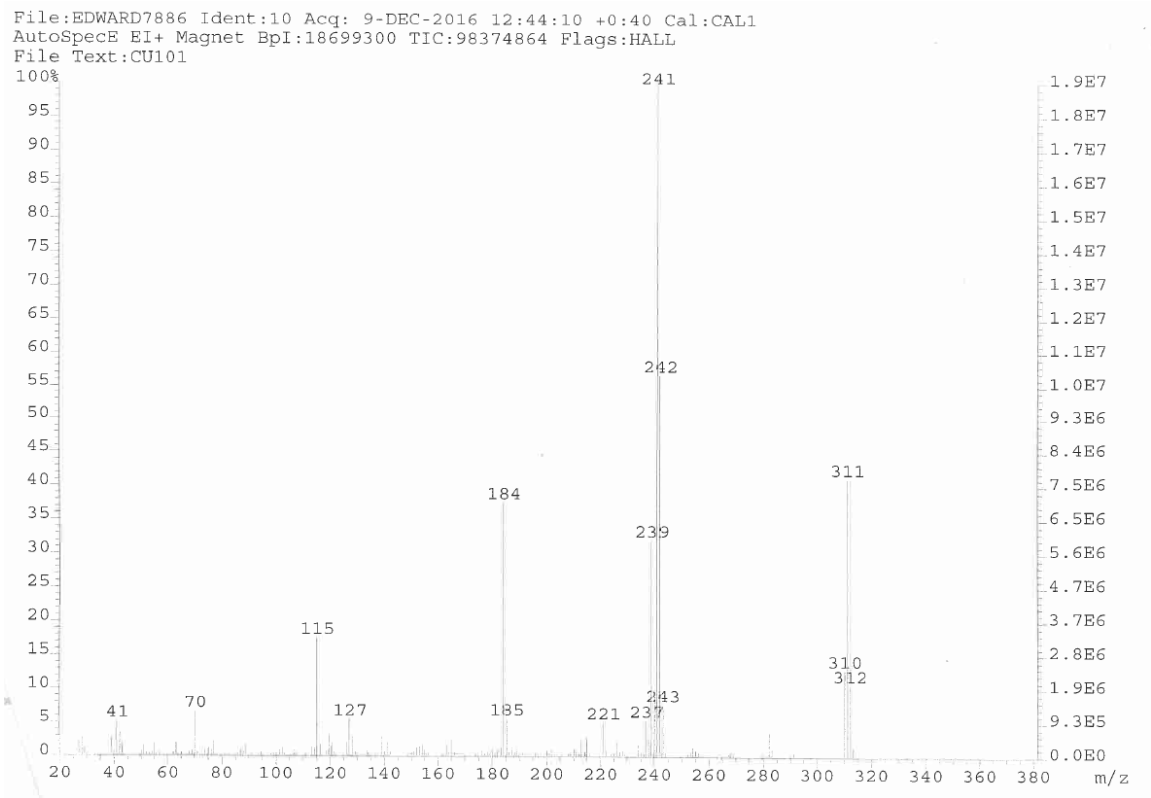

Figure S4.41. EI spectrum of propargylamine **C4P8**.

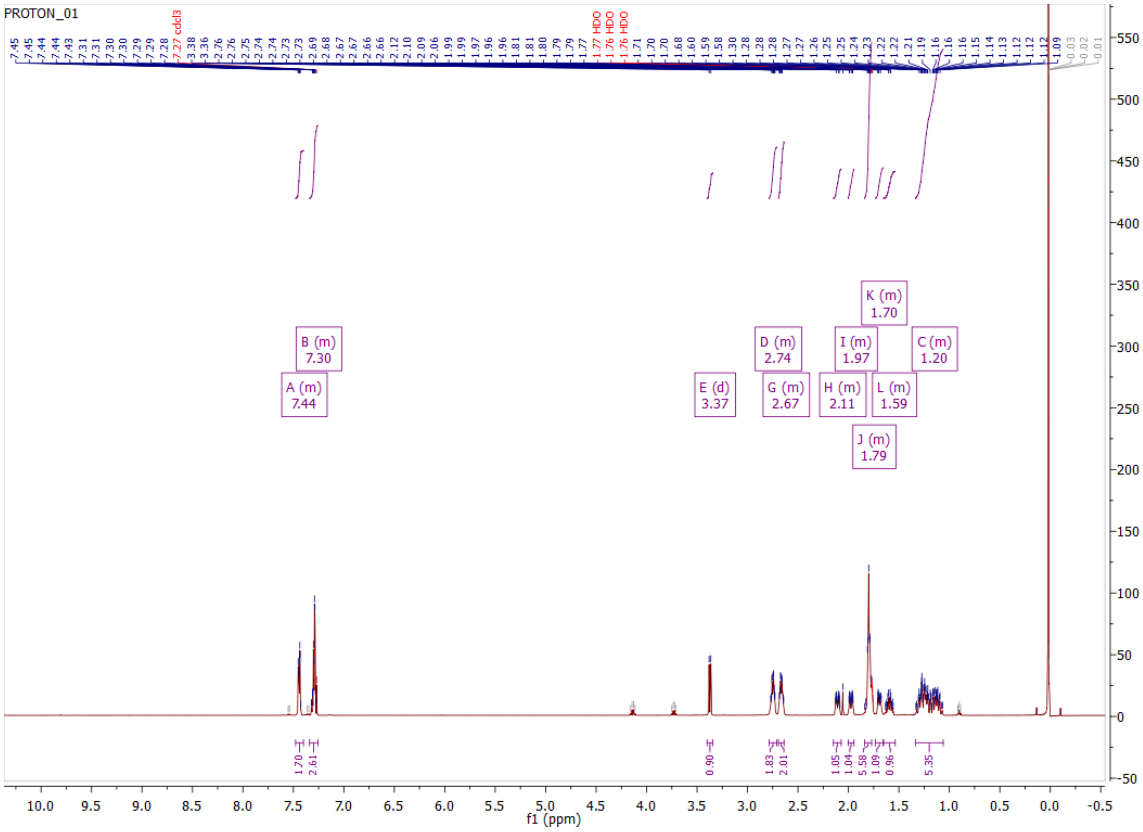

Figure S4.42. ^{1}H NMR spectrum of propargylamine **C4P9**.

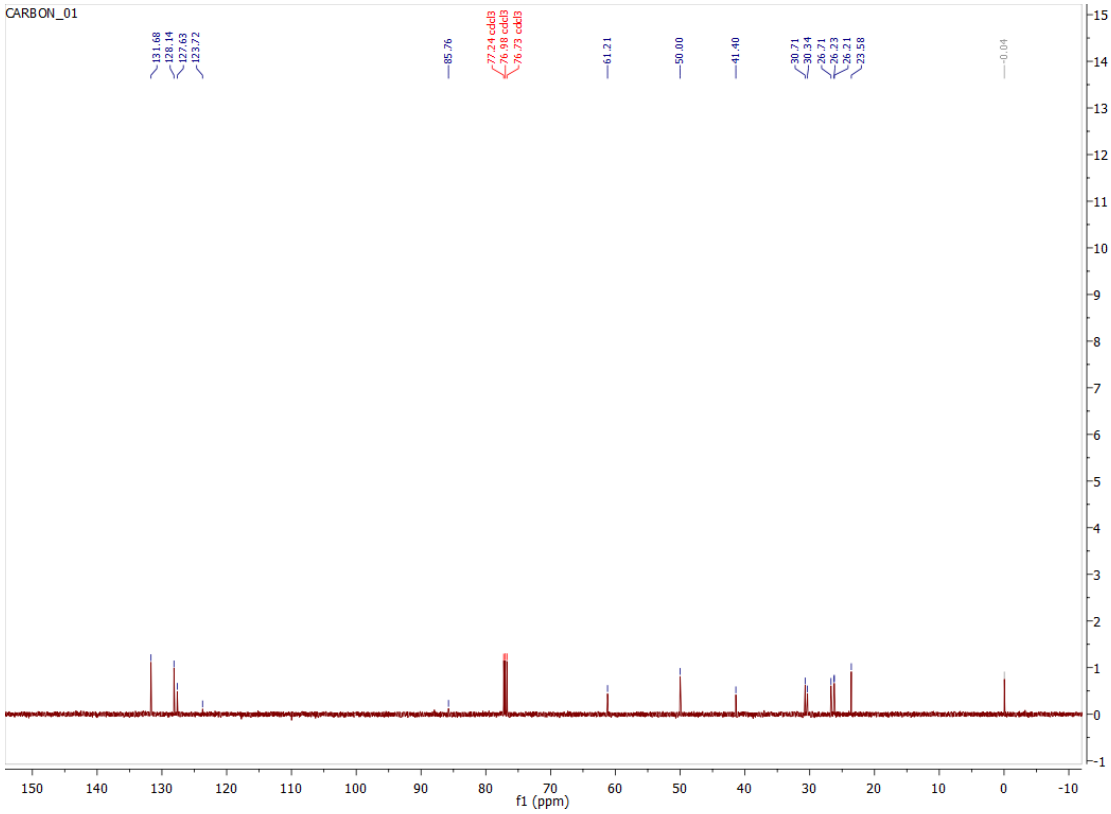

Figure S4.43. ^{13}C NMR spectrum of propargylamine **C4P9**.

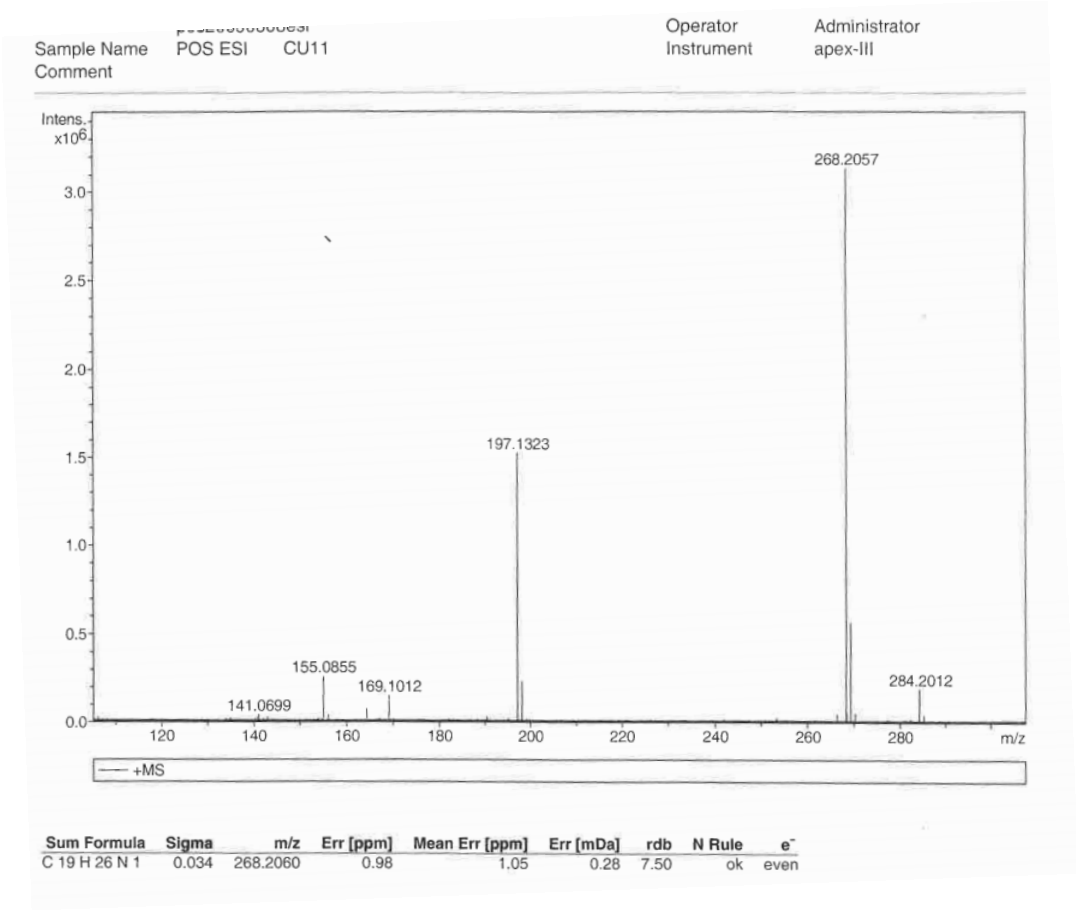

Figure S4.44. HRMS spectrum of propargylamine **C4P9**.

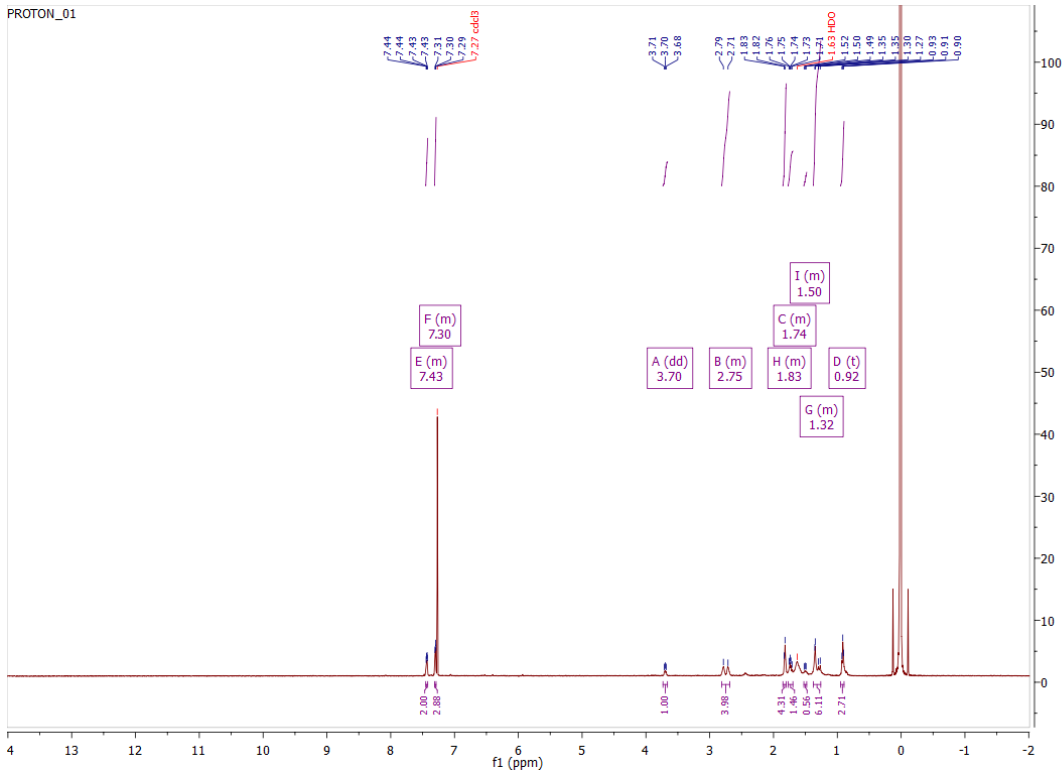

Figure S4.45. ^{1}H NMR spectrum of propargylamine **C4P10**.

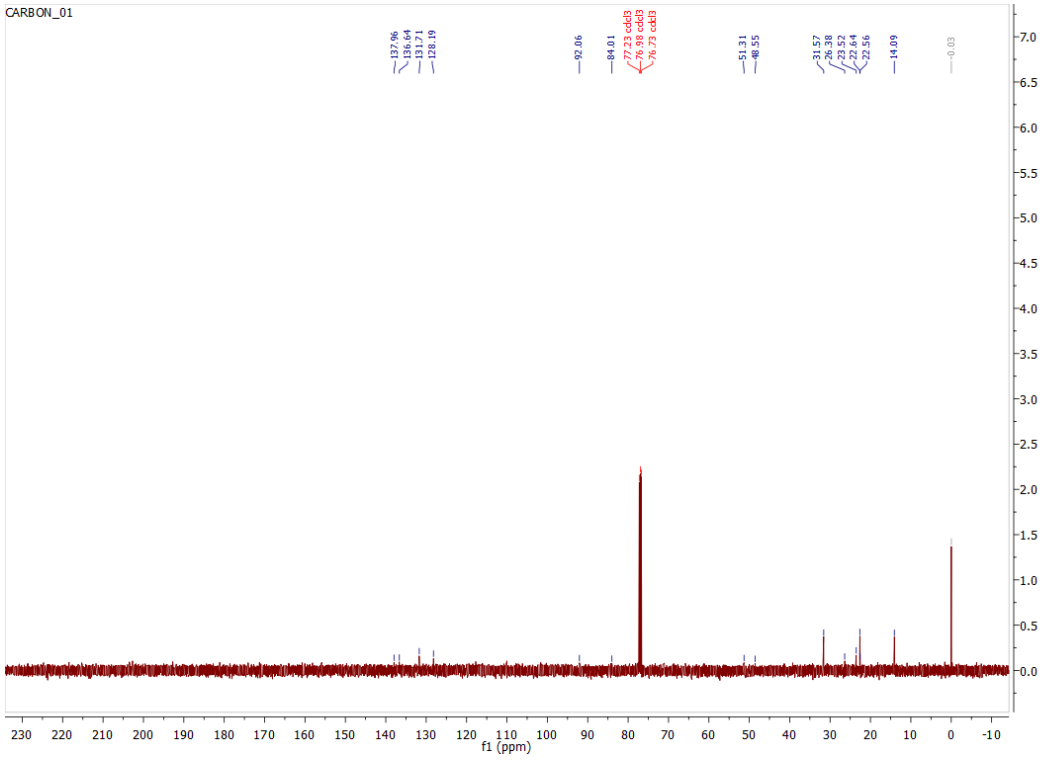

Figure S4.46. ^{13}C NMR spectrum of propargylamine **C4P10**.

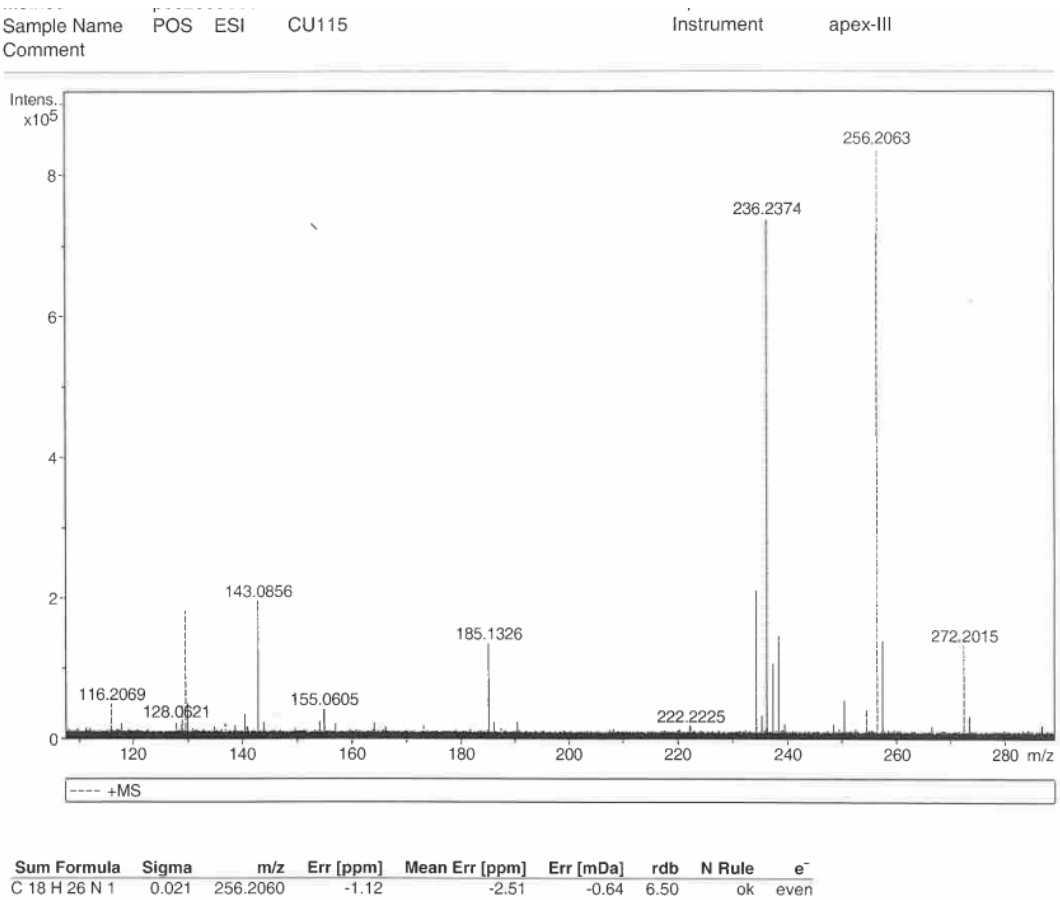

Figure S4.47. HRMS spectrum of propargylamine **C4P10**.

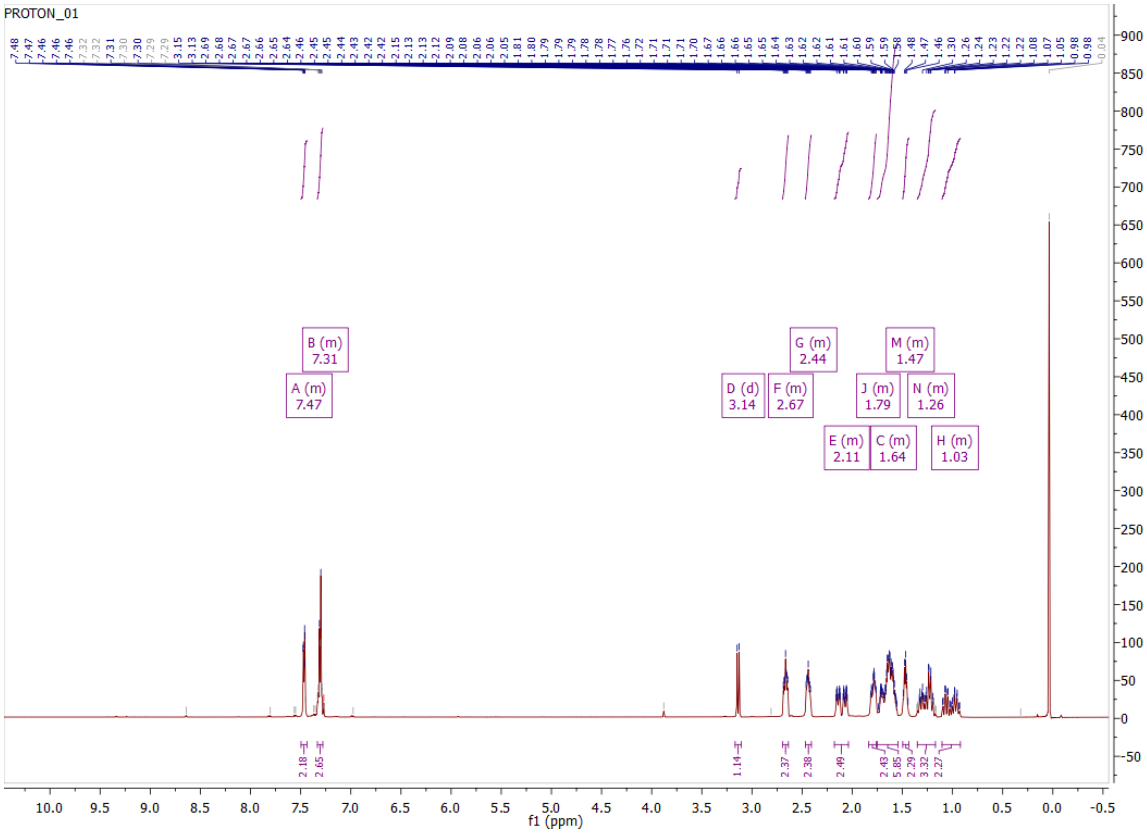

Figure S4.48. ^{1}H NMR spectrum of propargylamine **C4P12**.

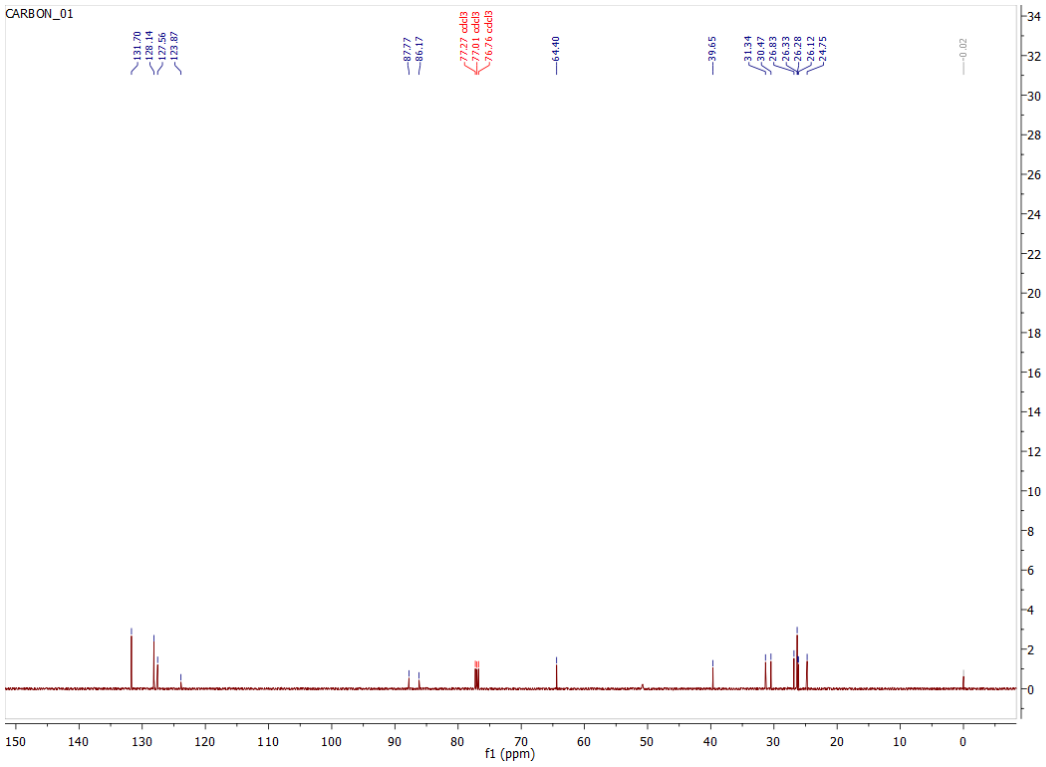

Figure S4.49. ^{13}C NMR spectrum of propargylamine **C4P12**.

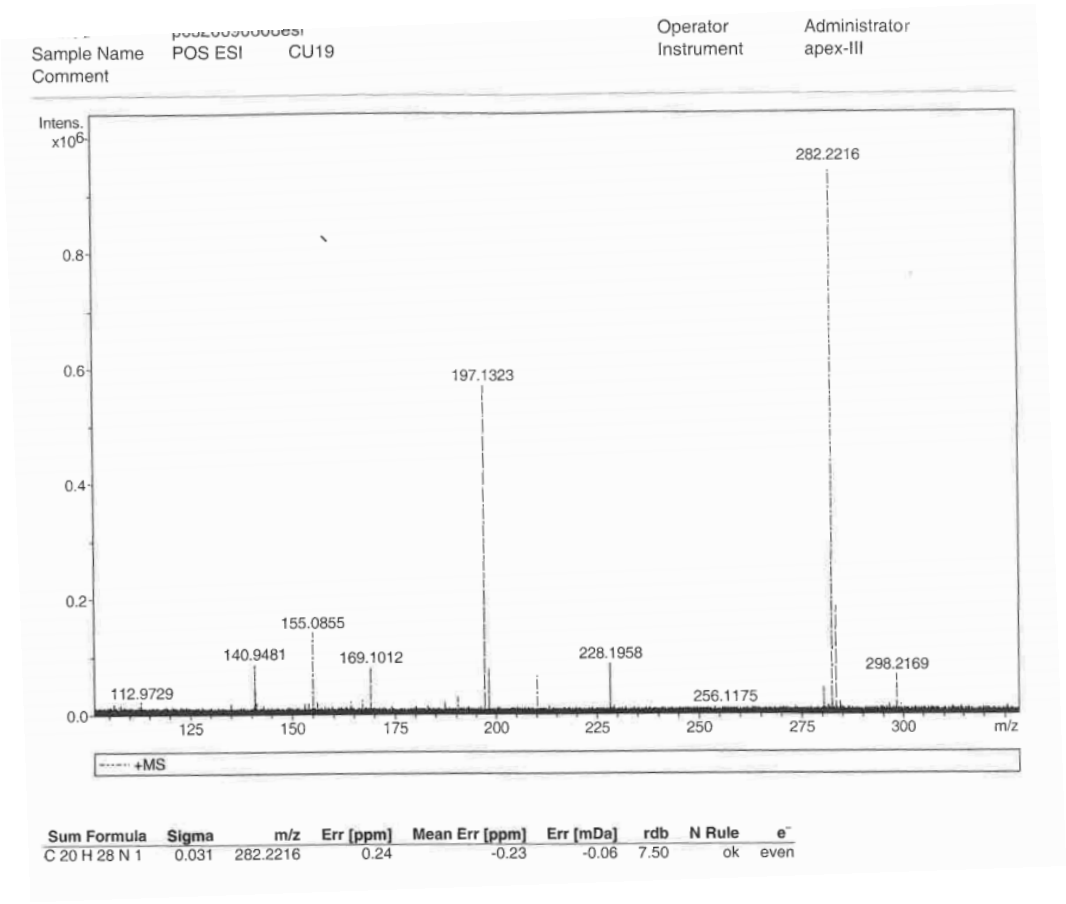

Figure S4.50. HRMS spectrum of propargylamine **C4P12**.

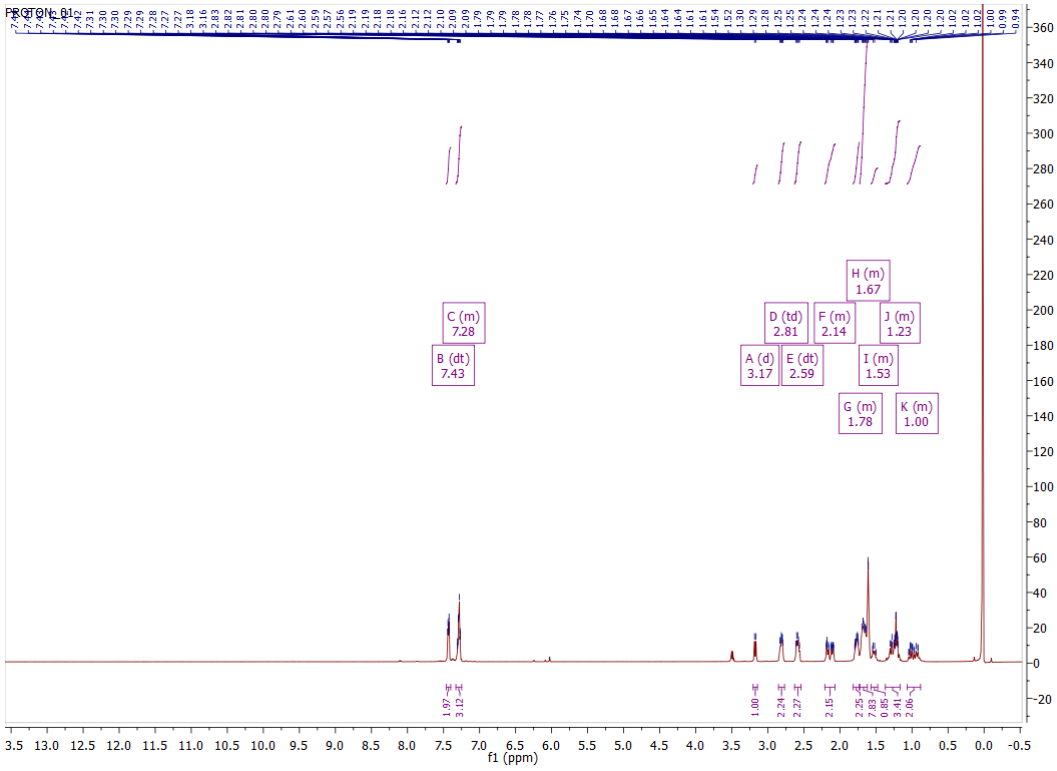

Figure S4.51. ^{1}H NMR spectrum of propargylamine **C4P13**.

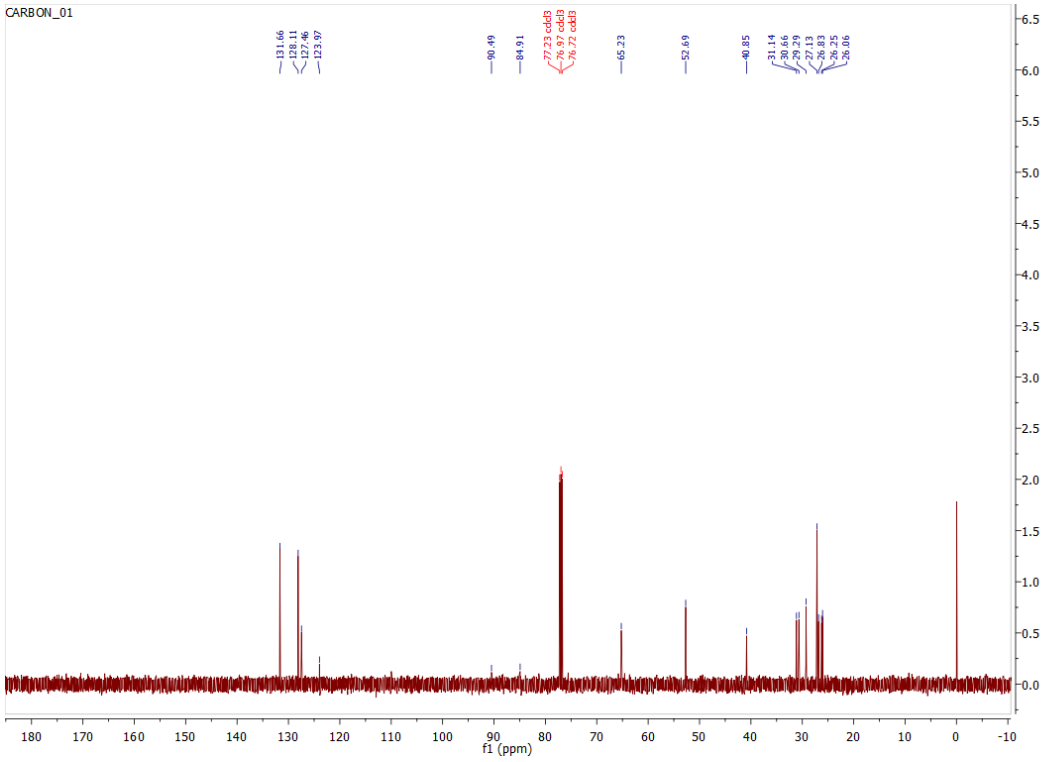

Figure S4.52. ^{13}C NMR spectrum of propargylamine **C4P13**.

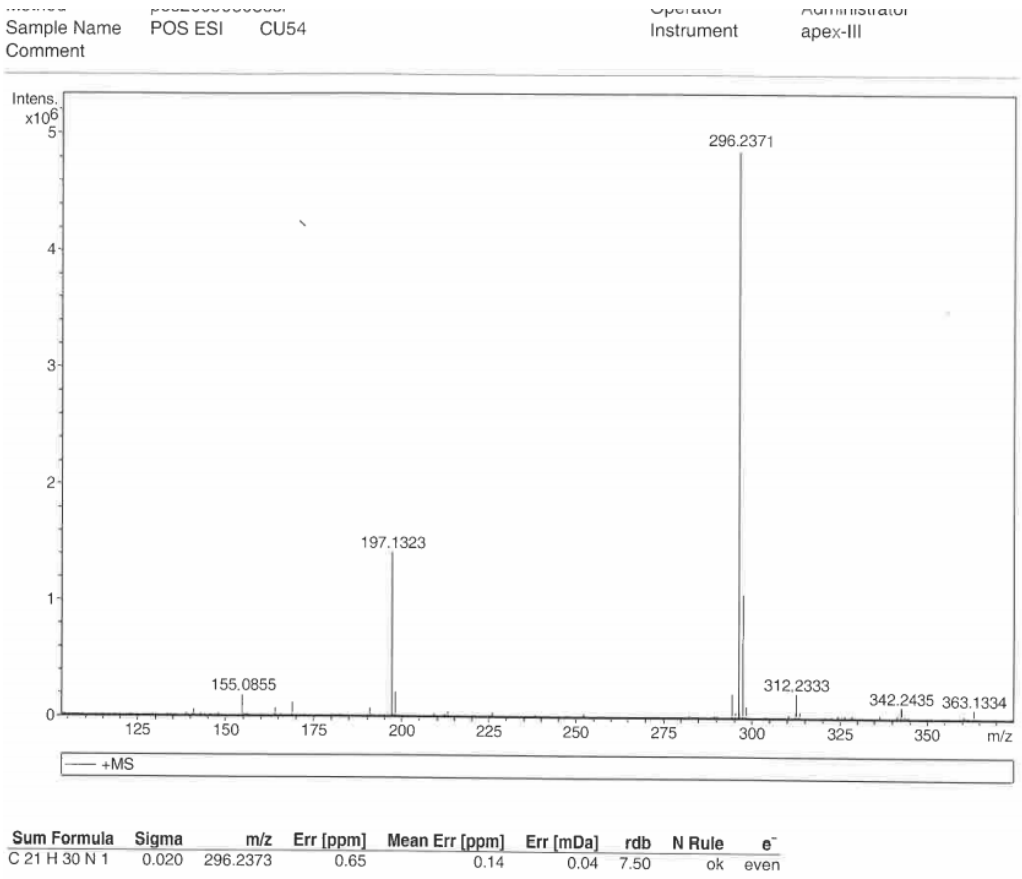

Figure S4.53. HRMS spectrum of propargylamine **C4P13**.

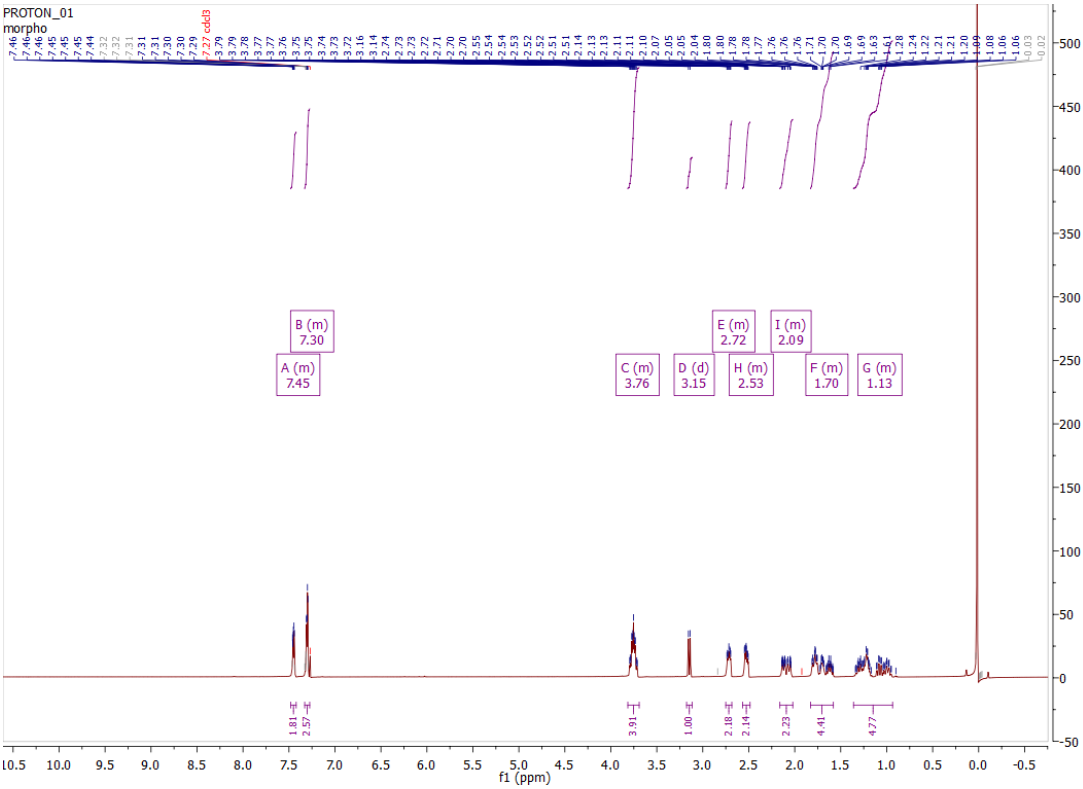

Figure S4.54. ^{1}H NMR spectrum of propargylamine **C4P14**.

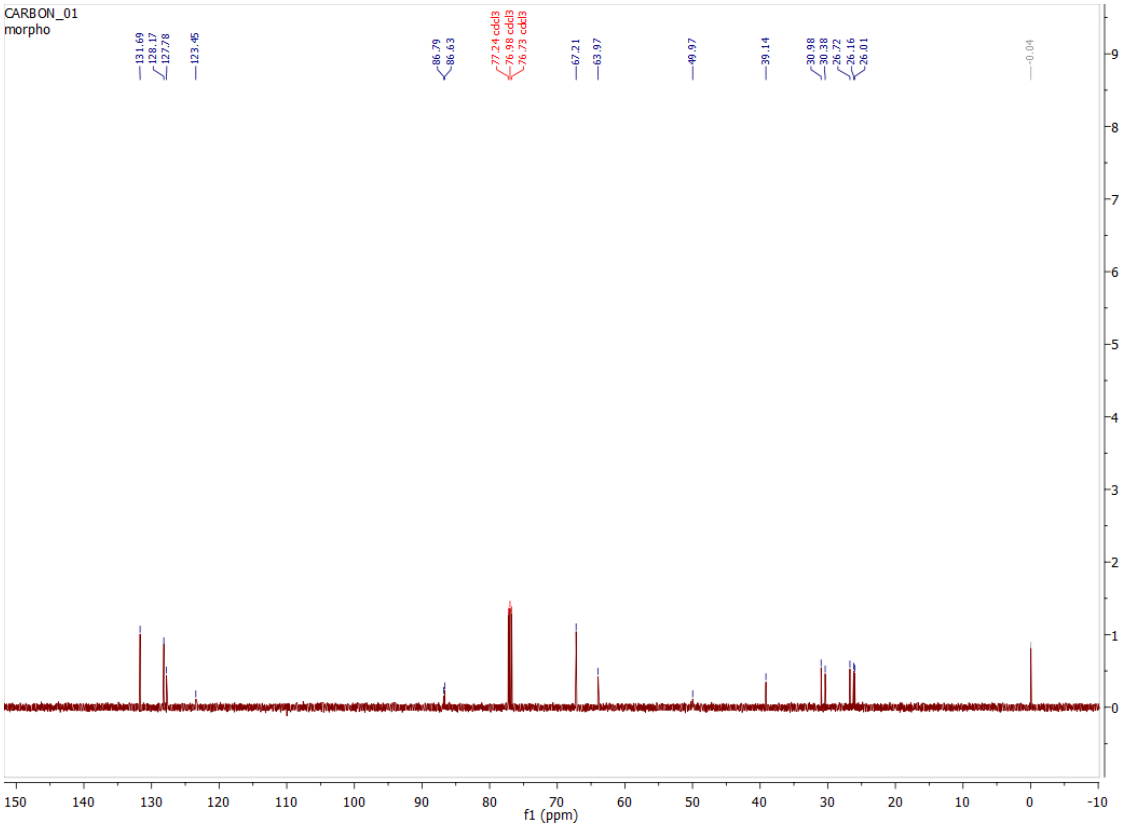

Figure S4.55. ^{13}C NMR spectrum of propargylamine **C4P14**.

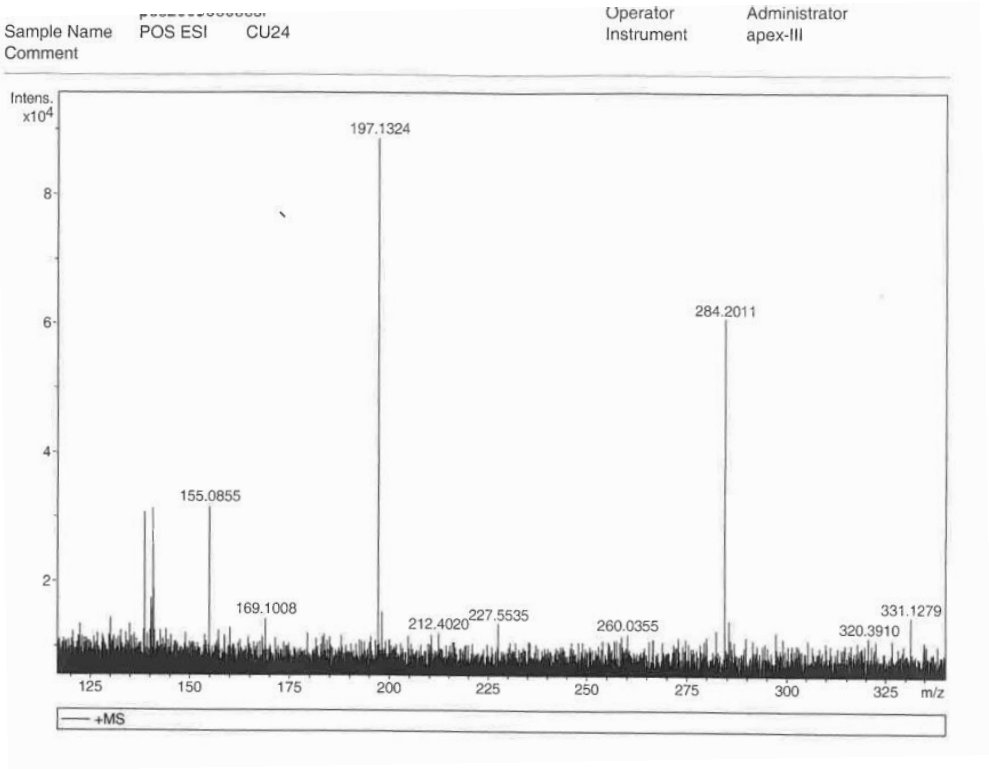

Figure S4.56. HRMS spectrum of propargylamine **C4P14**.

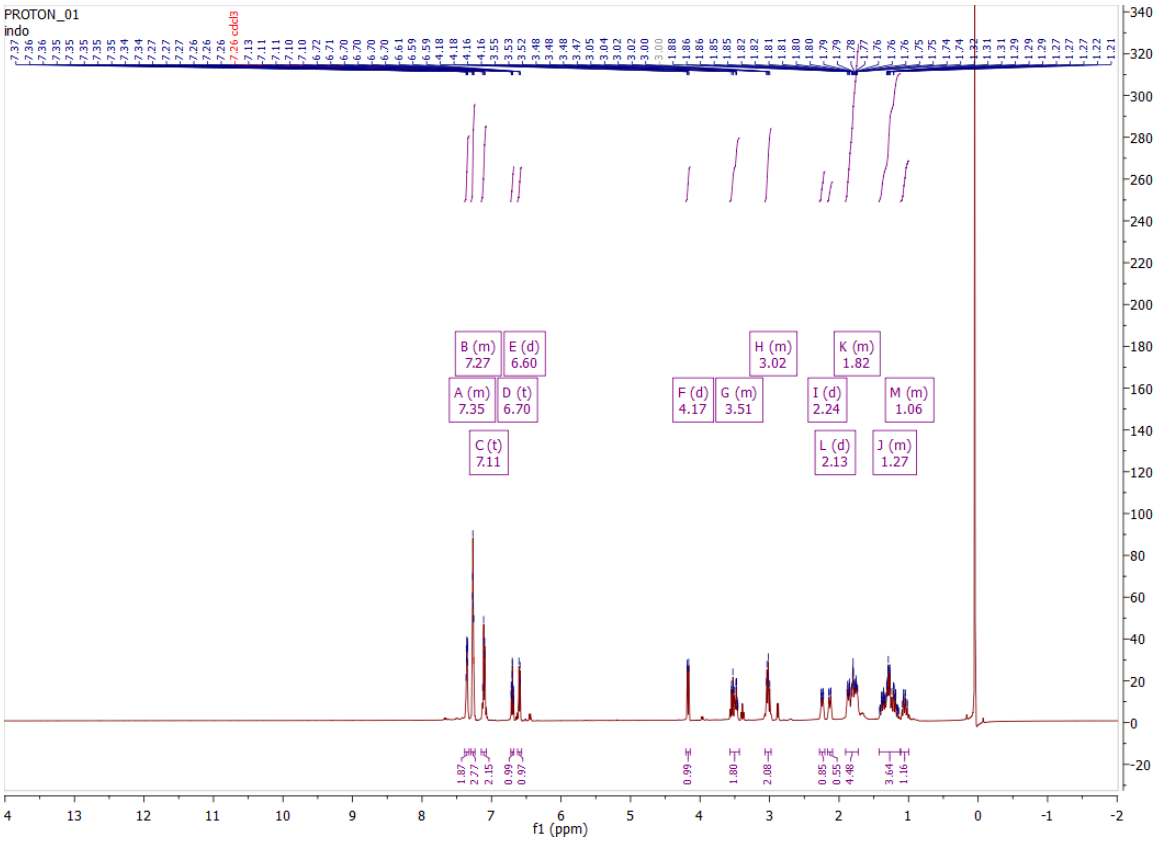

Figure S4.57. ^{1}H NMR spectrum of propargylamine **C4P15**.

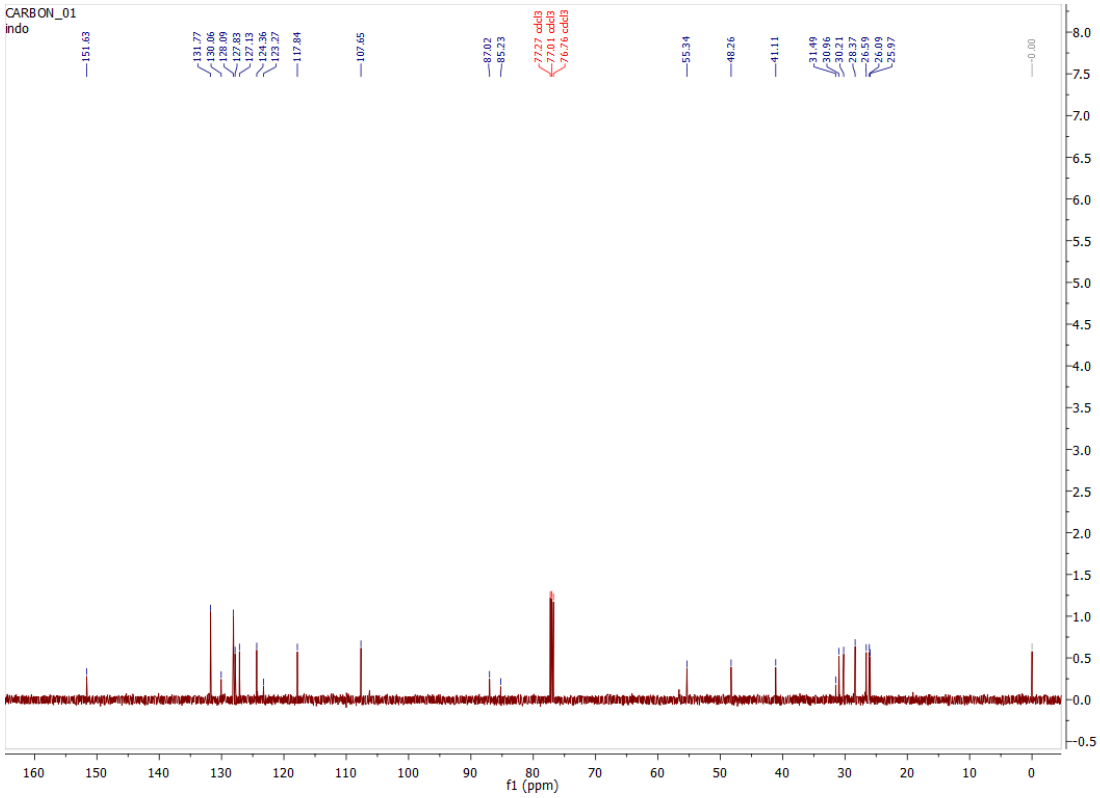

Figure S4.58. ^{13}C NMR spectrum of propargylamine **C4P15**.

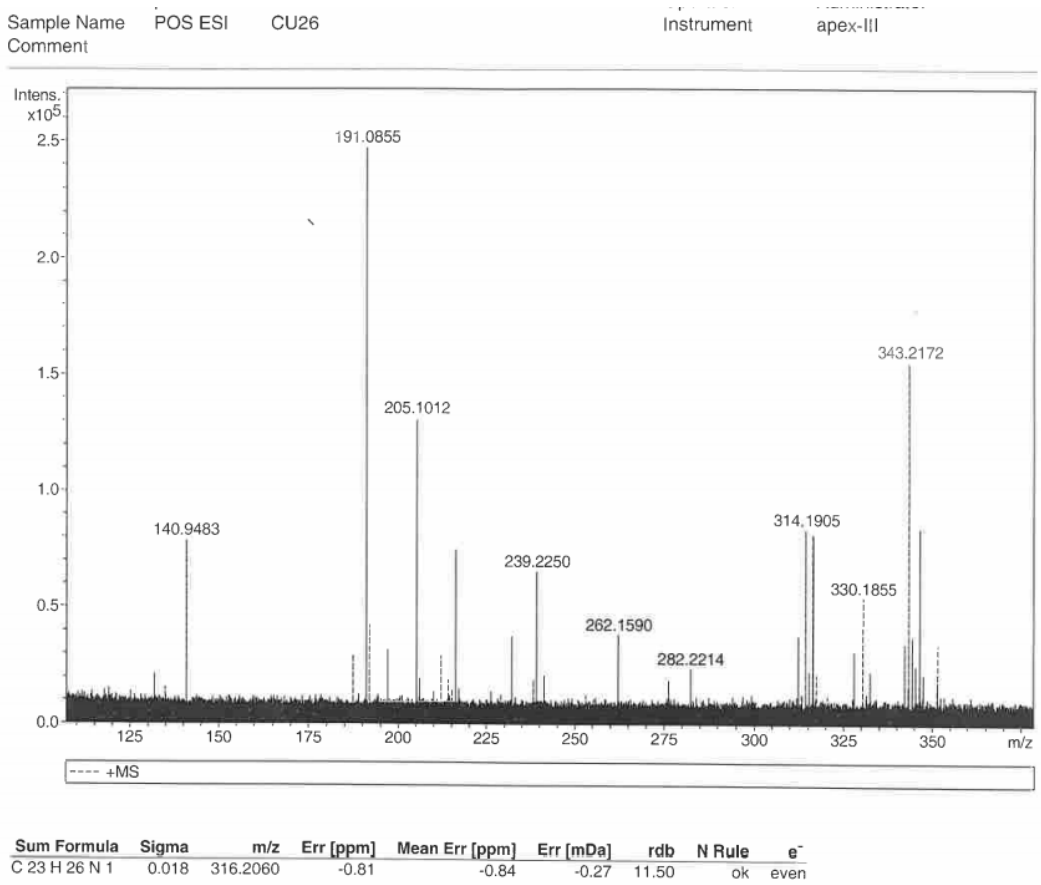

Figure S4.59. HRMS spectrum of propargylamine **C4P15**.

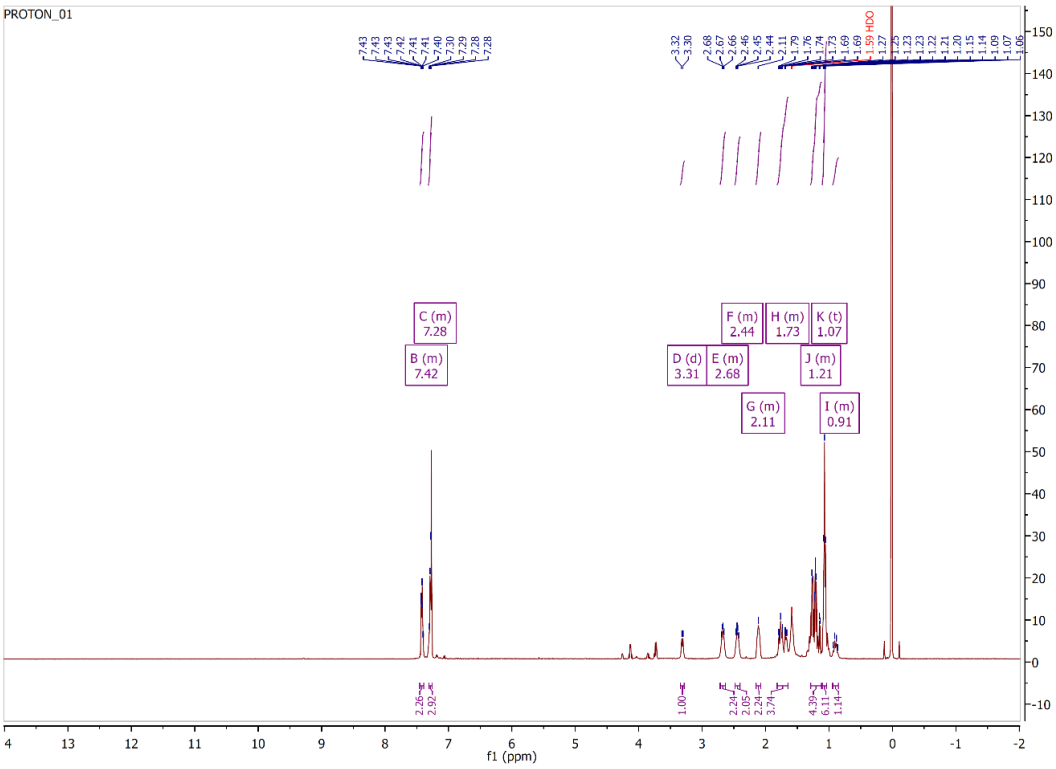

Figure S4.60. ^{1}H NMR spectrum of propargylamine **C4P16**.

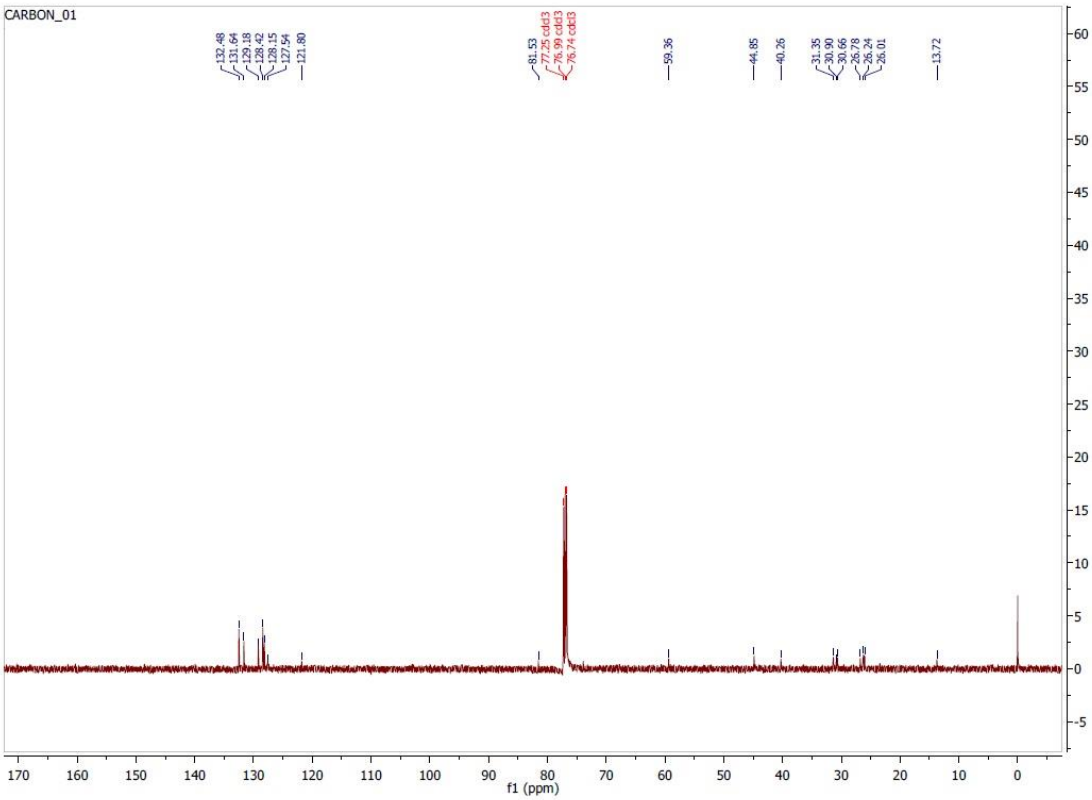

Figure S4.61. ^{13}C NMR spectrum of propargylamine **C4P16**.

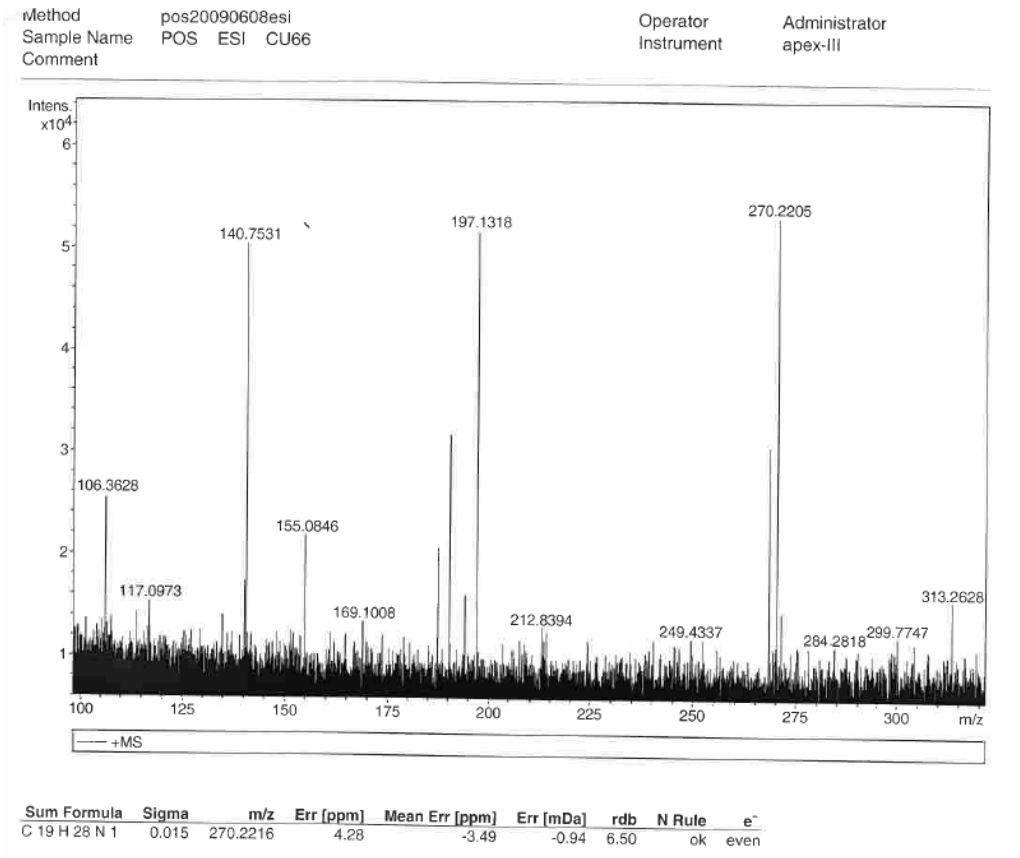

Figure S4.62. HRMS spectrum of propargylamine **C4P16**.

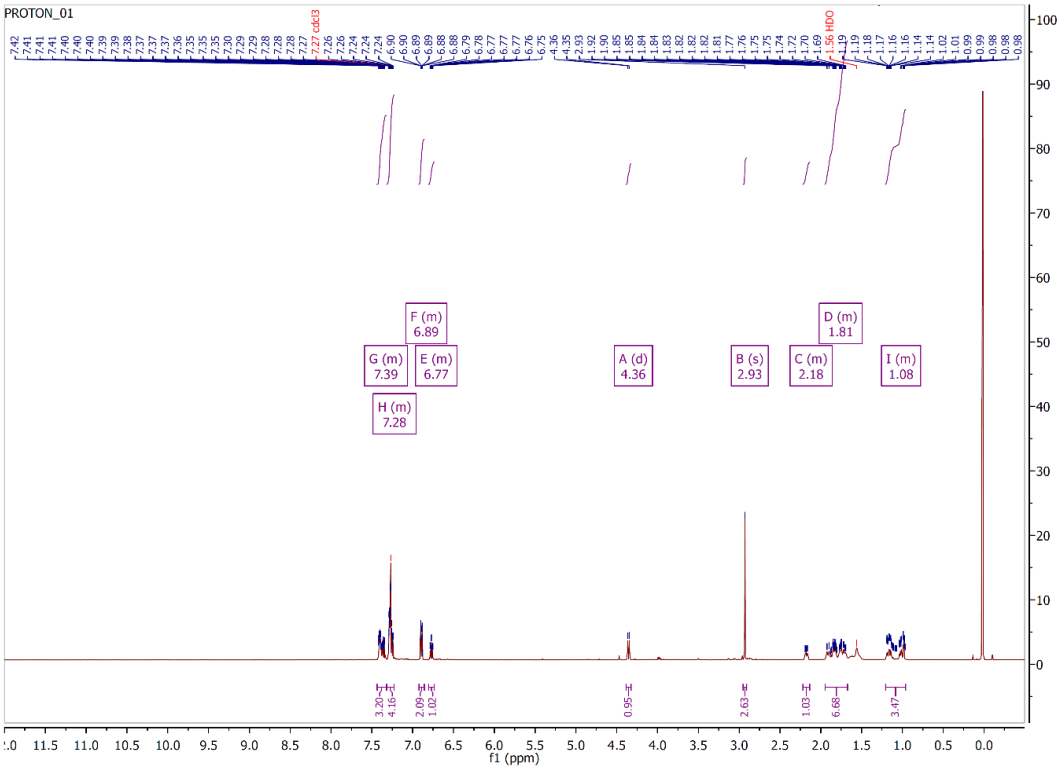

Figure S4.63. ^{1}H NMR spectrum of propargylamine **C4P17**.

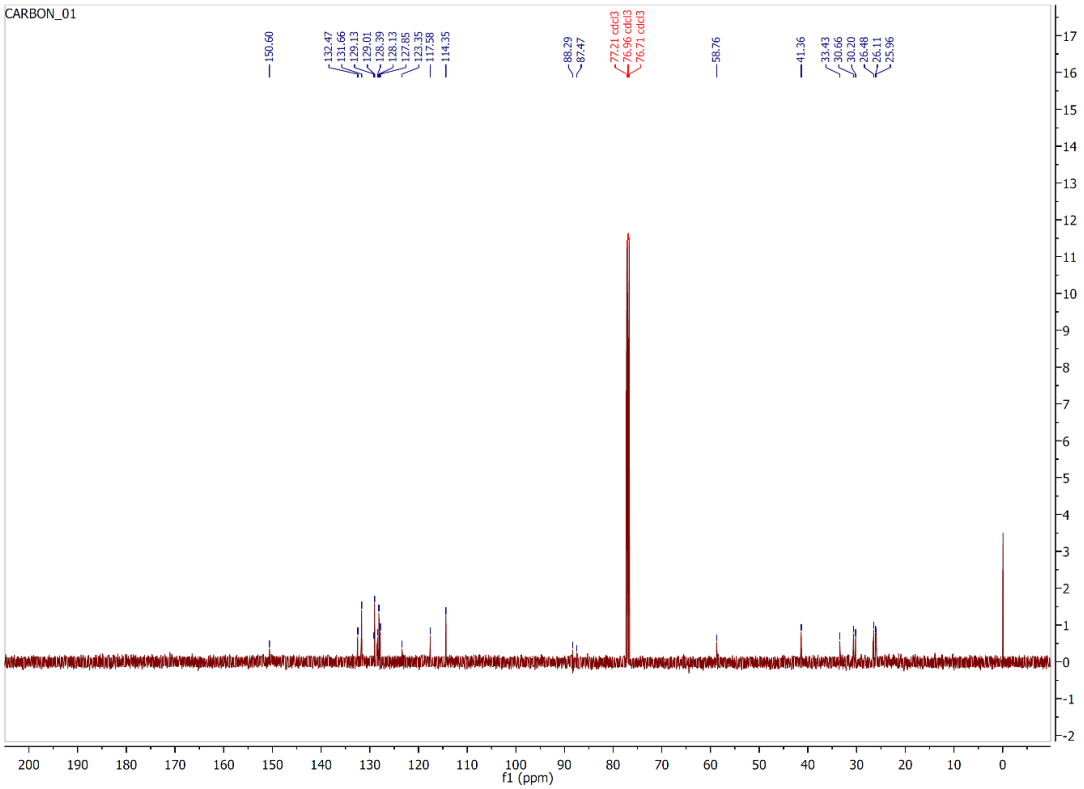

Figure S4.64. ^{13}C NMR spectrum of propargylamine **C4P17**.

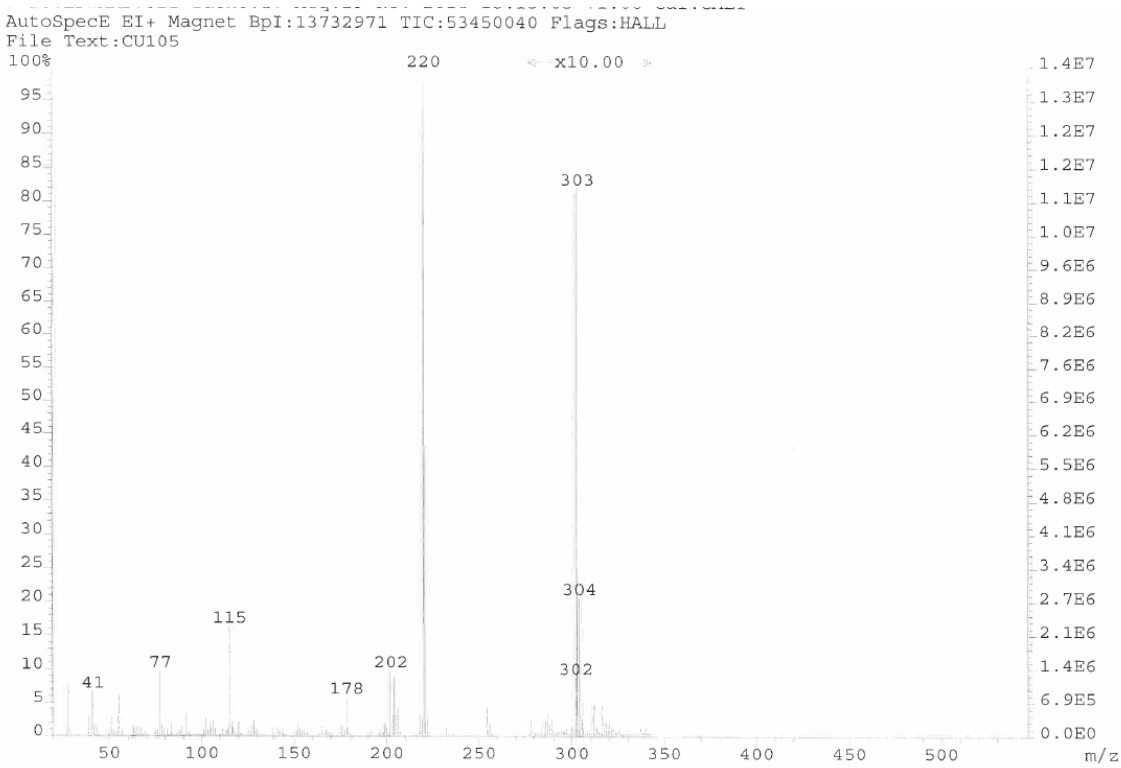

Figure S4.65. EI spectrum of propargylamine **C4P17**.

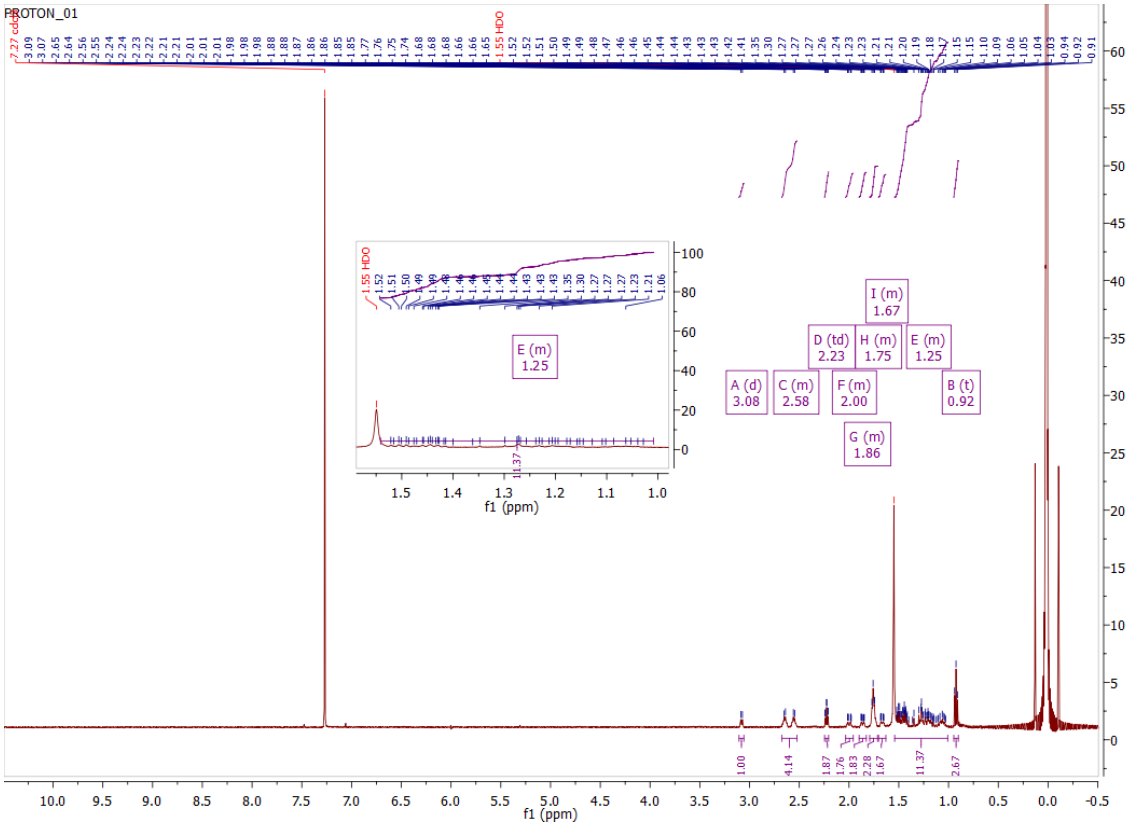

Figure S4.66. ^{1}H NMR spectrum of propargylamine **C4P22**.

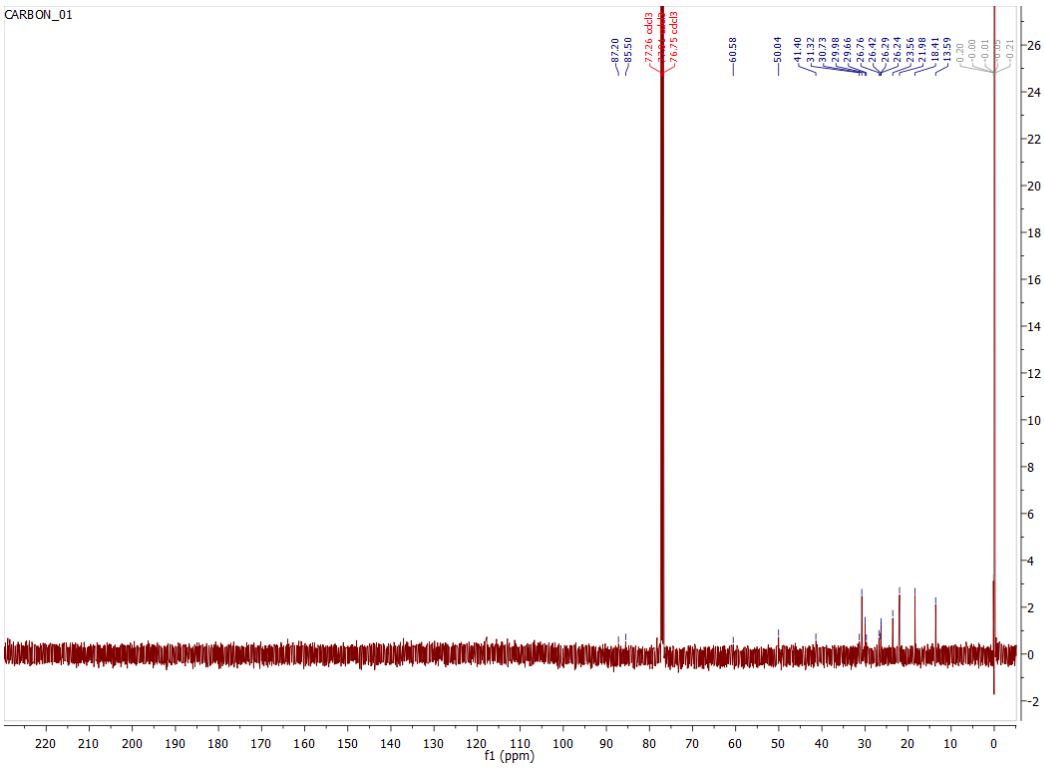

Figure S4.67. ^{13}C NMR spectrum of propargylamine **C4P22**.

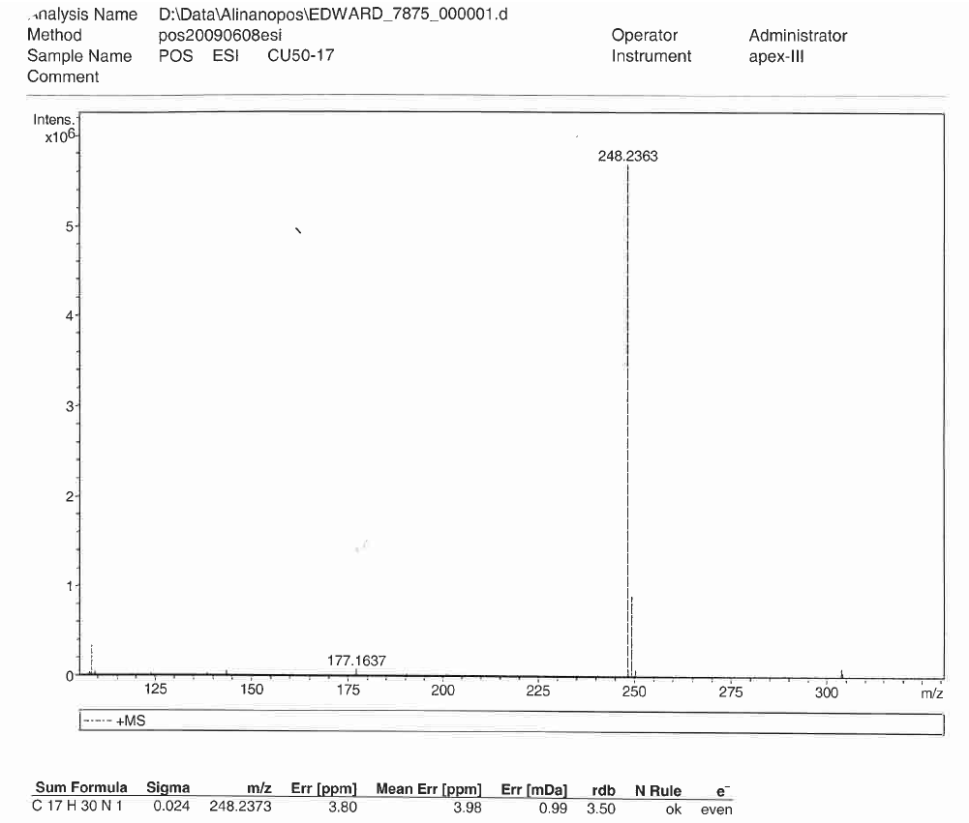

Figure S4.68. HRMS spectrum of propargylamine **C4P22**.

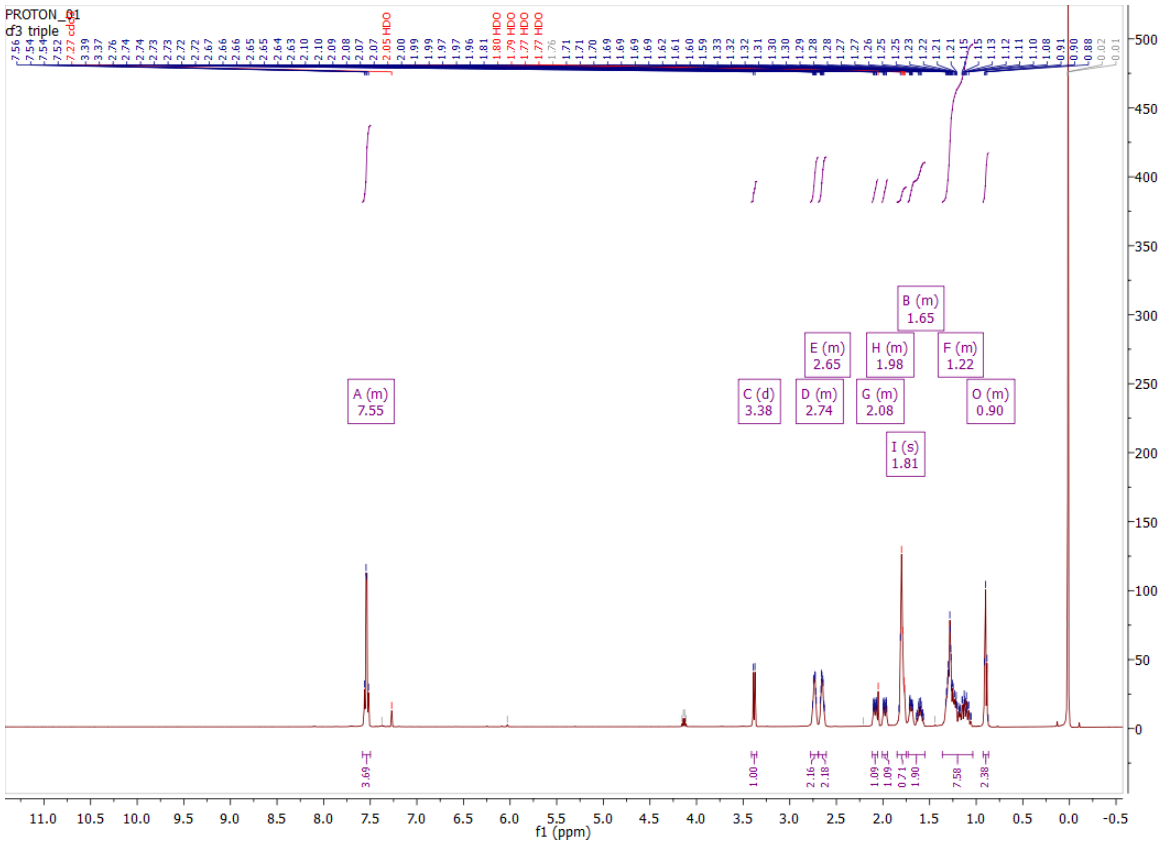

Figure S4.69. ^{1}H NMR spectrum of propargylamine **C4P23**.

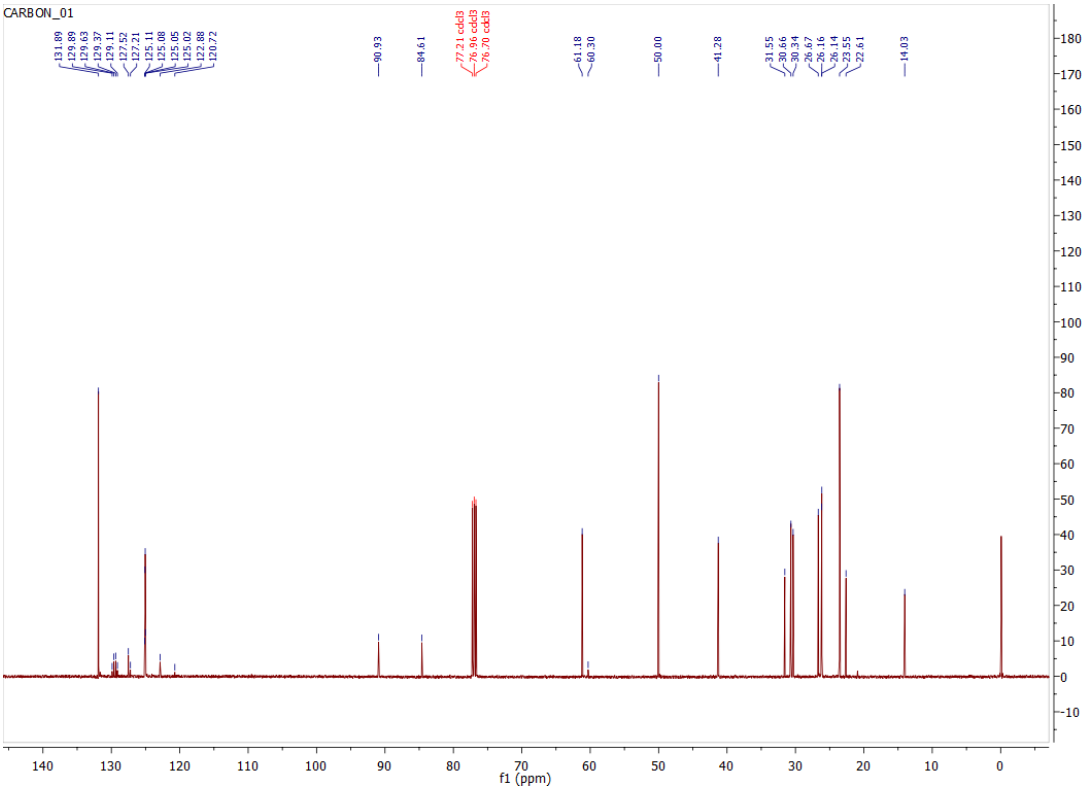

Figure S4.70. ^{13}C NMR spectrum of propargylamine **C4P23**.

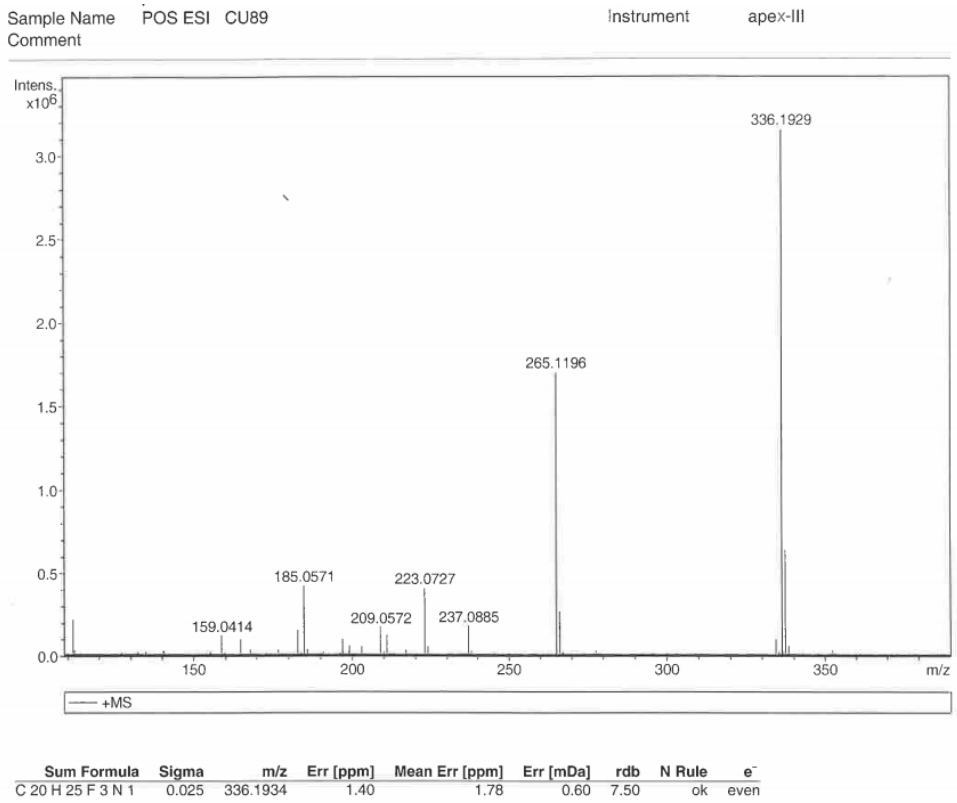

Figure S4.71. HRMS spectrum of propargylamine **C4P23**.

Chapter 5

5.1. Characterization data of 22 – 26

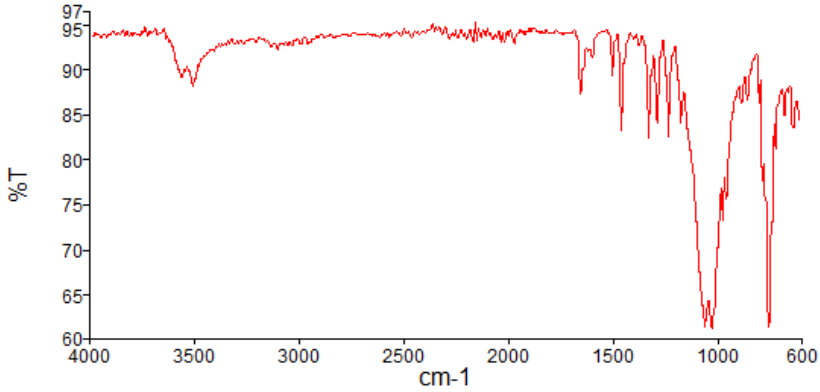

Figure S5.1. IR spectrum of **22**.

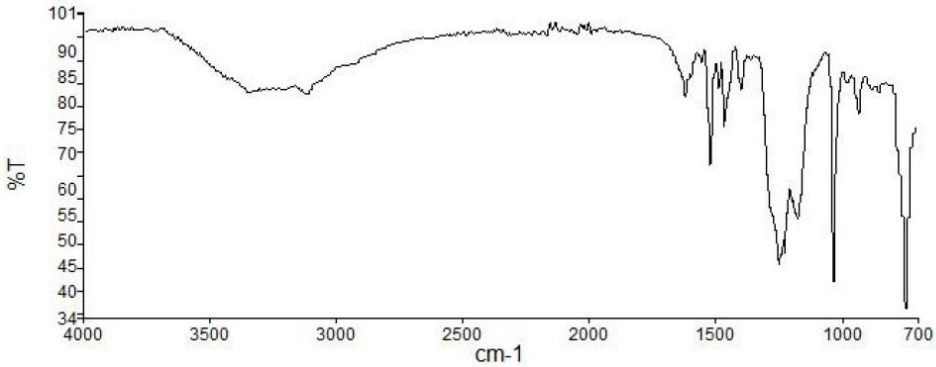

Figure S5.2. IR spectrum of **23**.

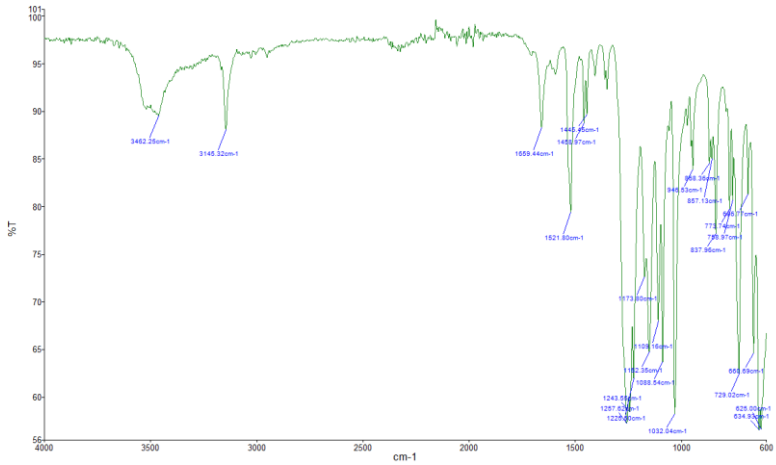

Figure S5.3. IR spectrum of **24**.

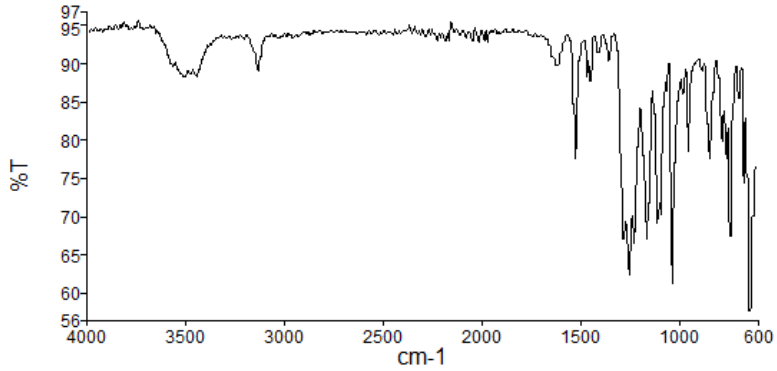

Figure S5.4. IR spectrum of **25**.

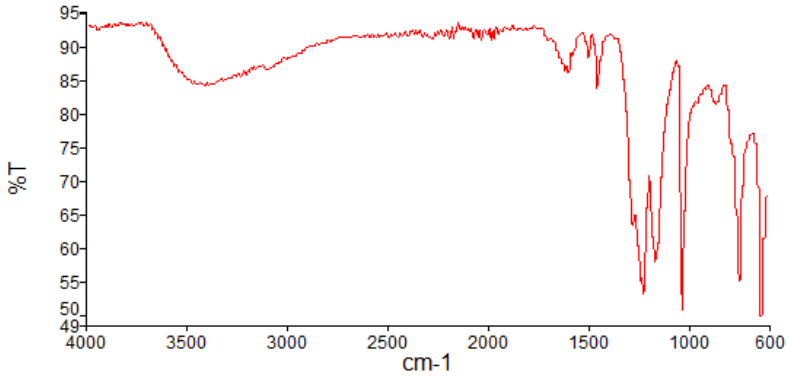

Figure S5.5. IR spectrum of **26**.

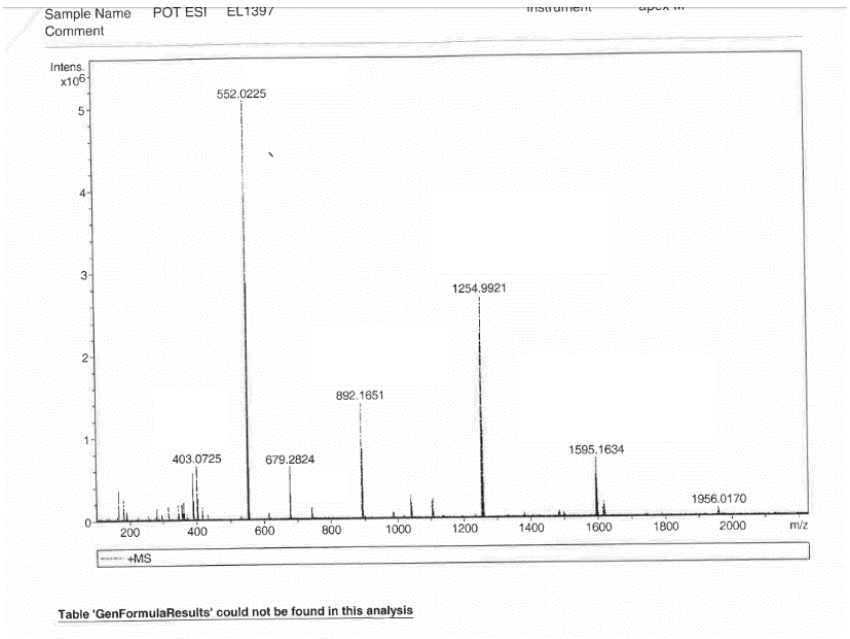

Figure S5.6. ESI-MS data for compound **22** in methanol. Main fragments: 403.07 m/z $[Cu(\mathbf{L^2})]^+$, 552.02 m/z $[Cu(\mathbf{L^2})(CF_3SO_3)]^+$, 614.96 m/z $[Cu_2(\mathbf{L^2})(CF_3SO_3)]^+$, 679.28 m/z $[Cu_3(\mathbf{L^2})(CF_3SO_3)]^+$, 743.22 m/z $[Cu(\mathbf{L^2})_2]^+$, 892.17 m/z $[Cu(\mathbf{L^2})_2(CF_3SO_3)]^+$, 1040.12 m/z

$[Cu(\mathbf{L^2})_2(CF_3SO_3)_2]^+$, 1106.07 m/z $[Cu_2(\mathbf{L^2})_2(CF_3SO_3)_2]^+$, 1232.35 m/z $[Cu(\mathbf{L^2})_3(CF_3SO_3)]^+$, 1254.99 m/z $[Cu_2(\mathbf{L^2})_2(CF_3SO_3)_3]^+$, 1595.16 m/z $[Cu_2(\mathbf{L^2})_3(CF_3SO_3)_3]^+$, 1956.02 m/z $[Cu_4(\mathbf{L^2})_5]^+$.

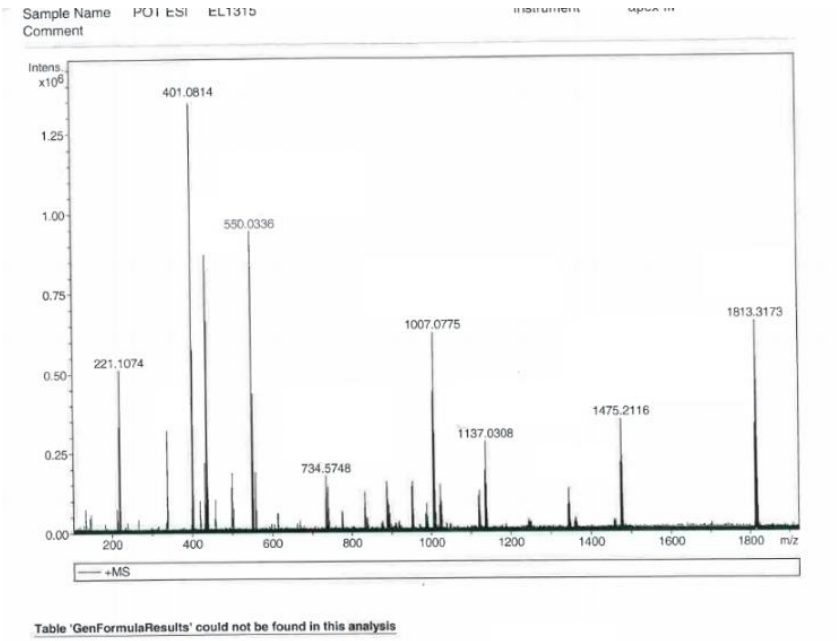

Figure S5.7. ESI-MS data for compound **23** in methanol. Main fragments: 339.16 m/z $[(\mathbf{L^6})+H]^+$, 401.08 m/z $[Cu(\mathbf{L^6})]^+$, 437.05 m/z $[Cu(\mathbf{L^6})(H_2O)_2]^+$, 464.03 m/z $[Cu_2(\mathbf{L^6})]^+$, 500.08 m/z $[Cu_2(\mathbf{L^6})(H_2O)_2]^+$, 550.03 m/z $[Cu(\mathbf{L^6})(CF_3SO_3)]^+$, 612.96 m/z $[Cu_2(\mathbf{L^6})(CF_3SO_3)]^+$, 734.57 m/z $[Cu(\mathbf{L^6})(CF_3SO_3)_2(H_2O)_2]^+$, 739.25 m/z $[Cu(\mathbf{L^6})_2]^+$, 888.19 m/z $[Cu(\mathbf{L^6})_2(CF_3SO_3)]^1$, 953.11 m/z $[Cu_2(\mathbf{L^6})_2(CF_3SO_3)]^+$, 1007.08 m/z $[Cu_2(\mathbf{L^6})_2(CF_3SO_3)(H_2O)_3]^+$, 1037.14 m/z $[Cu(\mathbf{L^6})_2(CF_3SO_3)_2]^+$, 1120.10 m/z $[Cu_2(\mathbf{L^6})_2(CF_3SO_3)_2(H_2O)]^+$, 1137.03 m/z $[Cu_2(\mathbf{L^6})_2(CF_3SO_3)_2(H_2O)_2]^+$, 1245.19 m/z $[Cu(\mathbf{L^6})_3(CF_3SO_3)_2(H_2O)]^+$, 1350.00 m/z $[Cu_3(\mathbf{L^6})_2(CF_3SO_3)_3(H_2O)_2]^+$, 1475.21 m/z $[Cu_2(\mathbf{L^6})_3(CF_3SO_3)_2(H_2O)_2]^+$, 1813.32 m/z $[Cu_2(\mathbf{L^6})_4(CF_3SO_3)_2(H_2O)_2]^+$.

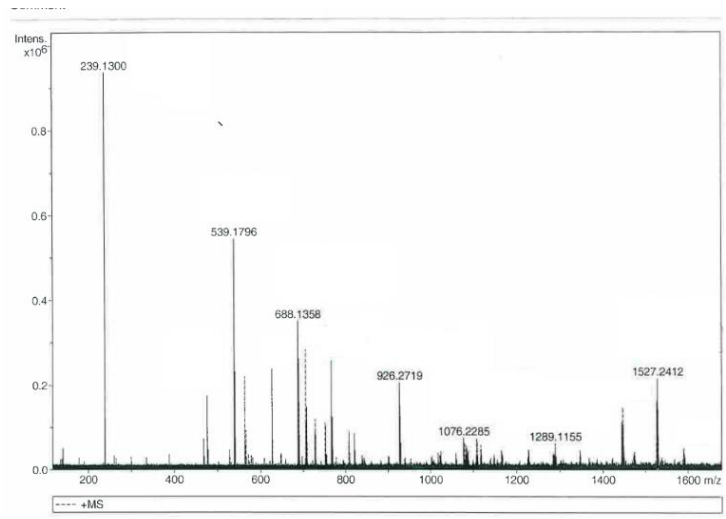

Figure S5.8. ESI-MS data for compound **24** in methanol. Main fragments: 239.13 m/z $[(\mathbf{L^7})+H]^+$, 301.05 m/z $[Cu(\mathbf{L^7})]^+$, 360.06 m/z $[Cu(\mathbf{L^7})_2(CF_3SO_3)(MeOH)]^{2+}$, 450.00 m/z $[Cu(\mathbf{L^7})(CF_3SO_3)]^+$, 477.26 m/z $[(\mathbf{L^7})_2+H]^+$, 539.18 m/z $[Cu(\mathbf{L^7})_2]^+$, 598.18 m/z $[Cu(\mathbf{L^7})(CF_3SO_3)_2]^+$, 627.22 m/z $[(\mathbf{L^7})_2(CF_3SO_3)]^+$, 688.14 m/z $[Cu(\mathbf{L^7})_2(CF_3SO_3)]^+$, 715.36 m/z $[(\mathbf{L^7})_3+H]^+$, 737.36 m/z $[(\mathbf{L^7})_3+Na]$, 753.07 m/z $[Cu_2(\mathbf{L^7})_2(CF_3SO_3)]^+$, 777.39 m/z $[Cu(\mathbf{L^7})_3]^+$, 808.20 m/z $[Cu(\mathbf{L^7})_3(MeOH)]^+$, 838.09 m/z $[Cu(\mathbf{L^7})_2(CF_3SO_3)_2]^+$, 902.00 m/z $[Cu_2(\mathbf{L^7})_2(CF_3SO_3)_2]^+$, 926.27 m/z $[Cu(\mathbf{L^7})_3(CF_3SO_3)]^+$, 1018.22 m/z $[Cu(\mathbf{L^7})_2(CF_3SO_3)_3(MeOH)]^+$, 1076.23 m/z $[Cu(\mathbf{L^7})_3(CF_3SO_3)_2]^+$, 1164.40 m/z $[(\mathbf{L^7})_3(CF_3SO_3)_3]^+$, 1224.78 m/z $[Cu(\mathbf{L^7})_3(CF_3SO_3)_3]^+$, 1289.12 m/z $[Cu_2(\mathbf{L^7})_3(CF_3SO_3)_3]^+$, 1352.34 m/z $[Cu_3(\mathbf{L^7})_3(CF_3SO_3)_3]^+$, 1445.63 m/z $[Cu_3(\mathbf{L^7})_4(CF_3SO_3)_2]^+$, 1527.24 m/z $[Cu_2(\mathbf{L^7})_4(CF_3SO_3)_3]^+$, 1589.32 m/z $[Cu_3(\mathbf{L^7})_4(CF_3SO_3)_3]^+$.

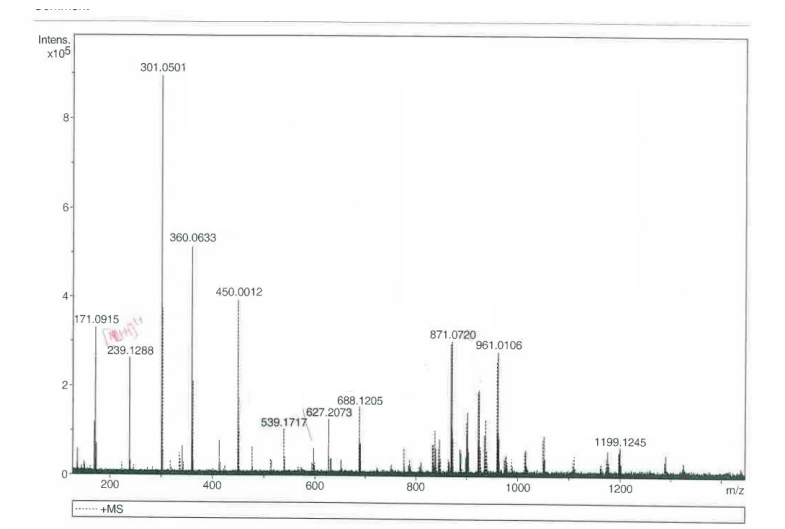

Figure S5.9. ESI-MS data for compound **25** in methanol. Main fragments: Main fragments: 239.13 m/z $[(\mathbf{L^7})+H]^+$, 301.05 m/z $[Cu(\mathbf{L^7})]^+$, 360.06 m/z $[Cu(\mathbf{L^7})_2(CF_3SO_3)(MeOH)]^{2+}$,

450.00 m/z $[Cu(\mathbf{L^7})(CF_3SO_3)]^+$, 539.17 m/z $[Cu(\mathbf{L^7})_2]^+$, 598.18 m/z $[Cu(\mathbf{L^7})(CF_3SO_3)_2]^+$, 627.21 m/z $[(\mathbf{L^7})_2(CF_3SO_3)]^+$, 688.12 m/z $[Cu(L^6)_2(CF_3SO_3)]^+$, 838.09 m/z $[Cu(\mathbf{L^7})_2(CF_3SO_3)_2]^+$, 871.07 m/z $[Cu(\mathbf{L^7})_2(CF_3SO_3)_2(MeOH)]^+$, 902.00 m/z $[Cu_2(\mathbf{L^7})_2(CF_3SO_3)_2]^+$, 925.04 m/z $[Cu(\mathbf{L^7})_3(CF_3SO_3)]^+$, 961.01 m/z $[Cu_3(\mathbf{L^7})(CF_3SO_3)_2]^+$, 986.04 m/z $[Cu(\mathbf{L^7})_2(CF_3SO_3)_3]^+$, 1050.95 m/z $[Cu_2(\mathbf{L^7})_2(CF_3SO_3)_3]^+$, 1199.12 m/z $[Cu_3(\mathbf{L^7})_3(CF_3SO_3)_2]^+$.

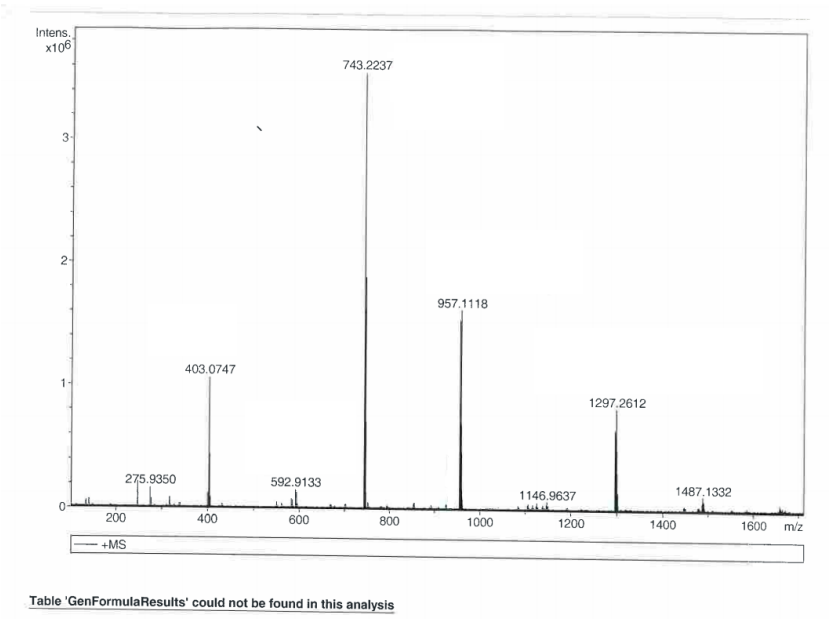

Figure S5.10. ESI-MS data for compound **26** in methanol. Main fragments: 403.07 m/z $[Cu(\mathbf{L^3})]^+$, 592.91 m/z $[Cu(\mathbf{L^3})_2(CF_3SO_3)_3]^{2+}$, 743.22 m/z $[Cu(\mathbf{L^3})_2]^+$, 957.11 m/z $[Cu_2(\mathbf{L^3})_2(CF_3SO_3)]^+$, 1297.26 m/z $[Cu_2(\mathbf{L^3})_3(CF_3SO_3)]^+$.

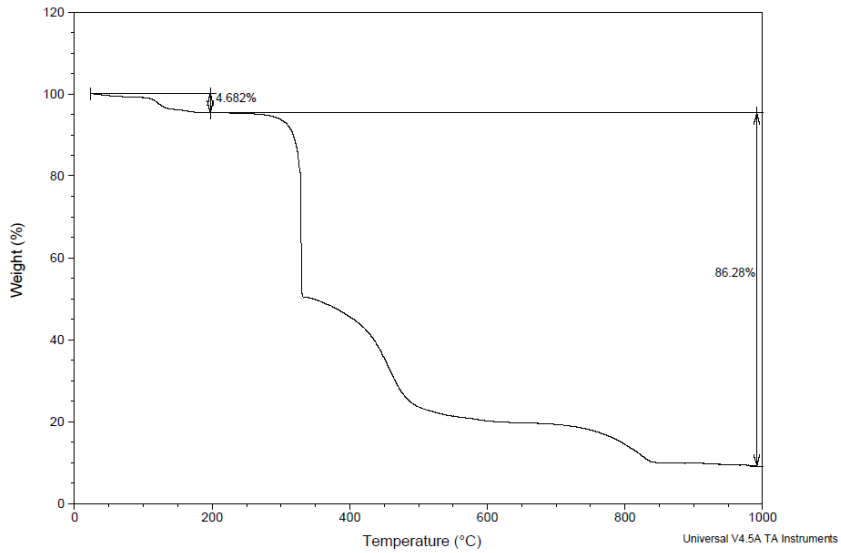

Figure S5.11. TGA graph for compound **22**.

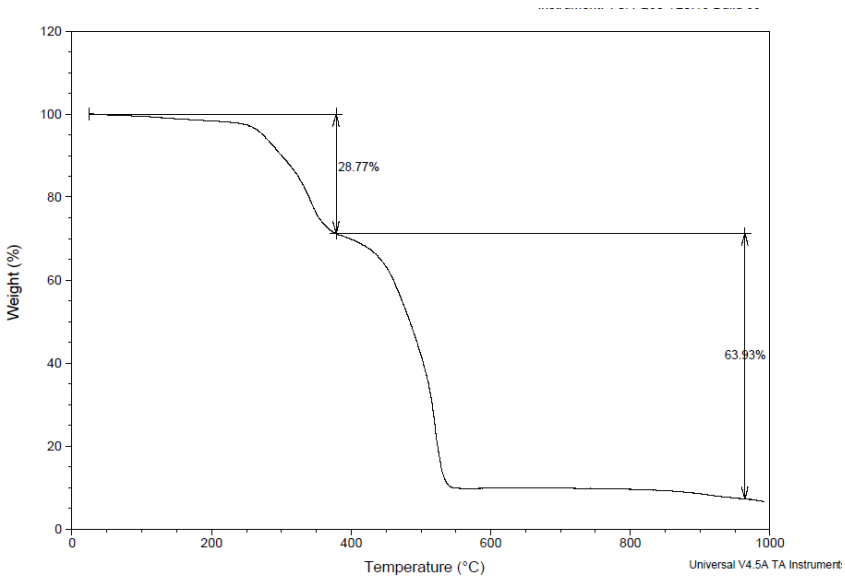

Figure S5.12. TGA graph for compound **23**.

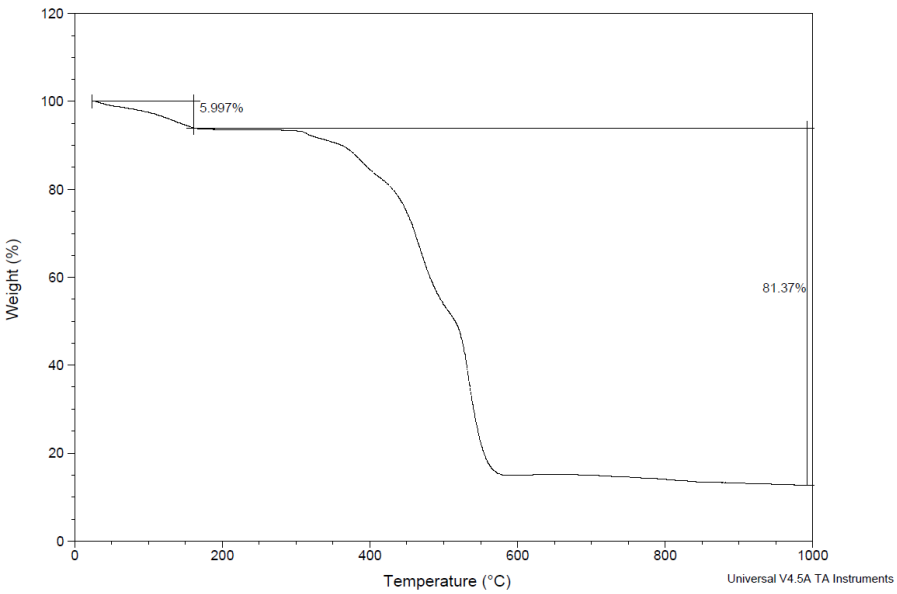

Figure S5.13. TGA graph for compound **24**.

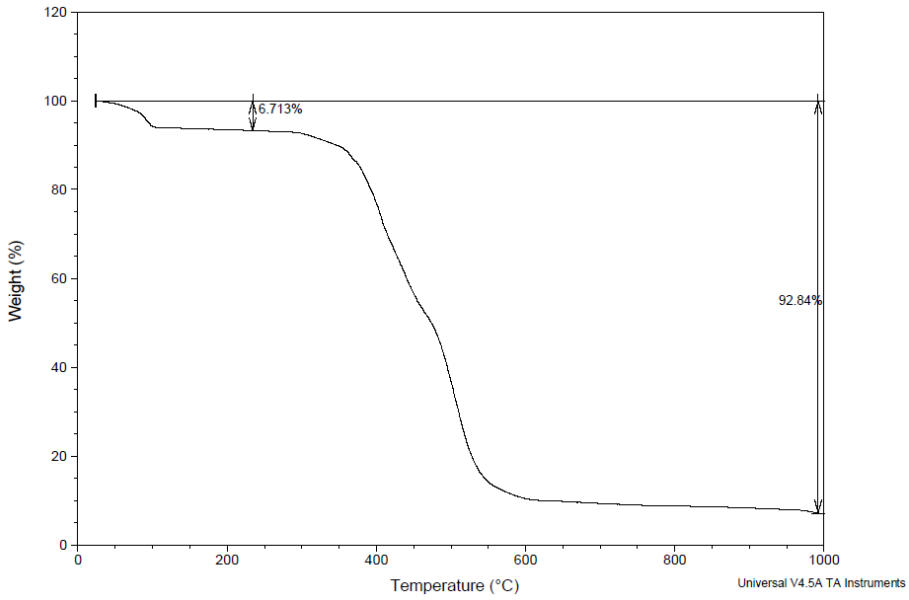

Figure S5.14. TGA graph for compound **25**.

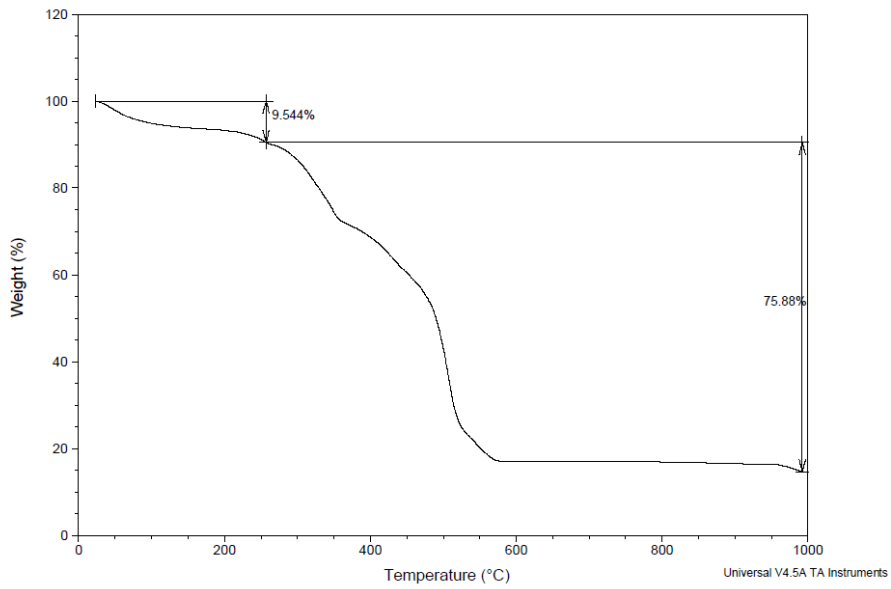

Figure S5.15. TGA graph for compound **26**.

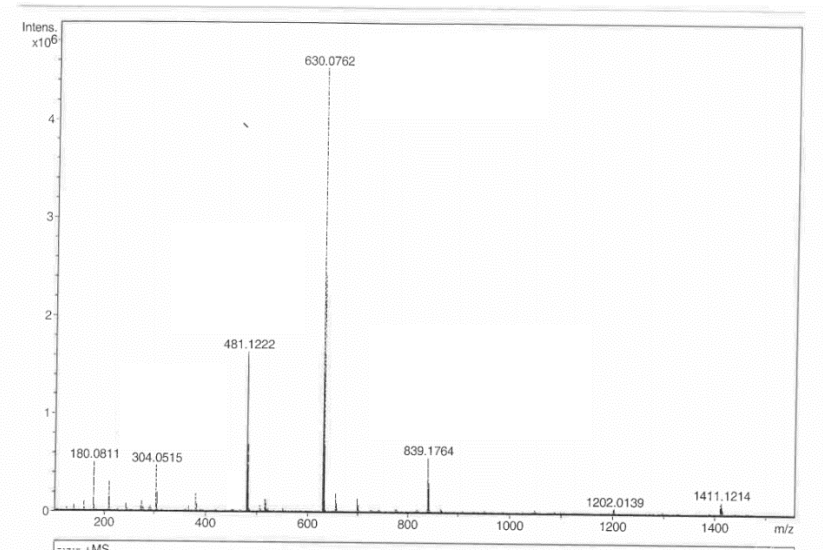

Figure S5.16. ESI-MS data for the *in situ* generated catalyst from $Cu(OTf)_2 \cdot H_2O$ and $\mathbf{L^8}$ in methanol. Main fragments: 304.05 m/z $[Cu(\mathbf{L^8})(MeOH)]^{+1}$, 481.12 m/z $[Cu(\mathbf{L^8})_2]^{1+}$, 630.08 m/z $[Cu(\mathbf{L^8})_2(CF_3SO_3)]^{+1}$, 839.18 m/z $[Cu(\mathbf{L^8})_3(CF_3SO_3)]^{+1}$, 1048.27 m/z $[Cu(\mathbf{L^8})_4(CF_3SO_3)]^{+1}$, 1202.01 m/z $[Cu_2(\mathbf{L^8})_3(CF_3SO_3)_3]^{+1}$, 1411.12 m/z $[Cu_2(\mathbf{L^8})_4(CF_3SO_3)_3]^{+1}$.

Table S5.1. The electrochemical data of the Cu^{II} complexes **18**, **20**, **23** (Parameters of the voltammetric measurements: glassy carbon electrode, DMF or DMSO, 0.1 M TBAP, 100 mV/s).

Complex	E_c (V)	I_c (μA)	E_a (V)	I_a (μA)	ΔE (V)	$E_{1/2}$ (V)	E^0 (V)	I_a/I_k	Solvent
Compound **20**	0.345	-7.1	0.464	19.6					DMF
	0.0507	-16.8	0.182	73.1					
	-0.215	-24.6							
Compound **18**	0.429	-6.91	0.556	8.45	0.127	0.493	0.702	1.2	
Compound **23**	0.409	-13.5	0.528	16.5	0.119	0.469	0.678	1.2	
$Cu(NO_3)_2$	0.371	-8.75	0.529	16.5					
	-0.0137	-14.9	0.182	32.6					
	-0.243	-15.1							
Compound **20**	0.224	-4.73	0.436	9.92					DMSO
	0.0185	-12.8	0.133	27.4					
	-0.392	-15.1	0.07	35.9					
Compound **18**	0.22	-3.07	0.45	3.31	0.23	0.335	0.544	1.1	
Compound **23**	0.22	-11.8	0.443	12.1	0.223	0.332	0.541	1.0	
$Cu(NO_3)_2$	0.226	-4.48	0.44	9.55					
	0.0251	-15.5	0.158	32.1					
	-0.321	-24	0.081	47.2					

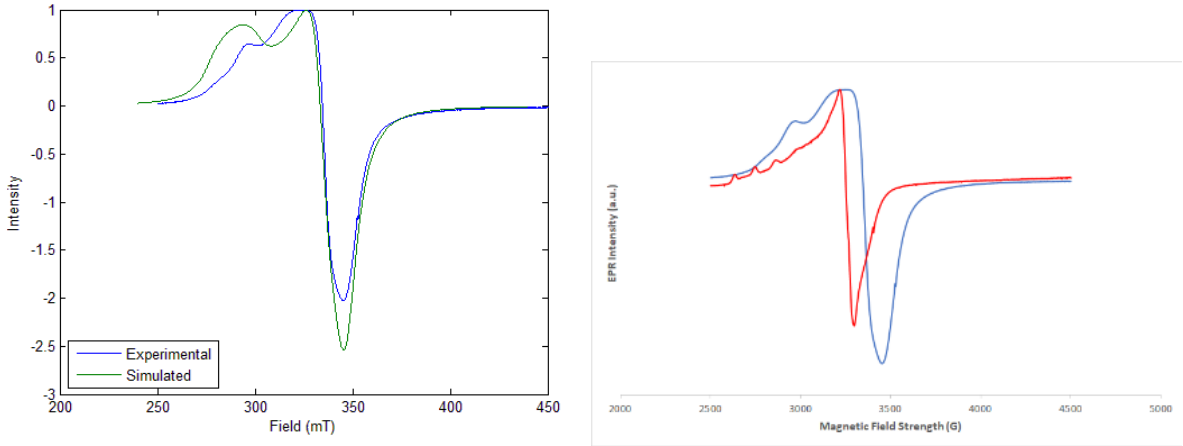

Figure S5.17. (left) Experimental (blue traces) and simulated (green traces) X-band EPR spectra for **23** at 9.496899 GHz and 5 K. (right) Overlay of EPR spectra in solid state (blue traces) and in methanolic solution (red traces) for **23** at 9.496899 GHz and 5 K.

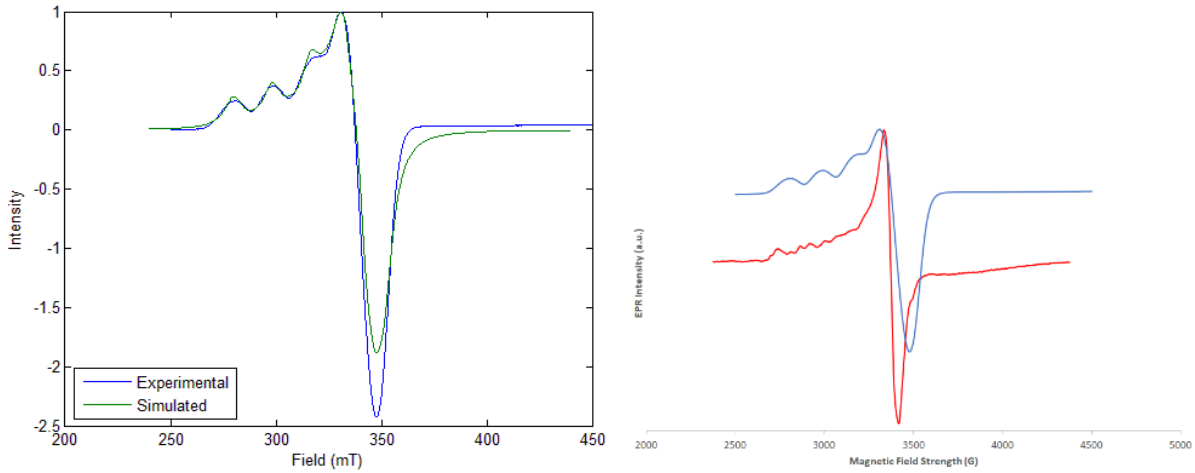

Figure S5.18. (left) Experimental (blue traces) and simulated (green traces) X-band EPR spectra for **18** at 9.383448 GHz and 5 K. (right) Overlay of EPR spectra in solid state (blue traces) and in ethanolic solution (red traces) for **18** at 9.383448 GHz and 5 K.

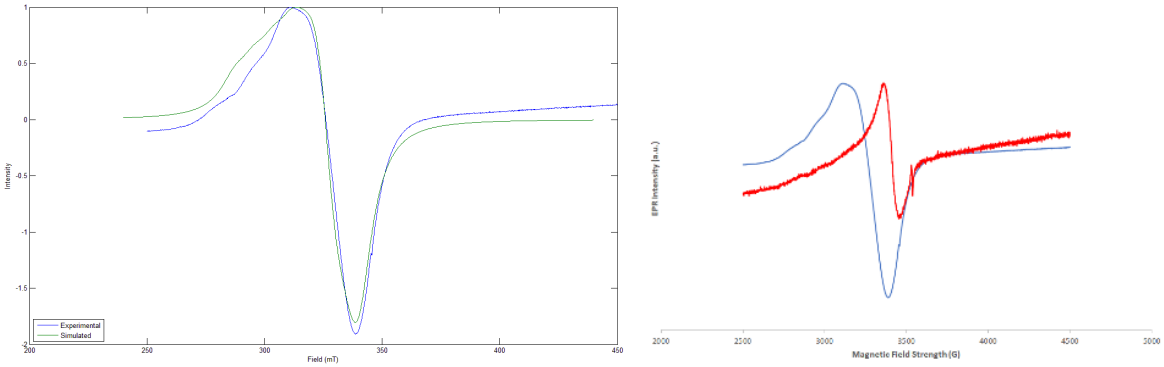

Figure S5.19. (left) Experimental (blue traces) and simulated (green traces) X-band EPR spectra for **20** at 9.303858 GHz and 5 K. (right) Overlay of EPR spectra in solid state (blue traces) and in methanolic solution (red traces) for **20** at 9.303858 GHz and 5 K.

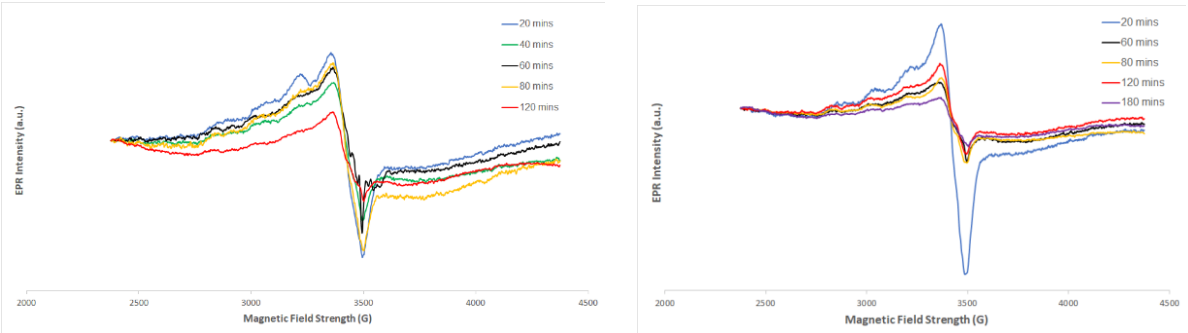

Figure S5.20. (left) Overlay of EPR spectra of aliquots from the catalytic reaction (**18** used as catalyst) during the synthesis of triazole **C5T1** in selected times. (right) Overlay of EPR spectra of aliquots from the catalytic reaction (**18** used as catalyst), with 15% Sodium-L-ascorbate added, during the synthesis of triazole **C5T1** in selected times.

5.2. ^{1}H, ^{13}C NMR and HRMS spectra of triazole products

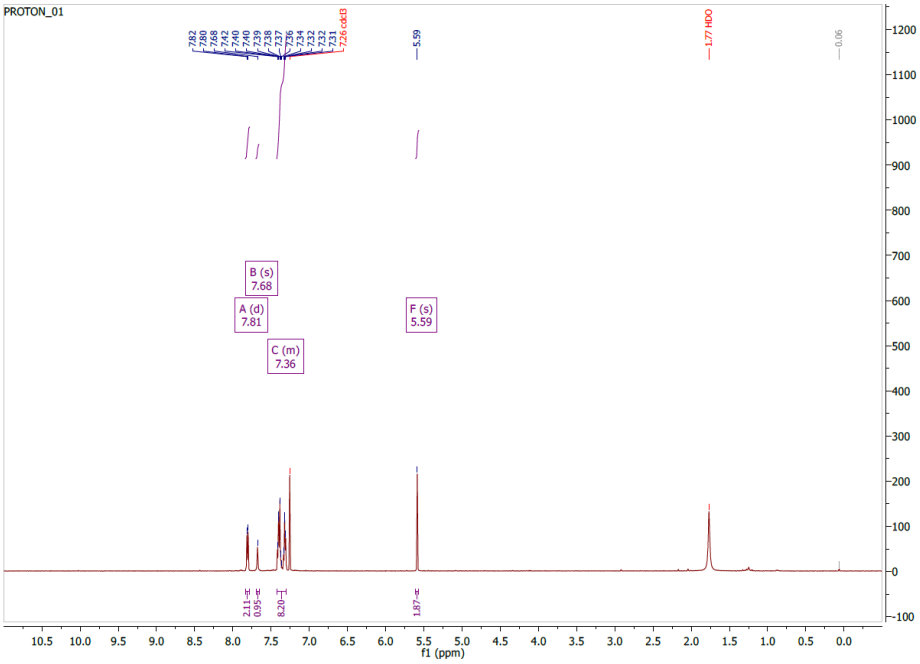

Figure S5.21. ^{1}H NMR spectrum of triazole **C5T1**.

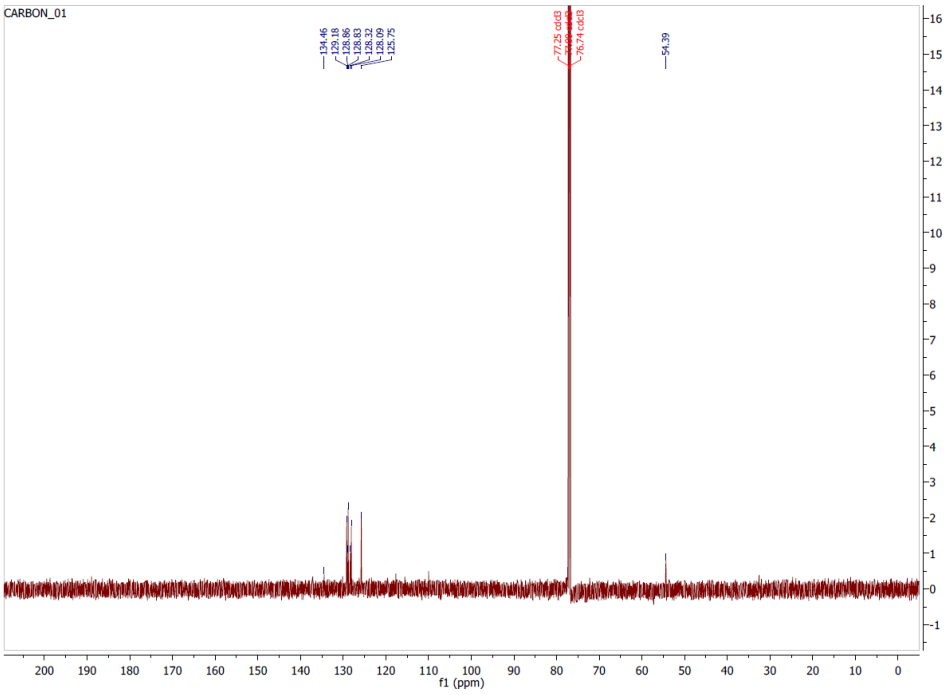

Figure S5.22. ^{13}C NMR spectrum of triazole **C5T1**.

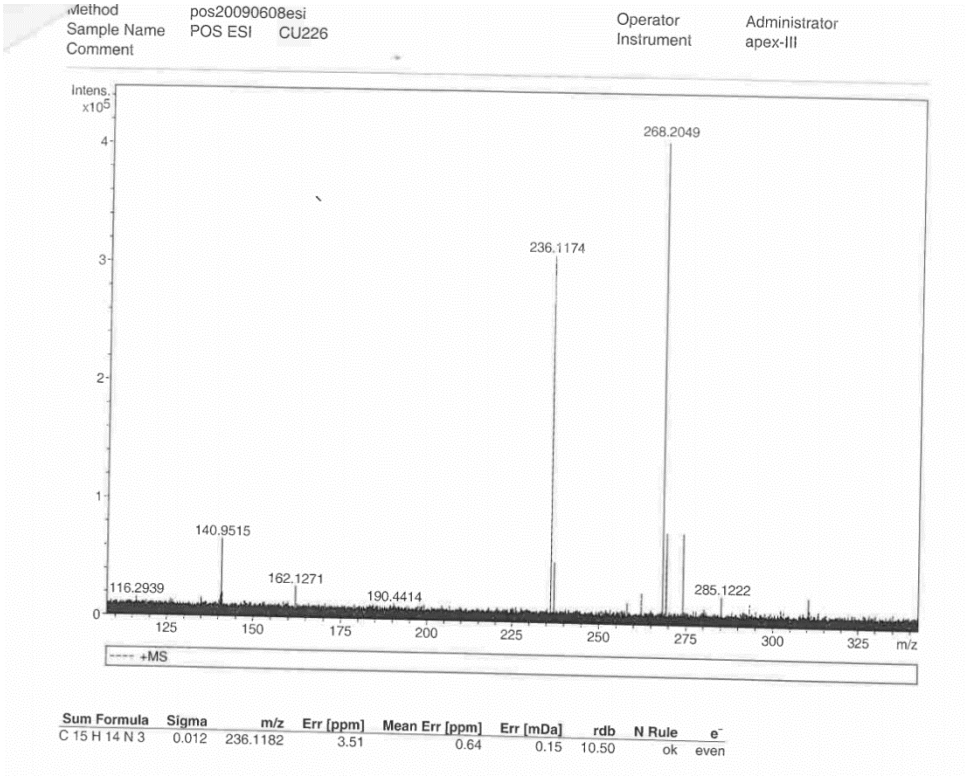

Figure S5.23. HRMS spectrum of triazole **C5T1**.

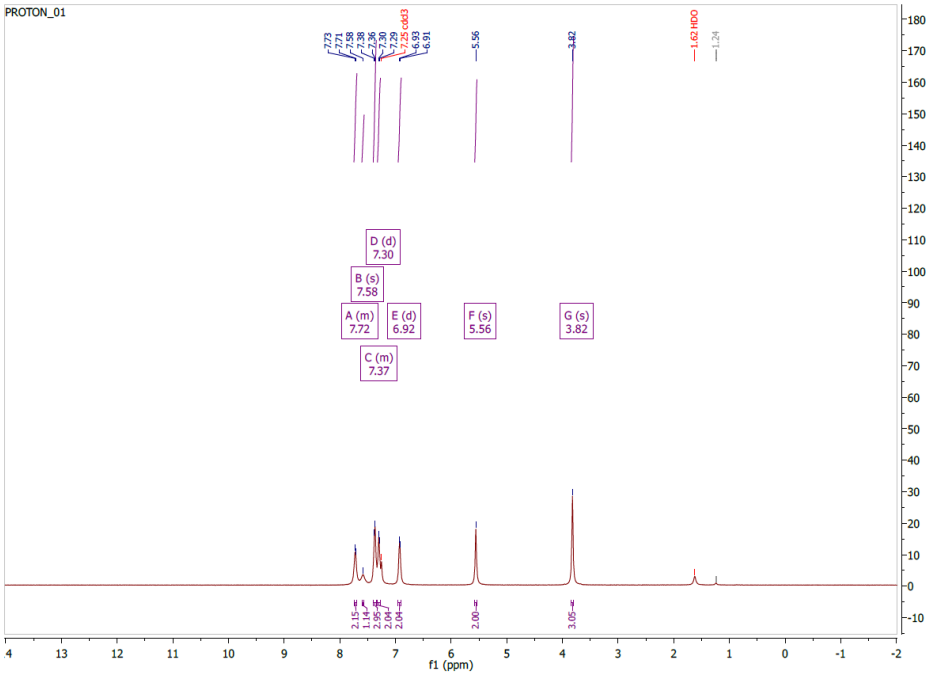

Figure S5.24. ^{1}H NMR spectrum of triazole **C5T2**.

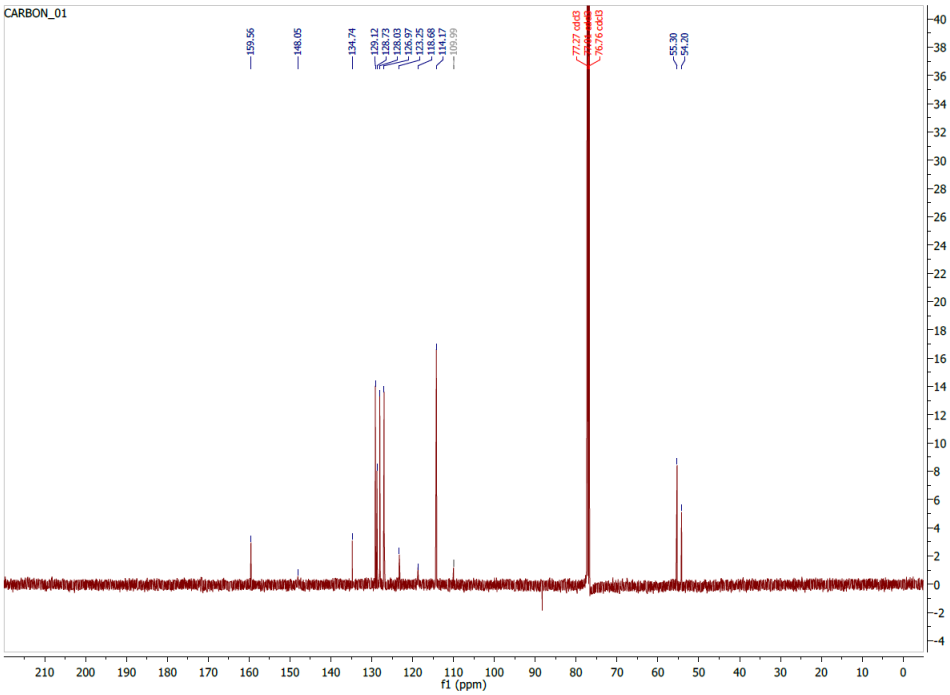

Figure S5.25. ^{13}C NMR spectrum of triazole **C5T2**.

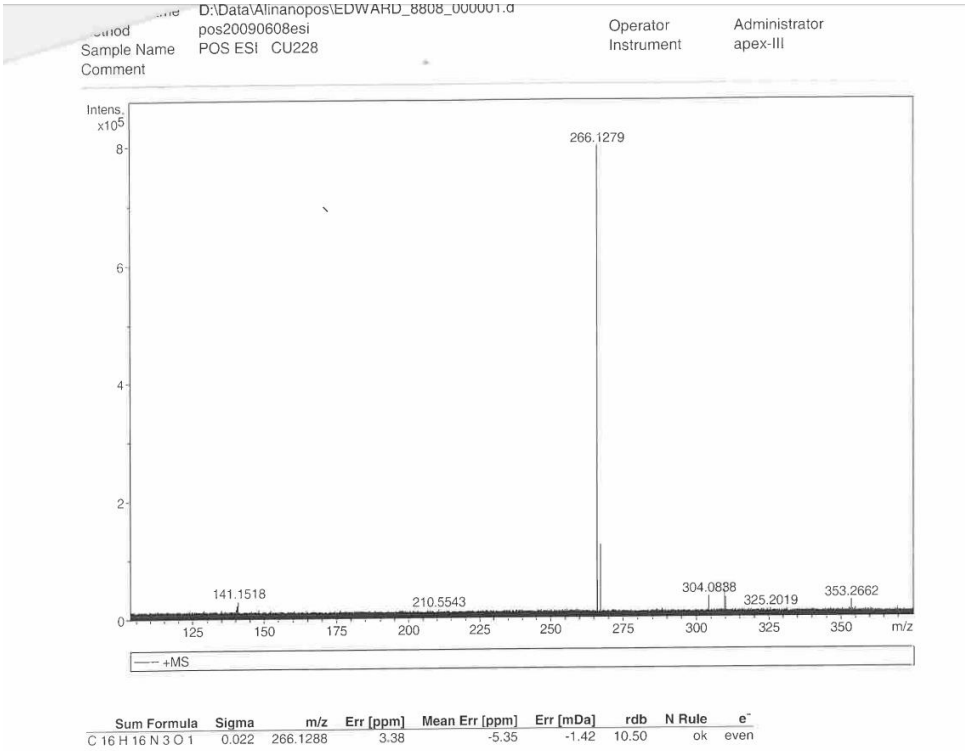

Figure S5.26. HRMS spectrum of triazole **C5T2**.

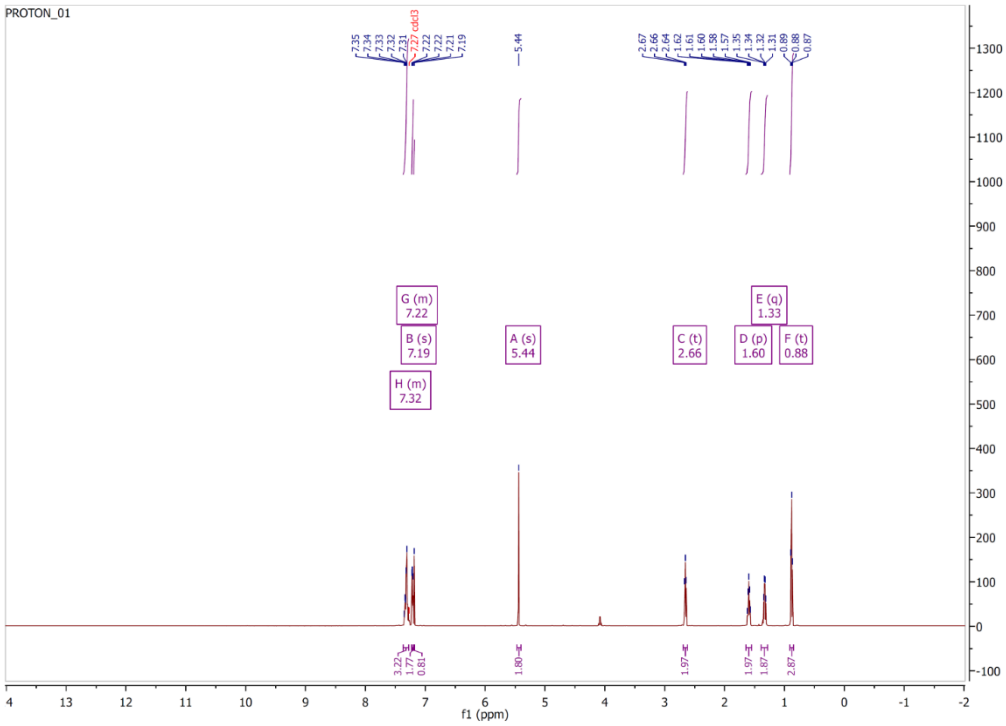

Figure S5.27. ^{1}H NMR spectrum of triazole **C5T3**.

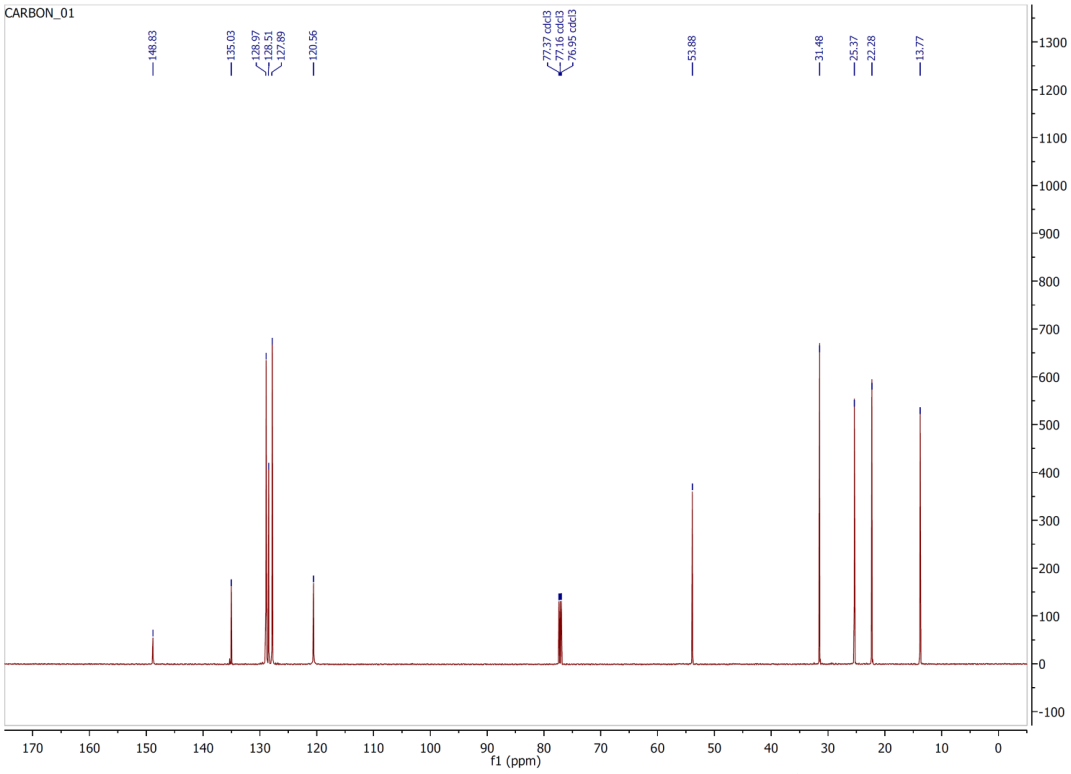

Figure S5.28. ^{13}C NMR spectrum of triazole **C5T3**.

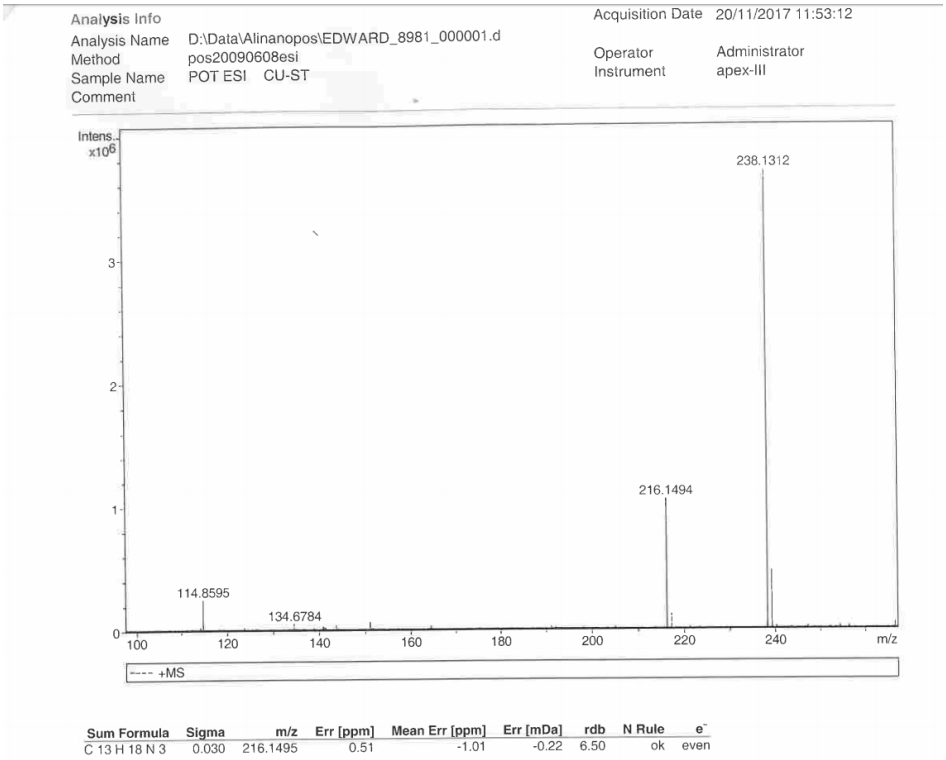

Figure S5.29. HRMS spectrum of triazole **C5T3**.

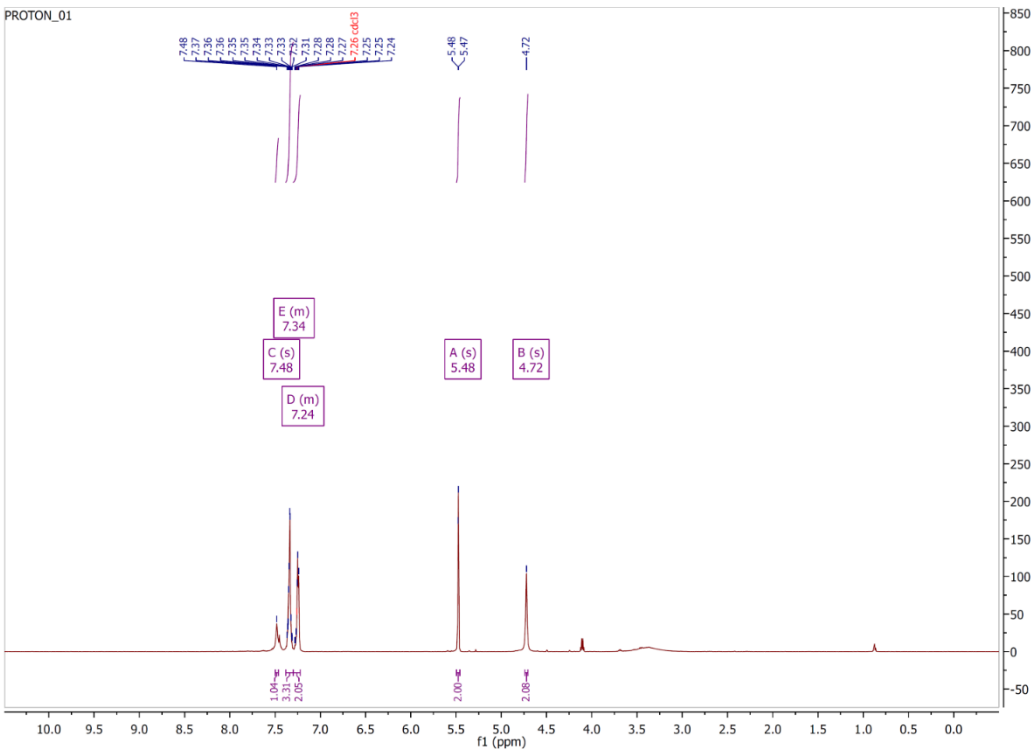

Figure S5.30. ^{1}H NMR spectrum of triazole **C5T4**.

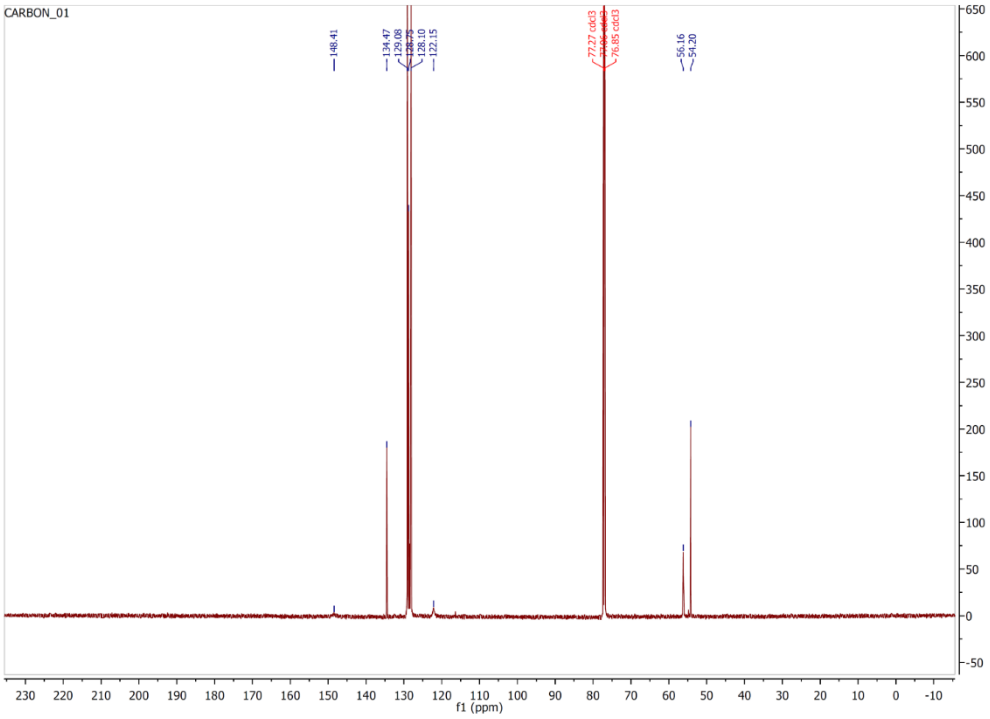

Figure S5.31. ^{13}C NMR spectrum of triazole **C5T4**.

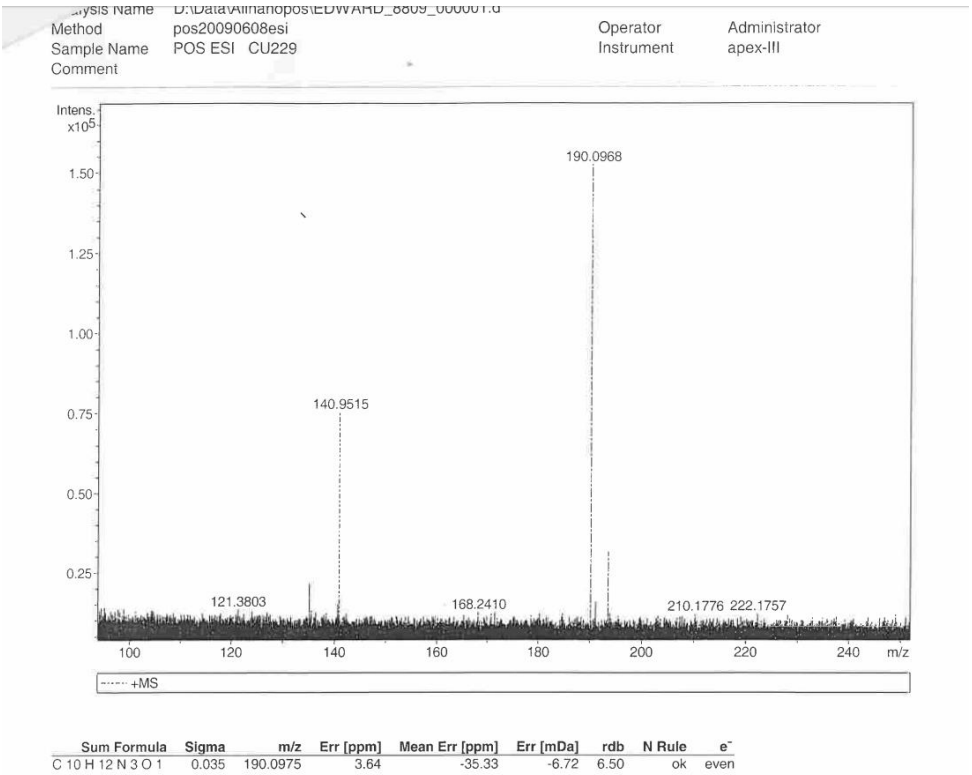

Figure S5.32. HRMS spectrum of triazole **C5T4**.

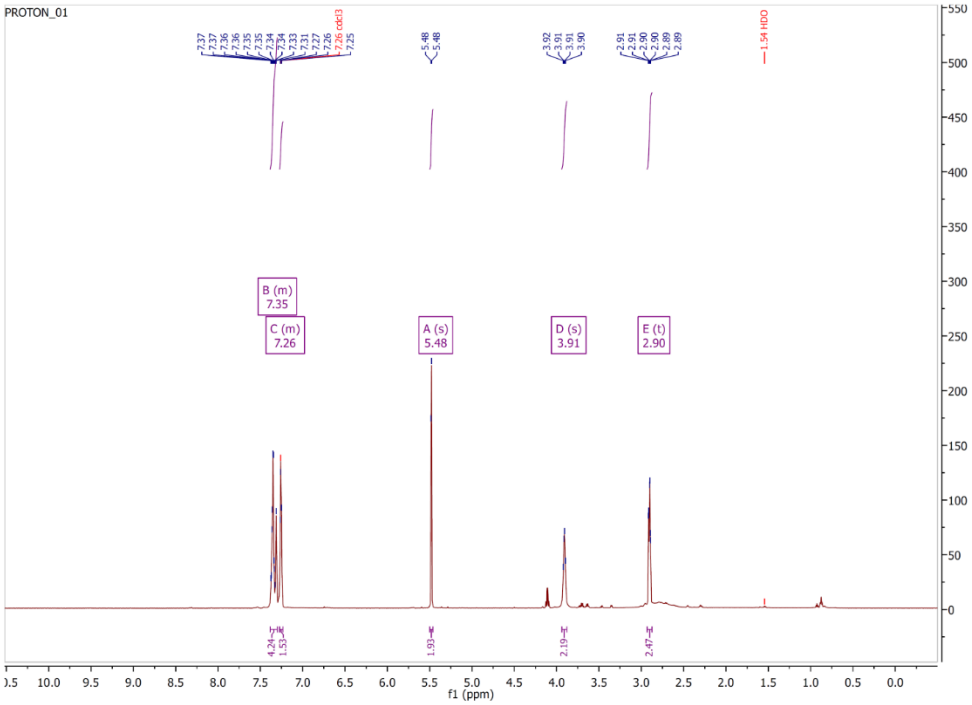

Figure S5.33. ^{1}H NMR spectrum of triazole **C5T5**.

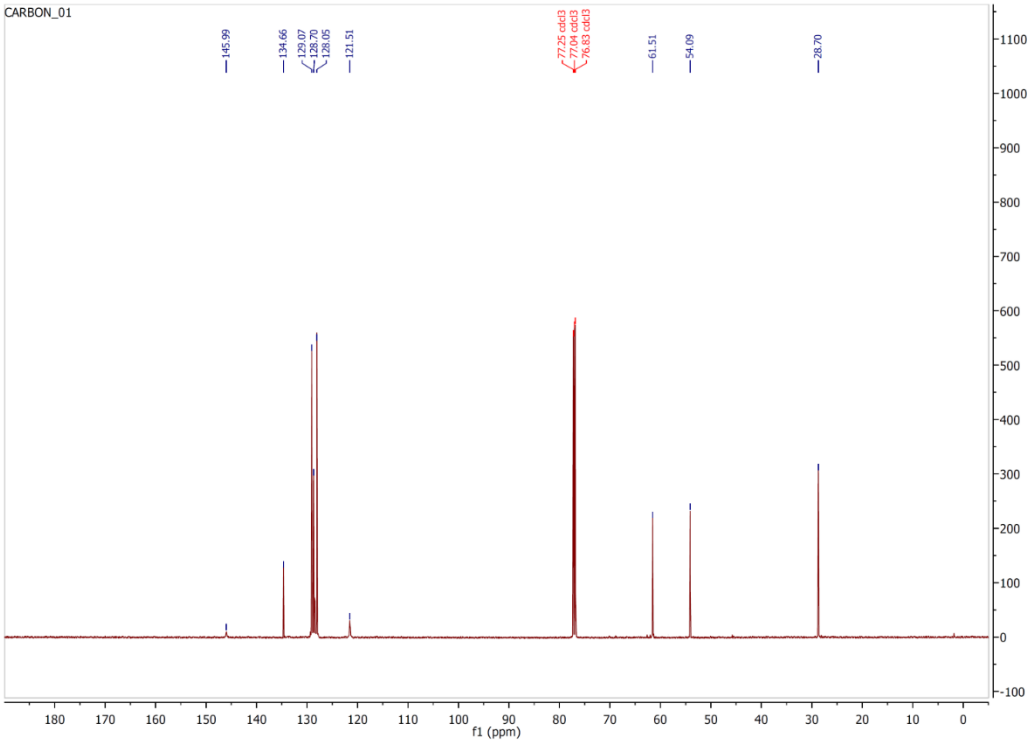

Figure S5.34. ^{13}C NMR spectrum of triazole **C5T5**.

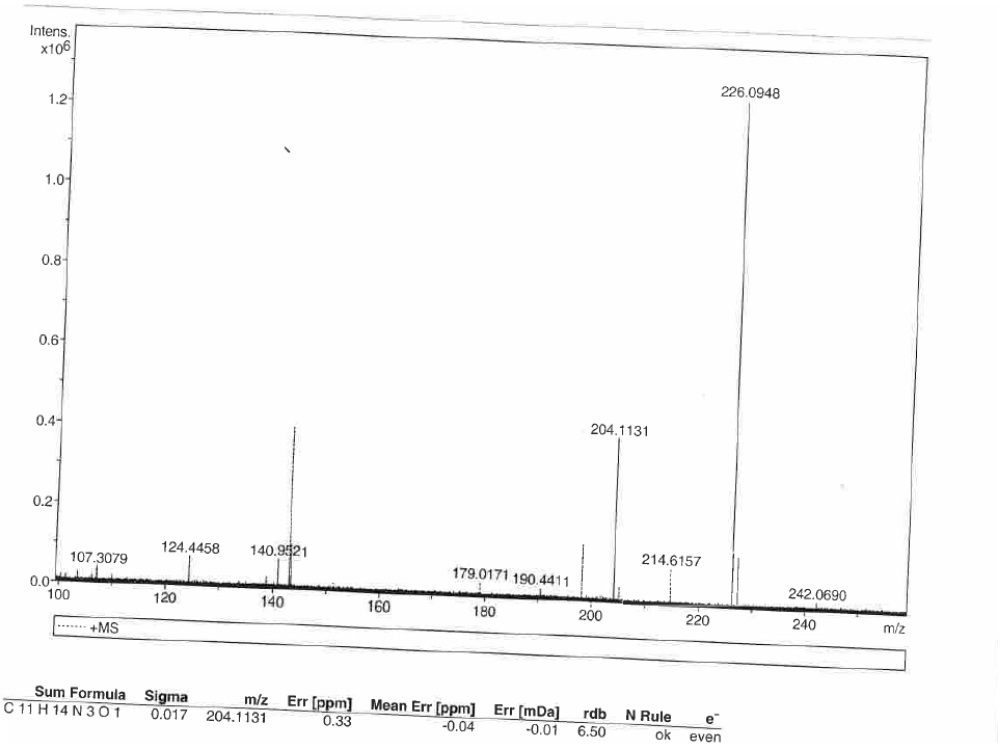

Figure S5.35. HRMS spectrum of triazole **C5T5**.

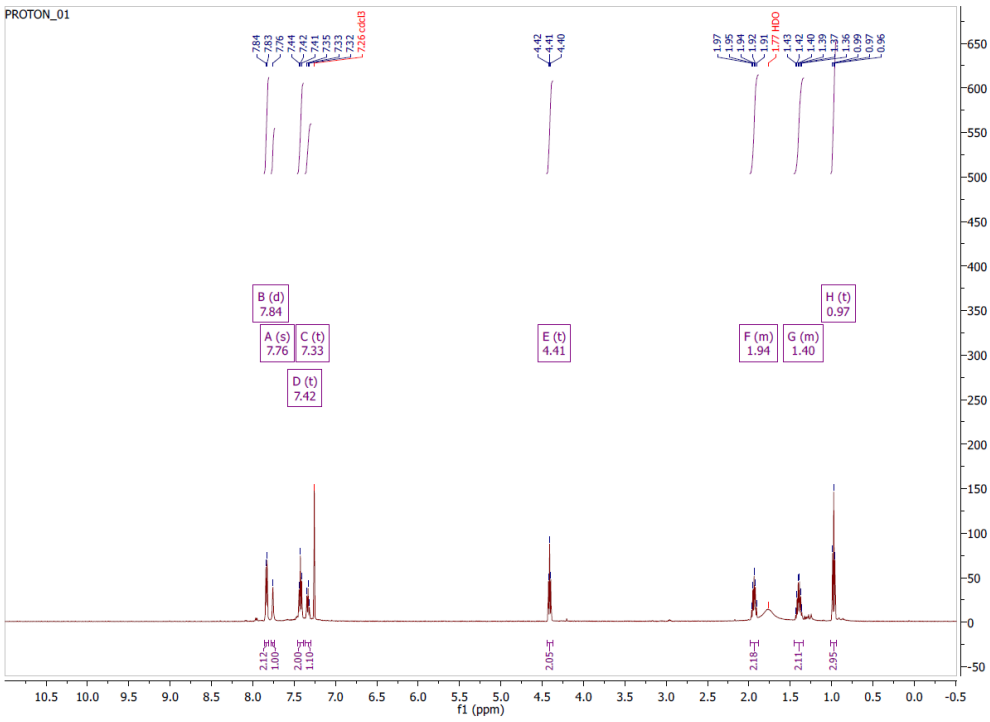

Figure S5.36. ^{1}H NMR spectrum of triazole **C5T7**.

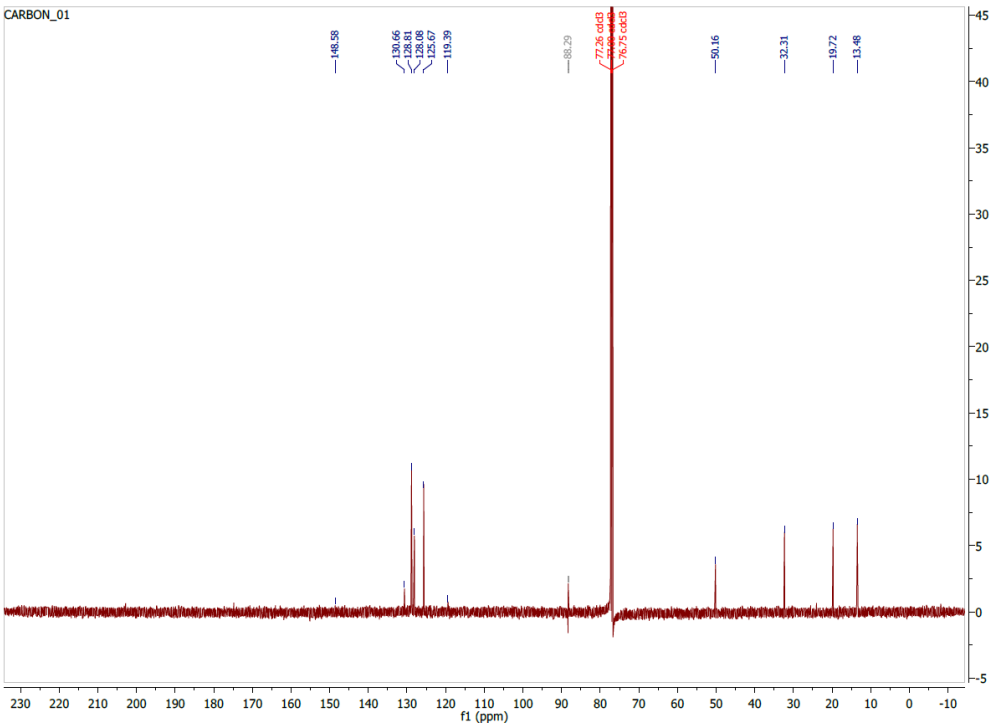

Figure S5.37. ^{13}C NMR spectrum of triazole **C5T7**.

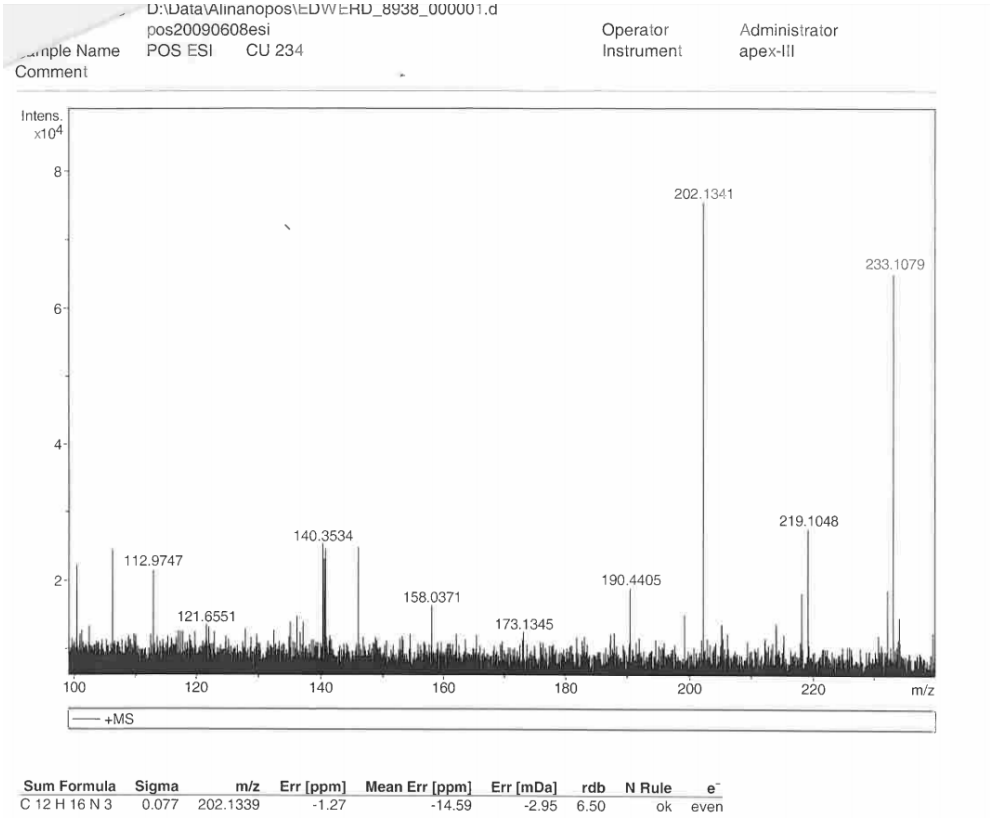

Figure S5.38. HRMS spectrum of triazole **C5T7**.

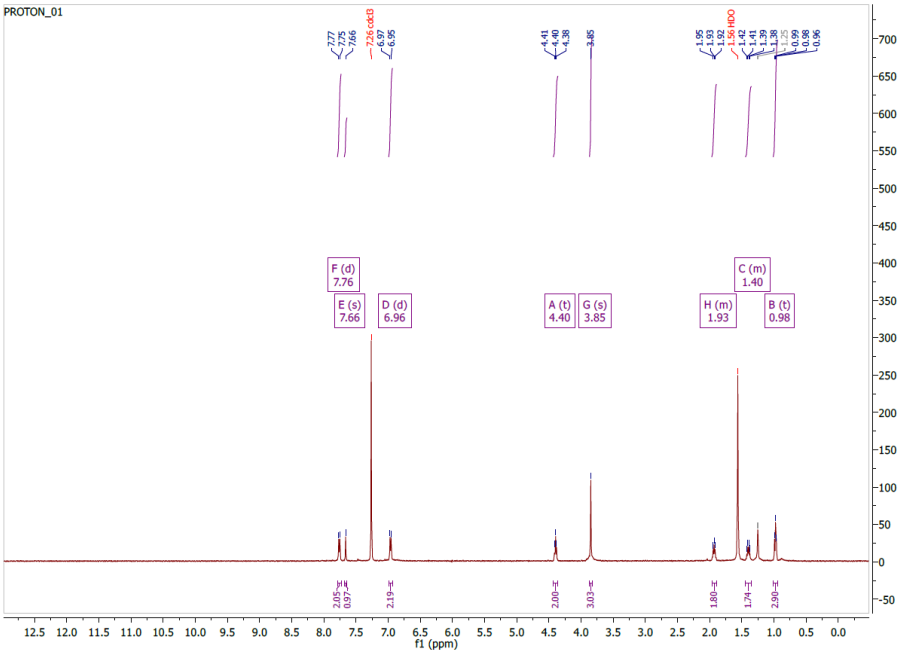

Figure S5.39. ^{1}H NMR spectrum of triazole **C5T8**.

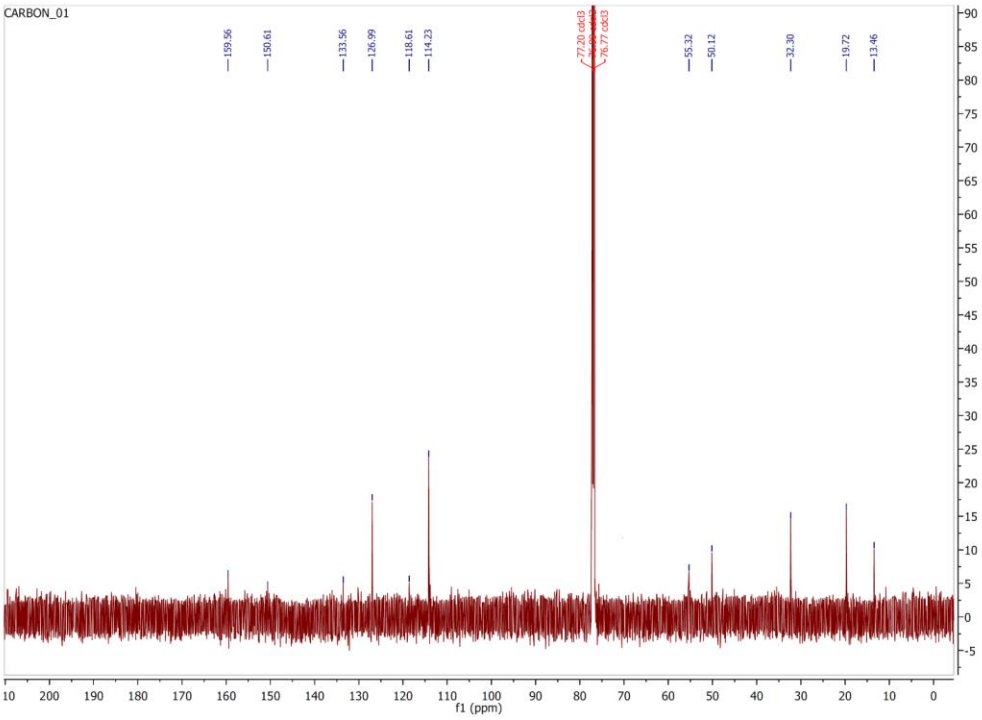

Figure S5.40. ^{13}C NMR spectrum of triazole **C5T8**.

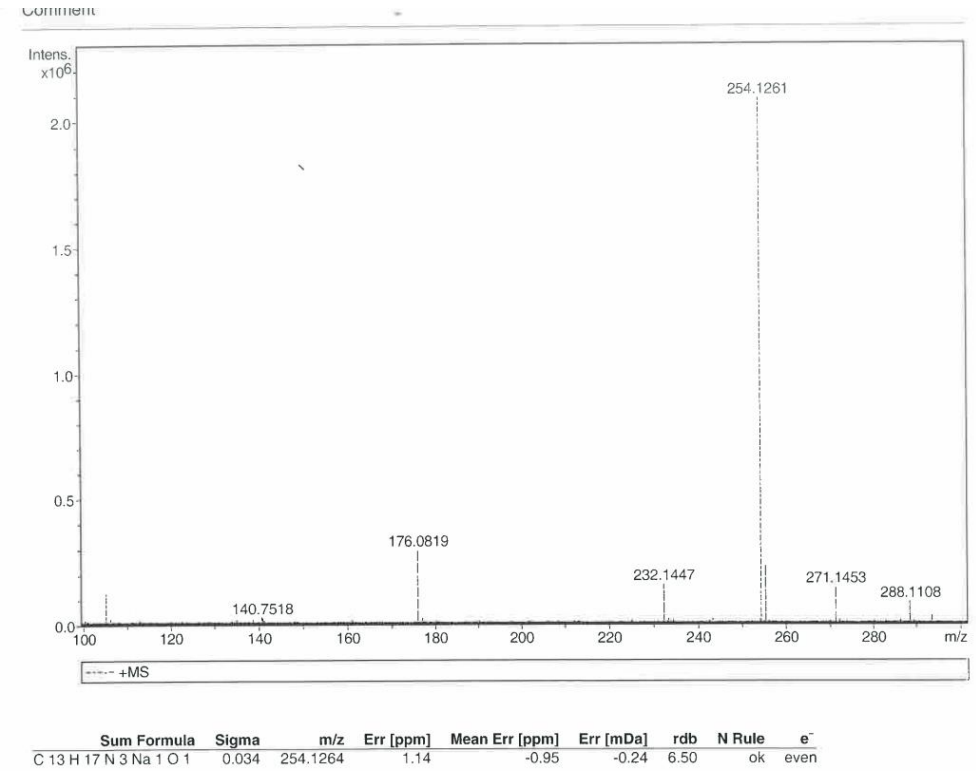

Figure S5.41. HRMS spectrum of triazole **C5T8**.

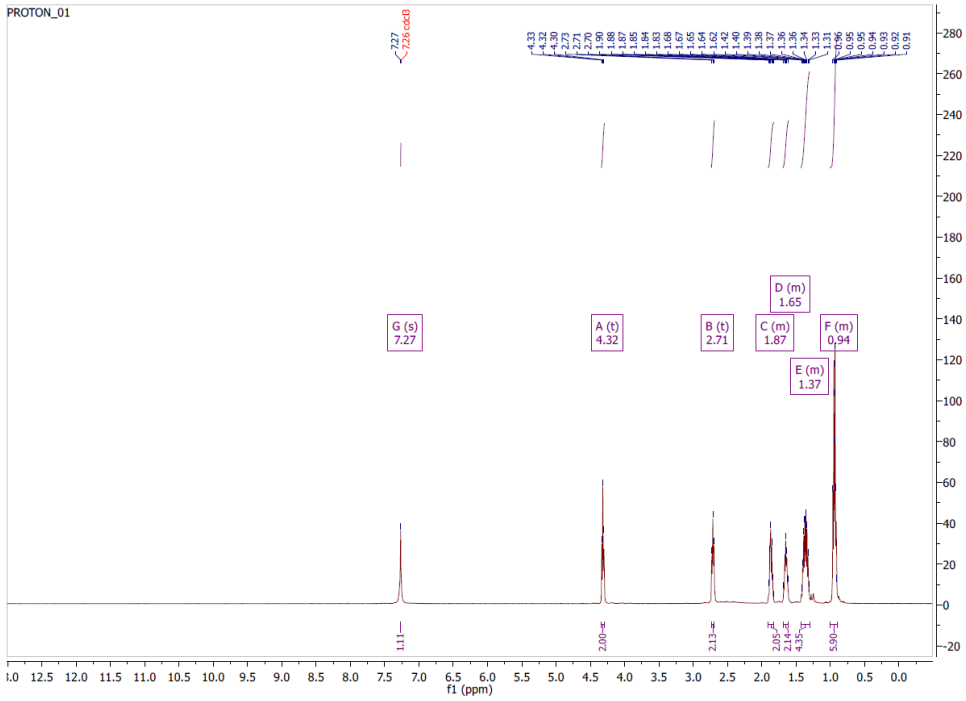

Figure S5.42. ^{1}H NMR spectrum of triazole **C5T9**.

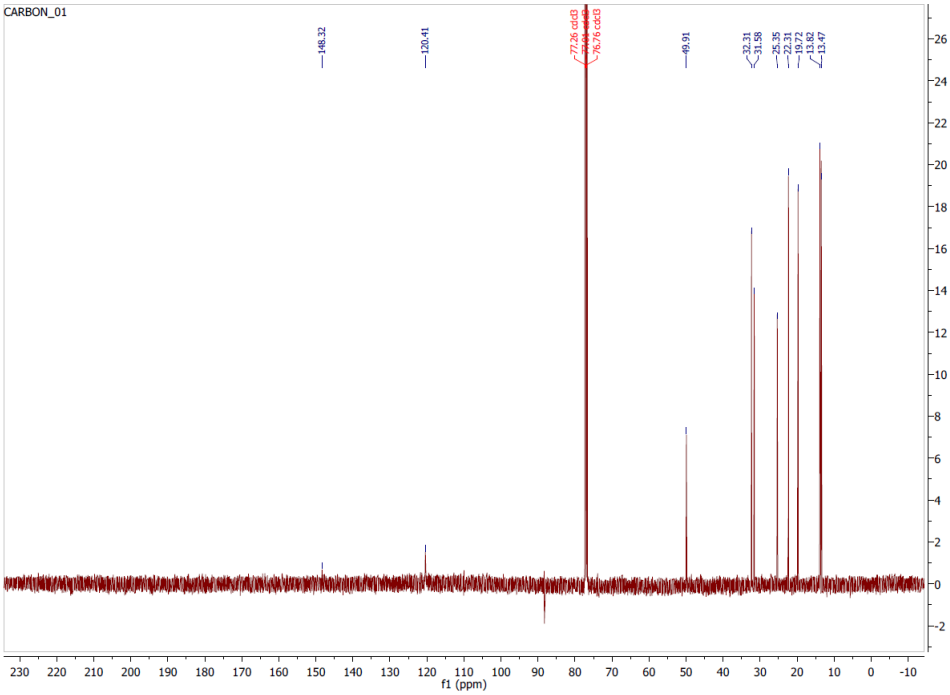

Figure S5.43. ^{13}C NMR spectrum of triazole **C5T9**.

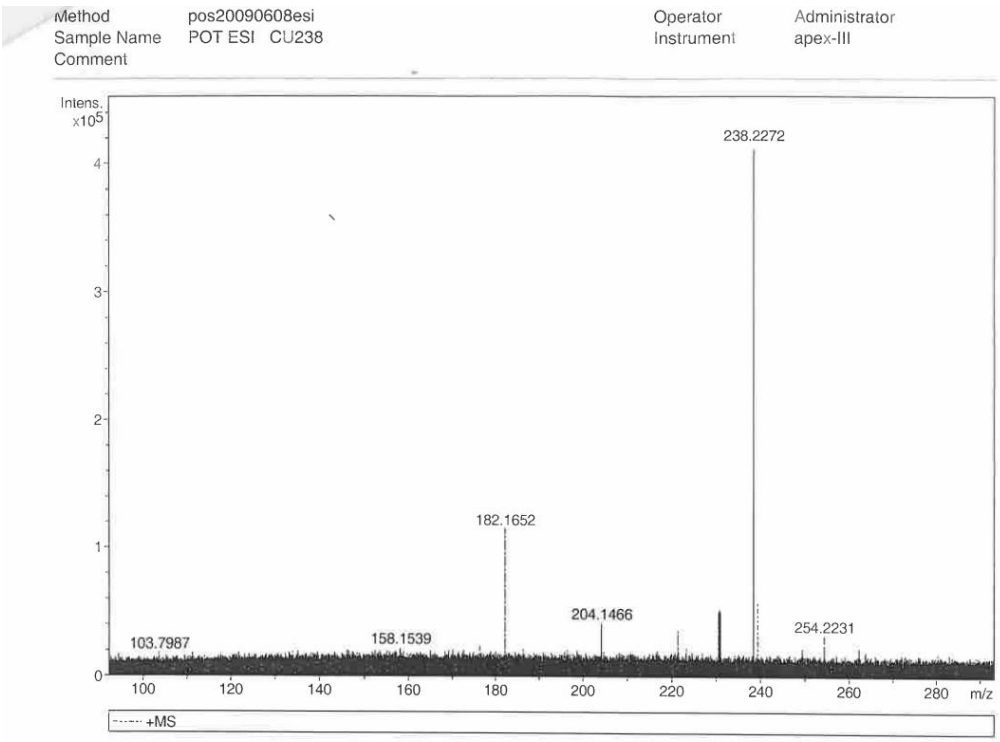

Sum Formula	Sigma	m/z	Err [ppm]	Mean Err [ppm]	Err [mDa]	rdb	N Rule	e⁻
C 10 H 20 N 3	0.010	182.1652	0.06	-9.82	-1.79	2.50	ok	even

Figure S5.44. HRMS spectrum of triazole **C5T9**.

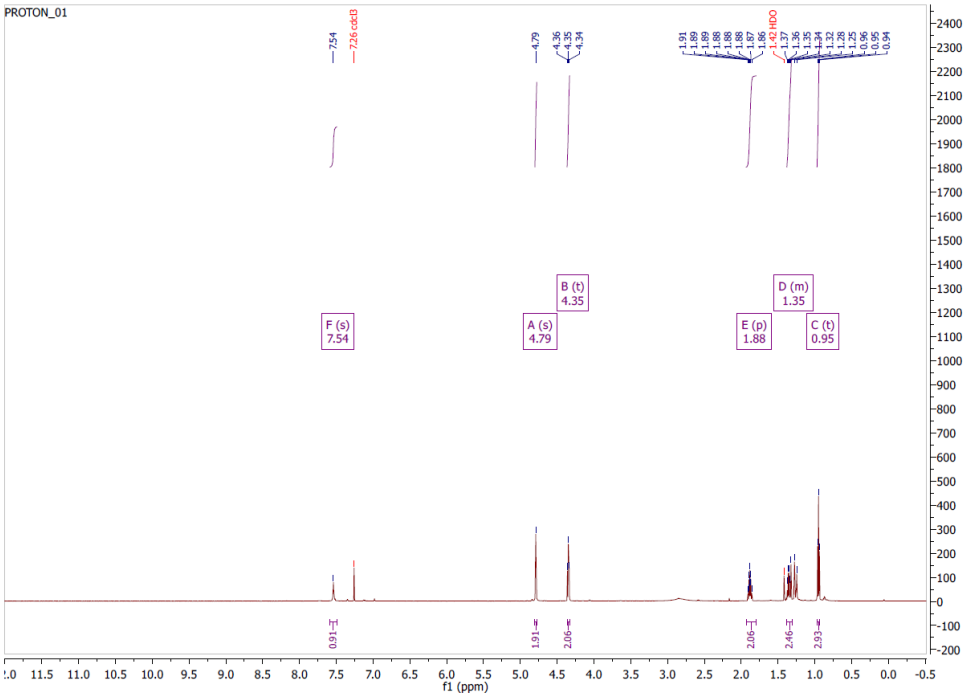

Figure S5.45. ^{1}H NMR spectrum of triazole **C5T10**.

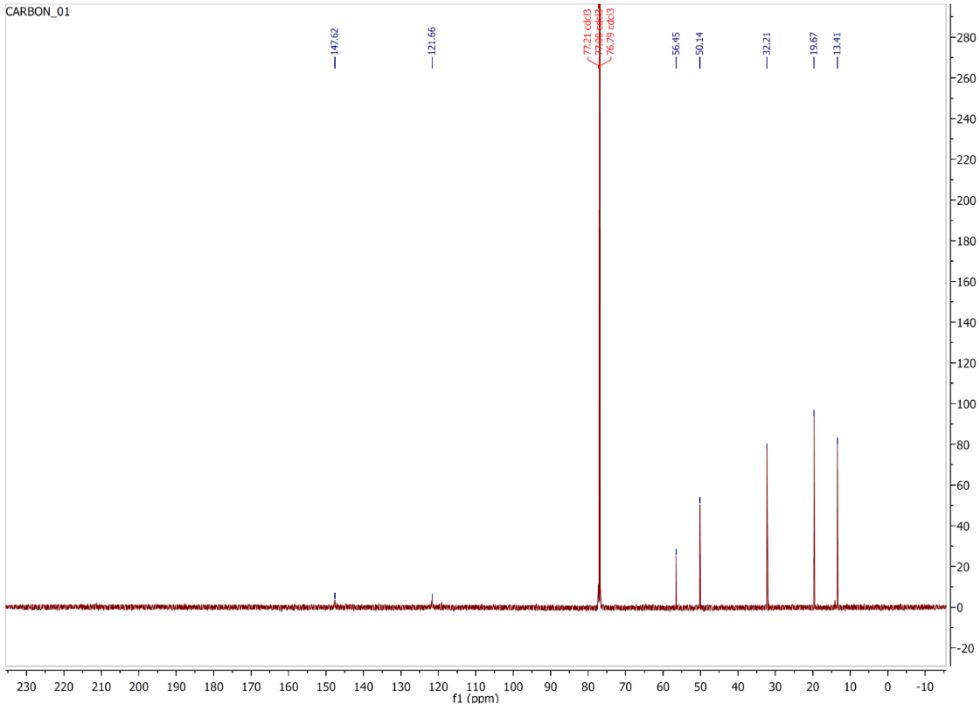

Figure S5.46. ^{13}C NMR spectrum of triazole **C5T10**.

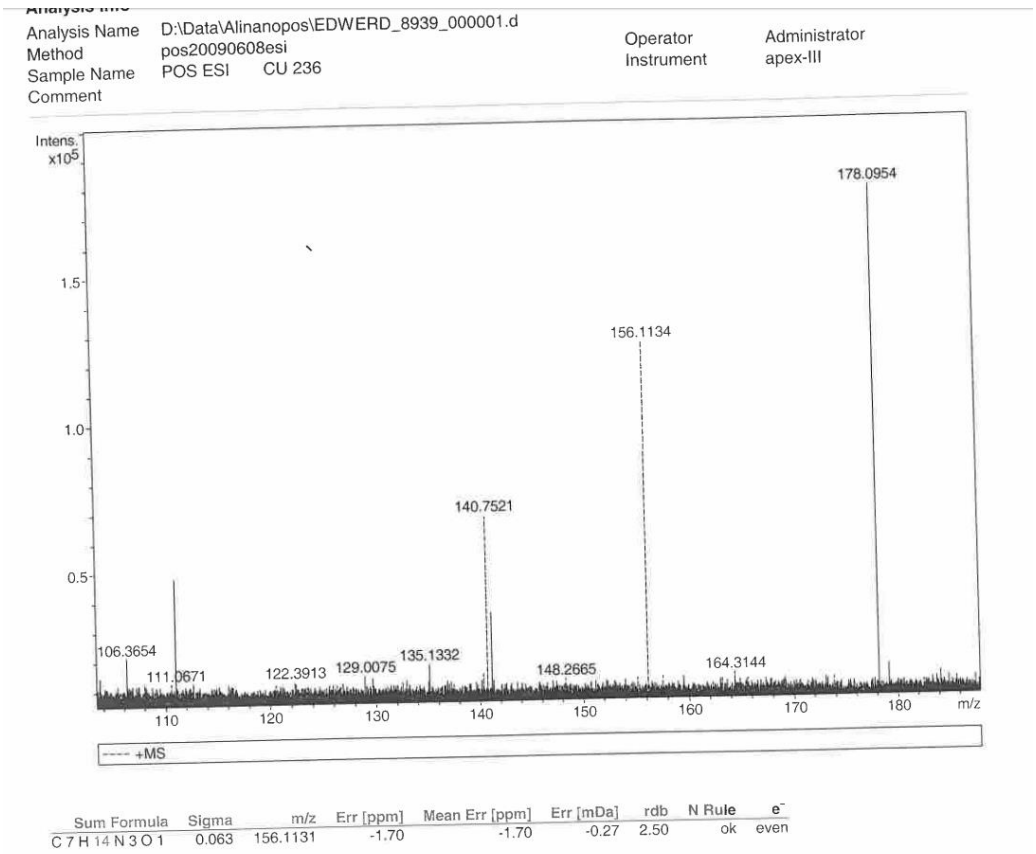

Figure S5.47. HRMS spectrum of triazole **C5T10**.

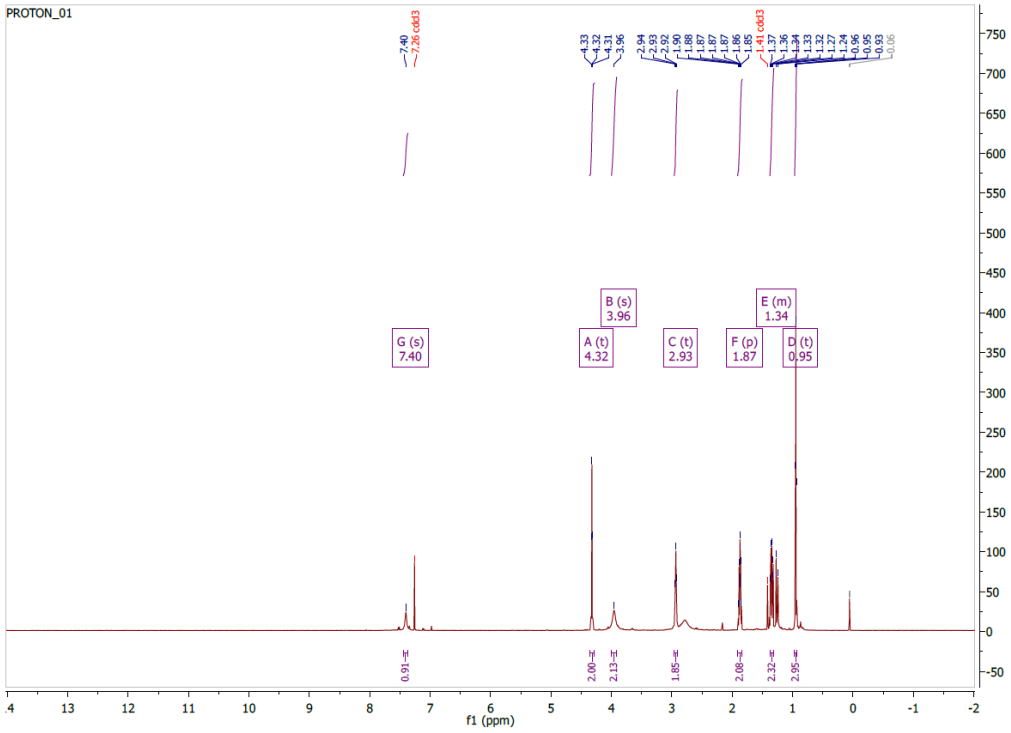

Figure S5.48. ^{1}H NMR spectrum of triazole **C5T11**.

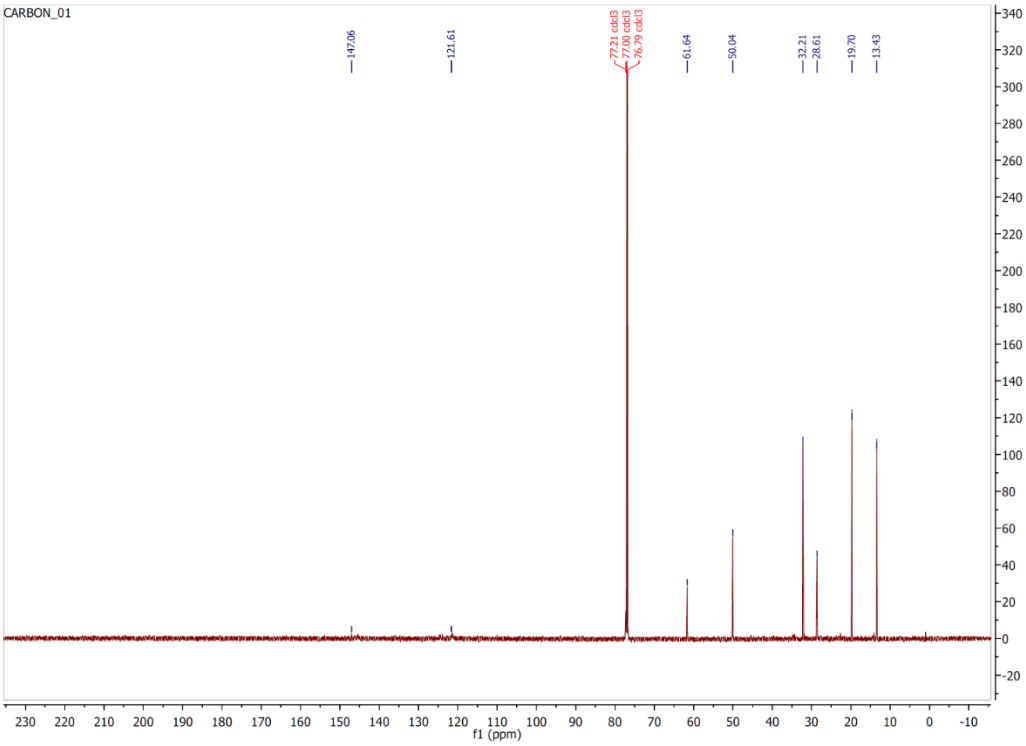

Figure S5.49. ^{13}C NMR spectrum of triazole **C5T11**.

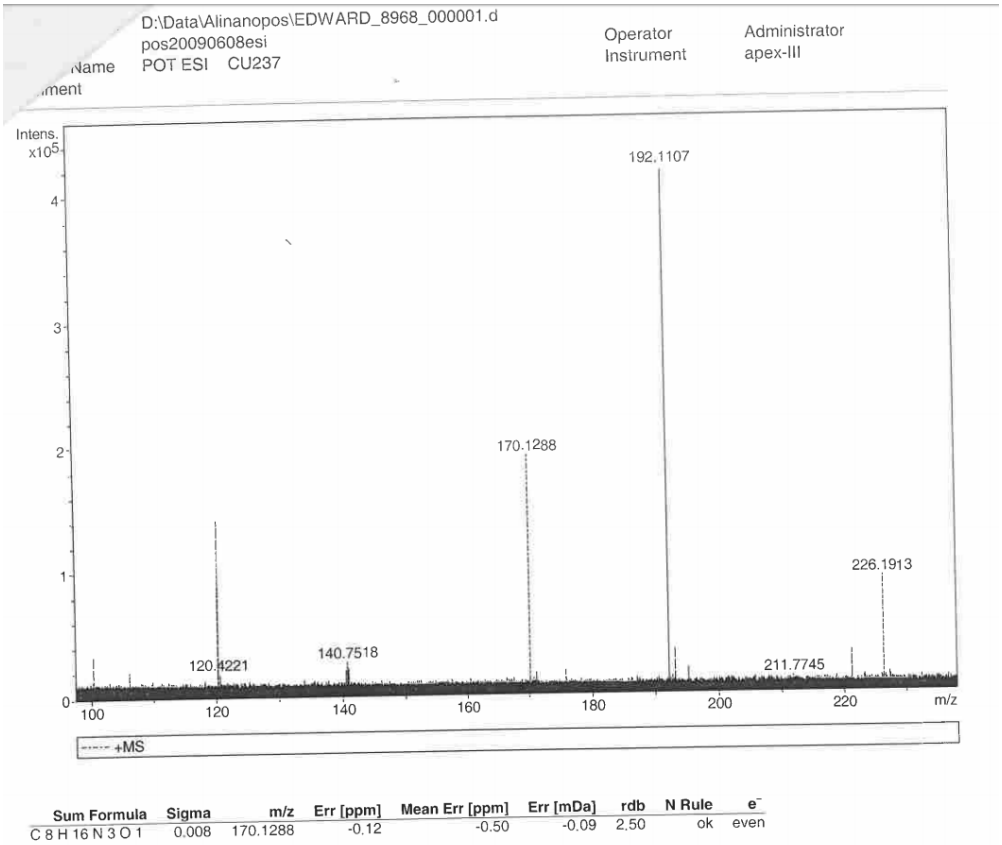

Figure S5.50. HRMS spectrum of triazole **C5T11**.

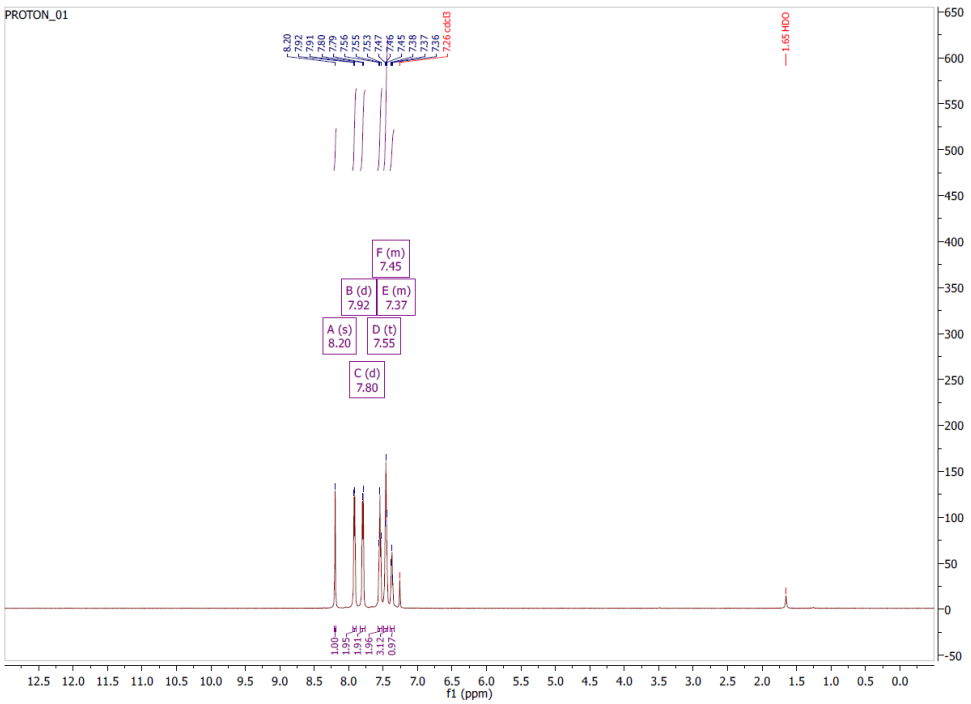

Figure S5.51. ^{1}H NMR spectrum of triazole **C5T12**.

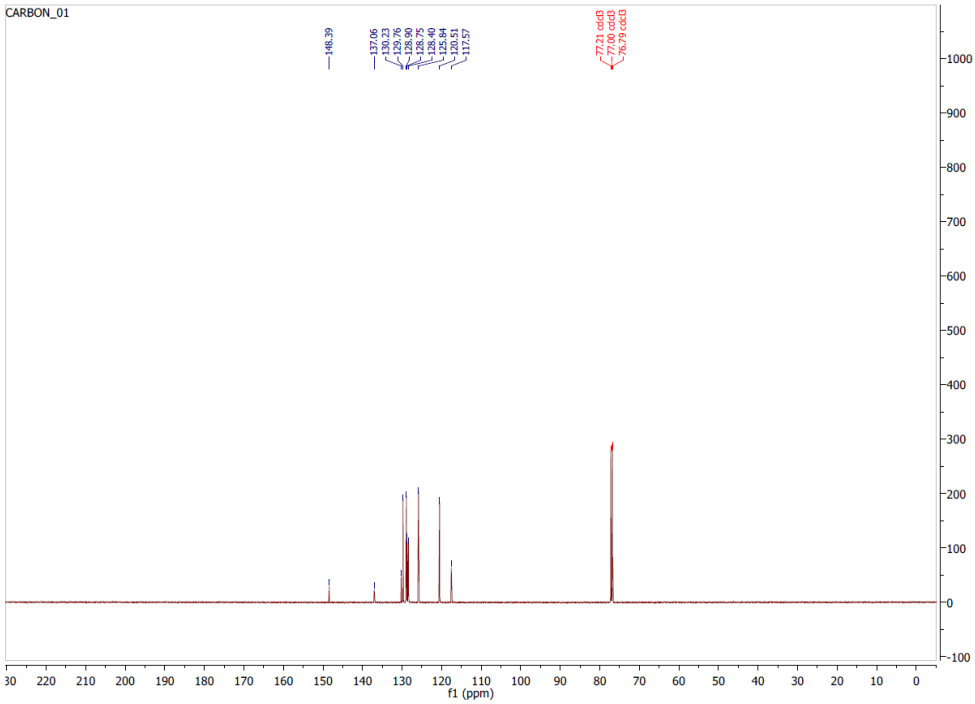

Figure S5.52. ^{13}C NMR spectrum of triazole **C5T12**.

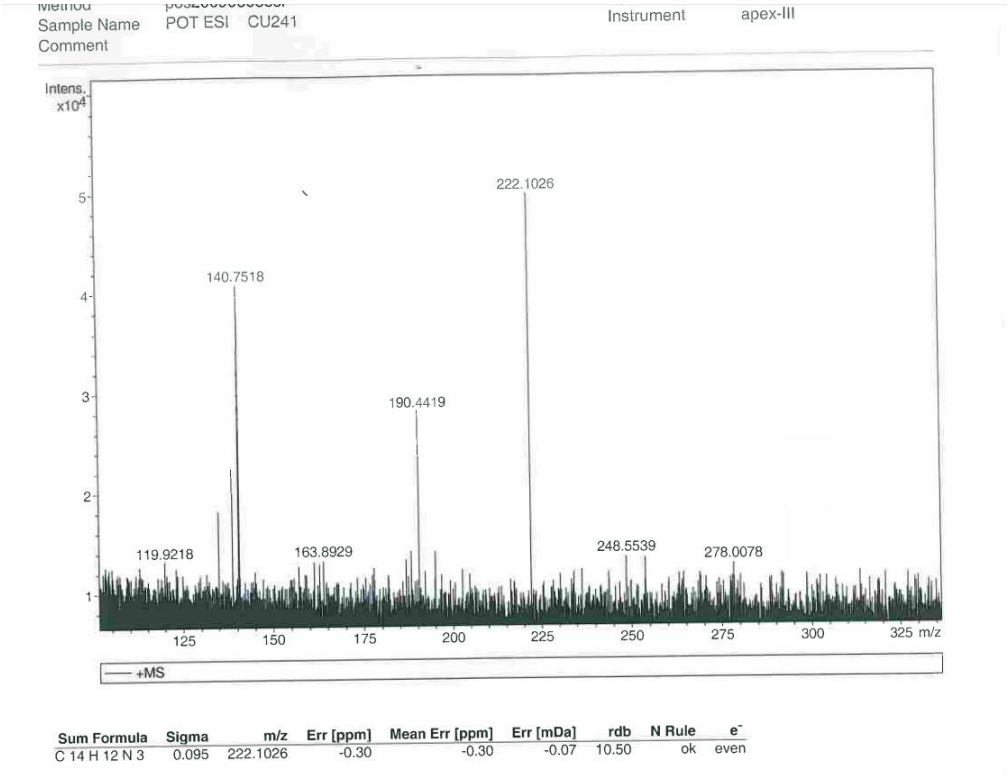

Figure S5.53. HRMS spectrum of triazole **C5T12**.

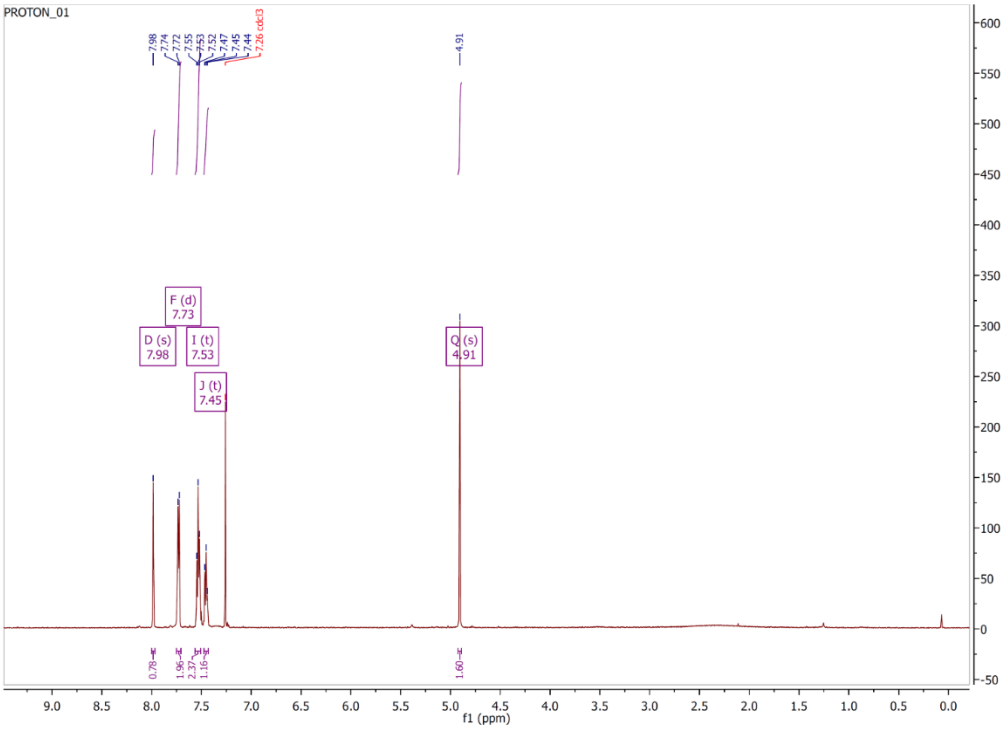

Figure S5.54. ^{1}H NMR spectrum of triazole **C5T14**.

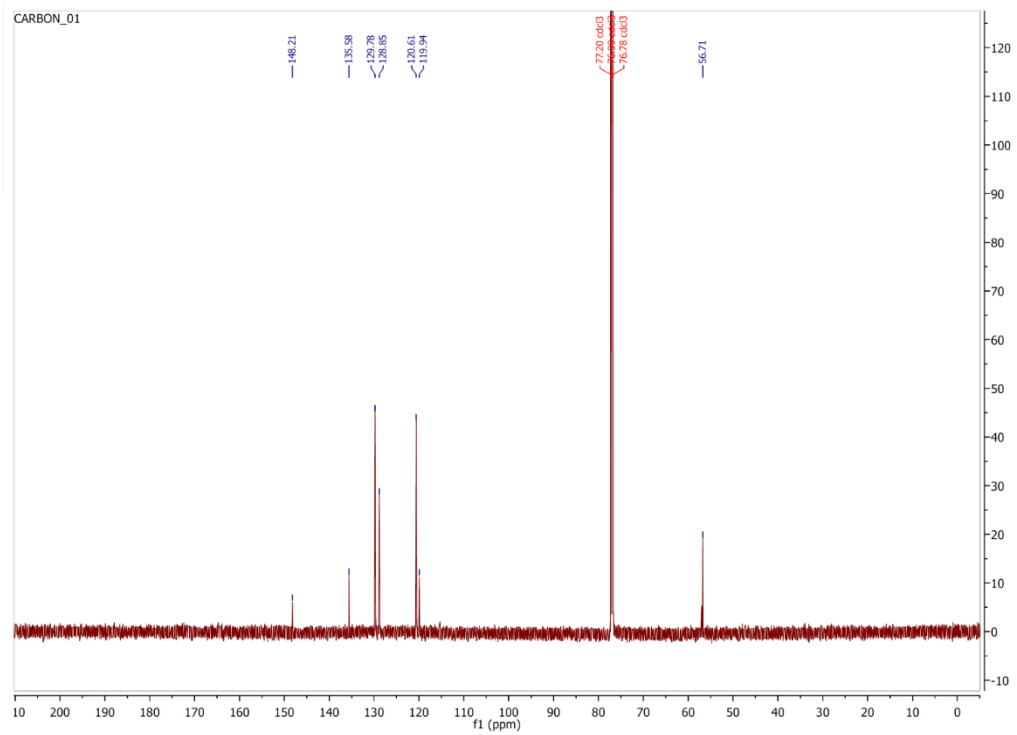

Figure S5.55. ^{13}C NMR spectrum of triazole **C5T14**.

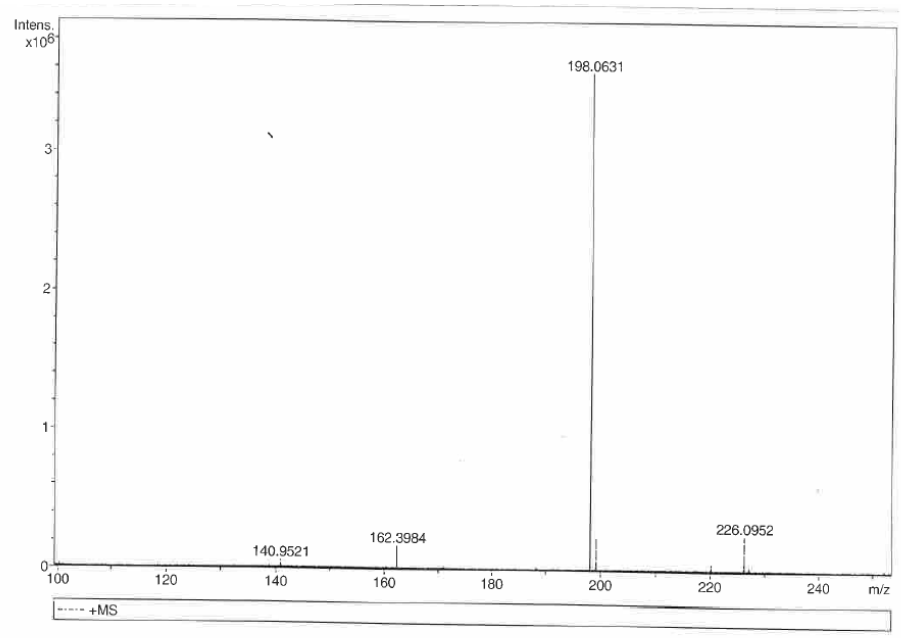

Sum Formula	Sigma	m/z	Err [ppm]	Mean Err [ppm]	Err [mDa]	rdb	N Rule	e⁻
C 9 H 9 N 3 Na 1 O 1	0.030	198.0638	3.56	4.61	0.91	6.50	ok	even

Figure S5.56. HRMS spectrum of triazole **C5T14**.

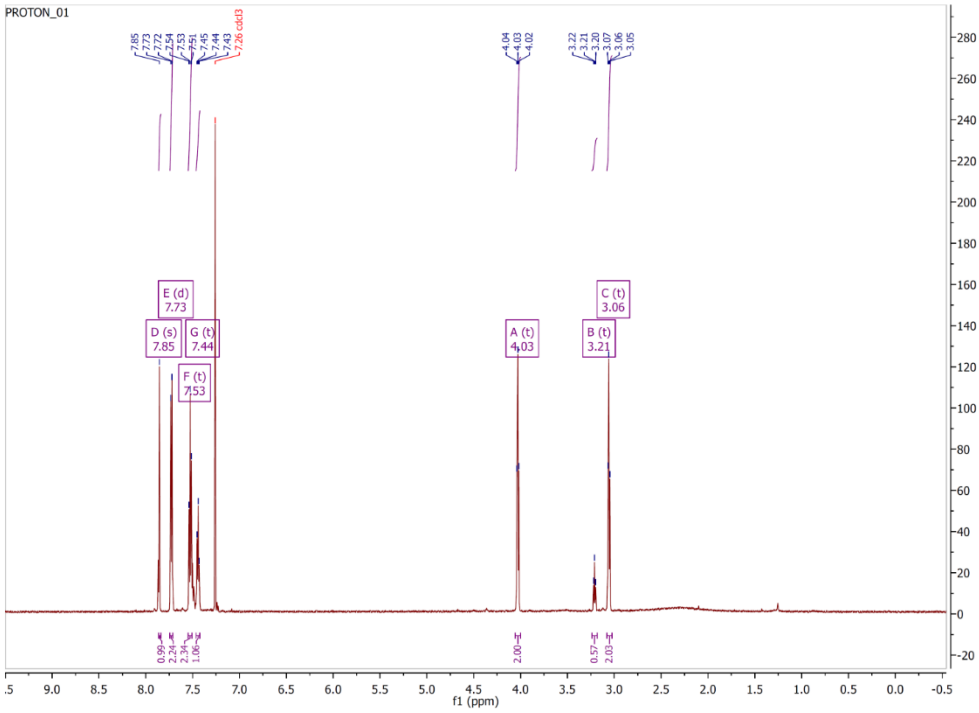

Figure S5.57. ^{1}H NMR spectrum of triazole **C5T15**.

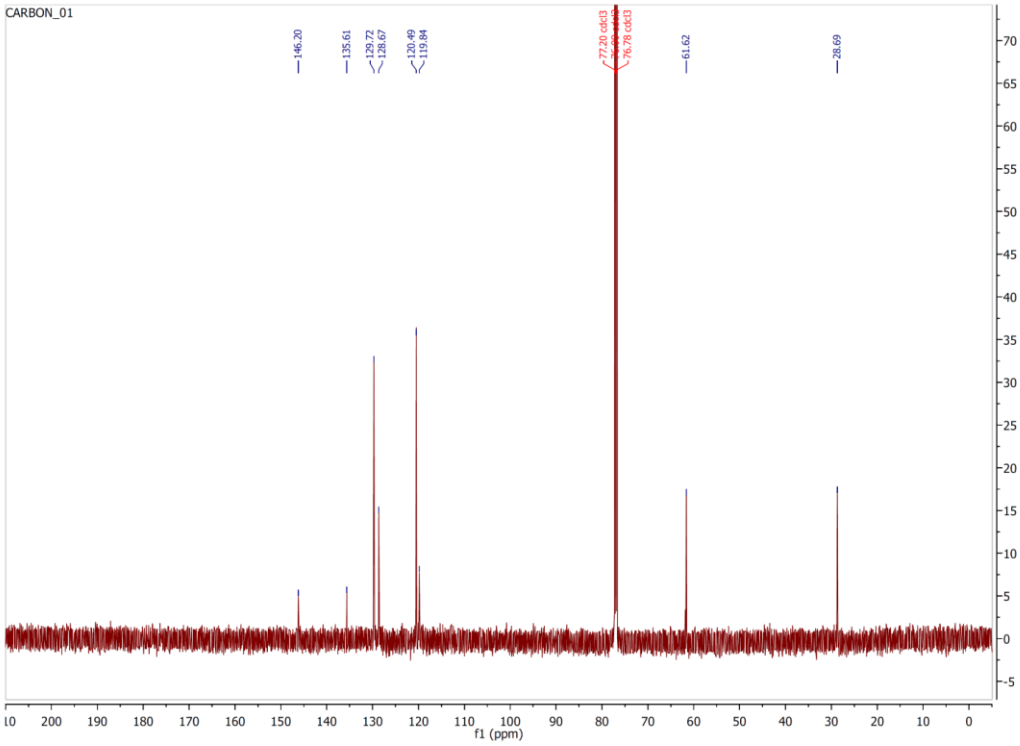

Figure S5.58. ^{13}C NMR spectrum of triazole **C5T15**.

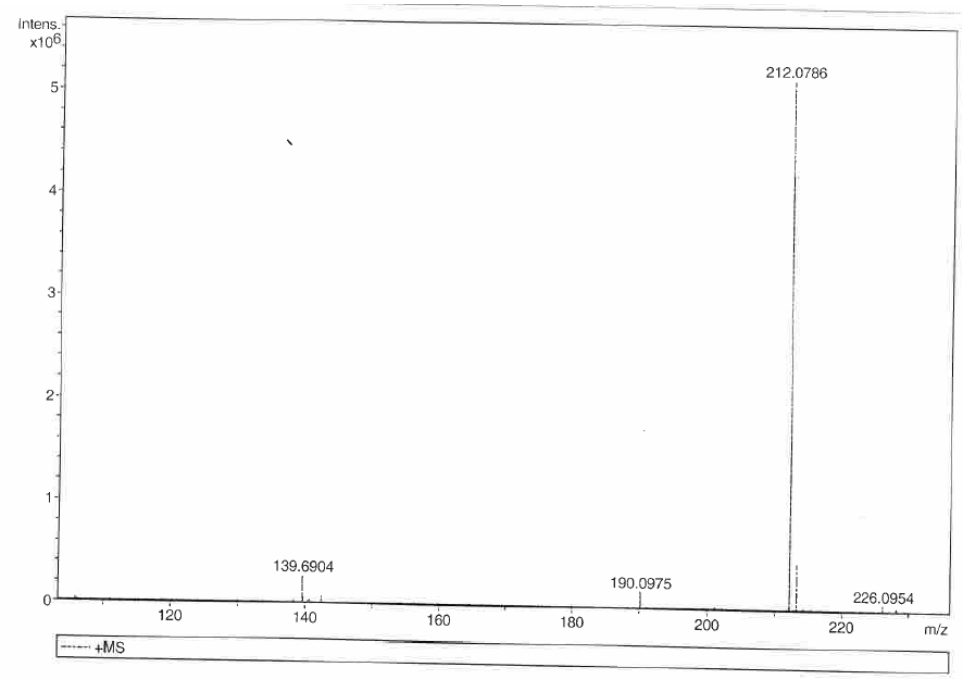

Sum Formula	Sigma	m/z	Err [ppm]	Mean Err [ppm]	Err [mDa]	rdb	N Rule	e⁻
C 10 H 11 N 3 Na 1 O 1	0.028	212.0794	3.87	6.43	1.36	6.50	ok	even

Figure S5.59. HRMS spectrum of triazole **C5T15**.

Chapter 6

6.1. Weak interactions

Table S6.1. π–π stacking distances (Å) and angles (º) in compound **28**.

Rings	Distance between ring centroids (Å)	Perpendicular distance between ring planes (Å)	Dihedral angle between ring mean-planes (˚)
A-B^{i}	3.588(7)	3.532(5)	5.7(6)
B-A^{ii}	3.589(7)	3.536(5)	5.7(6)
C-D^{iii}	3.592(7)	3.514(5)	2.7(6)
D-C^{iv}	3.592(7)	3.506(4)	2.7(6)

Ring A: N4-N5-N6-C20-C15. Ring B: C8-C9-C10-C11-C12-C13. Ring C: N7-N8-N9-C26-C21. Ring D: C28-C29-C30-C31-C32-C33.

Symmetry codes: ^{i}: 2-X,-1/2+Y,-Z. ^{ii}: 2-X,1/2+Y,-Z. ^{iii}: 2-X,-1/2+Y,1-Z. ^{iv}: 2-X,1/2+Y,1-Z.

Table S6.2. π–π stacking distances (Å) and angles (º) in compound **30**.

Rings	Distance between ring centroids (Å)	Perpendicular distance between ring planes (Å)	Dihedral angle between ring mean-planes (˚)
A-B^{i}	3.571(4)	3.500(2)	4.4(3)
B-A^{ii}	3.571(4)	3.488(3)	4.4(3)

Ring A: C1-C2-C3-C4-C5-C6. Ring B: C15-C16-C17-C18-C19-C20.

Symmetry codes: ^{i}: -1+X,Y,Z. ^{ii}: 1+X,Y,Z.

Table S6.3. π–π stacking distances (Å) and angles (º) in compound **31**.

Rings	Distance between ring centroids (Å)	Perpendicular distance between ring planes (Å)	Centroid offset (Å)	Dihedral angle between ring mean-planes (˚)
A-B^{i}	3.742(3)	3.3815(18)	-	1.9(2)
C-D^{ii}	3.352(2)	3.2803(17)	-	8.0(2)

C-B^{ii}	3.594(2)	3.2926(17)	-	5.9(2)
D-A^{i}	3.457(2)	3.4238(17)	-	3.8(2)
D-C^{ii}	3.352(2)	3.1795(17)	-	8.0(2)
E-B^{ii}	3.698(3)	3.4604(18)	-	4.7(2)
F-F^{iii}	3.623(3)	3.2603(18)	1.580	0
B-A^{i}	3.742(3)	3.3367(19)	-	1.9(2)
B-C^{ii}	3.593(2)	3.4233(19)	-	5.9(2)
B-E^{ii}	3.698(3)	3.4080(19)	-	4.7(2)

Ring A: C15-C16-C17-C18-C19-C20. Ring B: C35-C36-C37-C38-C39-C40. Ring C: N7-N8-N9-C26-C21. Ring D: N10-N11-N12-C40-C35. Ring E: C21-C22-C23-C24-C25-C26. Ring F: C28-C29-C30-C31-C32-C33.

Symmetry codes: ^{i}: 1-X,1-Y,2-Z. ^{ii}: X,Y,Z. ^{iii}: -X,2-Y,2-Z.

Table S6.4. π–π stacking distances (Å) and angles (º) in compound **33**.

Rings	Distance between ring centroids (Å)	Perpendicular distance between ring planes (Å)	Dihedral angle between ring mean-planes (˚)
A-B^{i}	3.300(2)	3.2538(14)	9.7(2)
A-C^{i}	3.644(2)	3.2668(14)	8.71(18)
B-A^{i}	3.300(2)	3.1466(15)	9.7(2)
B-C^{ii}	3.687(2)	3.3511(15)	1.06(18)
C-A^{i}	3.644(2)	3.4729(14)	8.71(18)
C-B^{ii}	3.687(2)	3.3396(14)	1.06(18)
C-D^{i}	3.804(2)	3.4712(11)	6.87(17)
D-C^{i}	3.804(2)	3.4371(16)	6.87(17)

Ring A: N003-N004-N007-C00G-C00I. Ring B: N005-N006-N008-C00H-C00F. Ring C: C00F-C00H-C00K-C00V-C00O-C00S. Ring D: C00G-C00M-C00W-C00X-C00T-C00I.

Symmetry codes: ^{i}: X,Y,Z. ^{ii}: 1-X,1-Y,1-Z.

Table S6.5. π–π stacking distances (Å) and angles (º) in compound **34**.

Rings	Distance between ring centroids (Å)	Perpendicular distance between ring planes (Å)	Dihedral angle between ring mean-planes (˚)
A-B^{i}	3.429(3)	3.298(2)	12.6(3)
B-A^{i}	3.429(3)	3.228(2)	12.6(3)
C-D^{i}	3.777(4)	3.654(3)	11.9(3)
D-C^{i}	3.776(4)	3.653(3)	11.9(3)

Ring A: N1-N2-N3-C6-C1. Ring B: N4-N5-N6-C15-C20. Ring C: C1-C2-C3-C4-C5-C6. Ring D: C15-C16-C17-C18-C19-C20.

Symmetry codes: ^{i}: X,Y,Z.

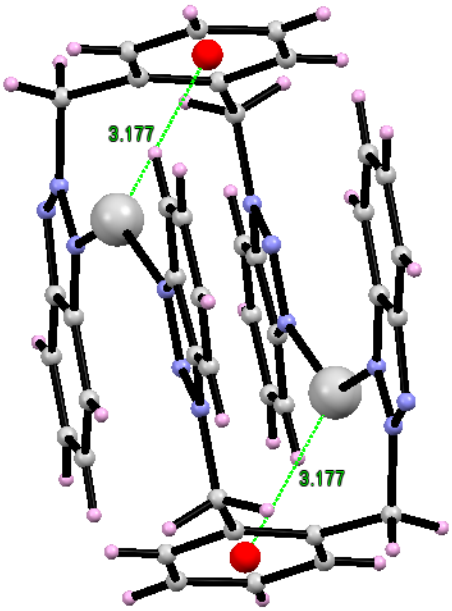

Figure S6.1. The Ag···π interactions in compound **31**, with the centroid-metal distance (in Å) represented as green dashed line. Color code Ag (grey), C (light grey), N (light blue), H (pink), centroid (red).

6.2. Additional figures of crystal structures

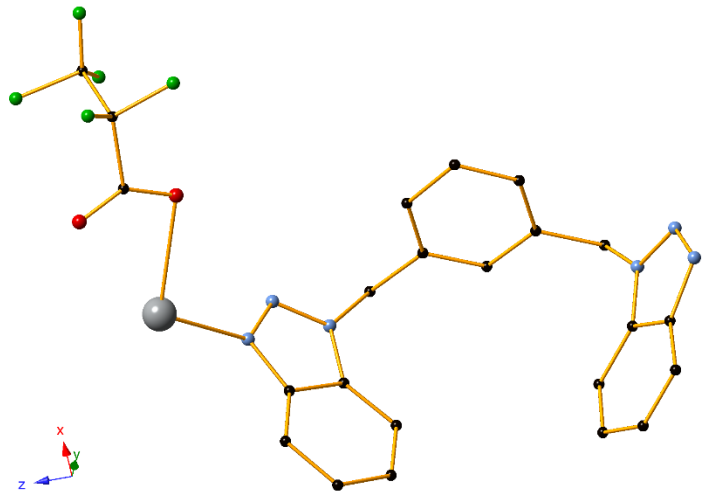

Figure S6.2. The asymmetric unit of compound [Ag(**L**^{2})($CF_3CF_2CO_2$)]. Colour code Ag (grey), C (black), N (light blue), F (green), O (red).

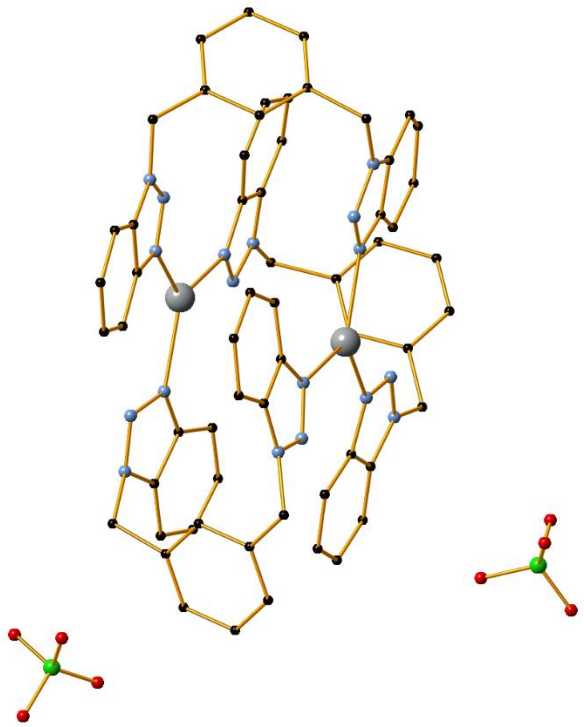

Figure S6.3. The structure of compound [Ag_2(**L**^{2})$_3$]·2ClO_4^-. Colour code Ag (grey), C (black), N (light blue), Cl (green), O (red).

6.3. Characterization data of 27 – 35

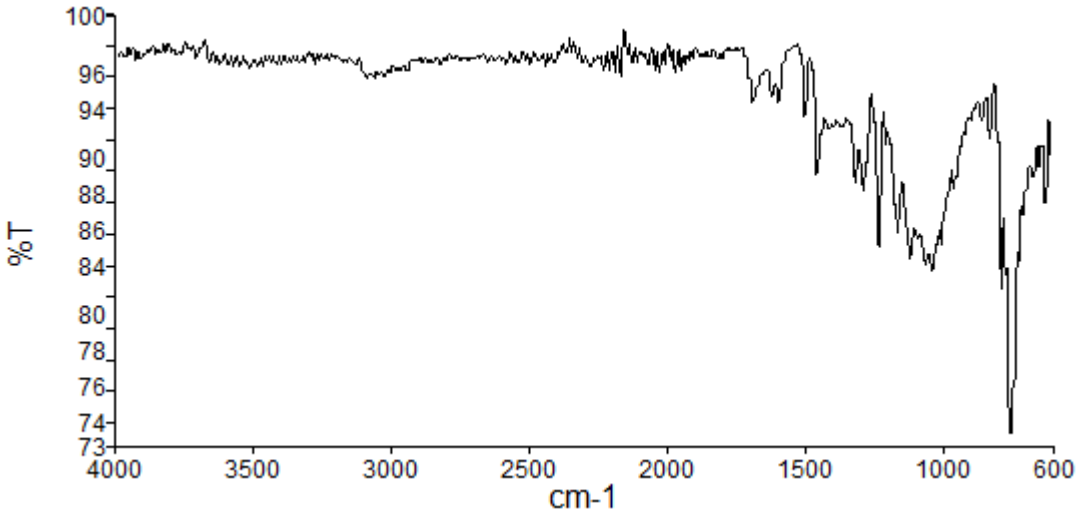

Figure S6.4. IR spectrum of **27**.

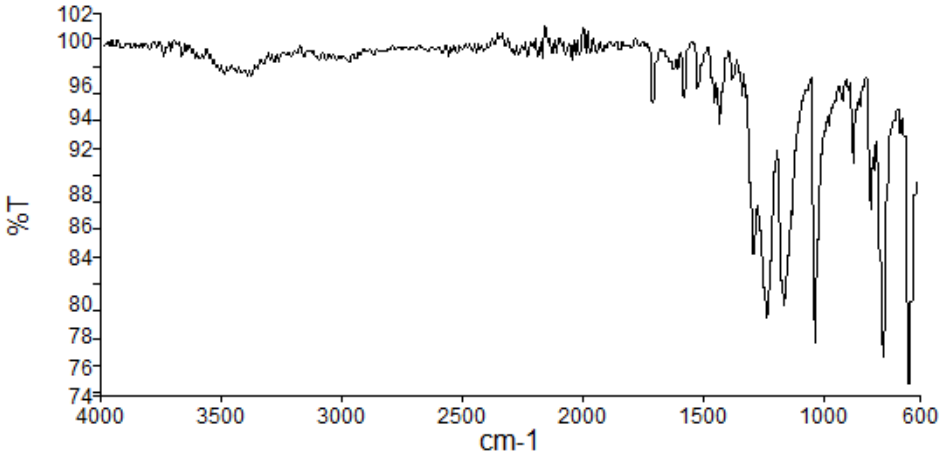

Figure S6.5. IR spectrum of **28**.

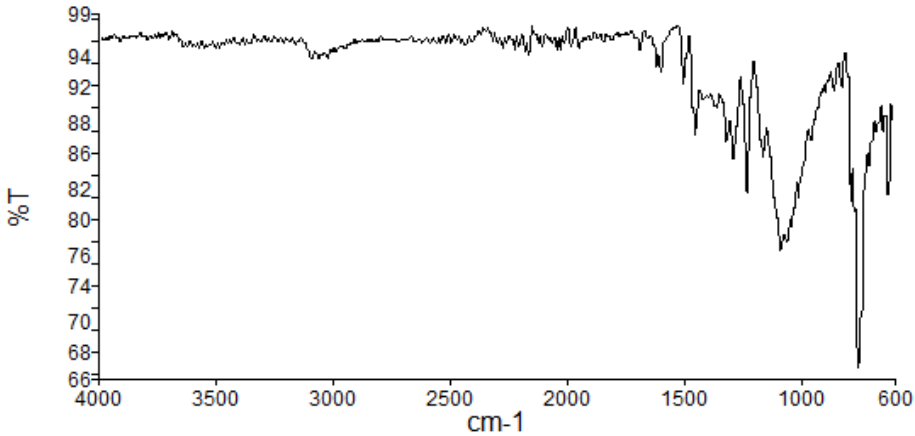

Figure S6.6. IR spectrum of **29**.

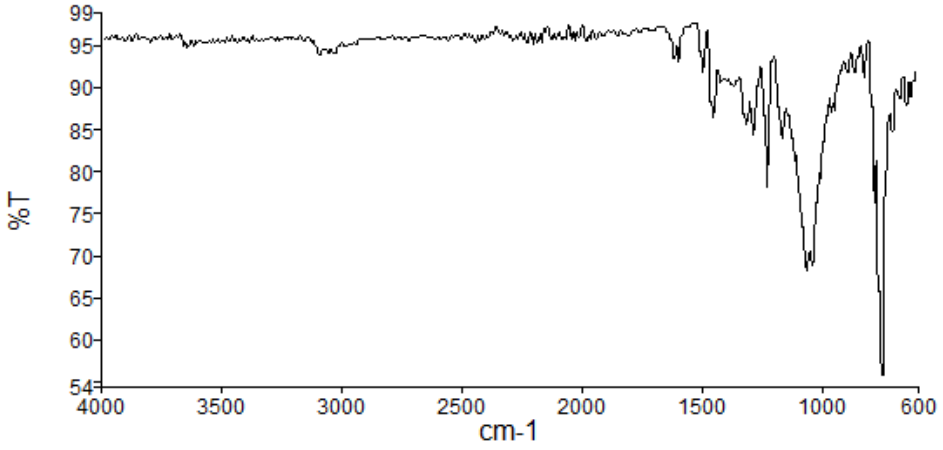

Figure S6.7. IR spectrum of **30**.

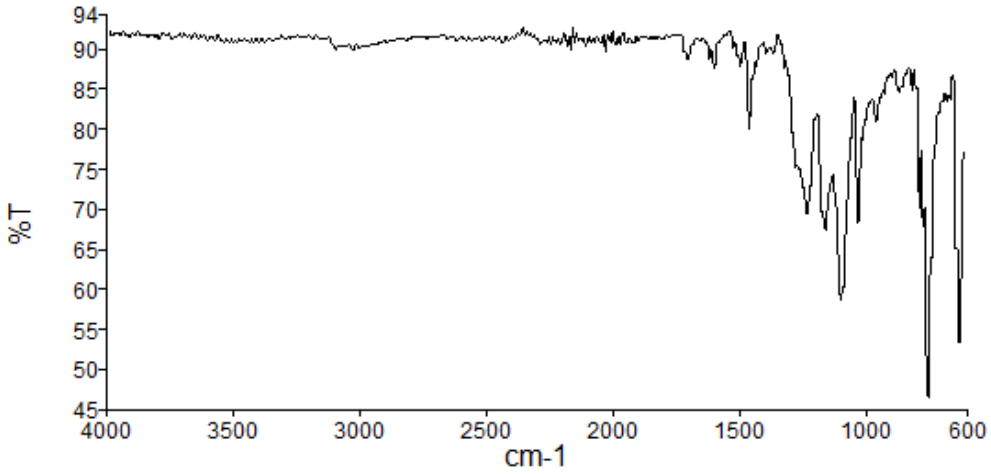

Figure S6.8. IR spectrum of **31**.

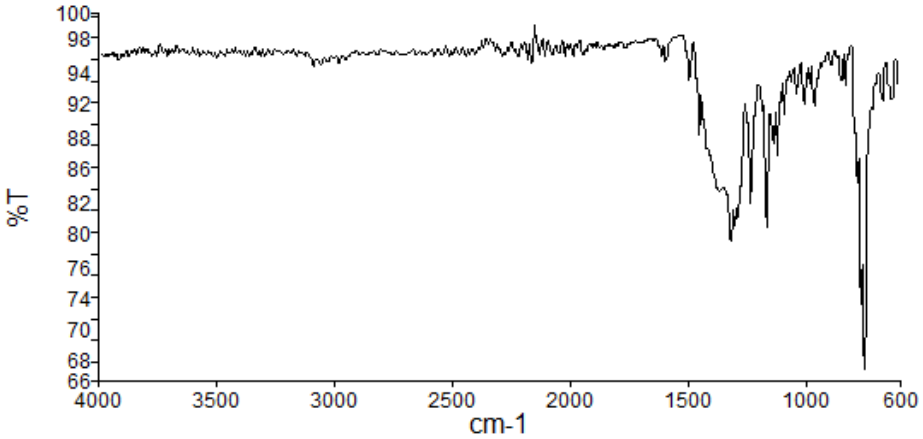

Figure S6.9. IR spectrum of **32**.

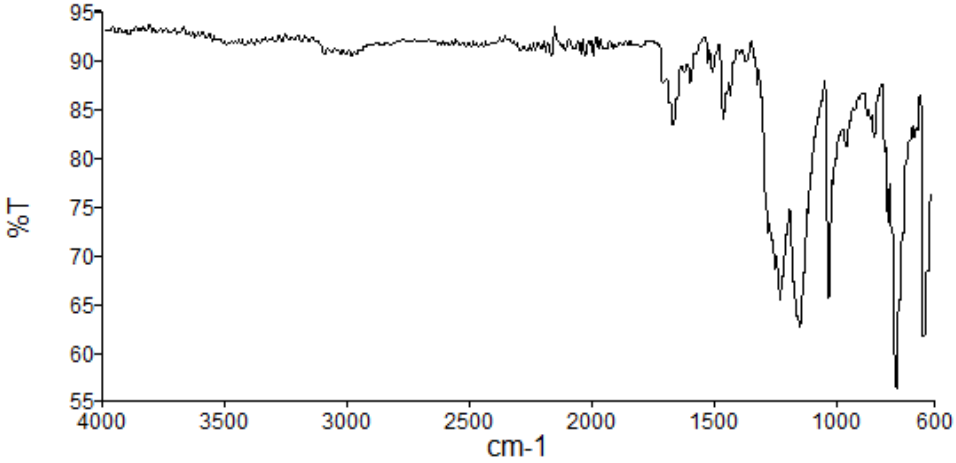

Figure S6.10. IR spectrum of **33**.

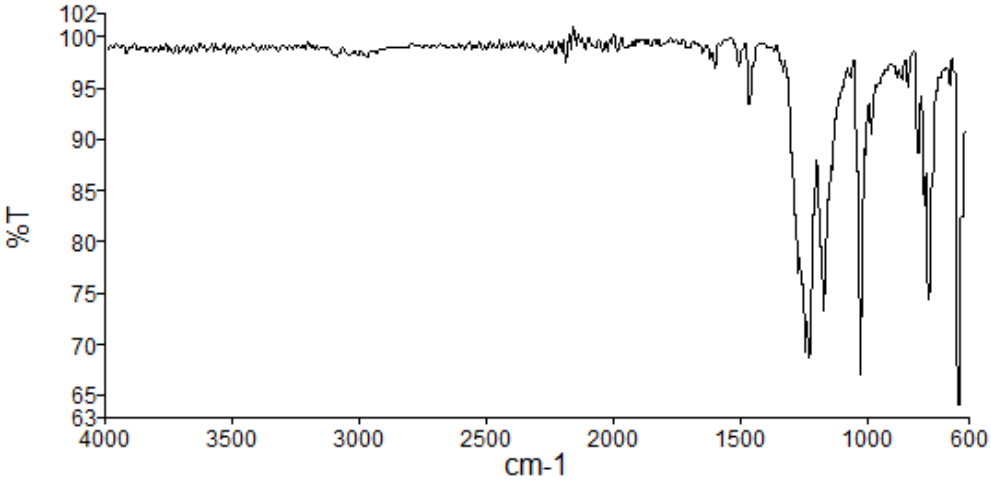

Figure S6.11. IR spectrum of **34**.

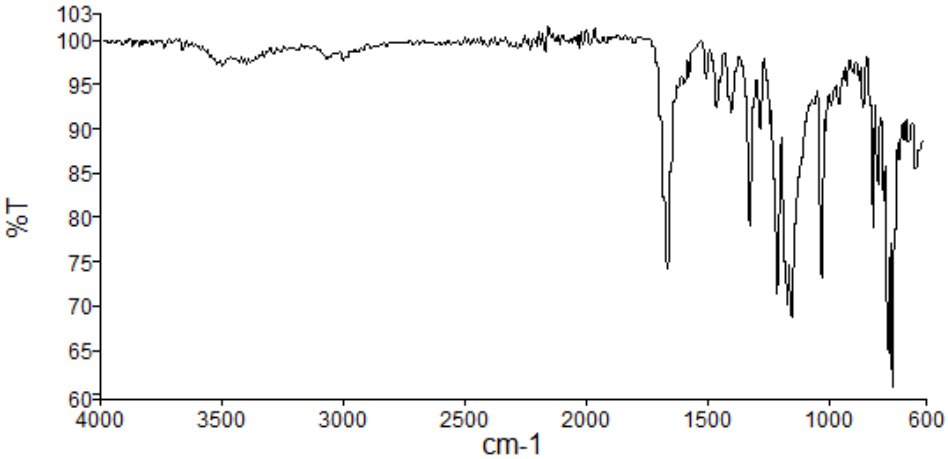

Figure S6.12. IR spectrum of **35**.

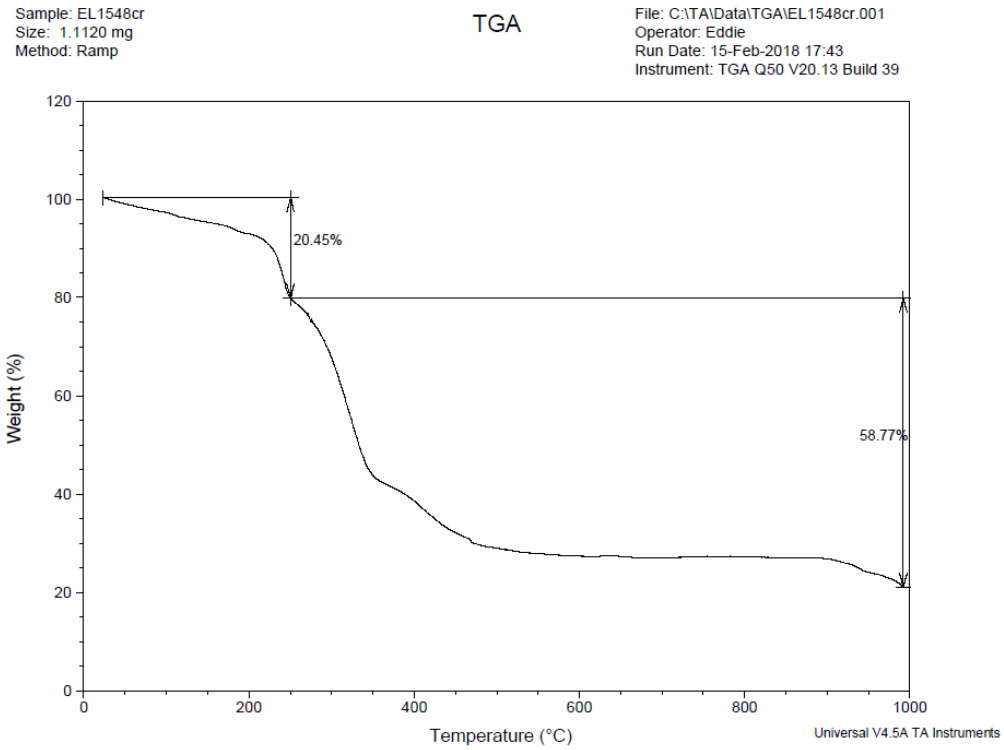

Figure S6.13. TGA graph of **27**.

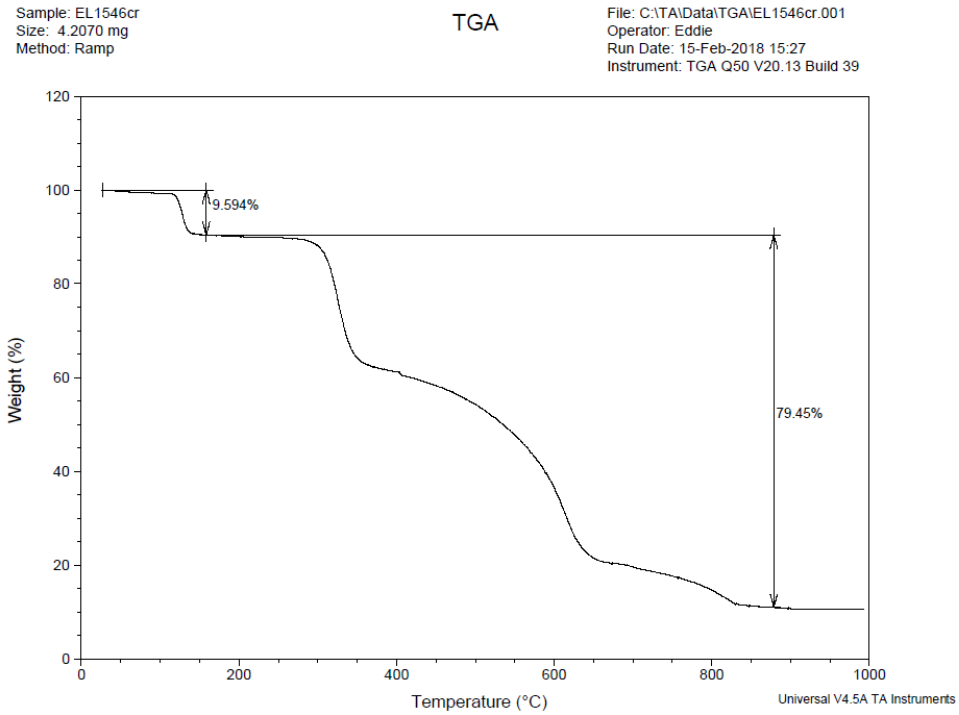

Figure S6.14. TGA graph of **28**.

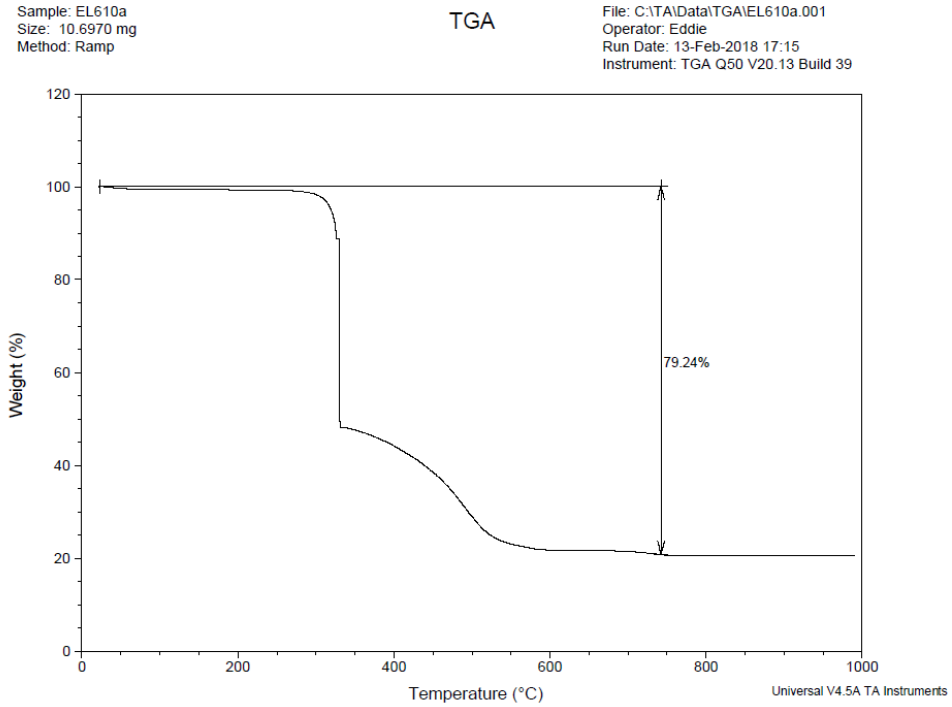

Figure S6.15. TGA graph of **29**.

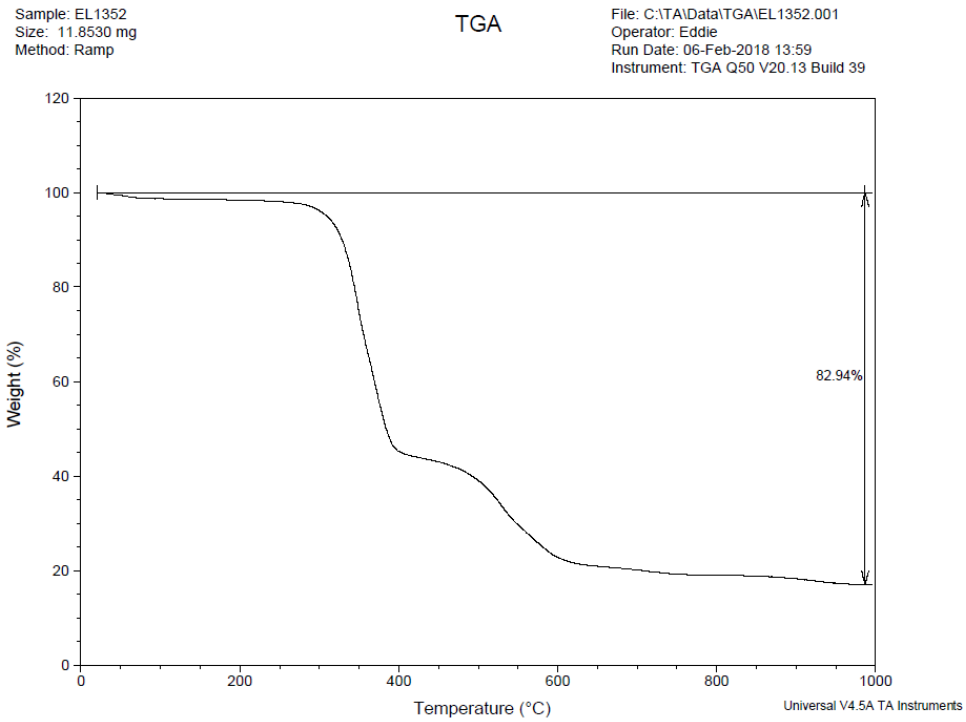

Figure S6.16. TGA graph of **30**.

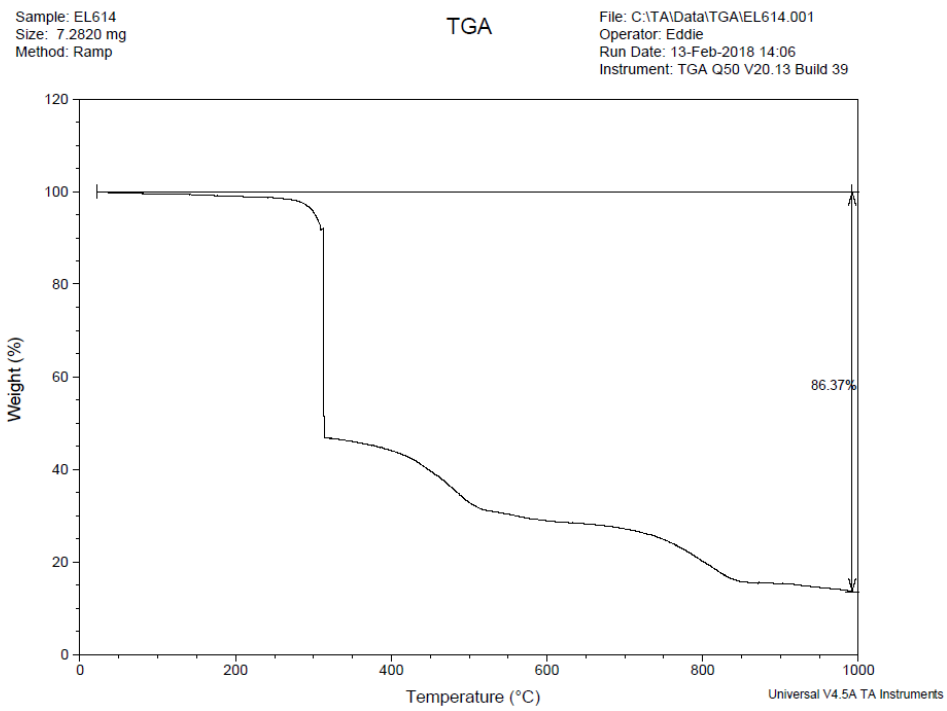

Figure S6.17. TGA graph of **31**.

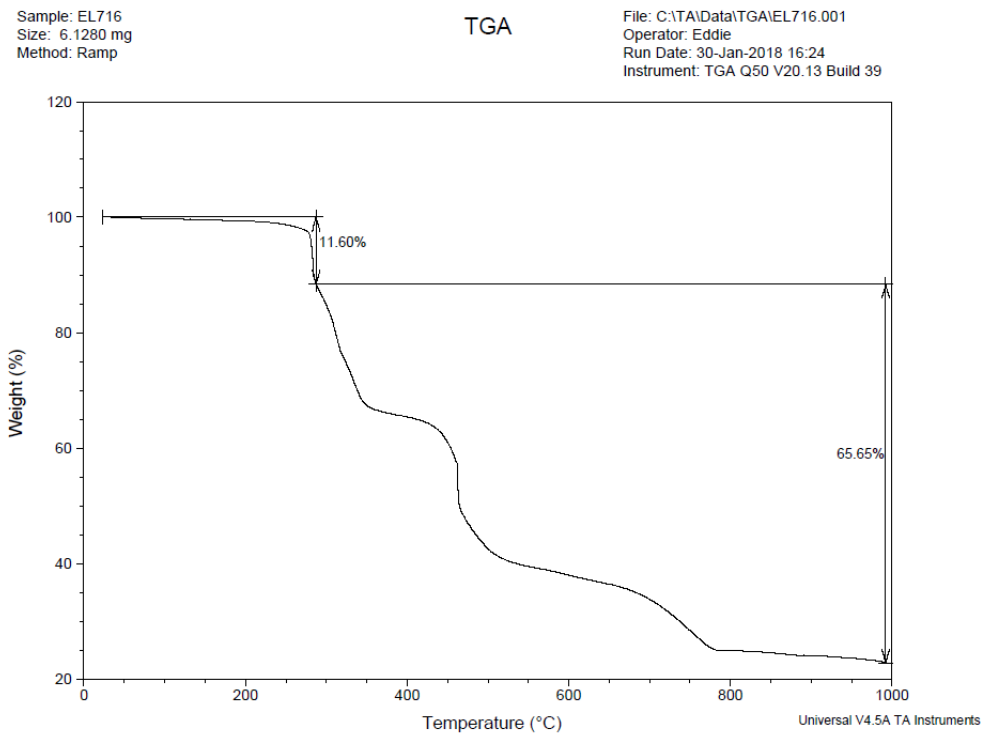

Figure S6.18. TGA graph of **32**.

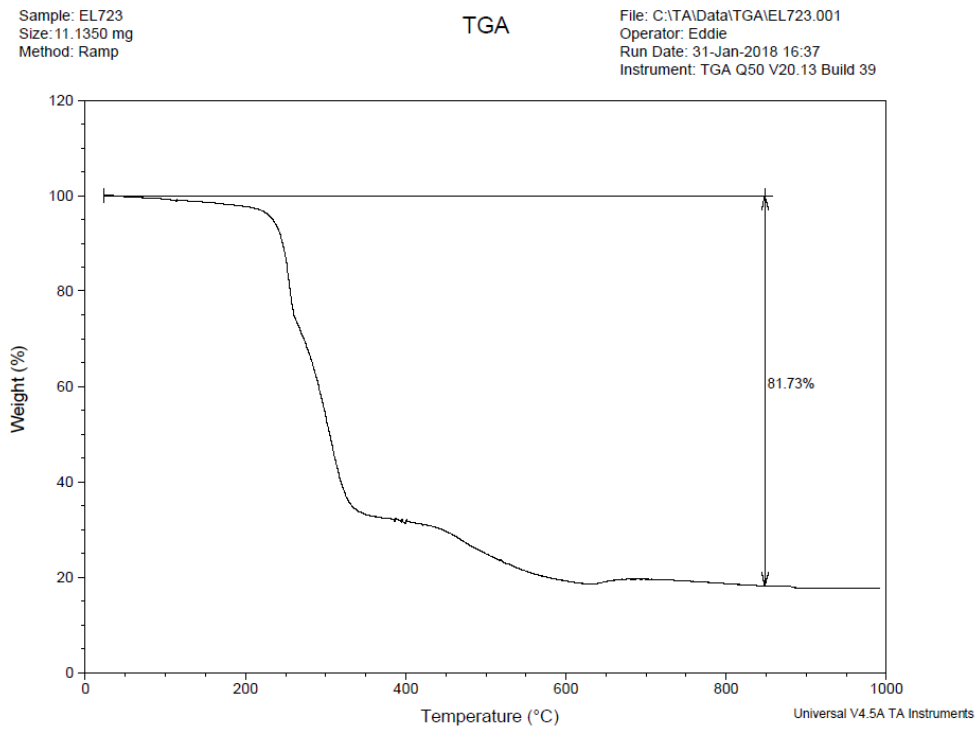

Figure S6.19. TGA graph of **33**.

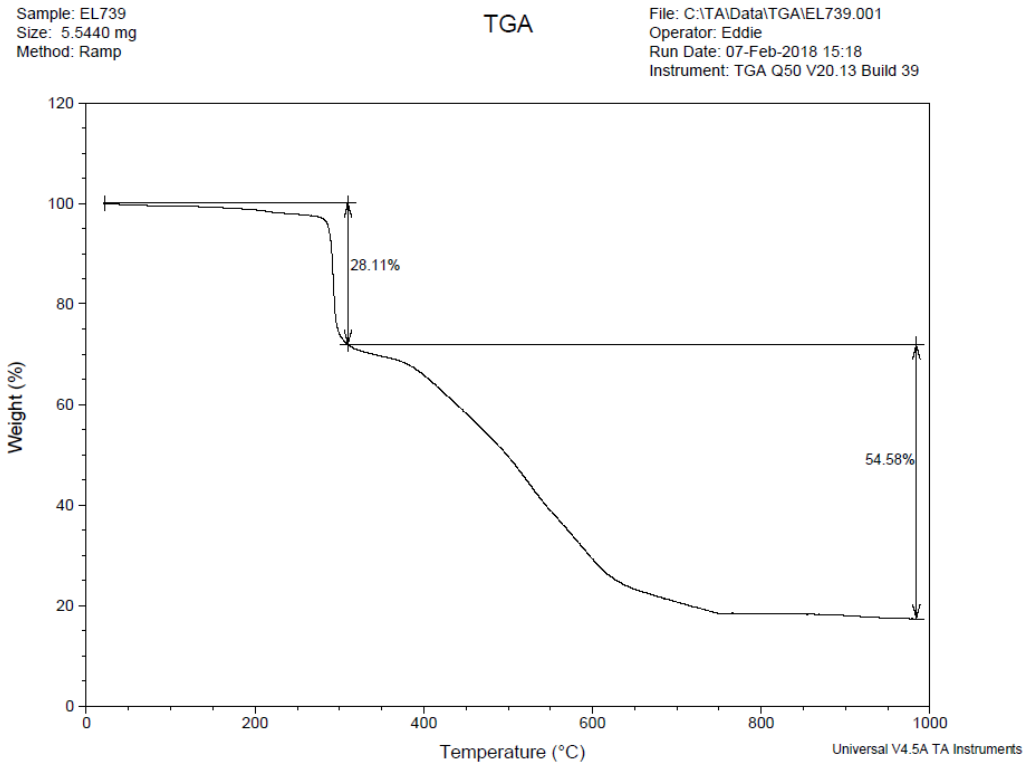

Figure S6.20. TGA graph of **34**.

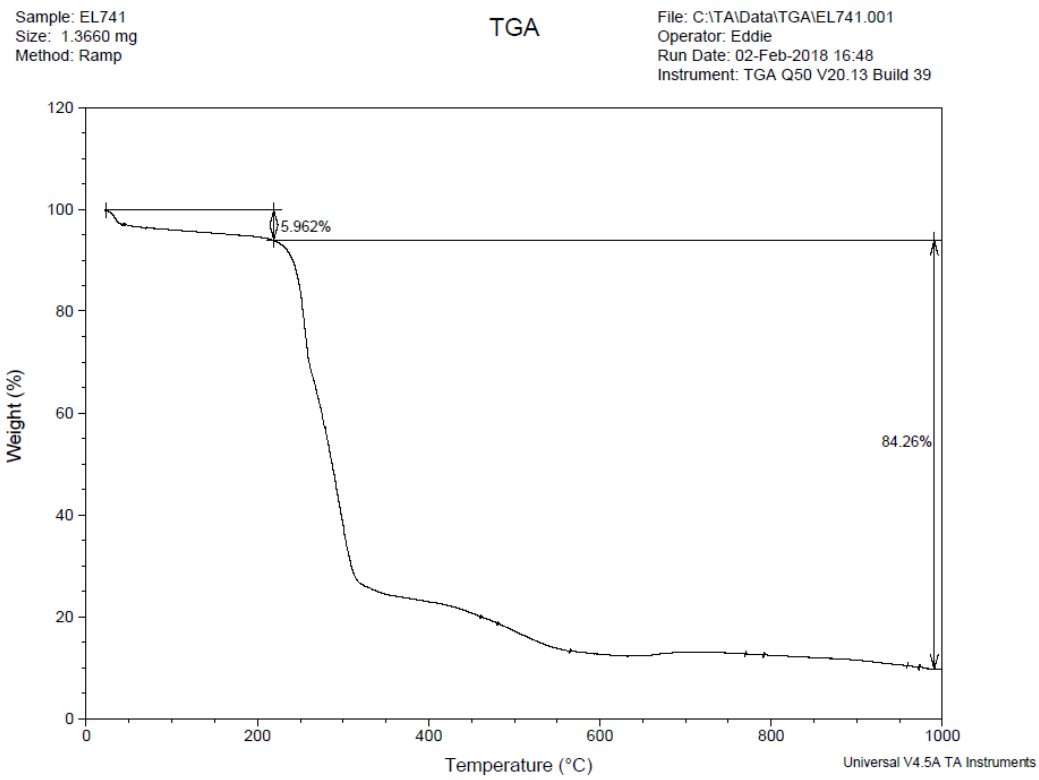

Figure S6.21. TGA graph of **35**.

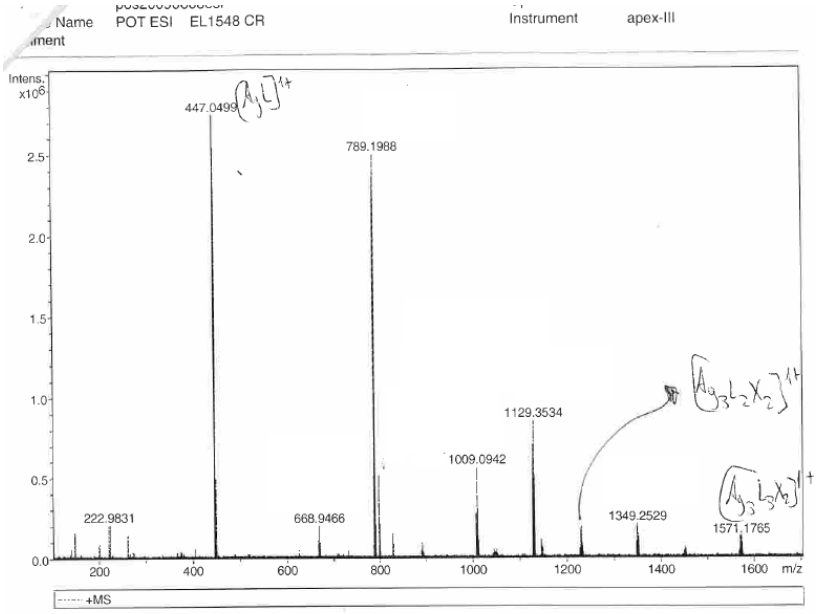

Figure S6.22. ESI-MS data for compound **27** in methanol. Main fragments: 447.05 m/z $[Ag(\mathbf{L^1})]^+$, 668.95 m/z $[Ag_2(\mathbf{L^1})\ (CF_3CO_2)]^+$, 789.20 m/z $[Ag(\mathbf{L^1})_2]^+$, 799.21 m/z $[(\mathbf{L^1})_2(MeOH)_3Na]^+$, 1009.09 m/z $[Ag_2(\mathbf{L^1})_2(CF_3CO_2)]^+$, 1129.35 m/z $[Ag(\mathbf{L^1})_3]^+$, 1231.95 m/z $[Ag_3(\mathbf{L^1})_2(CF_3CO_2)_2]^+$, 1349.25 m/z $[Ag_2(\mathbf{L^1})_3(CF_3CO_2)]^+$, 1571.18 m/z $[Ag_3(\mathbf{L^1})_3(CF_3CO_2)_2]^+$.

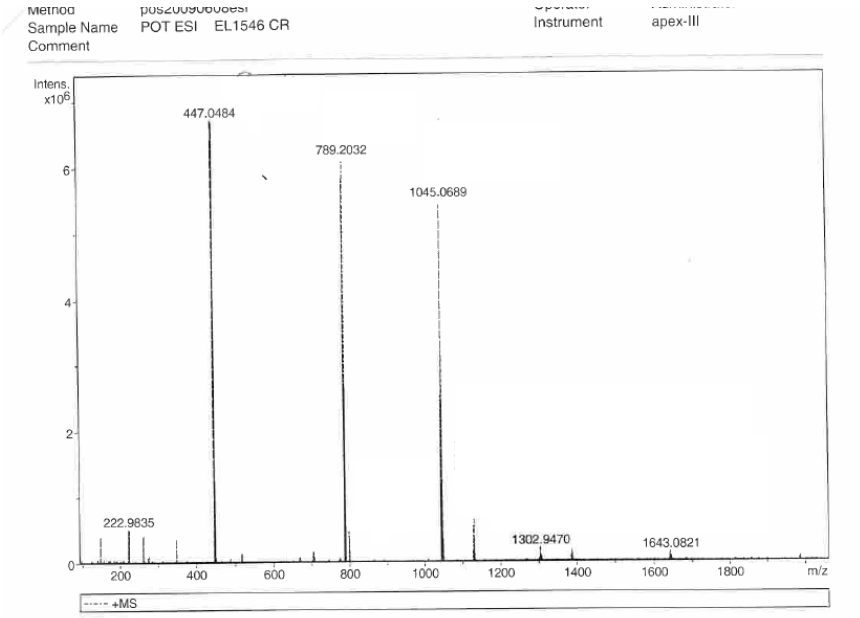

Figure S6.23. ESI-MS data for compound **28** in methanol. Main fragments: 447.05 m/z $[Ag(\mathbf{L^1})]^+$, 789.20 m/z $[Ag(\mathbf{L^1})_2]^+$, 799.21 m/z $[(\mathbf{L^1})_2(MeOH)_3Na]^+$, 1045.07 m/z $[Ag_2(\mathbf{L^1})_2(CF_3SO_3)]^+$, 1129.35 m/z $[Ag(\mathbf{L^1})_3]^+$, 1302.95 m/z $[Ag_3(\mathbf{L^1})_2(CF_3SO_3)_2]^+$, 1643.08 m/z $[Ag_3(\mathbf{L^1})_3(CF_3SO_3)_2]^+$.

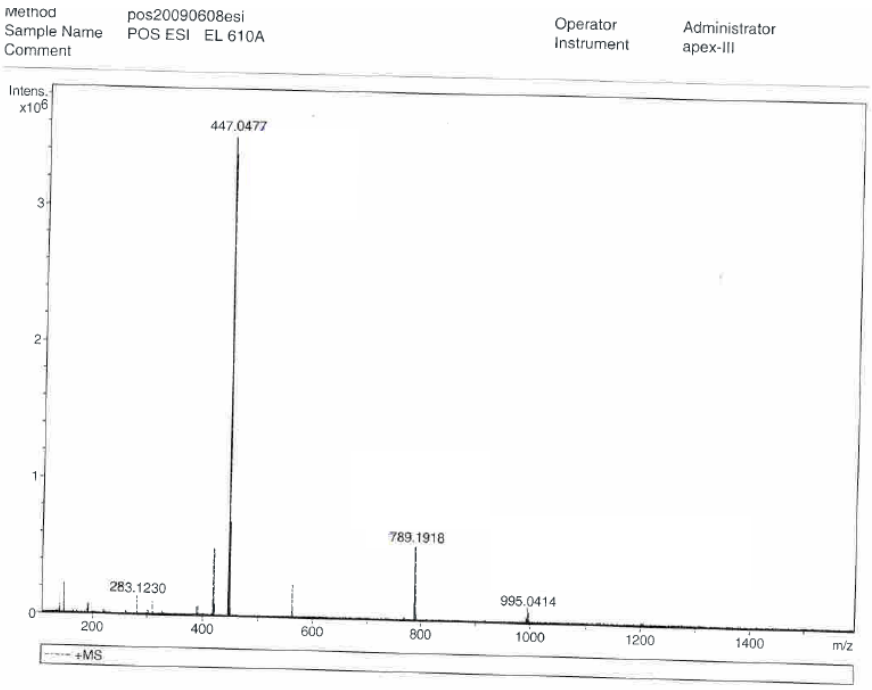

Figure S6.24. ESI-MS data for compound **29** in methanol. Main fragments: 428.20 m/z $[(\mathbf{L^2})(MeOH)_2Na]^+$, 447.05 m/z $[Ag(\mathbf{L^2})]^+$, 556.97 m/z $[Ag_2(\mathbf{L^2})]^+$, 789.19 m/z $[Ag(\mathbf{L^2})_2]^+$, 995.04 m/z $[Ag_2(\mathbf{L^2})_2(ClO_4)]^+$.

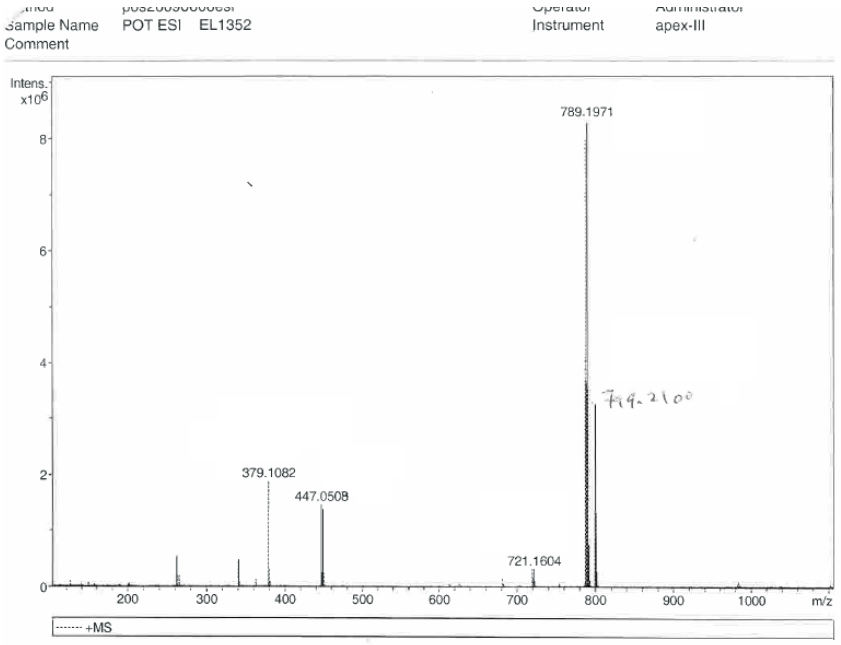

Figure S6.25. ESI-MS data for compound **30** in methanol. Main fragments: 379.11 m/z [(**L²**) + K]$^+$, 447.05 m/z [Ag(**L²**)]$^+$, 721.16 m/z [(**L²**)$_2$ + K]$^+$, 789.20 m/z [Ag(**L²**)$_2$]$^+$, 799.21 m/z [(**L²**)$_2$(MeOH)$_3$Na]$^+$.

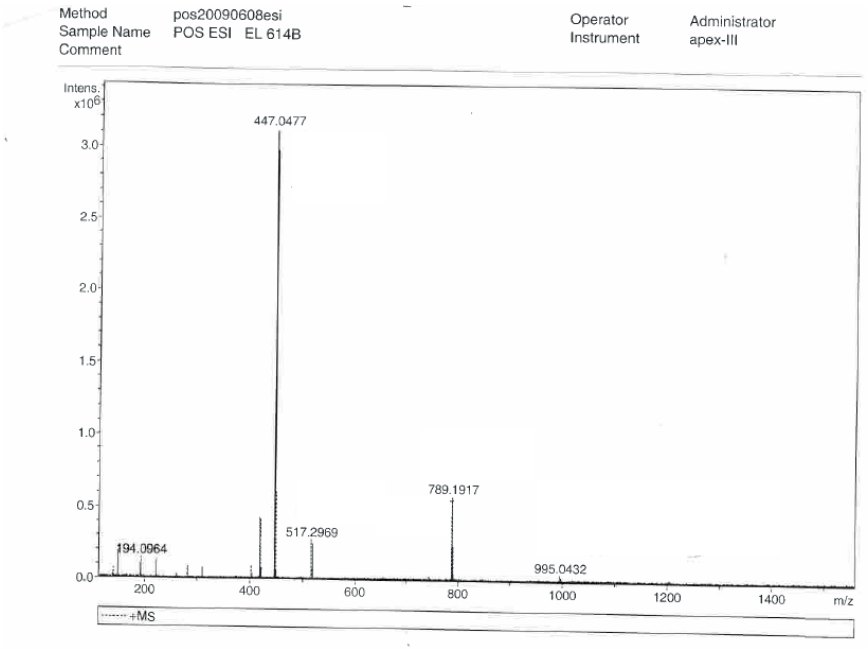

Figure S6.26. ESI-MS data for compound **31** in methanol. Main fragments: 428.20 m/z [(**L³**)(MeOH)$_2$Na]$^+$, 447.05 m/z [Ag(**L³**)]$^+$, 517.30 m/z [Ag$_2$(**L³**)$_2$(ClO$_4$)(MeOH)]$^{2+}$, 789.19 m/z [Ag(**L³**)$_2$]$^+$, 995.04 m/z [Ag$_2$(**L³**)$_2$(ClO$_4$)]$^+$.

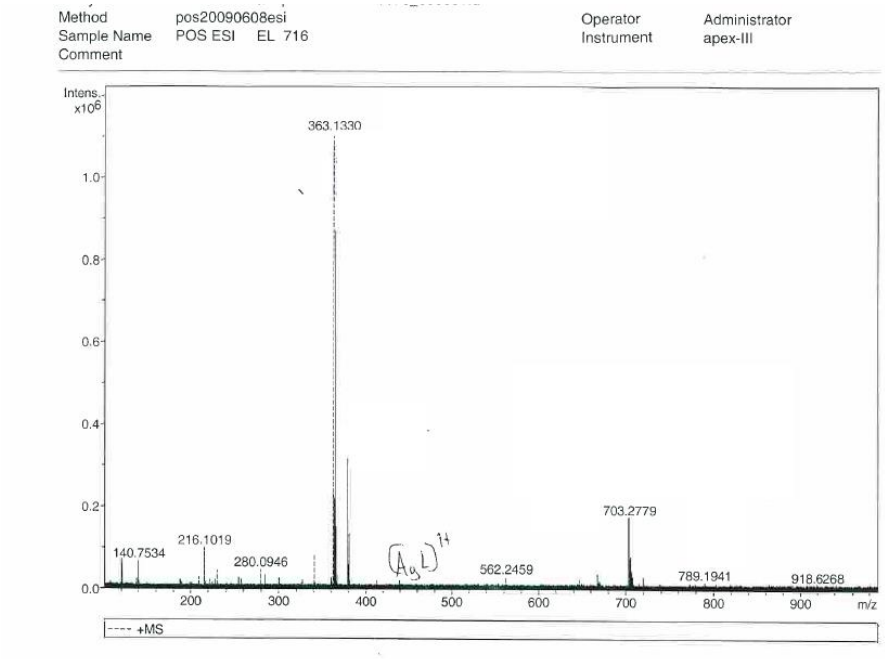

Figure S6.27. ESI-MS data for compound **32** in methanol. Main fragments: 363.13 m/z [(**L**^{3}) + Na]$^{+}$, 379.10 m/z [(**L**^{3}) + K]$^{+}$, 447.05 m/z [Ag(**L**^{3})]$^{+}$, 703.28 m/z [(**L**^{3})$_2$ + Na]$^{+}$, 789.19 m/z [Ag(**L**^{3})$_2$]$^{+}$.

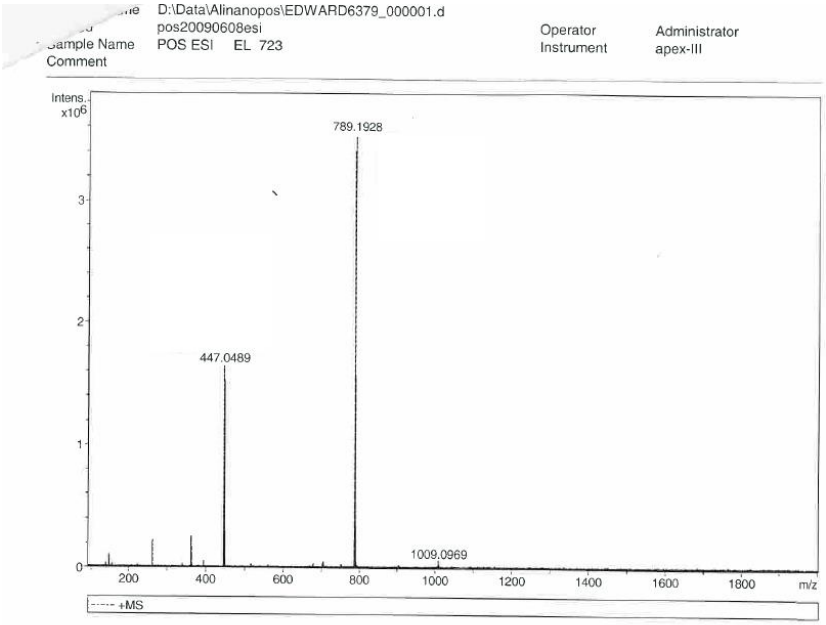

Figure S6.28. ESI-MS data for compound **33** in methanol. Main fragments: 363.13 m/z [(**L**^{3}) + Na]$^{+}$, 447.05 m/z [Ag(**L**^{3})]$^{+}$, 789.19 m/z [Ag(**L**^{3})$_2$]$^{+}$, 1009.09 m/z [Ag$_2$(**L**^{3})$_2$(CF_3CO_2)]$^{+}$.

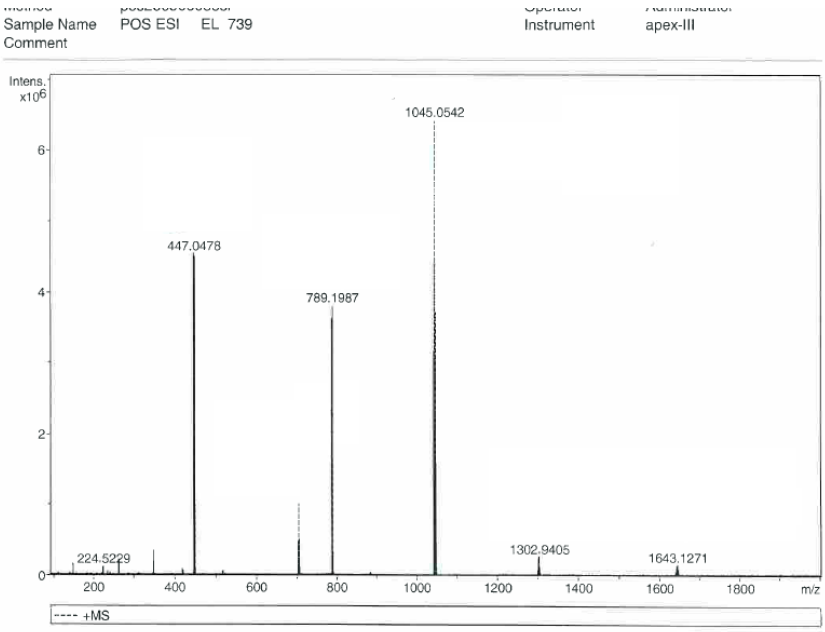

Figure S6.29. ESI-MS data for compound **34** in methanol. Main fragments: 447.05 m/z $[Ag(\mathbf{L^3})]^+$, 705.93 m/z $[Ag_2(\mathbf{L^3})\ (CF_3SO_3)]^+$, 789.20 m/z $[Ag(\mathbf{L^3})_2]^+$, 1045.05 m/z $[Ag_2(\mathbf{L^3})_2(CF_3SO_3)]^+$, 1302.94 m/z $[Ag_3(\mathbf{L^3})_2(CF_3SO_3)_2]^+$, 1643.13 m/z $[Ag_3(\mathbf{L^3})_3(CF_3SO_3)_2]^+$.

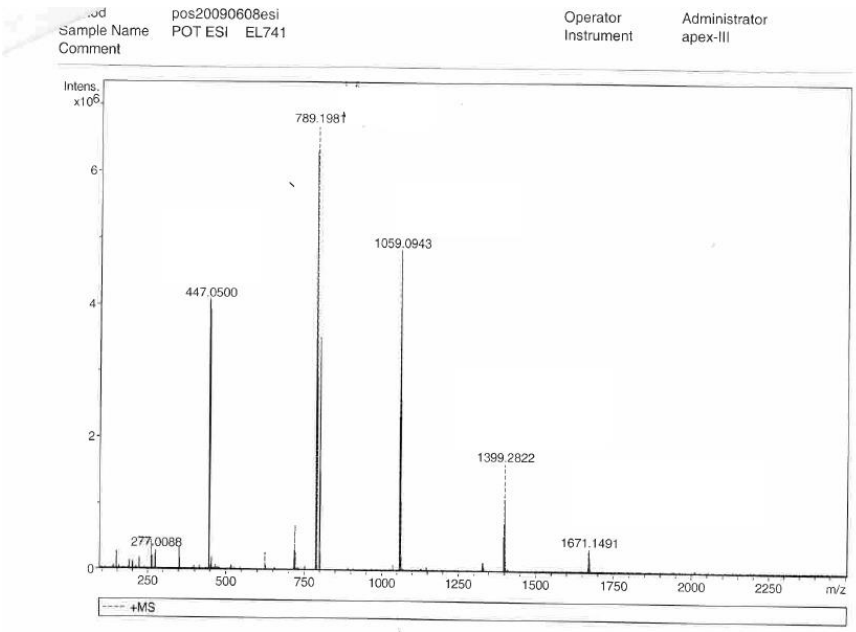

Figure S6.30. ESI-MS data for compound **35** in methanol. Main fragments: 447.05 m/z $[Ag(\mathbf{L^3})]^+$, 718.93 m/z $[Ag_2(\mathbf{L^3})\ (CF_3CF_2CO_2)]^+$, 789.20 m/z $[Ag(\mathbf{L^3})_2]^+$, 1059.09 m/z $[Ag_2(\mathbf{L^3})_2(CF_3CF_2CO_2)]^+$, 1399.28 m/z $[Ag_2(\mathbf{L^3})_3(CF_3CF_2CO_2)]^+$, 1671.15 m/z $[Ag_3(\mathbf{L^3})_3(CF_3CF_2CO_2)_2]^+$.

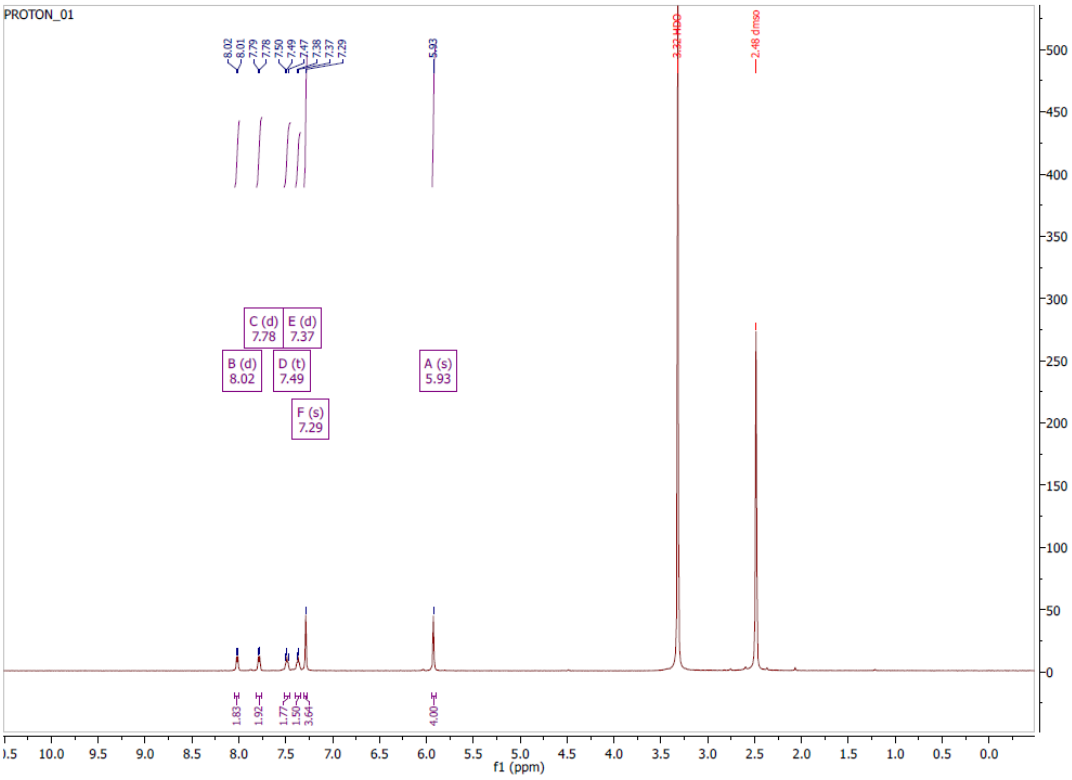

Figure S6.31. ^{1}H NMR spectrum of **27.**

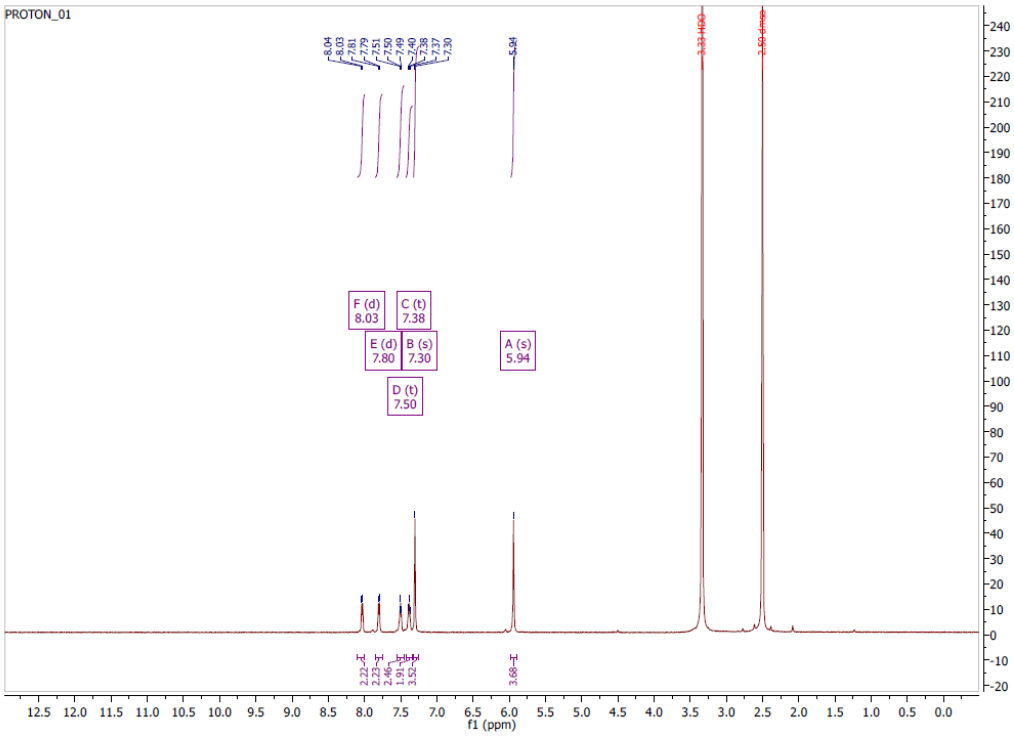

Figure S6.32. ^{1}H NMR spectrum of **28.**

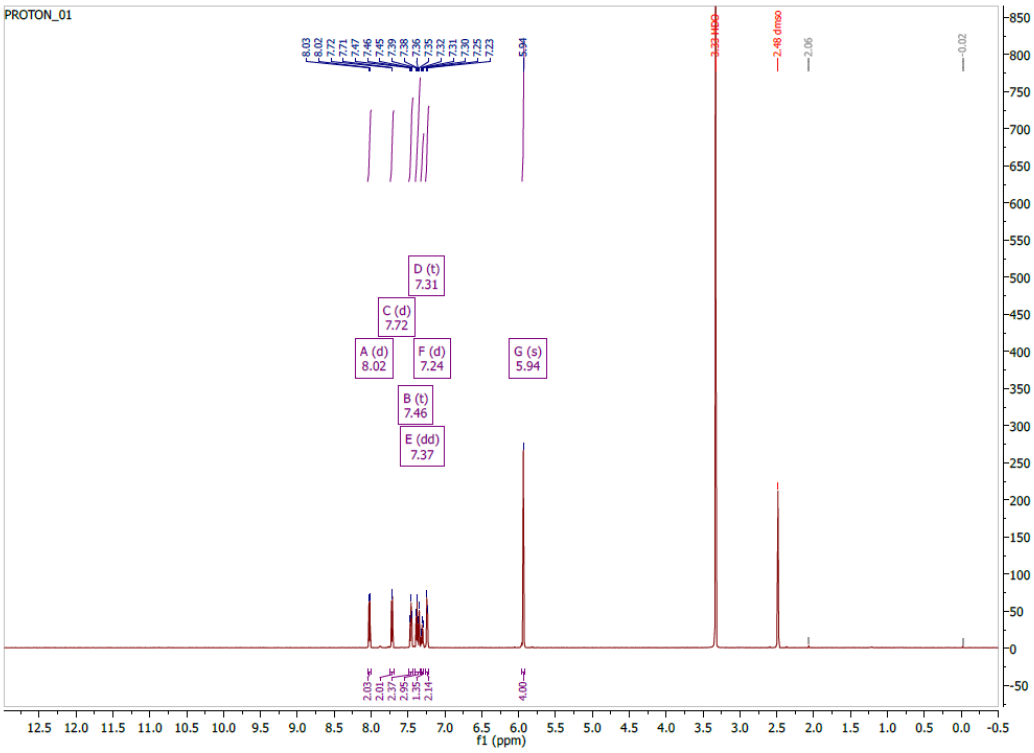

Figure S6.33. ^{1}H NMR spectrum of **29.**

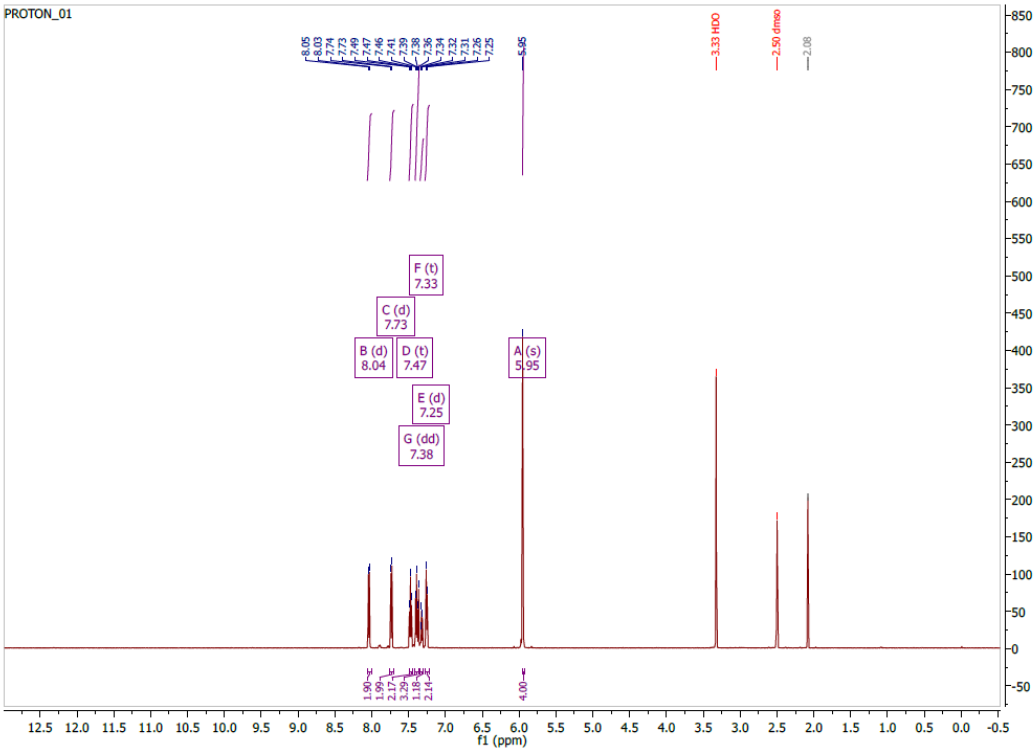

Figure S6.34. ^{1}H NMR spectrum of **30.**

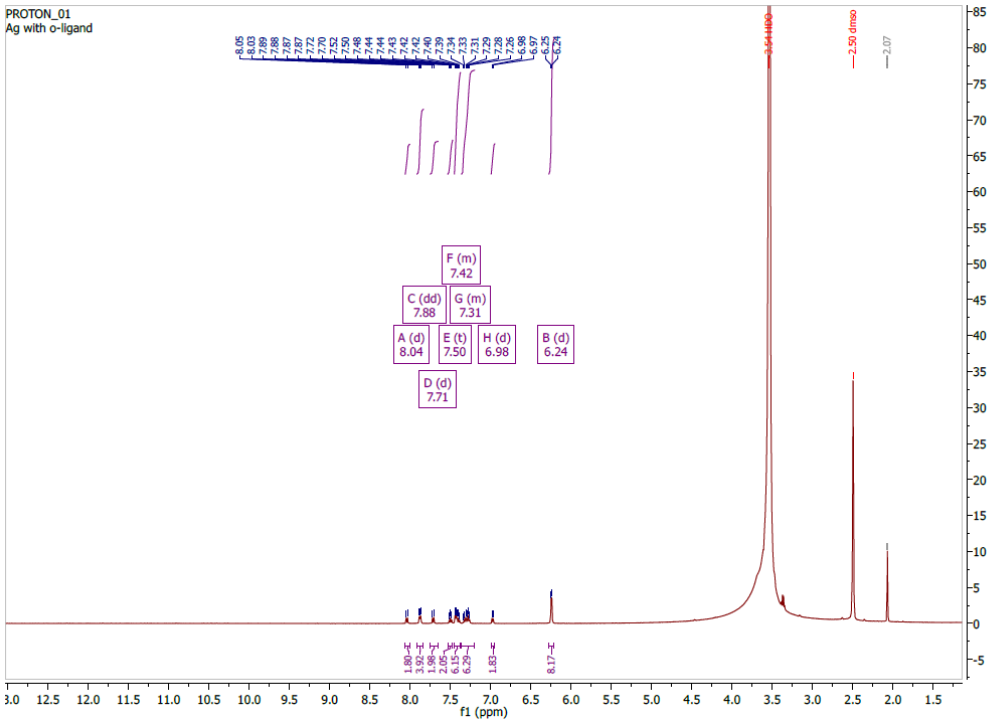

Figure S6.35. ^{1}H NMR spectrum of **31.**

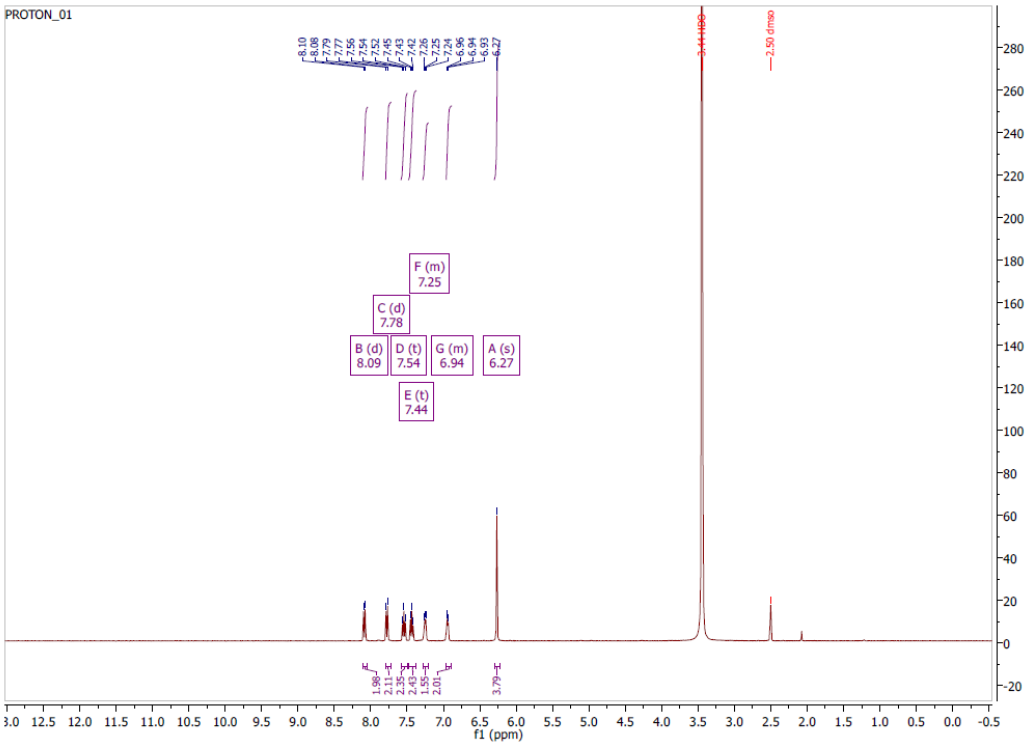

Figure S6.36. ^{1}H NMR spectrum of **32.**

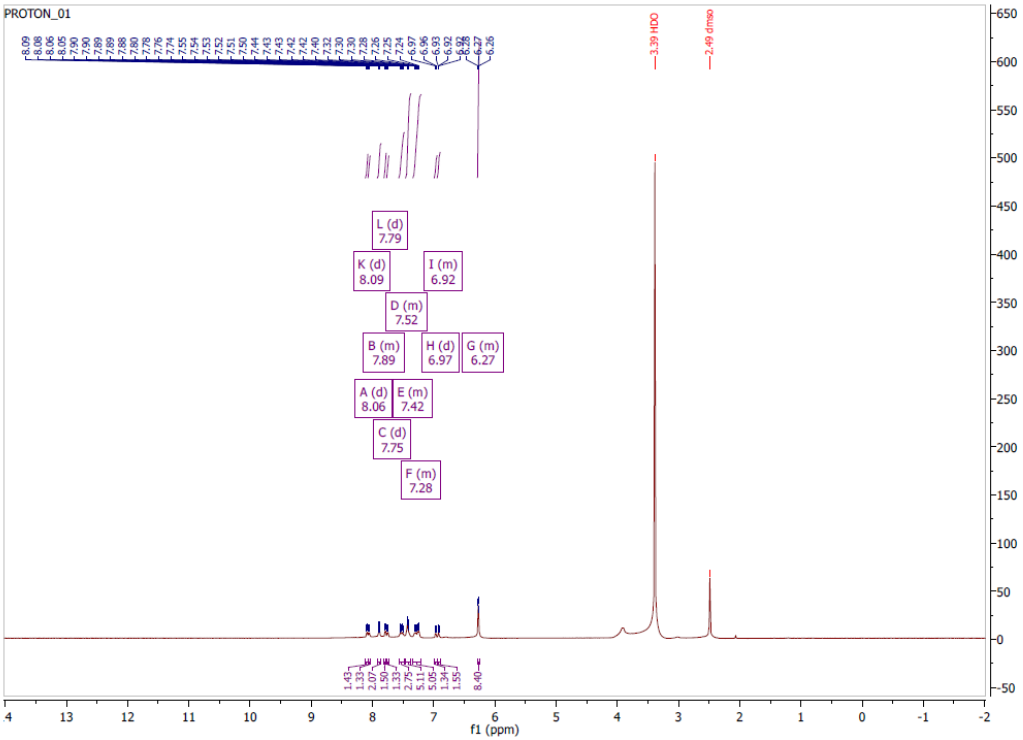

Figure S6.37. ^{1}H NMR spectrum of **33.**

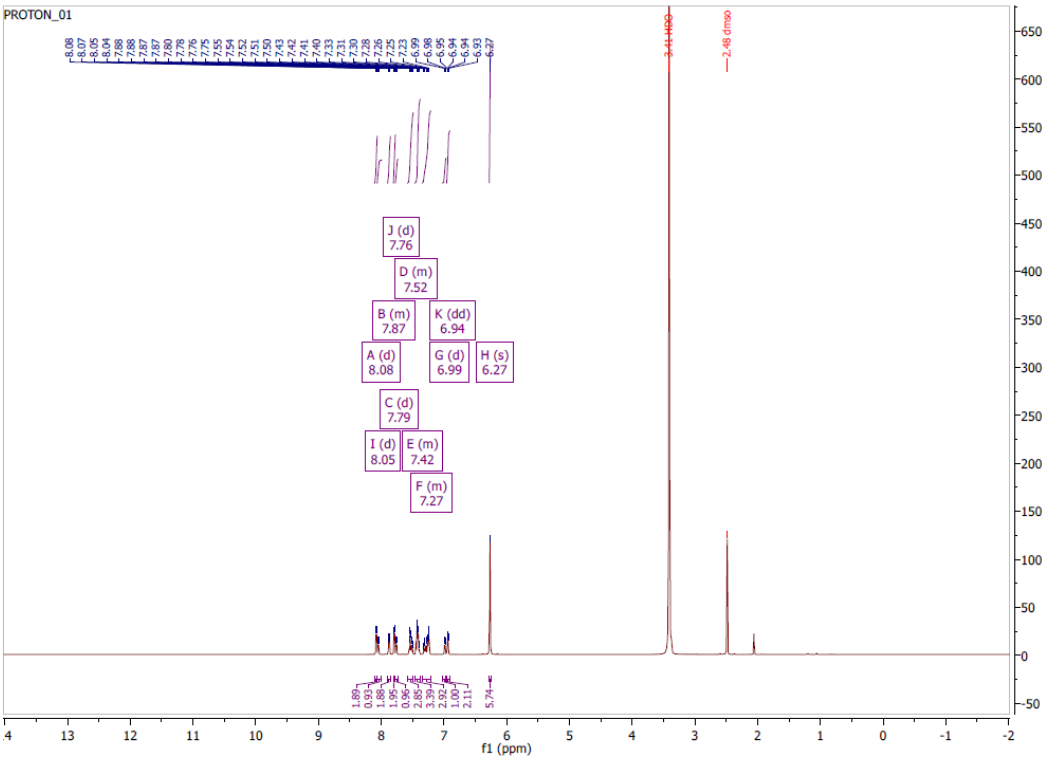

Figure S6.38. ^{1}H NMR spectrum of **34.**

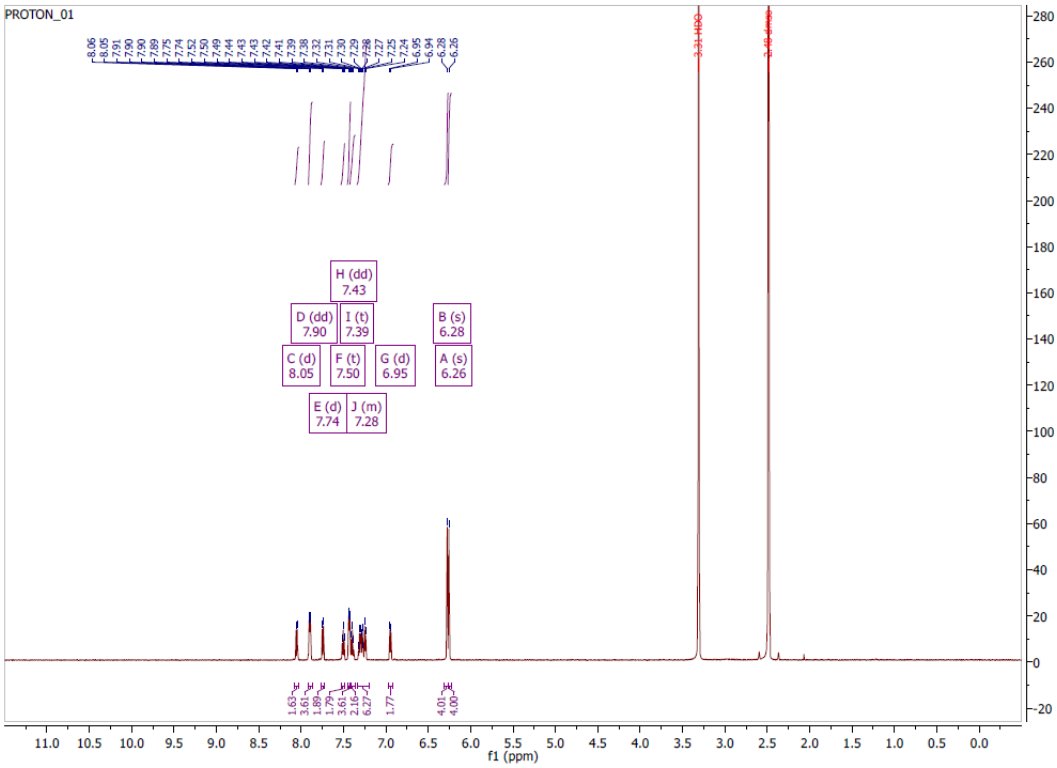

Figure S6.39. ^{1}H NMR spectrum of **35.**

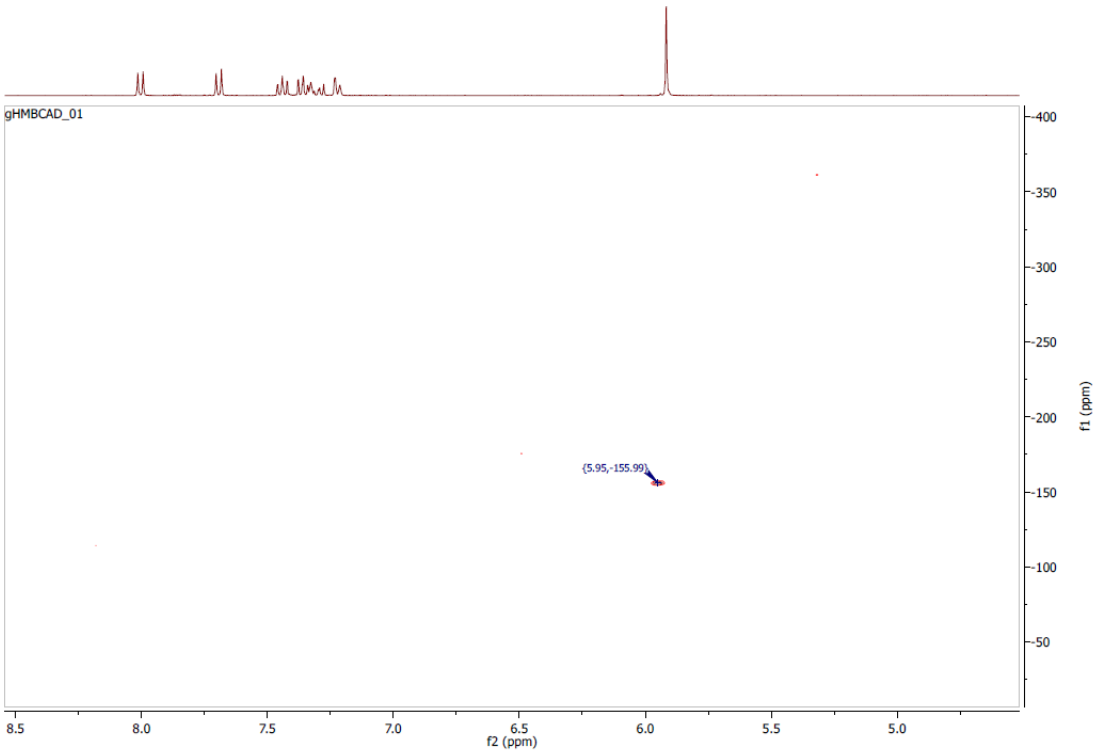

Figure S6.40. ^{15}N HMBC NMR spectrum of **30.**

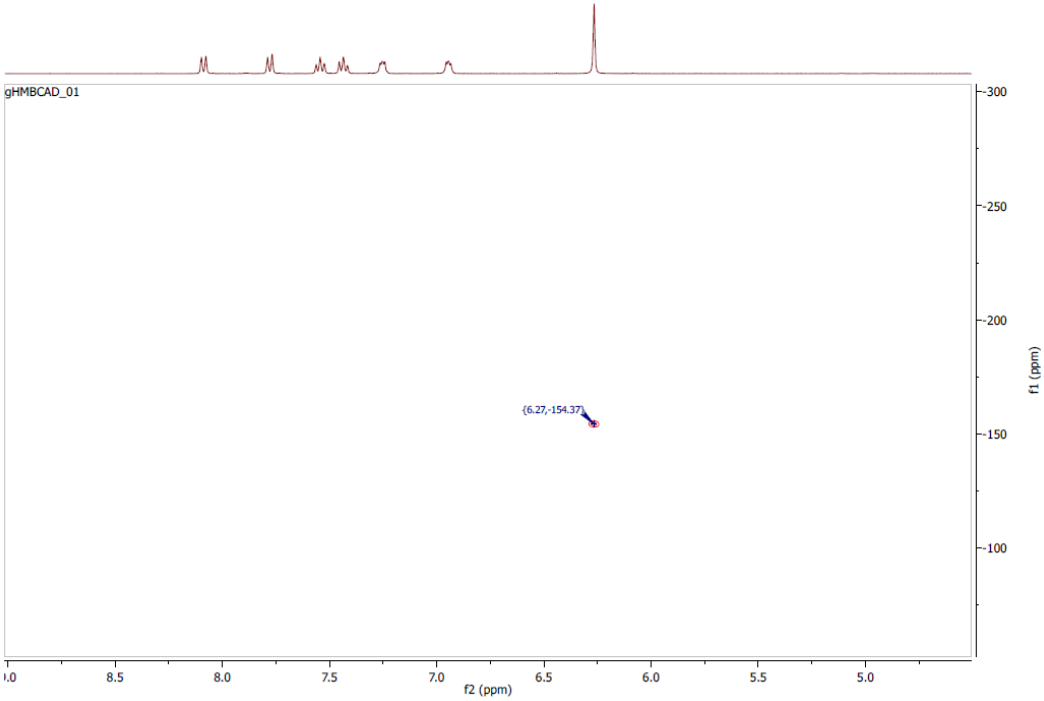

Figure S6.41. ^{15}N HMBC NMR spectrum of **32.**

6.4. ^{1}H, ^{13}C NMR and HRMS spectra of ketone products

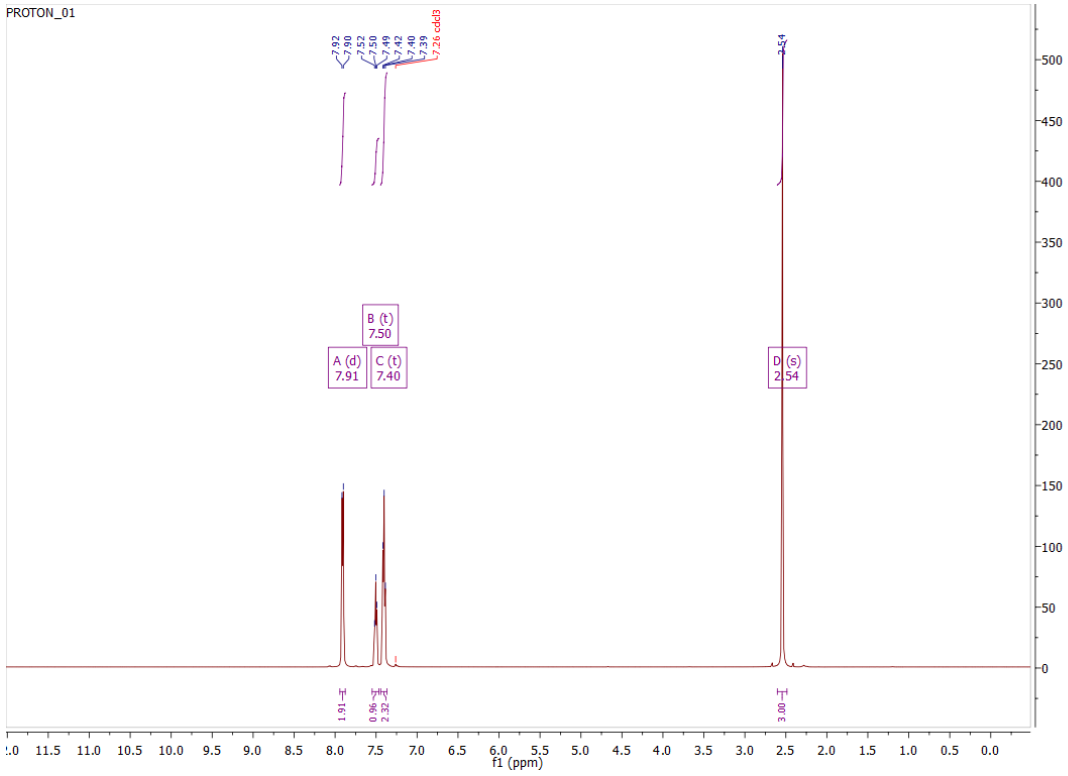

Figure S6.42. ^{1}H NMR spectrum of ketone **C6K1**.

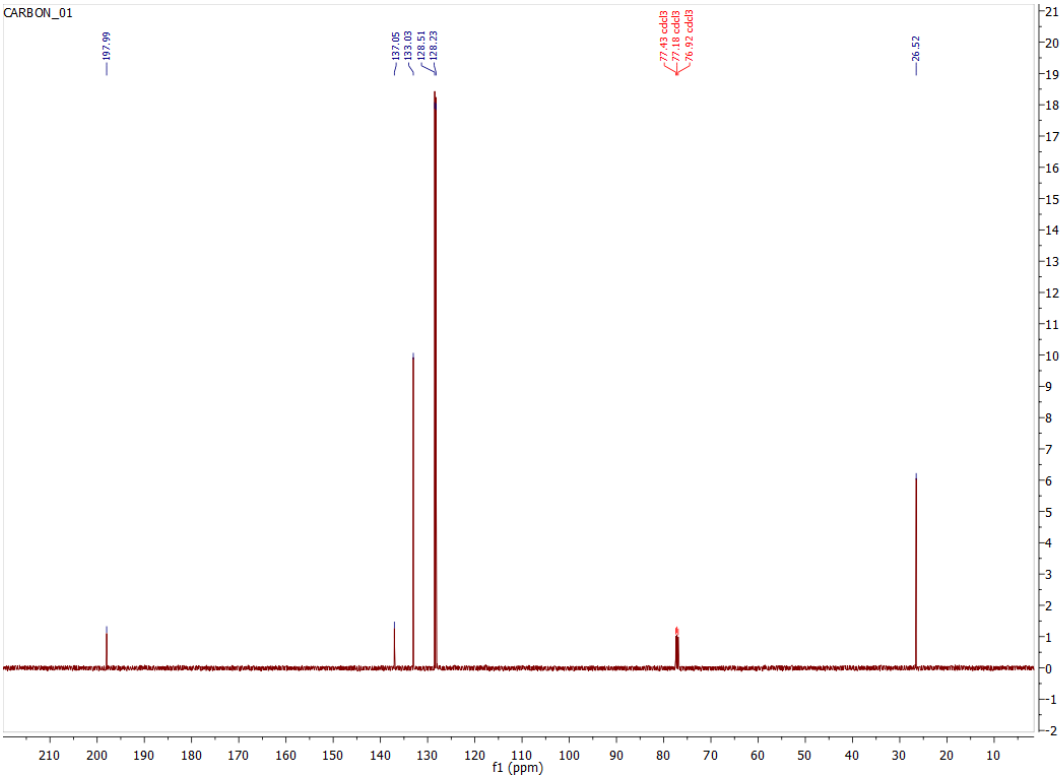

Figure S6.43. ^{13}C NMR spectrum of ketone **C6K1**.

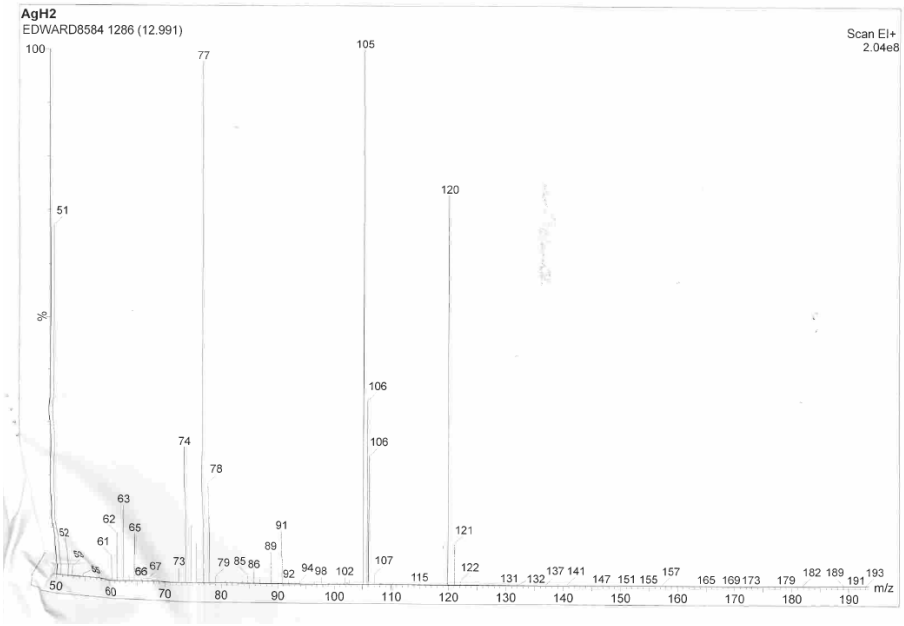

Figure S6.44. EI spectrum of ketone **15a**.

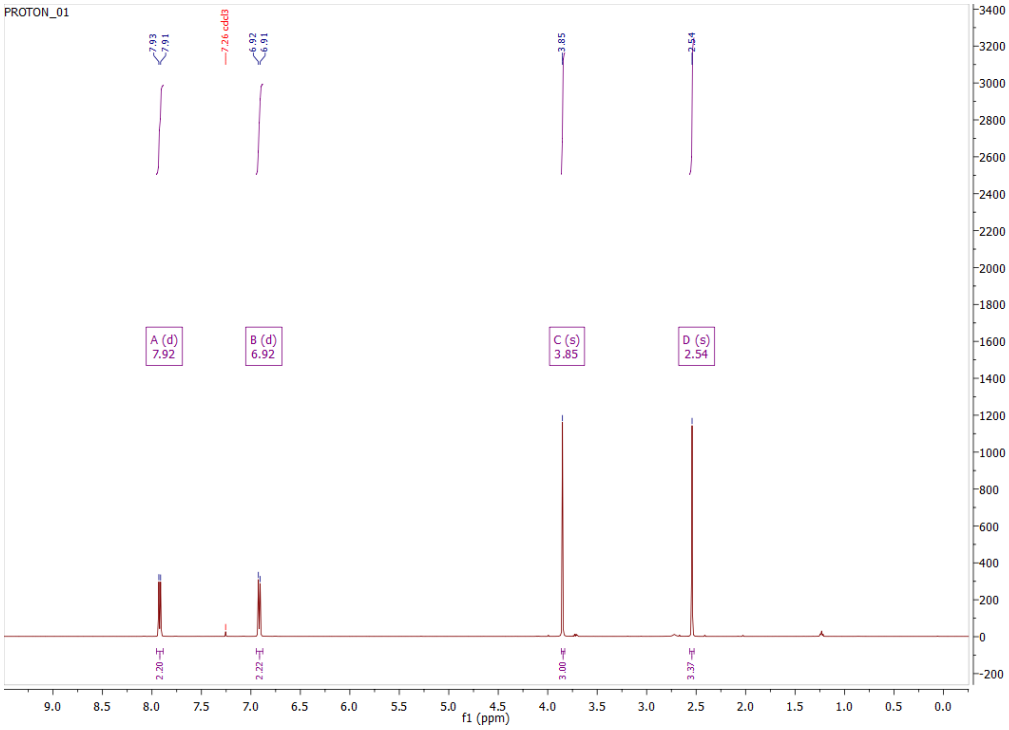

Figure S6.45. ^{1}H NMR spectrum of ketone **C6K2**.

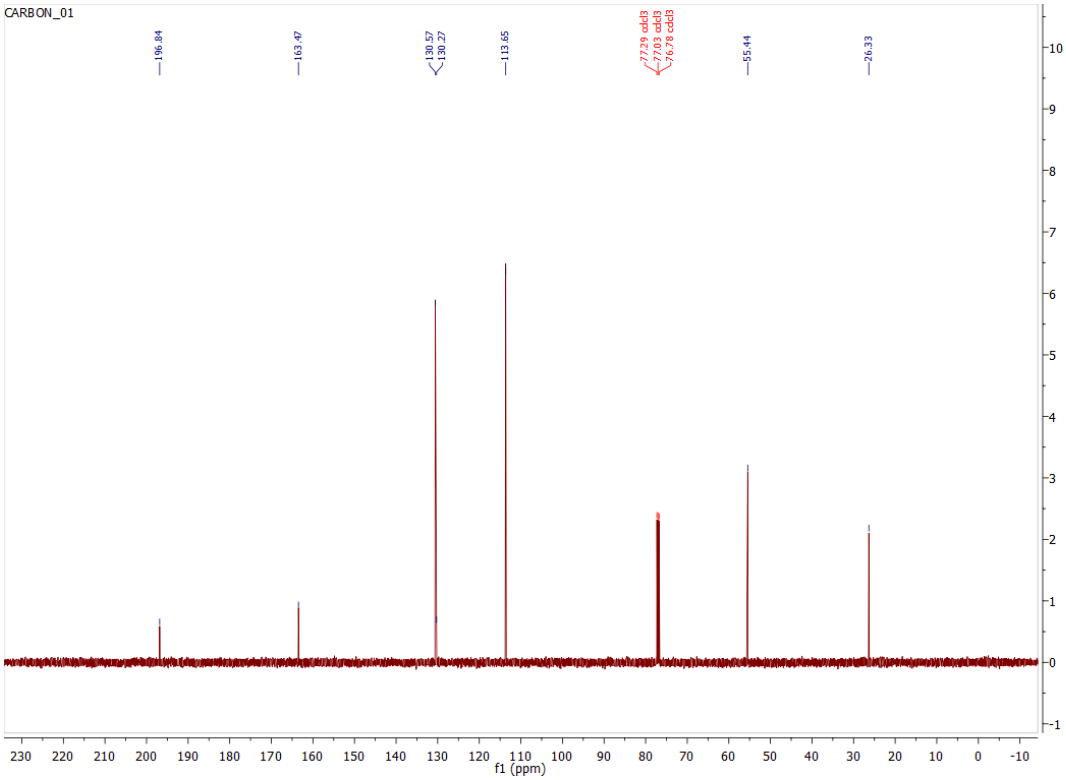

Figure S6.46. ^{13}C NMR spectrum of ketone **C6K2**.

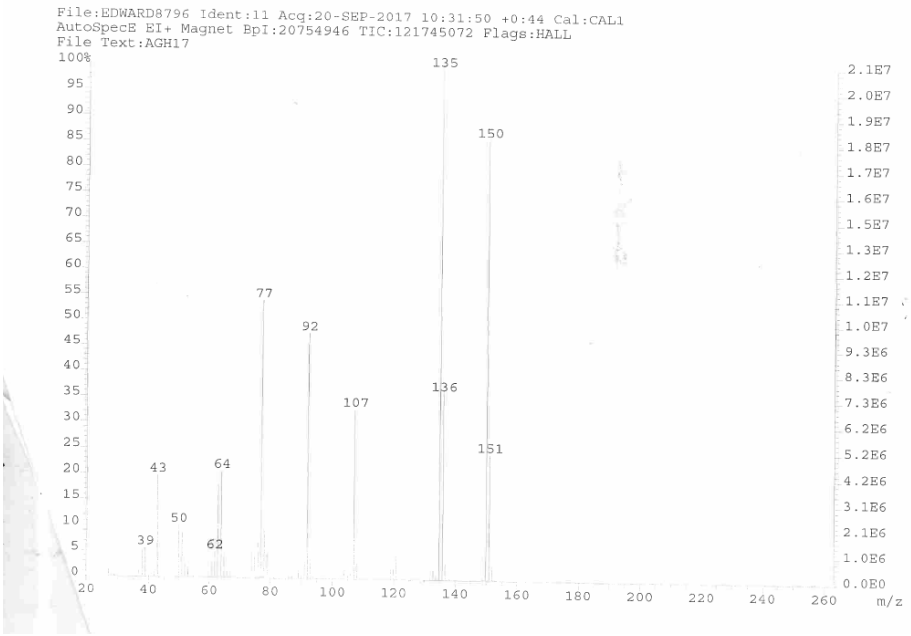

Figure S6.47. EI spectrum of ketone **C6K2**.

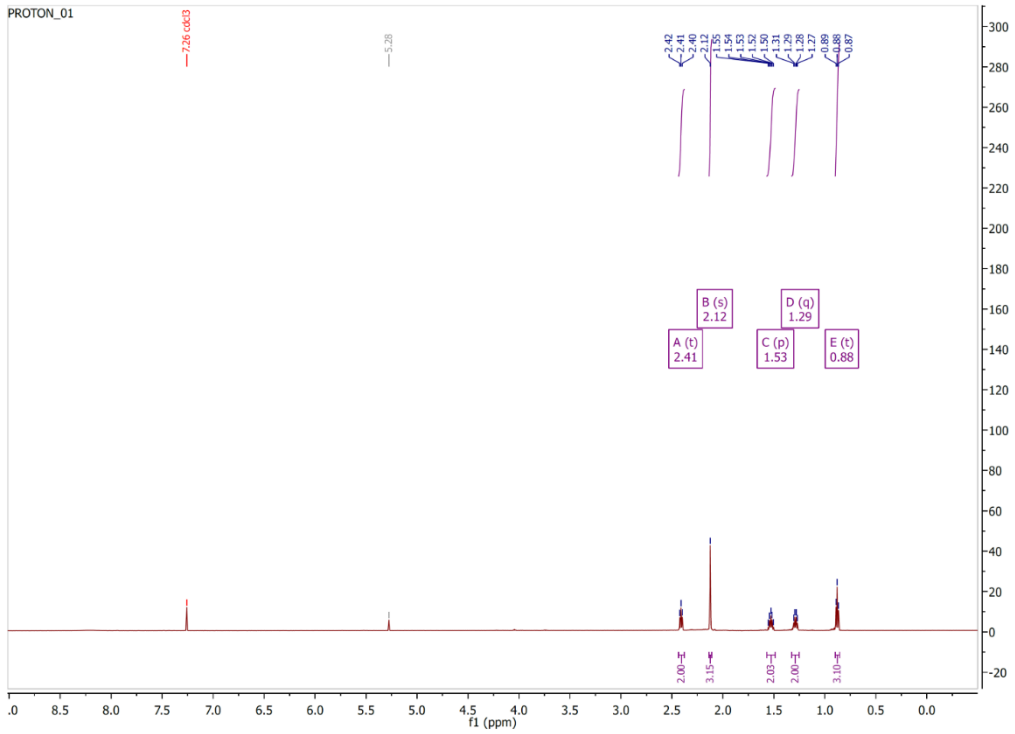

Figure S6.48. ^{1}H NMR spectrum of ketone **C6K3**.

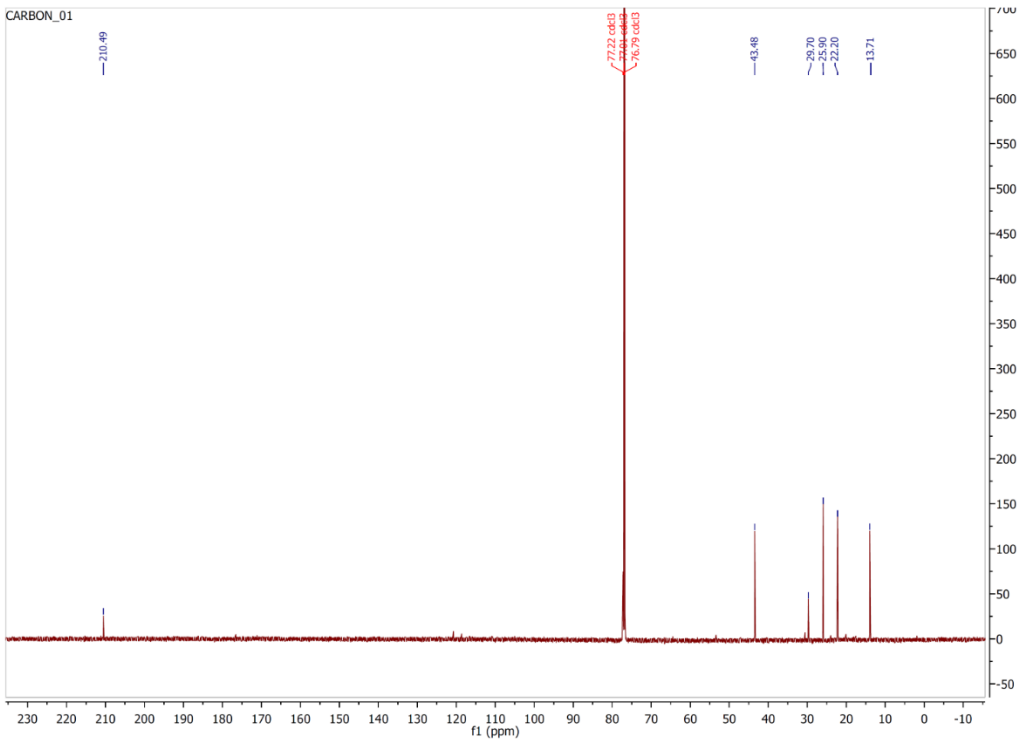

Figure S6.49. ^{13}C NMR spectrum of ketone **C6K3**.

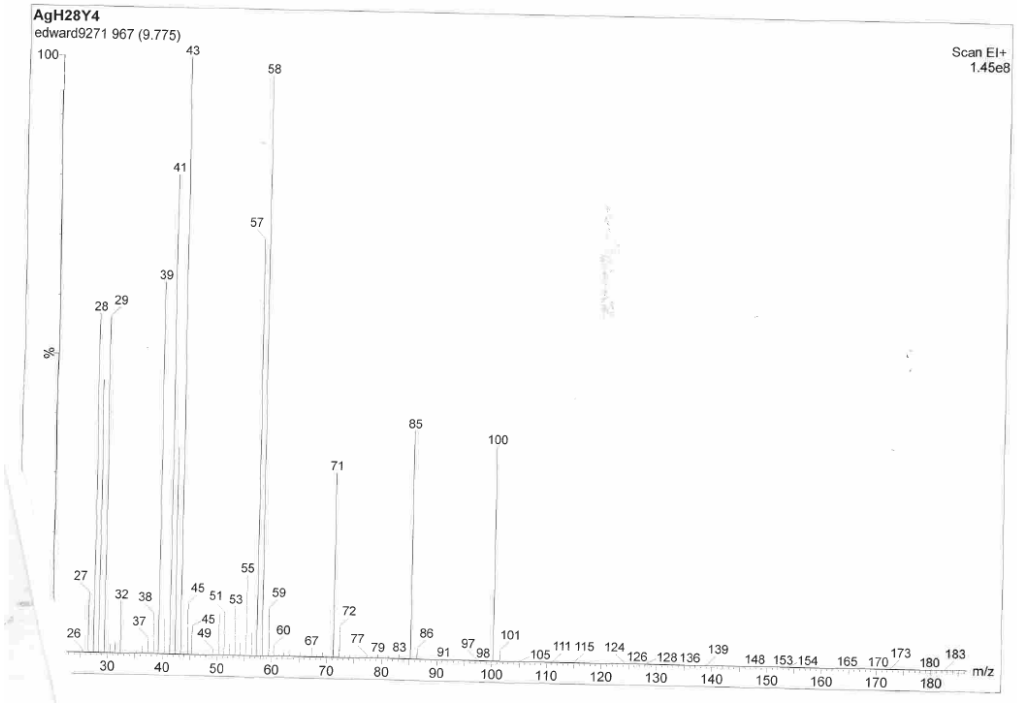

Figure S6.50. EI spectrum of ketone **C6K3**.